3.0 THERMAL EVALUATION

This chapter identifies and describes the principal thermal design aspects of the TRUPACT–III package. Further, this chapter presents the evaluations that demonstrate the thermal safety of the TRUPACT–III packaging and compliance with the thermal requirements of 10 CFR 71[1] when transporting a payload of contact-handled (CH) transuranic (TRU) waste generating a maximum of 80 watts of decay heat. Specifically, all package components are shown to remain within their respective temperature limits under the design basis normal conditions of transport (NCT). Further, per 10 CFR §71.43(g), the maximum accessible package surface temperature is demonstrated to be less than 50 °C for the maximum decay heat loading, an ambient temperature of 38 °C, and no insolation.

The bulk temperature of the impact absorbing foam is shown to be less than 65 °C, based on the NCT maximum temperature conditions. As such, the foam will retain sufficient structural integrity to protect the payload during the subsequent hypothetical accident condition (HAC) drop scenarios described in Chapter 2.0, *Structural Evaluation.* Finally, the package is shown to structurally withstand the damage arising from the HAC drop scenarios and retain sufficient thermal protection to maintain all package component temperatures within their respective short term limits during the regulatory fire event and the post-fire package cool-down period.

3.1 Description of Thermal Design

The TRUPACT–III packaging, as illustrated in Figure 1.1-1 through Figure 1.1-7 from Section 1.1, *Introduction*, is a rectangular body assembly with a bolted, flat closure lid and an energy absorbing overpack cover that protects the closure lid. The body assembly consists of an integral, energy-absorbing and thermally-protective overpack structure that surrounds and protects a rigid containment structural assembly (CSA) from the hypothetical accident conditions of transport (HAC). The external dimensions of the package are 4,288 mm long × 2,500 mm wide × 2,650 mm high, while the internal dimensions of the payload compartment are 2,790 mm long × 1,840 mm wide × 2,000 mm high. The maximum gross shipping weight of the package is 25,000 kg, with an empty weight of approximately 19,790 kg.

The primary heat transfer mechanisms within the TRUPACT–III packaging are conduction and radiation, while the principal heat transfer from the exterior of the packaging is via convection and radiation to the ambient environment. The potential for convective heat transfer within the payload cavity is conservatively neglected due to the relatively close coupling of the bodies within the package cavity.

3.1.1 Design Features

The TRUPACT–III package (see Figure 1.1-1 and Figure 1.1-2) is designed as a totally passive thermal system. The principal thermal characteristic of the TRUPACT–III package is that the structure of both the overpack and CSA are fabricated of relatively light weight sheetmetal. This design feature results in a package design that exhibits a rapid thermal response for the overpack sheetmetal under

[1] Title 10, Code of Federal Regulations, Part 71 (10 CFR 71), *Packaging and Transportation of Radioactive Material*, 01–01–09 Edition.

transient heat loads. The CSA is thermally protected from temperature swings on the package exterior through the balsa wood and polyurethane foam used to provide thermal and impact protection.

3.1.1.1 TRUPACT–III Packaging

CSA

The CSA (the body plus the bolted closure lid) is a rigid, lightweight, and high strength structure fabricated of Alloy UNS S31803 stainless steel. The inner wall of the CSA serves as the containment boundary for the package. Surrounding the 8-mm inner containment stainless steel sheets is an 8-mm stainless steel structural sheet that is attached to the containment sheets via V-shaped, 4-mm thick stainless steel stiffener ribs. Continuous seam welds attach the 4-mm thick ribs to the containment sheet, while 20-mm plug welds spaced approximately 55-mm apart are utilized to attach the ribs to the structural sheet. The overall cross-sectional thickness of the CSA body is 140-mm. Guide bars with a cross section of 25 mm × 76 mm are attached to the side, back, and roof of the CSA inner cavity. The guide bars are made of ASTM Type 304/304L stainless steel and are located to correspond to the bumpers on the SLB2 payload container.

The containment boundary of the CSA is formed by the following components:

- the inner stainless steel sheets of the CSA body (four sides plus the closed end),
- the closure lid inner sheet,
- the inner O-ring seal located in the outer flange of the closure lid,
- the vent port insert located in the closure lid,
- the vent port insert inner O-ring seal.

Packaging Overpack

The CSA is surrounded on the sides by an overpack of 109 to 114-mm thick polyurethane foam (nominal density of 0.10 kg/dm^3), followed by a 10-mm puncture resistant stainless steel sheet, then a 60-mm thick layer of low density balsa wood, and, finally, a 6-mm outer stainless steel sheet. The exterior surface of the outer sheet is painted white, with the coating being optional for the bottom surfaces. The steel sheets are fabricated of Alloy UNS S31803 stainless steel. The 109-mm foam thickness is used on the top and bottom of the package, while the sides of the package use a 114-mm thick foam layer. Figure 1.1-3 illustrates the typical buildup of components through a typical package section.

While the CSA is essentially surrounded by low thermal conductivity material (i.e., the polyurethane foam and balsa wood), the 6-mm support sheets connecting each edge of the CSA to the exterior of the package (see Figure 3.1-1) provide a direct heat transfer path between the CSA and the exterior surface of the package. As seen from the figure, the 6-mm support sheets are an integral part of the corner sheet metal component. This feature, plus the use of a continuous weld at the joint with the CSA structural sheet, provides a direct, metallic heat transfer path between the CSA and outer sheet. The impact protection at the corners is enhanced by the use of a higher density polyurethane foam (nominal density of 0.29 kg/dm^3) than that used along the sides of the package.

Packaging Closures

The ends of the package are similar to each other in construction and design layout. The principal differences are that the closure lid end contains the temperature sensitive O-ring seals and is more

complex in its design due to its ability to be removed. As such, while the following discussion is specific to the closure lid end, it is generally applicable to the design of the closed end as well.

The closure lid is fabricated in a similar manner as the sidewalls of the CSA body. However, for additional rigidity, the inner and outer sheets are 12-mm thick vs. the 8-mm thick sheets used for the CSA body sidewalls. In addition, the structural sheet of the closure lid is fabricated of multiple sheetmetal strips vs. a continuous sheet. The V-stiffeners are attached to the outside of the inner (containment) sheet using continuous fillet welds, while the outer structural sheets are connected to each other and the V-stiffeners using continuous slot welds (as opposed to the plug welds used for the CSA body). The total thickness of the lid is 148-mm, the width is 2,108 mm, and the height is 2,280 mm. The perimeter of the lid assembly is formed by a rigid box beam flange that incorporates two dovetail grooves to retain the containment and test O-rings and which mates with a similar box beam flange on the CSA body.

The closure lid incorporates a debris shield to protect the containment O-ring from debris originating from the payload. The debris shield assembly consists of a holder, a U-shaped foam insert, and the receptacle. The debris shield extends inward from the shear lip of the closure lid and mates with a receptacle mounted on the sides of the CSA inner cavity (see Figure 1.1-7). The holder is fabricated of UNS S31803 duplex stainless steel, the receptacle is UNS S31803 or Type 304L stainless steel, and the foam insert is made of silicone foam rubber. Double-sided tape is used to mount the foam insert to the holder. Each of the four shear lips features two, 5/16-inch (7.9 mm) diameter filters made from porous polyethylene. These filtered passages prevent a pressure differential across the debris shield and permit helium to reach the containment O-ring seal during leakage rate testing.

A 200-mm × 320-mm recess located in the lower right-hand corner of the lid contains the vent port and the seal test port. The vent port, which is a containment boundary penetration, is closed by an aluminum-bronze insert and sealed by a O-ring seal. The containment, test, and vent port O-ring seals are fabricated from butyl rubber. The closure lid is attached to the CSA body by forty-four (44) bolts fabricated from ASTM A320, L43 alloy steel. Figure 1.1-5 illustrates a cross-section through the closure lid and the interface between lid and the CSA structure.

Impact and thermal protection of the closure lid is provided by the overpack cover assembly. Figure 3.1-2 illustrates an elevation view, while a perspective view is provided in Figure 1.1-1. Because of the diamond shaped recessed region incorporated into the design, the cross-section through the assembly is not uniform. Figure 3.1-3 illustrates the cross-section through the assembly along a section cut line depicted in Figure 3.1-2.

The recessed region of the overpack cover assembly utilizes a 6-mm thick outer sheet backed by a 60-mm thick layer of low-density balsa wood which, in turn, is backed by a 120-mm thick layer of polyurethane foam. The balsa wood and polyurethane foam materials are separated by a 15-mm thick stainless steel sheet to provide resistance to the HAC puncture drop accidents. An additional 6-mm thick sheet is used at the backside of the overpack cover to enclose the polyurethane foam and form the surface which is secured against the outer surface of the closure lid.

The outer region of the overpack cover assembly utilizes an 8-mm thick outer sheet. The joints at the edges of the outer sheets used a rolled, overlapping joint to provide additional tear resistance when deformed under the HAC drop events. The outer sheet is backed by a 140-mm thick layer of medium density polyurethane foam (nominal density of 0.16 kg/dm^3) which, in turn, is backed by a 380-mm

thick layer of higher density polyurethane foam (nominal density of 0.48 kg/dm^3). The layers of polyurethane foam are separated by a 6-mm thick stainless steel sheet to provide resistance to the HAC puncture drop accidents. To provide additional thermal protection around the perimeter of the closure lid where the containment O-ring seals are used, a 42-mm layer of calcium silicate insulation is used. The calcium silicate insulation is covered by a 16-mm thick stainless steel protection plate to provide impact protection to the underlying insulation. Similarly, the upper and lower extensions on the overpack cover assembly incorporate a 30-mm layer of calcium silicate insulation backed by 16-mm thick protection plate to provide lateral protection to the overlapped edges of the closure lid.

Packaging Cheeks

The extensions or 'cheeks' at the end of the package (see Figure 1.1-1 and Figure 3.1-4) provide additional impact protection and serve as lifting points for the package. The outer plates of the cheeks vary in thickness from approximately 2 to 8-mm, but are typically 6-mm or 8-mm. A 140-mm thick layer of medium density polyurethane foam (nominal density of 0.16 kg/dm^3) is used at the ends of the extensions, while the remainder of the extension is filled with high density polyurethane foam (nominal density of 0.48 kg/dm^3). A 30-mm layer of calcium silicate insulation backed by 16-mm thick protection plate provides lateral thermal protection to the overlapped edges of the closure lid.

3.1.1.2 Payload Configuration

As described in Section 1.2.2, *Contents*, the users of the TRUPACT–III package must comply with the payload requirements outlined in the TRUPACT–III TRAMPAC document[2]. That document specifies the Standard Large Box 2 (SLB2) as the only permissible waste box payload container to be utilized with the TRUPACT–III package. The SLB2 containers are fabricated of painted carbon steel and have outside dimensions of 2,743-mm (108-in) long, 1,753-mm (69-in) wide and 1,854-mm (73-in) tall. The containers are designed to be either top or bottom loaded and to accommodate a variety of CH-TRU waste. Figure 3.1-5 illustrates a prototypic top-loading SLB2 container. The waste may either be placed directly into the SLB2 container, or be housed within other containers which, in turn, are placed into the SLB2 container.

Because of the potential variability in the configuration of the waste stream to be loaded in a SLB2 container, a hypothetical waste box which provides a conservative lower bound on the waste stream volume expected to be transported within a SLB2 container is assumed. The dimension of the hypothetical waste box is 965 mm × 965 mm × 1,727 mm (i.e., 3 ft, 2 inches × 3 ft, 2 inches × 5 ft, 8 inches). This hypothetical waste box payload geometry represents 23% of the total available waste volume within the SLB2 container and bounds both the credible volumetric heat loading and the credible non-uniform distribution of decay heat generating waste within the SLB2 container. The hypothetical waste box is assumed to be horizontally and axially centered within the SLB2 container and to be resting against the bottom of the SLB2 container. This placement yields the maximum expected separation distance between the payload and the interior of the TRUPACT–III cavity.

Section 3.5.2.1, *Description of Thermal Model for NCT Conditions*, provides additional details of the payload modeling.

---

[2] U.S. Department of Energy (DOE), *TRUPACT–III TRU Waste Authorized Methods for Payload Control (TRUPACT–III TRAMPAC)*, U.S. Department of Energy, Carlsbad Field Office, Carlsbad, New Mexico.

3.1.2 Content's Decay Heat

The maximum decay heat dissipated by the contents of the TRUPACT–III payload will be 80 watts or less. Further, the decay heat is assumed to be uniformly distributed within the reduced hypothetical payload volume discussed above. The use of a uniform volumetric heat generation is justified by the following considerations:

1) first, the region of uniform volumetric heat generation is confined to a reduced, hypothetical volume that represents only 23% of the actual payload volume within the SLB2 container (see discussion in Section 3.1.1.2, *Payload Configuration*),
2) the thermal conductivity of the entire volume within the SLB2 container is conservatively assumed to be equal to air. Since the actual payload will have an effective bulk thermal conductivity substantially higher than air due to the presence of metals and/or other materials, the peak temperature predicted using the SAR assumptions will bound the peak payload temperature for any credible decay heat distribution within the SLB2 container based on an even greater non-uniform decay heat distribution and the actual payload thermal conductivity.

3.1.3 Summary Tables of Temperatures

Table 3.1-1 presents a summary of the maximum temperatures determined for the major components of the TRUPACT–III packaging under NCT and HAC conditions with an internal decay heat load of 80 watts. As seen from the table, the peak temperature for all components remain within their respective limits for both NCT and HAC conditions. Therefore, the TRUPACT–III Package design complies with the thermal requirements of 10 CFR 71.

Further details of the NCT results, plus those for lower decay heat loads, are presented in Section 3.3, *Thermal Evaluation for Normal Conditions of Transport*. Similarly, further discussion of the HAC thermal analysis is provided in Section 3.4, *Thermal Evaluation for Hypothetical Accident Conditions.*

3.1.4 Summary Tables of Maximum Pressures

The maximum normal operation pressure (MNOP) developed during the maximum shipping period is limited by administrative controls to 172 kPa gauge. The maximum pressure developed under HAC conditions will be 249.3 kPa gauge, or a + 45% increase from its maximum pre-fire level. Table 3.1-2 presents a summary of the maximum package pressures.

The primary mechanism for potential flammable gas generation in TRU wastes is radiolysis[2], while gas generation via chemical, biological, and thermal mechanisms are insignificant. The methods of compliance and verification for gas generation issues are provided in the TRAMPAC document[2].

Table 3.1-1 – Summary of Maximum Package Temperatures

Location / Component	Temperatures (°C)			
			Maximum Allowable [3]	
	NCT Hot [1,2]	HAC [2]	NCT	HAC
Bounding Waste Box Payload				
- Maximum	162.2	177	230	230
- Bulk Avg.	90.4	107	230	230
Standard Large Box (SLB2) Payload				
- Maximum sidewall	62.3	89	230	230
- Minimum sidewall (coincident) [4]	52.9	54	230	230
- Avg. sidewall	54.9	60	230	230
- Bulk Avg. (of void only)	55.4	76	230	230
- Bulk Avg. (of total volume) [5]	63.0	83	230	230
Containment O-ring Seal	52.6	95	107	204
Sampling/Vent Port O-ring Seal	51.2	80	107	204
Debris Shield	52.6	95	120	-
CaSi (Seal Protection) Insulation	60.9	688	982	982
CSA Structural Sheet (includes Lid outer sheet),	57.6	689 (Max) [6] 75 (Avg)	316	725 for < 1 hour / 316
CSA Containment Sheet (includes Lid inner sheet)				
- Maximum	55.6	222	316	316
- Minimum (coincident) [4]	50.4	51	316	316
CSA Lid Bolts	53.4	187	427	316
Outer Skin				
- Package Body, Peak	86.6	800	121	1,370
- Package Cheek, Peak	77.8	800	121	1,370
- Package Cover, Peak	84.2	800	121	1,370
Last-a-Foam				
- Package Body, Peak/Avg.	67.3 / 51.9	684 / 96	260 / 65	-
- Package Corner, Peak/Avg.	82.4 / 52.3	797 / 189	260 / 65	-
- Package Cheek, Peak/Avg.	77.3 / 49.7	800 / 373	260 / 65	-
- Overpack Cover Outer Area, Peak/Avg.	83.6 / 52.4	792 / 169	260 / 65	-
- Overpack Cover Recess Area, Peak/Avg.	58.6 / 50.5	695 / 99	260 / 65	-
Balsa				
- Package Body, Peak/Avg.	86.2 / 55.3	793 / 455	100 / 65	-
- Overpack Cover, Peak/Avg.	66.9 / 51.3	784 / 449	100 / 65	-

Notes:

1) Peak temperatures determined assuming one SLB2, diurnal insolation cycle, and a constant ambient temperature of 38 °C.
2) For conservatism, the decay heat is confined to a bounding minimum sub-volume within the SLB2. This sub-volume represents 23% of the total available volume. The remaining SLB2 volume is assumed to have zero decay heat and the thermal properties of air.
3) Maximum allowable temperatures are established in Section 3.2.2, *Technical Specifications of Components*.
4) The listed minimum temperature is taken at the same time point (i.e., 'coincident') as the listed maximum temperature as opposed to the actual minimum temperature occurring during the diurnal cycle.
5) Bulk average temperature computed assuming SLB2 internal volume of 7,394 liters and a bounding waste box volume of 1,609 liters.
6) The peak CSA structural sheet temperature occurs at the location of the puncture bar damage and lasts less than 1 hour. The temperature for the remaining portions of the structural sheet is substantially lower as demonstrated by the average temperature value.

Table 3.1-2 – Summary of Maximum Pressures

Condition	CSA Cavity Temperature	Pressure
NCT Hot	59 °C	172 kPa gauge
HAC Hot	153 °C	249.3 kPa gauge

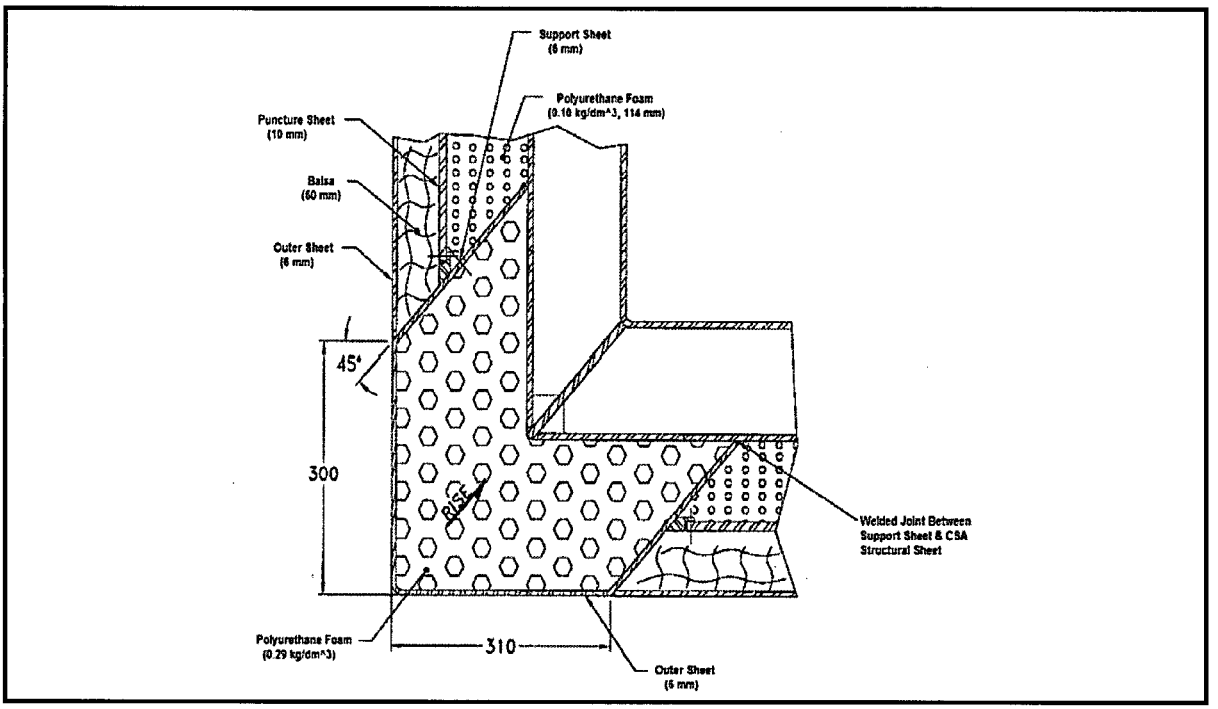

Figure 3.1-1 – Package Corner Detail

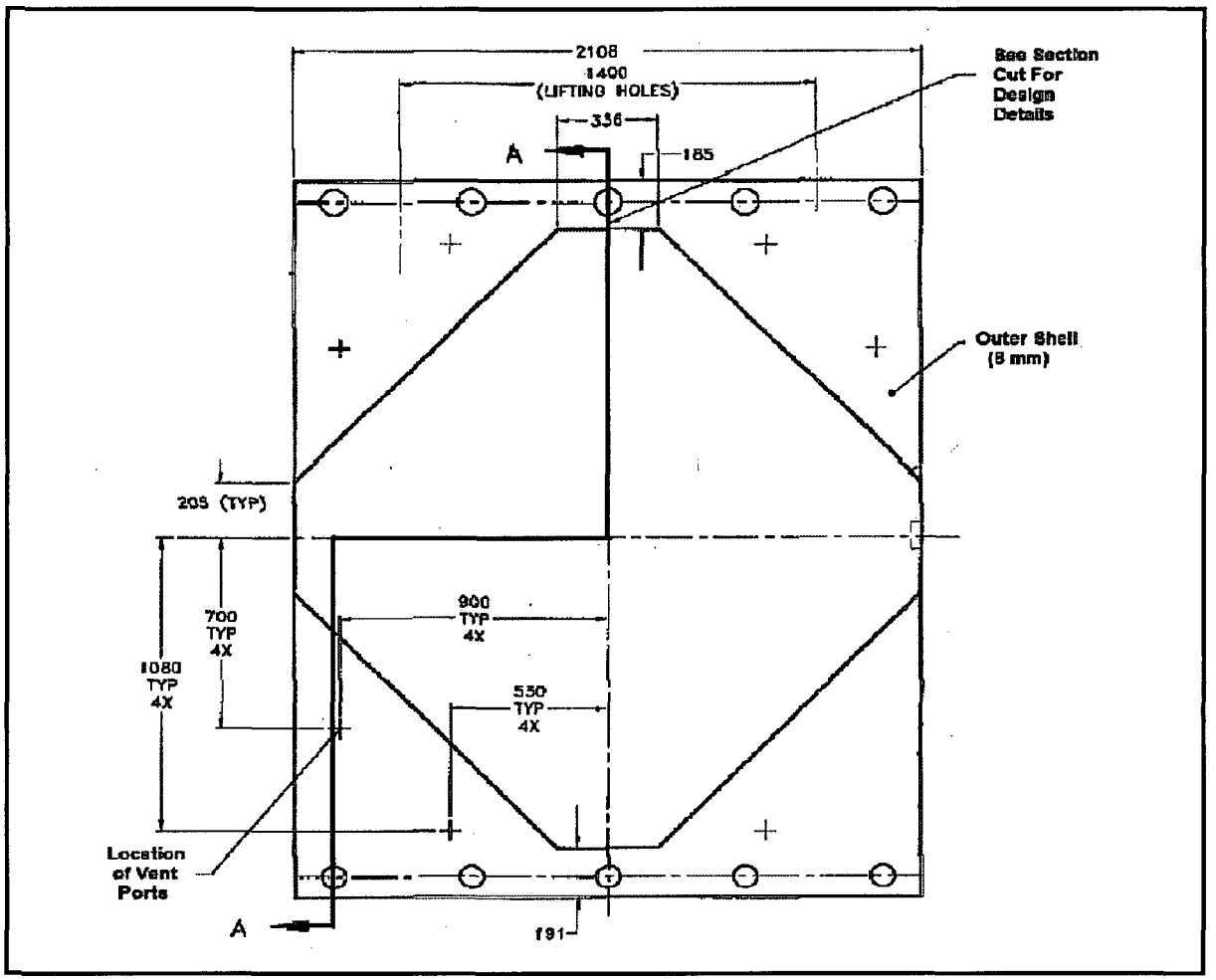

Figure 3.1-2 – Overpack Cover Elevation

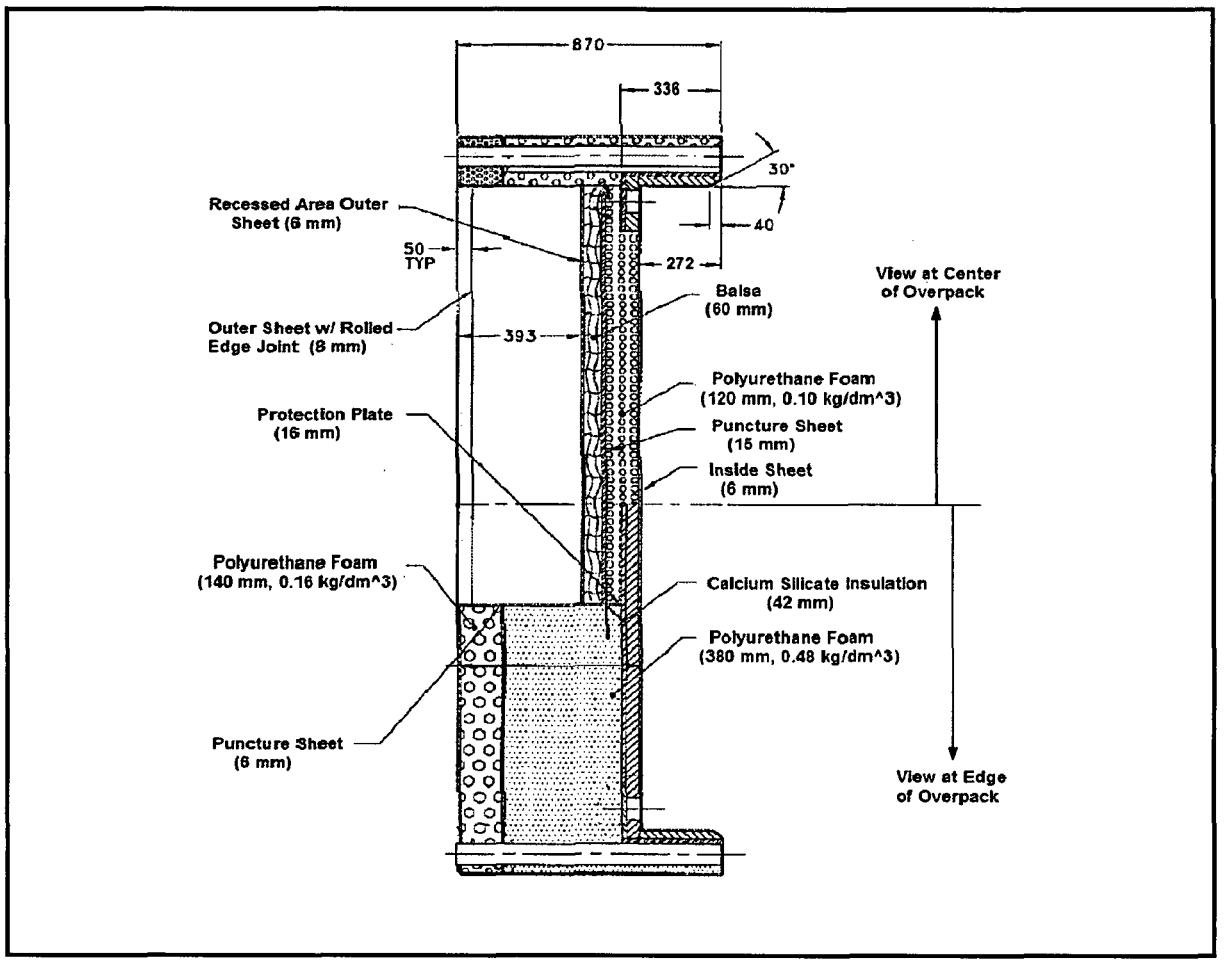

(See Figure 3.1-2 for depiction of section cut line.)

Figure 3.1-3 – Overpack Cover, Section Cut A-A

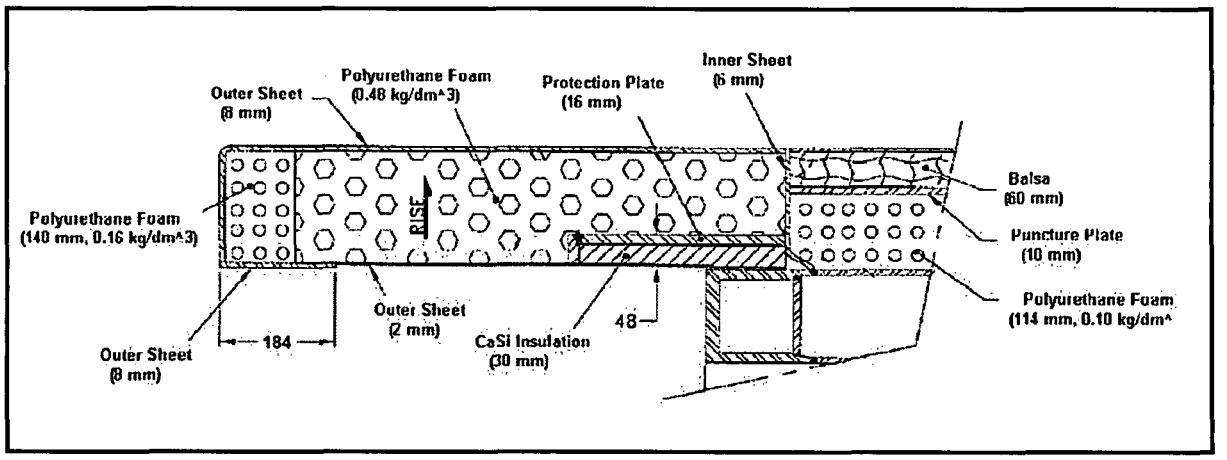

Figure 3.1-4 – Package Cheek Cross-Section

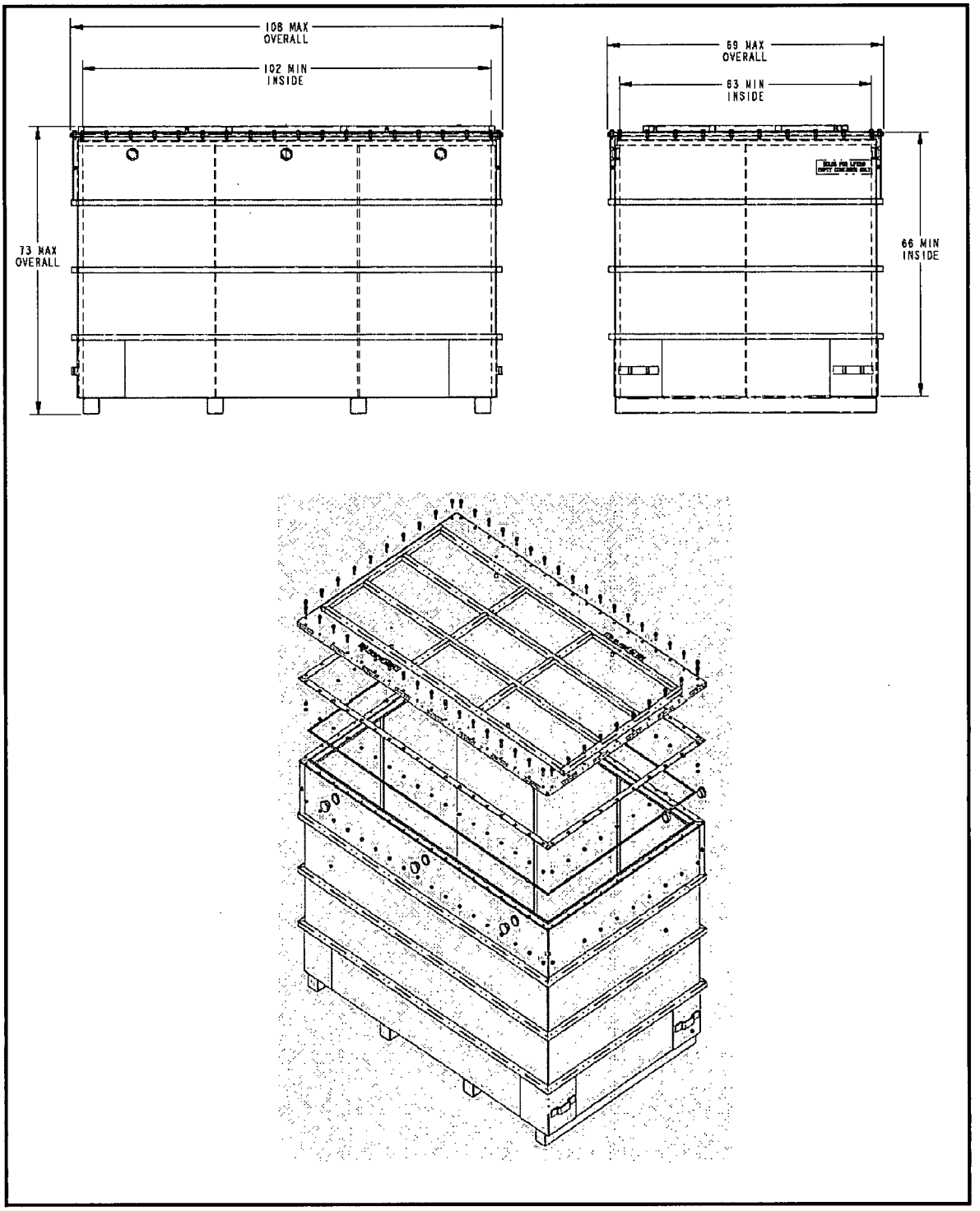

(Figure dimensions are in inches)

Figure 3.1-5 – Top-Loading SLB2 Waste Container

3.2 Material Properties and Component Specifications

The thermally significant materials used in the fabrication of the TRUPACT–III include the following:

- Alloy UNS S31803 used for all plate and sheet material
- ASTM Type 304/304L stainless steel used for parts made from round stock and any round tubes
- ASTM A320 L43 alloy steel, used for closure lid and overpack cover attachment bolts
- Balsa, used in the impact structure for the CSA body and the end overpacks
- Polyurethane foam, used in the body overpack and in the overpack cover
- Calcium silicate insulation, used for thermal protection around lid containment seal
- Air at atmospheric pressure, which fills all void volumes
- Closed-cell silicone foam and polyethylene used for the debris shield
- Plastic material (i.e., nylon, polyethylene, or polyurethane) attached to the guide bars

In addition to the above materials, the SLB2 waste boxes are assumed to be fabricated principally from ASTM A-36 carbon steel, while the roller floor is assumed to be fabricated of 6061 aluminum.

3.2.1 Material Properties

The thermal properties for the Alloy UNS S31803 and ASTM Type 304/304L stainless steels are provided in Table 3.2-1 as a function of temperature. The thermal properties, including thermal conductivity and specific heat, are taken from Table TCD of the ASME Boiler and Pressure Vessel Code[1] for material groups K and J, respectively. Since the NCT analysis requires evaluations for ambient temperatures down to -40 °C, the ASME table values are extrapolated to provide data for this temperature condition. The density of Alloy UNS S31803 stainless steel is 7.89 g/cm^3 and the density of the ASTM Type 304L stainless steel is 8.0 g/cm^3, as taken from an on-line database[2].

Instead of modeling the exact geometry of the structure for the CSA sidewall and lid, as illustrated in Figure 1.1-4, effective thermal properties were developed which permit the structures to be simulated as homogeneous solids. The effective thermal properties are based on the properties for Alloy UNS S31803 stainless steel and consist of a set of temperature dependant, anisotropic (i.e., directional dependant) thermal conductivities, a volume weighted density, and temperature dependant specific heat values. See Section 3.5.2.4, *Effective Thermal Properties for Corrugated Wall/Lid Structures*, for a discussion of the methodology used to develop these values. Table 3.2-2 and Table 3.2-3 present the computed effective thermal properties for the prototypic container wall and closure lid structures, respectively.

[1] American Society of Mechanical Engineers (ASME) Boiler and Pressure Vessel Code, Section II, *Materials, Part D – Properties*, Table TCD, 2004 Edition, 2005 and 2006 Addenda, New York, NY.

[2] Matweb, Online Material Data Sheets, www.matweb.com.

In a similar fashion, the box beam structures used at the end of the CSA body and around the perimeter of the closure lid are modeled using effective thermal properties. These effective properties are computed as a fraction of those for an equivalent volume of solid Alloy UNS S31803 stainless to account for the geometry of the structures. Section 3.5.2.5, *Effective Thermal Properties for CSA End Detail & Lid Perimeter*, presents the methodology used to develop these fractional multipliers with the computed values presented in Table 3.2-4.

The thermal properties for the ASTM A320 L43 (AISI 4340) alloy steel, as taken from Table TCD of the ASME Boiler and Pressure Vessel Code[1] for material group D, are presented in Table 3.2-5 as a function of temperature. The ASME table values are extrapolated to provide data for the -40°C temperature condition. A density of 7.86 g/cm^3 is used for the ASTM A320 Type L43 material, per an on-line database[2]. Similarly, the thermal properties for the carbon steel used for the SLB2 waste container and the aluminum used in the roller floor and the payload pallets are also taken from taken from the ASME Boiler and Pressure Vessel Code with their density based on an on-line database[2]. Table 3.2-6 and Table 3.2-7 present the thermal properties for 6061 aluminum and SA-36 carbon steel, respectively.

The thermal properties for the polyurethane foam, balsa, and calcium silicate insulation are assumed to be constant with temperature under NCT conditions. The values assumed for this analysis are presented in Table 3.2-8. Since the polyurethane foam used for the TRUPACT–III package is based on a proprietary formulation, the thermal properties for the four densities of polyurethane foam used are obtained from the manufacturer's on-line website[3]. These proprieties remain essentially constant over the range of temperatures encountered during NCT operations. The performance of the polyurethane foam under HAC conditions is addressed in Section 3.5.4, *'Last-A-Foam' Response under HAC Condition.*

The property values for balsa are based on information from the database for the SCALE computer code[4] which gives a thermal conductivity for balsa wood across its grain as approximately 0.05 W/m-K. Another database[5] gives a maximum ratio of 2.8 for the 'with-grain' versus the 'cross-grain' properties and indicates that the variation in property values may be of up to ±20%. Based on this guidance, the thermal conductivity for balsa obtained from the SCALE database is reduced to 0.0415 W/m-K to account for material variability. This value is conservatively used under NCT for both grain directions. For HAC conditions, where the concern is heat into the package, the SCALE database value of 0.05 W/m-K is multiply by 2.8 (for grain effects) and increased by 20% (for property variability effects), to yield a maximum expected thermal conductivity of 0.168 W/m-K. See Section 3.5.2.6, *Description of Thermal Model for HAC Conditions*, for a more detailed discussion of how the exposed and unexposed sections of balsa wood are modeled under HAC conditions.

[3] Last-A-Foam™ FR3700 On-line Data Sheet, www.generalplastics.com

[4] NuReg/CR-0200, Vol. 3, Rev. 6, SCALE, *A Modular Code System for Performing Standardized Computer Analyses for Licensing Evaluation.*

[5] *Wood Handbook--Wood As An Engineering Material*, General Technical Report #FPL-GTR-113. Madison, WI: U.S. Department of Agriculture, Forest Service, Forest Products Laboratory, 1999.

The calcium silicate insulation data presented in Table 3.2-8 is taken from a prototypic vendor's product sheet[6] for calcium silicate insulation with a nominal density of 0.45 kg/dm^3. The specific heat of the material is based on test data[7] obtained for generically similar materials.

The thermal properties of air are based on curve fits[8] and are presented in Table 3.2-9. Since the debris shield is not directly modeled, the thermal properties for closed-cell silicone foam and polyethylene are not needed. The same is true for the plastic material used on the surface of the guide bars at the closed end of the payload cavity. Instead, the temperatures for these components are assumed to be equal to the maximum of the surrounding structures.

The tested emissivity of as-received Type 304 stainless steel[9] varied from 0.25 to 0.28. Since Type 304 and Alloy UNS S31803 stainless steel are similar in chemical composition, they can be expected to exhibit similar emissivity properties. For the purpose of this evaluation, an emissivity of 0.25 is conservatively used for the emittance from all interior radiating stainless steel surfaces under NCT conditions.

The outer skin of the package will be coated with a white coating, with the coating being optional for the bottom surfaces. While the presence of a white coating[10] could increase the emittance of the outer skin to as high as 0.92 and reduce the solar absorptivity to as low as 0.20, conservative values of 0.8 and 0.52 (i.e., the same as uncoated stainless steel[11]), respectively, are used for these parameters. Besides allowing for flexibility in selecting a coating type, this assumption provides an allowance for degradation of the coating under ultraviolet exposure and for the accumulation of dirt and grime under transport conditions.

Exposure of the coating to the elevated temperatures experienced during the HAC event will blacken the coating and soot may accumulate on the surface. While it is possible that the coating could fail during the fire, thus exposing the underlying stainless steel surface with its associated lower emissivity, such a failure is not a certainty. Therefore, for the purpose of this analysis, an emissivity of 0.90 is used for all exterior surfaces during the regulatory transient fire condition. Further, as a result of oxidation under high temperatures, the inside surface of the outer skin will see an increase in its emittance from the 0.25 value assumed for NCT conditions to a conservatively high value of 0.60[12].

---

[6] Product sheet for Super Firetemp® M, Industrial Insulation Group, Fruita, CO, www.iig-llc.com.

[7] Ohmura, Tsuboi, Onondera, and Tomimura, *Specific Heat Measurements of High Temperature Thermal Insulations by Drop Calorimeter Method*, International Journal of Thermalphysics, Vol. 24, No. 2, March 2003.

[8] Rohsenow, Hartnett, and Choi, *Handbook of Heat Transfer*, 3rd edition, McGraw-Hill Publishers, 1998.

[9] Frank, R. C., and W. L. Plagemann, *Emissivity Testing of Metal Specimens.* Boeing Analytical Engineering coordination sheet No. 2-3623-2-RF-C86-349, August 21, 1986. Testing accomplished in support of the TRUPACT-II design program.

[10] Gilmore, D. G., Editor, Satellite Thermal Control Handbook, The Aerospace Corporation Press, El Segundo, CA, 1994.

[11] Tables 399 and 402, G. G. Gubareff, J. E. Janssen, and R. H. Torborg, *Thermal Radiation Properties Survey*, 2nd Edition, Honeywell Research Center, 1960.

[12] Tables 148 and 149, G. G. Gubareff, J. E. Janssen, and R. H. Torborg, *Thermal Radiation Properties Survey*, 2nd Edition, Honeywell Research Center, 1960.

For the purposes of this evaluation, an emissivity of 0.9[13] is assumed for the balsa surfaces at all temperatures. The same reference indicates that the other non-metallic solids used in the package, such as the polyurethane foam and the calcium silicate insulation, will exhibit a similar emissivity of 0.9 since these materials have a similar color and surface roughness.

The radiation properties of the SLB2 payload container is based on emissivity values of approximately 0.70 for "light-scale" or "rusted" surfaces[9] and values of approximately 0.82 or higher for various paints/coatings[10]. A value of 0.78 provides a conservative lower bound for the normally painted surface.

Table 3.2-10 presents a summary of the emittance and absorptivity data used for the NCT analysis. Specific changes to these values to account for the thermal conditions existing for the hypothetical fire are addressed in Section 3.4.2, *Fire Test Conditions* and Section 3.5.2.6, *Description of Thermal Model for HAC Conditions*.

3.2.2 Technical Specifications of Components

The materials used in the TRUPACT–III that are considered temperature sensitive are the Alloy UNS S31803 stainless steel, the butyl rubber seals, the silicone foam and porous polyethylene used in the debris shield for the CSA, the coating used on the outer skin, the balsa wood, and the rigid polyurethane foam components. The minimum allowable service temperature for all TRUPACT–III components is below the minimum -40°C thermal load condition.

Stainless steel exhibits material property variations within the operating temperature range of the transportation cask. In compliance with the ASME B&PV Code[14], an upper temperature limit of 316 °C (600 °F) has been placed on the use of the Alloy UNS S31803 stainless steel. This temperature point represents the maximum temperature listed for the material in the ASME Code Case N-635-1. Studies[15] have shown that duplex steels, such as Alloy UNS S31803, may experience a transition from ductile to brittle fracture if exposed to temperatures in excess of 300 °C (572 °F) for extended periods of time. The phenomenon consists of two hardening and embrittlement processes that may occur when the material is heated: (a) sigma phase (σ) precipitation in the range of 700 °C to 900 °C and (b) precipitation of a Cr-rich phase (α') in the range of 300 °C to 600 °C. The (α') precipitation leads to a progressive hardening and reduction of the material toughness. This precipitation occurs by spinodal decomposition, a mechanism by which the ferrite phase decomposes into a Cr-rich phase (α') and a Fe-rich phase. Because this reaction occurs more rapidly at 475 °C, this process is also known as "475 °C embrittlement". However this phase separation may also occur after thousands of hours at exposure temperatures as low as 300 °C, after about 11 hours at an exposure temperature of 650 °C, or after approximately 1 hour at an exposure temperature of 725 °C.

The maximum allowable temperature for the ASTM Type 304/304L stainless steel and the ASTM A320 L43 alloy steel used for structural purposes is 427 °C (800 °F)[16]. Both the Alloy

[13] Table 5-2, Kreith, Frank, *Principles of Heat Transfer*, 3rd edition, Harper & Row, 1973.

[14] American Society of Mechanical Engineers (ASME) Boiler & Pressure Vessel Code, Section III, *Code Case N-635-1*.

[15] Weng, K., Chen, T., and Yang, J, *The High-Temperature and Low-Temperature Aging Embrittlement in a 2205 Duplex Stainless Steel*, Bulletin of the College of Engineering, N.T.U., No. 89, October 2003, pp. 45–61.

[16] ASME Boiler & Pressure Vessel Code, Section II, Part D, 2004 Edition, with 2005 and 2006 Addendum.

UNS S31803 and ASTM Type 304/304L stainless steels have a melting point above 1,370 °C. The ASME limits on allowable temperature apply only to conditions where the component's structural properties are required to accommodate the structural loads arising from the respective operating mode or a load combination (such as NCT and HAC drop accidents).

Therefore, based on the above paragraphs, the temperature criteria applied to the various steel components of the package are as follows. A long-term temperature limit of 316 °C is used for the Alloy UNS S31803 stainless steel utilized for the CSA and the closure lid. While a 427 °C long-term temperature limit is applicable for the ASTM Type 304/304L and ASTM A320 L43 steels, a 316 °C long-term temperature limit is conservatively applied instead for consistency with the UNS S31803 limit. The 316 °C limit is also conservatively used for the short-term limit under HAC conditions for all UNS S31803, ASTM Type 304/304L, and A320 L43 steels with the exception of the small region of the CSA structural sheet affected by the puncture bar damage and the outer sheets of the package. For the portion of the CSA structural sheet affected by the puncture bar damage, the allowable short-term limit is based on the time-at-temperature exposure criterion summarized above. This variable temperature versus time criteria is used to assess the potential for incurring a ductile-to-brittle transition (i.e., embrittlement) when the CSA structural steel exceeds the long-term 316 °C temperature limit. A short-term limit of 1,370 °C is applied for the outer sheets of the package.

The outer surface coating has a continuous temperature range of -40 °C to 121 °C, with a maximum intermittent temperature rating of 135 °C[17]. Extended operations above 135 °C can be expected to result in the coating losing its surface adherence and flaking off. In compliance with 10 CFR §71.43(g), the maximum temperature of any accessible outer surface is further limited to 50 °C under NCT conditions when insolation is not present.

The butyl rubber O-rings used for the containment seals have a continuous service temperature range of approximately -54 °C to +107 °C[18]. The material is compatible with higher temperatures if the exposure period to the elevated temperatures is kept correspondingly shorter. Testing performed in support of the certification of the TRUPACT–II package and the Radioisotope Thermoelectric Generator (RTG) Transportation System Packaging[19] demonstrated the material's ability to maintain a leak tight containment boundary under a combination of elevated temperatures, time duration, and minimum seal compression. The testing demonstrated that the butyl rubber compound has a minimum temperature rating of 221 °C for exposure durations of 1 hour or less and 204 °C for exposures of 8 hours or less. For the purposes of this evaluation, the Butyl rubber O-rings are assumed to have an upper temperature limit of 204 °C for exposures of 8 hours or less, a maximum continuous rating of 107 °C, and a lower temperature limit of -54 °C. See Section 2.12.2, *Elastomer O-ring Seal Performance Tests*, for a further discussion of the thermal performance of Butyl rubber O-ring seals.

---

[17] Based on typical epoxy based coating performance based on the Tnemec line of epoxy coatings, Tnemec Company Inc. Kansas City, MO 64120-1323, www.tnemec.com.

[18] Parker O-Ring Handbook, ORD 5700/USA, 2007, www.parker.com.

[19] DOE Docket No. 94-6-9904, *Radioisotope Thermoelectric Generator Transportation System Safety Analysis Report for Packaging*, WHC-SD-RTG-SARP-001, prepared for the U.S. Department of Energy Office of Nuclear Energy under Contract No. DE-AC06-87RL10930 by Westinghouse Hanford Company, Richland, WA.

The silicone foam used in the debris shield assembly for the CSA has a recommended service temperature range of -50 to 200°C[20]. Under intermittent use, the allowable temperature range increases to -75 to 260°C. The porous polyethylene used to prevent a pressure gradient and allow the flow of helium across the debris shield during leak testing has a recommended service temperature range similar to HDPE (high density polyethylene), or -60 to 120 °C[2]. The melting point for HDPE is 135 °C[2]. Since the function of the debris shield is required only for the NCT and pre-fire HAC conditions, the appropriate temperature limit for the debris shield is -60 to 120 °C to protect the porous polyethylene. The same temperature limit applies to the plastic material on the guide bars. No temperature limit exists for the HAC fire condition as the debris shield and the plastic material on the guide bars may fail under this condition with no consequence for the safety of the packaging.

The calcium silicate insulation has a recommended maximum service temperature of 982 °C[6]. There is no minimum recommended service temperature.

Wood will degrade under elevated temperature, with the severity of the degradation depending on the temperature level achieved, the length of exposure, and the availability of oxygen[5]. While permanent reduction in strength can occur for prolonged exposure to temperatures >65 °C, significant thermal degradation occurs at temperatures >100 °C when the chemical bonds begin to break. As the temperature increases, the level and rate of decomposition also increases until at a temperature of approximately 450 °C the decomposition process forms volatile and flammable gases which can ignite and begin a self-sustaining process if sufficient oxygen is present. For the purposes of this evaluation, the maximum allowable temperature for the balsa wood under NCT conditions is assumed to be 100 °C for peak temperatures based on the onset of chemical decomposition and 65 °C for average temperatures based upon loss of strength considerations. No short-term temperature limit is applied to the balsa wood since the material is not required to survive the HAC fire event.

Section 3.5.4, *'Last-A-Foam' Response under HAC Condition*, describes the behavior of the rigid polyurethane foam as a function of temperature. Based on this information, an NCT temperature limit of approximately 260 °C is used to avoid non-reversible changes in the thermal properties. No temperature limit exists under HAC conditions since the thermal decomposition of the foam material plays a significant role in the level of thermal protection the material provides to underlying foam material and components. A design limit of 65 °C for the bulk average foam temperature under NCT conditions is imposed for this evaluation to establish a lower bound on the foam's structural properties which decrease with increased temperature level.

The maximum payload temperature is assumed to be 230 °C based on the commonly accepted auto-ignition temperature for paper.

[20] Product Cut Sheet, SS30 Expanded, Closed-Cell Silicone Sponge / Foam, Innovation in Polymer Technology, 41 Industrial Drive, Exeter, NH, 03833, www.ipotec.com.

Table 3.2-1 – Thermal Properties of Stainless Steels

Material	Temperature (°C)	Density (kg/dm^3)	Thermal Conductivity W/m-K	Specific Heat (J/g-K)
Alloy UNS S31803 Stainless Steel ①	-40	7.89	13.56	0.492
	21.1		14.19	0.502
	37.8		14.37	0.504
	93.3		15.23	0.516
	148.9		16.10	0.527
	204.4		16.96	0.538
	260.0		17.65	0.542
	315.6		18.52	0.551
	371.1		19.38	0.560
	426.7		20.08	0.564
	537.8		21.63	0.578
	648.9		23.19	0.587
	760.0		24.75	0.602
	815.6		25.44	0.604
ASTM Type 304/304L Stainless Steel ②	-40.0	8.00	14.25	0.469
	21.1		14.88	0.478
	37.8		15.06	0.480
	93.3		16.10	0.500
	148.9		16.96	0.514
	204.4		18.00	0.528
	260.0		18.87	0.538
	315.6		19.56	0.545
	371.1		20.42	0.553
	426.7		21.11	0.556
	537.8		22.85	0.570
	648.9		24.23	0.578
	760.0		25.79	0.589
	815.6		26.48	0.594

Notes:

① Data based on ASME Boiler and Pressure Vessel Code, Section II, *Materials*, *Part D – Properties*, Table TCD, Material Group K, 2004 Edition, 2005 and 2006 Addenda, New York.

② Data based on ASME Boiler and Pressure Vessel Code, Section II, *Materials*, *Part D – Properties*, Table TCD, Material Group J, 2004 Edition, 2005 and 2006 Addenda, New York.

Table 3.2-2 – Effective Thermal Properties for Corrugated Wall Structure

Temperature (°C)	Density (kg/dm^3)	Thermal Conductivity, (W/m-K)			Specific Heat (J/g-K)
		'Thru Wall'①	'Along Wall'①	'Axial'①	
-40	1.33	0.62	2.28	1.55	0.492
21.1		0.70	2.41	1.62	0.502
93.3		0.84	2.56	1.74	0.516
204.4		1.16	2.85	1.94	0.538
315.6		1.60	3.11	2.12	0.551
426.7		2.20	3.37	2.29	0.564
537.8		2.97	3.63	2.47	0.578
648.9		3.92	3.90	2.65	0.587
760.0		5.08	4.16	2.83	0.602

Note: ① For horizontal walls of the CSA, the 'Thru Wall' conductivity is aligned with y-axis of model, 'Along Wall' is aligned with x-axis of the model, and 'Axial' is aligned with the z-axis of model. For vertical walls of the CSA, the 'Thru Wall' conductivity is aligned with x-axis of model, 'Along Wall' is aligned with y-axis of the model, and 'Axial' is aligned with the z-axis of model.
② See Appendix 3.5.2.4, *Effective Thermal Properties for Corrugated Wall/Lid Structures*, for the development of the effective thermal properties.

Table 3.2-3 – Effective Thermal Properties for Corrugated Lid Structure

Temperature (°C)	Density (kg/dm^3)	Thermal Conductivity, (W/m-°K)			Specific Heat (J/g-K)
		'Thru Wall'①	'Along Wall'①	'Axial'①	
-40	1.69	0.65	2.91	2.20	0.492
21.1		0.74	3.04	2.30	0.502
93.3		0.89	3.26	2.47	0.516
204.4		1.23	3.64	2.75	0.538
315.6		1.71	3.97	3.00	0.551
426.7		2.35	4.30	3.26	0.564

Note: ① For horizontal walls of the CSA, the 'Thru Wall' conductivity is aligned with y-axis of model, 'Along Wall' is aligned with x-axis of the model.
② See Appendix 3.5.2.4, *Effective Thermal Properties for Corrugated Wall/Lid Structures*, for the development of the effective thermal properties.

Table 3.2-4 – Effective Thermal Properties for CSA End & Lid Perimeter Structures

Structure	Density Multiplier ①	Thermal Conductivity Multiplier ①			Specific Heat Multiplier ①
		'Axial' ②	'Transverse' ②	'Along' ②	
CSA End	0.455	0.318	0.200	0.321	1.0
Lid Perimeter	0.495	0.308	0.270	0.368	1.0

Note: ① The table values represent multiplier factors to be applied against the thermal property values presented in Table 3.2-1 to yield the appropriate temperature dependant properties for the subject structure. See Section 3.5.2.5, *Effective Thermal Properties for CSA End Detail & Lid Perimeter*, for development of the table values.
② The 'Axial' value is for heat transfer aligned with the z-axis of the model. The 'Transverse' value is for heat transfer perpendicular to the face of the structures (i.e., from inside to outside). The 'Along' value is for heat transfer around the perimeters of the structures.

Table 3.2-5 – Properties of Type A320 L43 Bolt Material

Temperature (°C)	Density (kg/dm^3)	Thermal Conductivity W/m-K	Specific Heat (J/g-K)
-40.0	7.86	35.54	0.401
21.1		36.17	0.437
37.8		36.35	0.447
93.3		36.86	0.473
148.9		37.21	0.494
204.4		37.21	0.514
260.0		37.04	0.534
315.6		36.52	0.556
371.1		35.83	0.581
426.7		34.96	0.607
537.8		33.06	0.673
648.9		31.15	0.800
760.0		27.00	1.823
815.6		26.48	0.663

Note: Data based on ASME Boiler and Pressure Vessel Code, Section II, *Materials, Part D – Properties*, Table TCD, Material Group D, 2004 Edition, 2005 and 2006 Addenda, New York

Table 3.2-6 – Properties of Type 6061 Aluminum

Temperature (°C)	Density (kg/dm^3)	Thermal Conductivity (W/m-K)	Specific Heat (J/g-K)
-40	2.70	161.3	0.866
21.1		166.3	0.893
37.8		167.7	0.901
65.6		169.6	0.914
93.3		171.3	0.924
121.1		172.7	0.935
148.9		174.1	0.946
176.7		175.3	0.956
204.4		176.4	0.962

Note: Data based on ASME Boiler and Pressure Vessel Code, Section II, *Materials, Part D – Properties*, Table TCD, 2004 Edition, 2005 and 2006 Addenda, New York.

Table 3.2-7 – Properties of ASTM SA-36 Carbon Steel

Temperature (°C)	Density (kg/dm^3)	Thermal Conductivity (W/m-K)	Specific Heat (J/g-K)
-40	7.86	45.35	0.390
21.1		47.25	0.439
37.8		47.77	0.453
93.3		48.11	0.487
148.9		47.25	0.512
204.4		45.86	0.531
260.0		44.48	0.550
315.6		43.10	0.570
371.1		41.71	0.594

Note: American Society of Mechanical Engineers (ASME) Boiler and Pressure Vessel Code, Section II, *Materials*, *Part D – Properties*, Table TCD, Material Group B, 2004 Edition, 2005 and 2006 Addenda, New York.

Table 3.2-8 – Thermal Properties of Non-Metallic Materials

Material	Temperature (°C)	Density (kg/dm^3)	Thermal Conductivity W/m-K	Specific Heat (J/g-K)	Comments
Polyurethane Foam	-	0.48	0.068	1.477	NCT properties
	-	0.29	0.046	1.477	"
	-	0.16	0.031	1.477	"
	-	0.10	0.029	1.477	"
Balsa	-	0.12	0.0415	1.8	NCT properties
	-	0.12	0.168	1.8	HAC properties
Calcium Silicate Insulation	20	0.45	0.083	0.95	Values for 20 and 500°C extrapolated from the available data
	93		0.088		
	204		0.095		
	316		0.105		
	427		0.115		
	500		0.121		

Table 3.2-9 – Thermal Properties of Air

Temperature (°C)	Thermal Conductivity① (W/m-°C)	Specific Heat① (J/g-K)	Dynamic Viscosity① (N-s/m^2 × 10^6)	Density (kg/dm^3)	Prandtl Number①	Coef. of Thermal Exp. (1/K)
-40	0.0209	1.0042	15.1836	Use Ideal Gas Law with Molecular wt = 28.966 g/mole	Compute as $Pr = c_p\mu/k$	Compute as β = 1/(°C+273.15)
-18	0.0227	1.0045	16.3407			
10	0.0248	1.0055	17.240			
38	0.0269	1.0071	19.0445			
93	0.0308	1.0121	21.5246			
149	0.0345	1.0191	23.8271			
204	0.0381	1.0278	25.9852			
260	0.0415	1.0378	28.0186			
316	0.0449	1.0488	29.9337			
371	0.0482	1.0606	31.7442			
427	0.0514	1.0730	33.4732			
482	0.0545	1.0857	35.1352			
538	0.0576	1.0986	36.7350			
649	0.0634	1.1242	39.7662			
760	0.0688	1.1487	42.6006			
816	0.0713	1.1603	43.9535			

Table 3.2-10 – Thermal Radiative Properties for NCT

Material	Assumed Conditions	Assumed Emissivity (ε)	Absorptivity (α)
Containment & Structural Sheets (UNS S31803 Stainless Steel) ①	Slightly oxidized, < 121 °C	0.25	---
Outer Sheet, Exterior Surface (Coated UNS S31803 Stainless Steel) ②	White coating	0.8	0.52
Outer Sheet, Interior Surface (UNS S31803 Stainless Steel) ①	Slightly oxidized, < 121 °C	0.25	---
Balsa Wood ③	Untreated	0.90	---
Polyurethane Foam & Calcium Silicate Insulation ③	---	0.90	---
SLB2 ④	Painted carbon steel	0.78	---
Bounding Waste Box ③	Wood or paper	0.90	---
Ambient Environment	---	1.00	N/A

Notes:

① Testing[9] indicates values of 0.25 to 0.28 for "as-received" stainless steel. An emissivity value of 0.25 represents a conservative lower-bound value for the unfinished stainless steel surfaces, leading to conservatively higher temperatures for NCT.

② Based on conservative estimate for emissivity and absorptivity. See Section 3.2.1, *Material Properties*, for more discussion.

③ The emissivity of 0.90 is a representative value for wood and most non-metallic solids (e.g., polyurethane foam & calcium silicate insulation)[13].

④ Emissivity values of approximately 0.70 for "light-scale" or "rusted" surfaces[9] and values of approximately 0.82 or higher for various paints/coatings[10]. A value of 0.78 provides a conservative lower bound for the normally painted surface.

3.3 Thermal Evaluation for Normal Conditions of Transport

This section presents the thermal analysis methodology and the evaluation results for the thermal performance of the TRUPACT–III package under NCT conditions to demonstrate compliance with the requirements of 10 CFR §71.43(g) and §71.71. The thermal evaluations are performed for the recommended design basis NCT cases[1] using conservative analytical techniques to assure that all materials are maintained within their applicable minimum and maximum allowable temperature during all modes of operation.

The analytical thermal model of the TRUPACT–III is developed for use with the Thermal Desktop® [2] and SINDA/FLUINT[3] computer programs. The SINDA/FLUINT and Thermal Desktop® computer programs have been validated for safety basis calculations for nuclear related projects[4,5]. Together, the Thermal Desktop® and SINDA/FLUINT codes provide the capability to simulate steady-state and transient temperatures using temperature dependent material properties and heat transfer via conduction, convection, and radiation. Complex algorithms may be programmed into the solution process for the purposes of computing heat transfer coefficients as a function of the local geometry, gas thermal properties as a function of temperature, and pressure.

The thermal model of the TRUPACT–III package defines a quarter symmetry model of the package's closure end (i.e., symmetrical about the package axial axis and 180° symmetry about the package vertical axis). This modeling choice captures the thermally sensitive seal region at the package closure lid and allows the incorporation of varying insolation loads that will occur at the top, sides, and ends of the package and the adiabatic conditions assumed to exist over the bottom surface of the package. The modeling assumes that the TRUPACT–III operations are conducted with the package in its normal, horizontal orientation. Appendix 3.5.2, *Thermal Model Details*, provides details of the thermal model used for the NCT evaluation.

3.3.1 Heat and Cold

3.3.1.1 Maximum NCT Temperatures

The thermal evaluation of the TRUPACT–III package with the SLB2 payload for the NCT Hot condition assumes a constant ambient air temperature of 38°C and regulatory insolation that follows a sine curve distribution. Given the relatively low thermal mass of the package exterior, the analysis is conducted as a transient simulation to properly account for the diurnal solar loading on the thermal response of the package. Figure 3.3-1 illustrates the expected warm up transient for

[1] Regulatory Guide 7.8, *Load Combinations for the Structural Analysis of Shipping Casks for Radioactive Material*, Revision 1, U. S. Nuclear Regulatory Commission, March 1989.

[2] Thermal Desktop®, Versions 4.8/5.1, Cullimore & Ring Technologies, Inc., Littleton, CO, 2005/2008.

[3] SINDA/FLUINT, Systems Improved Numerical Differencing Analyzer and Fluid Integrator, Versions 4.8/5.1, Cullimore & Ring Technologies, Inc., Littleton, CO, 2005/2008.

[4] Software Validation Test Report for Thermal Desktop® and SINDA/FLUINT, Version 4.8, Packaging Technology, Inc., File No. TR-VV-05-001, Rev. 1.

[5] AFS-TR-VV-006, Rev. 0, Thermal Desktop and SINDA/FLUINT Testing and Acceptance Report, V5.1, Windows XP, AREVA Federal Services LLC, September 2008.

the TRUPACT–III package loaded with a single SLB2 container dissipating 80 watts of decay heat. The package and payload are assumed to begin the transient at a uniform temperature of 20°C at the time of loading. The transient is conducted for a period of 18 days with the resulting temperatures plotted for every 6 hours until the last 48 hours when the output interval is decreased to every 1/2-hour to more accurately define the diurnal temperature response.

As seen from the figure, the maximum container skin temperature reaches a repeatable cycle within the first 2 or 3 days of the transient, while the internal package components (see the curves for the CSA containment sheet and the SLB2 shell) require in excess of 10 days to achieve the majority of their temperature rise and over 15 days to attain their maximum temperatures. Further, while an approximate 35°C swing in the exterior skin temperature will occur over each 24 hour period, the temperatures within the CSA will be essentially constant due to the insulating nature of the overpack. The relatively high temperature seen for the bounding waste box is due to the assumption that the thermal conductivity within the waste box and the SLB2 container is equal to that of air with no convection. As such, large thermal gradients are required to dissipate even low power levels.

Figure 3.3-2 illustrates the associated thermal response for the foam and balsa wood components of the package during the same time frame and for the closure and vent port/sampling seals. The temperature response is similar in that in excess of 10 days is required for the majority of the temperature increase to be attained and over 15 days are required to reach the maximum temperature levels.

A summary of the temperature results for this evaluation, plus those achieved for decay heat loads of 40 and 20 watts are presented in Table 3.3-1. As seen from the table, the level of payload decay heat loading has only a slight effect on the peak package temperatures. Instead, the package temperature levels achieved are driven primarily by the ambient conditions. The peak temperatures achieved for all of the components are significantly below the allowable temperature limits. The O-rings used on the containment boundaries remain well within the allowable temperature limits under NCT conditions. The same is true for the temperature sensitive components of the debris shield assembly. It should be noted that, since the debris shield assembly is not explicitly represented by the thermal model, its temperature is assumed to be the same as the containment O-ring due to their proximity.

The evaluation strategy of centering of the hypothetical waste box within the CSA was chosen to yield the maximum payload temperature and, thus, the highest level of CSA pressurization for a given decay heat loading. While positioning the hypothetical waste box against the forward wall of the SLB2 container could yield a higher containment seal temperature, the effect would be minor. First, even if the SLB2 container were slid against the CSA lid, direct contact between the SLB2 container (and the hypothetical waste box within it) and the lid would be highly limited by the 'bumpers' on the SLB2 container. These 38 mm square, thin walled, hollow tubes around the sides and ends of the SLB2 container (see Figure 3.1-5) will effectively maintain a 38 mm wide air gap between the SLB2 container and the lid. Second, the maximum SLB2 container sidewall temperature noted in Table 3.3-1 is 62.3 °C. This maximum temperature occurs where the hypothetical waste box is touching the SLB2 container wall and, as such, represents the maximum temperature the CSA lid could reach under the extreme scenario where the hypothetical waste box is located against the forward SLB2 container wall, the SLB2 container is slid against the CSA lid, and the thermal resistance of the thin walled, hollow tube bumpers is ignored. Further, contact with the CSA lid will act to lower the temperature level within both the SLB2 container and the

waste box such that the actual peak lid temperature would be between 62.3 °C and the 52.6 °C reported in Table 3.1-1 for the containment seal. In any case, the maximum seal temperature would still remain well below its established 107 °C temperature limit for NCT conditions.

To assess the effect of assuming no air gaps between the component interfaces, the various air gap conductors within the NCT thermal model were converted to direct contact conductors and the NCT evaluation for the 80 W decay heat payload repeated. As expected, the elimination of the thermal resistance associated with the air gaps resulted in the peak component temperatures decreasing. However, the level of decrease noted is less than 1 °C indicating that the size of the air gap is not thermally significant for this package due to a combination of its low decay heat loading, the surface area of the package for dissipating the heat through, and the metallic heat transfer path between the CSA and outer sheet provided by the corner ribs.

Figure 3.3-3 and Figure 3.3-4 present perspective views of the temperature distribution within the packaging and within the packaging and payload, respectively, for the 80 watt decay heat case at approximately mid-day during the diurnal cycle. The temperature distribution illustrates the heating due to a combination of decay heat and insolation on the external surfaces. As seen, the peak package temperature occurs at the outer skin due to the solar heating of the horizontal, flat surfaces. Those portions of the package that have a vertical orientation or are shaded exhibit temperatures that are 30 to 40°C cooler. The temperature variation across the face of the closure end impact structure is due to the variation of solar loading on each of the surfaces because of the orientation and the self-shading by portions of the structure. The presence of the puncture resistant sheets and the joint between the overpack cover and the package overpack structure can be seen in the temperature distribution illustrated in Figure 3.3-3. The temperature distribution illustrated in Figure 3.3-4 demonstrates that the principal thermal gradient within the packaging occurs between the center of the payload and the CSA containment sheet. As stated before, this relatively large thermal gradient occurs because of the assumption that the thermal conductivity within the CSA cavity is equal to that of still air.

The evaluation of the package's thermal performance for the NCT Hot condition without insolation is conducted to confirm the package design complies with the requirements of 10 CFR §71.43(g)[6]. As seen from the summary of component temperatures presented in Table 3.3-2, the maximum temperature of all accessible surfaces are below the allowable limit of 50°C for non-exclusive packages.

3.3.1.2 Minimum NCT Temperatures

The minimum temperature distribution for the packaging occurs with a zero decay heat load and an ambient air temperature of -40 °C per 10 CFR §71.71(c)(2). The steady-state analysis of this condition requires no thermal calculations to be performed. Instead, it is assumed that all package components achieve the -40 °C temperature under steady-state conditions. As discussed in Section 3.2.2, *Technical Specifications of Components*, the -40 °C temperature is within the allowable range of all components.

As a potential initial condition for all normal or accident events, a minimum uniform temperature of -29 °C and no insolation must be considered per 10 CFR §71.71(b) and §71.73(b). Table 3.3-3

[6] Title 10, Code of Federal Regulations, Part 71 (10 CFR 71), *Packaging and Transportation of Radioactive Materials*, United States Nuclear Regulatory Commission (USNRC), 01–01–09 Edition.

presents a summary of the resulting temperatures with 80, 40, and 20 watt payload decay heat loads and the evaluated SLB2 payload configuration. All component temperatures are within the allowable temperature limits.

3.3.2 Maximum Normal Operating Pressure

The maximum normal operation pressure (MNOP) developed during the maximum shipping period is limited to 172 kPa gauge by design. The pressure developed will be a function of the initial quantity of air filling the TRUPACT–III cavity, the quantity of gas generated by the waste stream in the payload containers, the thermal expansion of the gases under operating conditions, and the amount of water vapor that may exist within the package. The chemical, biological, and thermal mechanisms of gas generation within the payload are insignificant with radiolysis being the primary mechanism for potential flammable gas generation in TRU wastes[7].

The TRUPACT–III TRAMPAC[7] describes the basis for computing the maximum amount of gas that can be generated from any source within the payload based on the contribution of each component contributing to the total pressure in the package. The relatively low temperature attained within the CSA indicates that outgassing will not occur from either the silicone foam or porous polyethylene used in the debris shield nor will it occur from the plastic material used on the CSA's guide bars

[7] U.S. Department of Energy (DOE), *TRUPACT–III TRU Waste Authorized Methods for Payload Control (TRUPACT–III TRAMPAC)*, U.S. Department of Energy, Carlsbad Field Office, Carlsbad, New Mexico.

Table 3.3-1 – NCT Hot Temperatures w/ SLB2 Payload

Location / Component	Temperatures (°C)[1]			
	80 Watts [2]	40 Watts [2]	20 Watts [2]	Maximum Allowable [3]
Bounding Waste Box Payload				
- Maximum	162.2	108.5	79.2	230
- Bulk Avg.	90.4	69.8	59.0	230
Standard Large Box (SLB2) Payload				
- Maximum sidewall	62.3	54.5	51.8	230
- Minimum sidewall (coincident) [4]	52.9	50.0	48.5	230
- Avg. sidewall	54.9	51.5	49.8	230
- Bulk Avg. (of void only)	55.4	51.9	50.1	230
- Bulk Avg. (of total volume) [5]	63.0	55.8	52.0	230
Containment O-ring Seal	52.6	51.4	50.9	107
Sampling/Vent Port O-ring Seal	51.2	49.1	48.0	107
Debris Shield	52.6	51.4	50.9	120
CaSi (Seal Protection) Insulation	60.9	60.3	59.9	982
CSA Structural Sheet [6]	57.6	56.5	55.9	316
CSA Containment Sheet				
- Maximum	55.6	53.3	52.6	316
- Minimum (coincident) [4]	50.4	48.5	47.3	316
CSA Lid				
- Maximum	56.1	54.8	54.1	316
- Lid Bolt Maximum	53.4	52.4	51.9	316
Outer Skin				
- Package Body, Peak	86.6	86.5	86.5	121
- Package Cheek, Peak	77.8	77.8	77.7	121
- Package Cover, Peak	84.2	84.2	84.2	121
Last-a-Foam				
- Package Body, Peak/Avg.	67.3 / 51.9	66.6 / 50.3	66.2 / 49.4	260 / 65
- Package Corner, Peak/Avg.	82.4 / 52.3	82.3 / 51.1	82.3 / 50.5	260 / 65
- Package Cheek, Peak/Avg.	77.3 / 49.7	77.2 / 49.4	77.2 / 49.3	260 / 65
- Overpack Cover Outer Area, Peak/Avg.	83.6 / 52.4	83.6 / 51.8	83.6 / 51.5	260 / 65
- Overpack Cover Recess Area, Peak/Avg.	58.6 / 50.5	58.0 / 49.4	57.7 / 48.8	260 / 65
Balsa				
- Package Body, Peak/Avg.	86.2 / 55.3	86.1 / 54.5	86.1 / 54.2	100 / 65
- Overpack Cover, Peak/Avg.	66.9 / 51.3	66.6 / 51.0	66.5 / 50.9	100 / 65

Notes:

1) Peak temperatures determined assuming one SLB2, diurnal cycle for insolation, and a constant ambient temperature of 38 °C.
2) For conservatism, the decay heat is confined to a bounding minimum sub-volume within the SLB2. This sub-volume represents 23% of the total available volume. The remaining SLB2 volume is assumed to have zero decay heat and the thermal properties of air.
3) Maximum allowable temperatures are established in Section 3.2.2, *Technical Specifications of Components*.
4) The listed minimum temperature is taken at the same time point (i.e., 'coincident') as the listed maximum temperature as opposed to the actual minimum temperature occurring during the diurnal cycle.
5) Bulk average temperature computed assuming SLB2 internal volume of 7,394 liters and a bounding waste box volume of 1,609 liters.
6) The peak CSA structural sheet temperature occurs at joint with overpack cover where enclosing sheet metal and corner ribs form thermal bridges to outer skin. Generally, the CSA structural sheet temperature is within 1°C of containment sheet temperature.

Table 3.3-2 – NCT Hot, No Solar Temperatures w/ SLB2 Payload

Location / Component	Temperatures (°C)[1]			
	80 Watts [2]	40 Watts [2]	20 Watts [2]	Maximum Allowable [3]
Bounding Waste Box Payload				
- Maximum	155.1	100.3	70.2	230
- Bulk Avg.	81.9	60.8	49.6	230
Standard Large Box (SLB2) Payload				
- Maximum sidewall	54.6	46.5	42.2	230
- Minimum sidewall	42.0	39.9	38.9	230
- Avg. sidewall	45.0	41.5	39.6	230
- Bulk Avg. (of void only)	45.3	41.6	39.7	230
- Bulk Avg. (of total volume) [4]	53.3	45.8	41.9	230
Containment O-ring Seal	42.6	40.2	39.0	107
Sampling/Vent Port O-ring Seal	42.2	40.0	38.9	107
Debris Shield	42.6	40.2	39.0	120
CaSi (Seal Protection) Insulation	42.0	39.9	38.8	982
CSA Structural Sheet [5]	44.2	41.0	39.4	316
CSA Containment Sheet				
- Maximum	44.7	41.3	39.5	316
- Minimum	40.3	39.1	38.4	316
CSA Lid				
- Maximum	43.6	40.7	39.2	316
- Lid Bolt Maximum	42.8	40.3	39.1	316
Outer Skin				
- Package Body, Peak	41.9	39.8	38.8	50
- Package Cheek, Peak	41.5	39.7	38.7	50
- Package Cover, Peak	42.2	40.0	38.9	50
Last-a-Foam				
- Package Body, Peak/Avg.	44.2 / 41.2	41.0 / 39.5	39.4 / 38.6	260 / 65
- Package Corner, Peak/Avg.	43.4 / 40.4	40.6 / 39.1	39.2 / 38.4	260 / 65
- Package Cheek, Peak/Avg.	40.6 / 38.4	39.2 / 38.1	38.5 / 37.9	260 / 65
- Overpack Cover Outer Area, Peak/Avg.	41.4 / 39.0	39.6 / 38.4	38.7 / 38.1	260 / 65
- Overpack Cover Recess Area, Peak/Avg.	42.2 / 40.1	40.0 / 39.0	38.9 / 38.4	260 / 65
Balsa				
- Package Body, Peak/Avg.	42.3 / 39.4	40.0 / 38.6	38.9 / 38.2	100 / 65
- Overpack Cover, Peak/Avg.	39.2 / 38.5	38.5 / 38.1	38.1 / 38.0	100 / 65

Notes:

1) Peak temperatures determined assuming one SLB2, diurnal cycle for insolation, and a constant ambient temperature of 38 °C.
2) For conservatism, the decay heat is confined to a volume within the SLB2 defined by the bounding waste box form (i.e., 965mm × 965mm × 1,727mm). This bounding volume is assumed to be centered within the SLB2 in the lateral and axial directions and to be resting against the bottom of the SLB2. The remaining volume of the SLB2 is assumed to have zero watts of decay heat and the thermal properties of air.
3) Maximum allowable temperatures are established in Section 3.2.2, *Technical Specifications of Components*. Maximum outer skin temperature limited to 50 °C in compliance with the requirements of §71.43(g).
4) Bulk average temperature computed assuming SLB2 internal volume of 7,394 liters and a bounding waste box volume of 1,609 liters.
5) The peak CSA structural sheet temperature occurs at joint with overpack cover where enclosing sheet metal and corner ribs form thermal bridges to outer skin. Generally, the CSA structural sheet temperature is within 1°C of containment sheet temperature.

Table 3.3-3 – NCT Cold Temperatures w/ SLB2 Payload

Location / Component	Temperatures (°C)[1]			
	80 Watts [2]	40 Watts [2]	20 Watts [2]	Minimum Allowable [3]
Bounding Waste Box Payload				
- Maximum	108.7	46.4	10.9	<-40
- Bulk Avg.	25.7	0.2	-13.8	<-40
Standard Large Box (SLB2) Payload				
- Maximum sidewall	-3.9	-15.7	-22.2	<-40
- Minimum sidewall	-23.2	-26.0	-27.5	<-40
- Avg. sidewall	-19.3	-24.0	-26.5	<-40
- Bulk Avg. (of void only)	-18.7	-23.7	-26.3	<-40
- Bulk Avg. (of total volume) [4]	-9.0	-18.5	-23.6	<-40
Containment O-ring Seal	-23.5	-26.2	-27.6	<-40
Sampling/Vent Port O-ring Seal	-23.9	-26.4	-27.7	<-40
Debris Shield	-23.5	-26.2	-27.6	<-40
CaSi (Seal Protection) Insulation	-24.3	-26.6	-27.8	<-40
CSA Structural Sheet [5]	-21.8	-25.4	-27.2	<-40
CSA Containment Sheet				
- Maximum	-21.4	-25.2	-27.1	<-40
- Minimum	-26.1	-27.5	-28.2	<-40
CSA Lid				
- Maximum	-22.4	-25.7	-27.3	<-40
- Lid Bolt Maximum	-23.3	-26.1	-27.6	<-40
Outer Skin				
- Package Body, Peak	-24.1	-26.5	-27.7	<-40
- Package Cheek, Peak	-24.7	-26.8	-27.9	<-40
- Package Cover, Peak	-24.0	-26.5	-27.7	<-40
Last-a-Foam				
- Package Body, Peak/Avg.	-21.8 /-25.1	-25.4 /-27.0	-27.2 /-28.0	<-40
- Package Corner, Peak/Avg.	-22.7 /-26.0	-25.8 /-27.5	-27.4 /-28.2	<-40
- Package Cheek, Peak/Avg.	-25.8 /-28.2	-27.4 /-28.6	-28.2 /-28.8	<-40
- Overpack Cover Outer Area, Peak/Avg.	-24.9 /-27.5	-26.9 /-28.2	-28.0 /-28.6	<-40
- Overpack Cover Recess Area, Peak/Avg.	-24.0 /-26.3	-26.5 /-27.6	-27.7 /-28.3	<-40
Balsa				
- Package Body, Peak/Avg.	-23.7 /-27.0	-26.3 /-28.0	-27.7 /-28.5	<-40
- Overpack Cover, Peak/Avg.	-27.3 /-28.1	-28.1 /-28.5	-28.6 /-28.8	<-40

Notes:

1) Peak temperatures determined assuming one SLB2, no insolation, and a constant ambient temperature of -29 °C. Minimum temperature of all components is ≥ -29 °C.
2) For conservatism, the decay heat is confined to a volume within the SLB2 defined by the bounding waste box form (i.e., 965mm × 965mm × 1,727mm). This bounding volume is assumed to be centered within the SLB2 in the lateral and axial directions and to be resting against the bottom of the SLB2. The remaining volume of the SLB2 is assumed to have zero watts of decay heat and the thermal properties of air.
3) Minimum allowable temperatures are established in Section 3.2.2, *Technical Specifications of Components*.
4) Bulk average temperature computed assuming SLB2 internal volume of 7,394 liters and a bounding waste box volume of 1,609 liters.
5) The peak CSA structural sheet temperature occurs at joint with overpack cover where enclosing sheet metal and corner ribs form thermal bridges to outer skin. Generally, the CSA structural sheet temperature is within 1°C of containment sheet temperature.

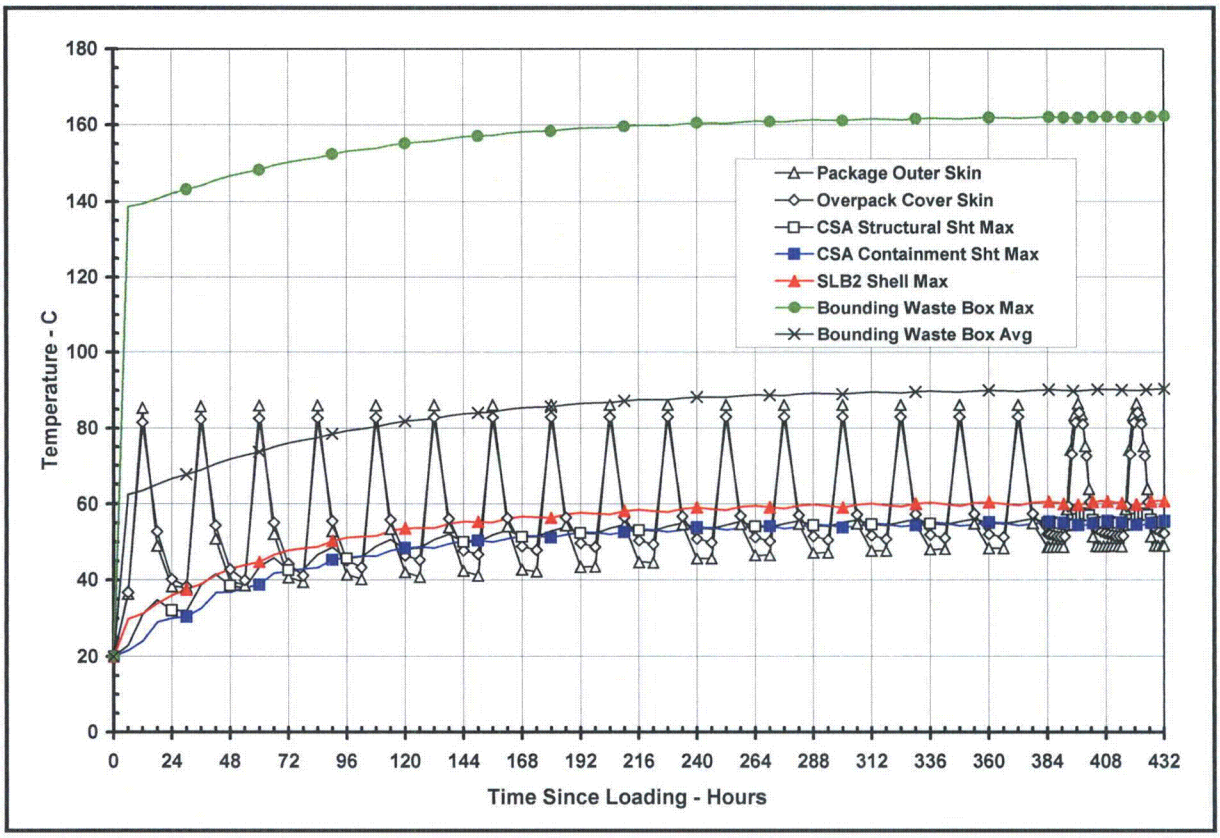

Figure 3.3-1 – Transient Package Thermal Response with 80 Watt SLB2 Payload

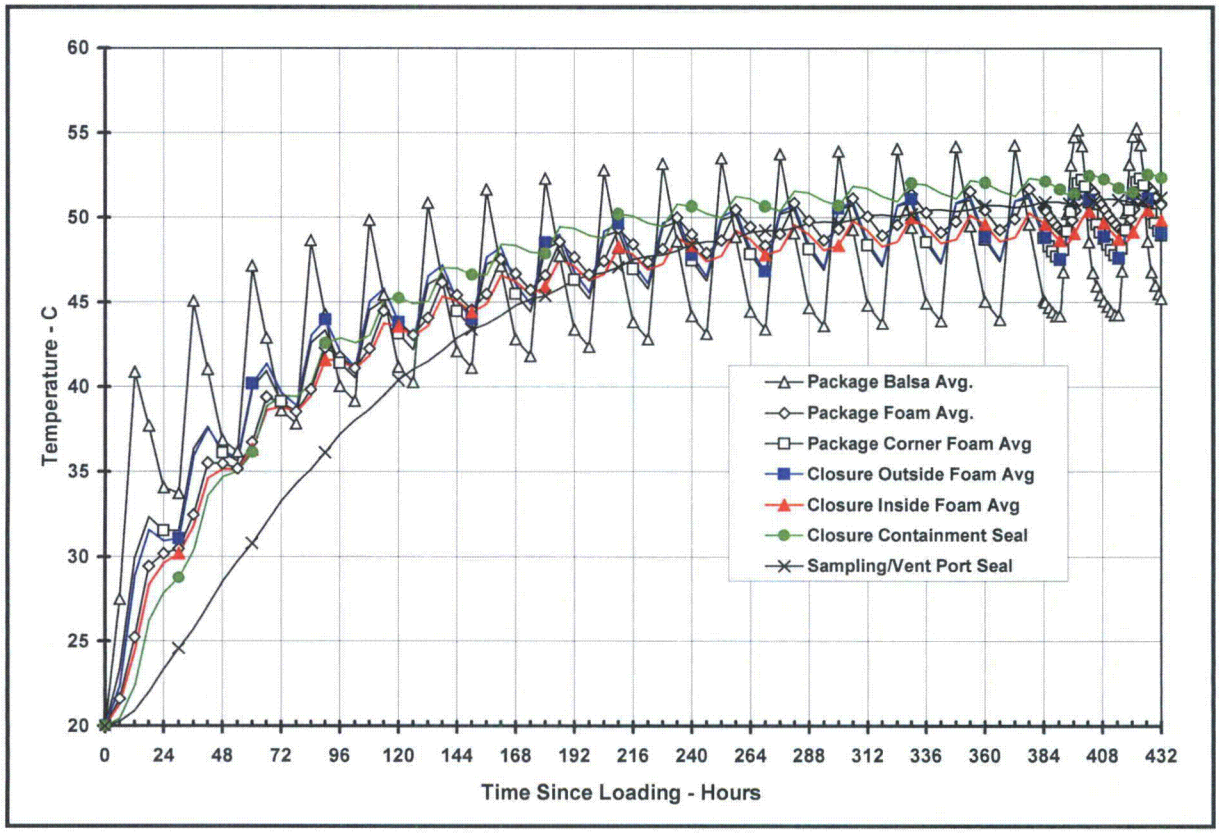

Figure 3.3-2 – Transient Foam, Balsa, and Seal Thermal Response with 80 Watt SLB2 Payload

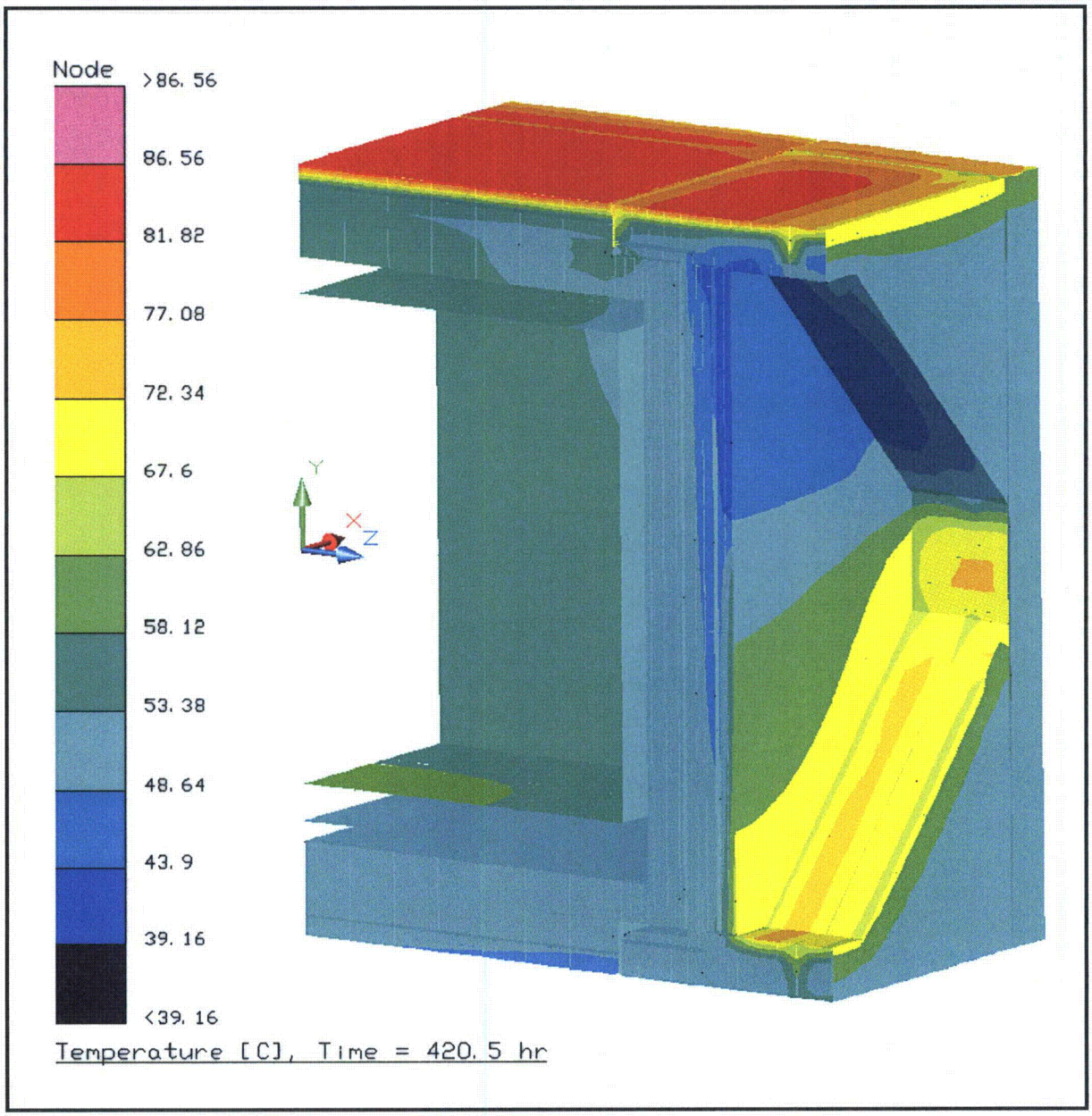

Figure 3.3-3 – Temperature Distribution within Packaging

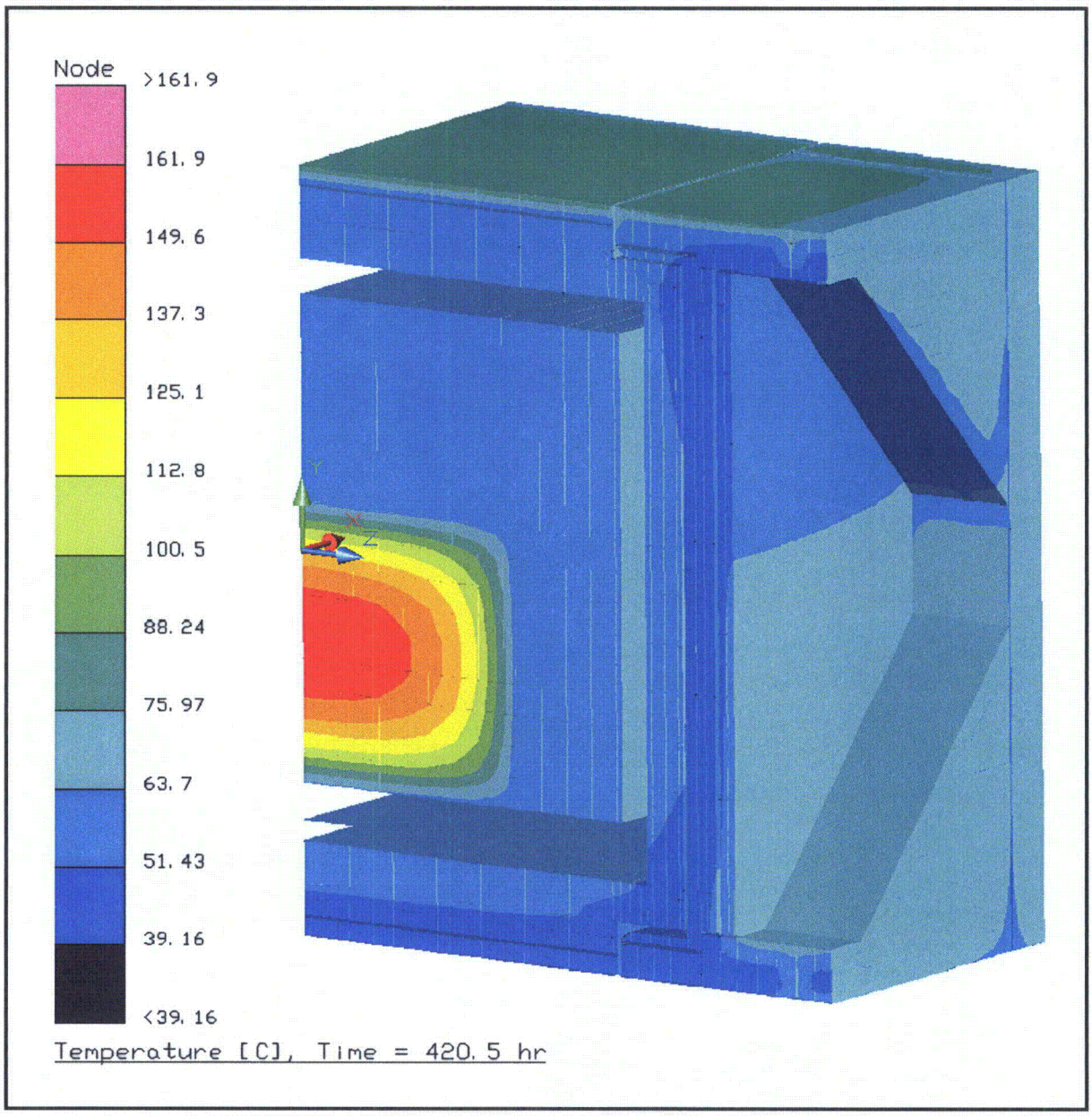

Figure 3.3-4 – Temperature Distribution within Packaging and Payload

This page intentionally left blank.

3.4 Thermal Evaluation for Hypothetical Accident Conditions

This section presents the evaluation methodology and results for the thermal analysis of the TRUPACT–III package under the hypothetical accident condition (HAC) specified in 10 CFR §71.73(c)(4) [1]. The evaluation is based on an analytical model of the TRUPACT–III package which takes into account the damage expected to the package as result of the HAC free and puncture bar drops that precede the fire event, as well as the changes expected to the thermal characteristics and survivability of the various package components.

3.4.1 Initial Conditions

The initial conditions of the TRUPACT–III package prior to the HAC fire event is based on drop testing of two full scale certification test units (i.e., CTU-1 and CTU-2) to establish the expected level of damage sustained by the package as a result of the NCT and HAC free and puncture drop tests. Section 2.7, *Hypothetical Accident Conditions*, documents the series of accident drops conducted on the test articles. Section 3.5.3, *Review of TRUPACT–III Package Full Scale Drop Test Results*, provides a further overview of the test results and the rationale for selecting the worst-case damage scenario based on the test results.

Based on the referenced evaluation of the potential package damage, it is concluded that the bounding damage scenario for the TRUPACT–III package will consist of an oblique free drop on the side-edge of the package (test LD5, see Section 2.7.1.1.2(B), *Drops on the Sides*), followed by a puncture bar impact just aft of the cheek to body joint. The oblique free drop on the side-edge of the package will impart the most significant damage over the greatest surface area compared to any of the other free drop scenarios, while the puncture bar impact location will generate the greatest level of damage in comparison with the other puncture bar impacts and places that damage as close to the thermally sensitive closure seals as feasible. It is further assumed that the TRUPACT–III package will come to rest in a horizontal position prior to the initiation of the fire. Since the package geometry is nearly symmetrical about its axis, there are no significant thermal differences whether the package is right-side up, up-side down, or even on its side. The potential for the SLB2 payload being re-positioned depending upon the package orientation is not significant to the peak temperatures developed under HAC conditions given the payload's relatively low shell temperatures noted for the NCT conditions.

The temperature of the package components prior to the start of the HAC fire event are based on those observed for the 424 hour point in the transient NCT Hot analysis presented in Section 3.3.1.1, *Maximum NCT Temperatures*, for a payload of one SLB2 with a maximum decay heat load of 80 watts. While the effects of solar radiation may be neglected before and during the thermal test [2], the initial package condition for the HAC thermal event for this evaluation are conservatively based the presence of insolation prior to the fire event. It should be noted that an exact temperature match between the maximum temperatures from the NCT results and the HAC pre-fire initial temperatures does not occur since, given the diurnal cycle used for the insolation

[1] Title 10, Code of Federal Regulations, Part 71 (10 CFR 71), *Packaging and Transportation of Radioactive Material*, United States Nuclear Regulatory Commission (USNRC), 01–01–09 Edition.

[2] NUREG-1609, *Standard Review Plan for Transportation Packages for Radioactive Material*, U.S. Regulatory Commission, Office of Nuclear Materials Safety and Standards, March 1999.

loading, each package component reaches its peak temperature at a different time point. As such, while the selected time point in the NCT transient used for the HAC pre-fire temperatures occurs when the CSA is reaching its maximum temperature, the outer shell temperatures of the package are slightly below their noted peak temperatures. This difference is not significant since the outer shell temperature quickly rises when exposed to the HAC fire event.

3.4.2 Fire Test Conditions

The thermal performance of the TRUPACT–III package under HAC conditions is evaluated using an analytical thermal model. The HAC model is a modified version of the quarter symmetry NCT model described in Appendix 3.5.2.1, *Description of Thermal Model for NCT Conditions*. This is appropriate since the use of a quarter symmetry model to simulate the non-symmetric damages arising from the HAC drop events is inherently conservative. The primary modifications made to the NCT model for the HAC modeling consist of the following:

- Simulated the worst-case HAC free and puncture drops consisting of an oblique side-edge drop and subsequent puncture bar damage adjacent to the side-edge damage and just aft of the cheek to body joint (see Figure 3.5-16). As described in Appendix 3.5.2.6, *Description of Thermal Model for HAC Conditions*, the oblique side-edge drop creates a flattened region approximately 305 mm (12 inches) wide along the package length, reducing to approximately 178 mm (7 inches) wide at the cheek areas due to the additional structure and the higher density polyurethane foam used in the cheeks. The puncture bar damage is assumed to have penetrated both the outer skin and the underlying 10 mm thick puncture-resistant plate and to have opened a hole in the outer skin that is approximately 254 mm (10 inches) long by 178 mm (7 inches) wide following the package rotation after impact. While the hole in the underlying 10 mm thick puncture-resistant plate and polyurethane foam was 178 mm (7 inches) in diameter, or 54% of the opening in the outer skin, the full 254 mm x 178 mm opening is assumed all the way to the surface of the CSA for conservatism. Further, all compacted material within the affected area is assumed to have fallen out prior to the HAC fire, thus exposing the underlying CSA surface to the HAC environment. These assumptions provide a significant level of conservatism.
- Changed the thermal conductivity of the balsa wood from the value consistent with the low end of the observed range to a value that represent the high end of the range,
- Increased the emissivity of the external surfaces from 0.8 to 0.9 to account for possible soot accumulation on the surfaces,
- The balsa wood surfaces adjacent to undamaged portions of the outer skin will be charred from the HAC fire, but not consumed due to the lack of air. However, since the thermal conductivity of solid wood is greater than that for charred wood, the thermal properties of undamaged wood are assumed for computing the heat flow into the package. Exposed sections of balsa wood are conservatively assumed to be fully consumed at the start of the fire,
- Replaced the assumed air gaps between the layered components of the package side wall with direct contact,

- Replaced the adiabatic boundary condition applied to the bottom of the package for NCT conditions with convective and radiation thermal conductors to the ambient,
- Apply convection heat transfer coefficients between the package and the ambient that are appropriate for gas velocities of 10 m/sec during the 30-minute fire event[3]. The elevated convection heat transfer rate is conservatively applied to the surfaces of the CSA exposed by the puncture bar attack, even though convection will be significantly reduced by the recessed cavity formed by the puncture bar damage. Convection coefficients based on still air are assumed following the 30-minute fire event,
- An 800 °C ambient condition with an effective emissivity of 1.0 is used to simulate the elevated temperature of the fire for convective and radiation heat transfer during the 30-minute fire event. The ambient condition is re-set at the end of the 30-minute fire to the pre-fire ambient condition of 38 °C with an effective emissivity of 1.0 and with the addition of insolation.

3.4.3 Maximum Temperatures and Pressure

3.4.3.1 Maximum HAC Temperatures

Figure 3.4-1 presents the thermal response curves for selected package components to the simulated HAC fire event. As illustrated in the figure, while the exterior of the package quickly rises to nearly the temperature of the fire, the CSA containment sheet and its enclosed SLB2 payload container and bounding waste box configuration show only moderate thermal response to the presence of the 30-minute fire event. The noted transient response reflects the significant thermal protection afforded to the CSA and its payload by the presence of the outer skin, the balsa wood, polyurethane foam, and the calcium silicate insulation.

This result is further illustrated by the perspective and reverse perspective views presented in Figure 3.4-2 of the temperature distribution in the TRUPACT–III Package after 30 minutes of exposure to the HAC fire. The figure clearly shows that the balsa wood and polyurethane foam limits the elevated temperatures resulting from the fire event to narrow regions adjacent to the outer shell. The presence of the 6-mm puncture resistant sheet in the overpack cover can be seen via the thermal path it provides between the layers of polyurethane foam. Similar thermal paths occur at the corner ribs and the end sheets separating the package body and the overpack cover.

This thermal protection of the CSA is further illustrated by the temperature response curves presented in Figure 3.4-3 and the temperature distribution illustrated in Figure 3.4-4. As seen from the figures, the maximum temperature noted on the CSA occurs only on the structural sheet and only for the relatively small portion of the CSA affected by the puncture bar damage. In addition to the region of elevated temperature caused by the puncture bar damage, Figure 3.4-4 also shows a smaller region of slightly elevated temperature approximately mid-height on the CSA. This region of slightly elevated temperature results from heat conducted axially into the package via the exposed sheet metal of the recessed area of the overpack cover (see Figure 3.5-2) and the opposing sheet metal in the package cheek area and not as the result of the HAC free or puncture bar damage.

[3] Schneider, M.E and Kent, L.A., *Measurements Of Gas Velocities And Temperatures In A Large Open Pool Fire, Heat and Mass Transfer in Fire* - HTD Vol. 73, 1987, ASME, New York, NY.

Figure 3.4-5 presents an enlarged view of the portion of the CSA affected by the puncture bar damage and which exceeds the NCT design limit of 316 °C. The region of elevated temperatures is predicted to extend only a short distance below the structural sheet and does not extend to the containment sheet. The large thermal gradient through the segment of the CSA wall affected by the puncture bar attack depicted in Figure 3.4-5 results from the 'corrugated' makeup of the 140 mm thick CSA wall (see Appendix 3.5.2.4, *Effective Thermal Properties for Corrugated Wall/Lid Structures*, for details). In this type of construction, the structural sheet of the CSA is separated from the containment sheet by a 124-mm airspace and 4-mm thick V-stiffeners inclined at an approximately 67 degree angle. The V-stiffeners act as a thermal shield by preventing direct radiation heat transfer between the structural and containment sheets, while their thinness, length, and stainless steel makeup greatly restrict heat conduction between the sheets.

As discussed in Section 3.2.2, *Technical Specifications of Components*, the NCT 316 °C temperature limit for the CSA represents the maximum temperature for continuous use listed for the material in the ASME Code Case N-635-1 and not the limit under the transient HAC conditions. The temperature limit under HAC is established to avoid what is known as "475 °C Embrittlement". Section 3.2.2 indicates that an aging time of 1 hour at 725 °C (i.e., a temperature that bounds the peak predicted CSA temperature) or approximately 11 hours at 650 °C is required to transition from ductile to brittle fracture. Per Figure 3.4-3, the entire time the peak CSA structural sheet temperature is above 650 °C is only about 30 minutes, while the CSA containment sheet remains well below 316 °C. As such, while a reduction in ductility may occur for the section of the CSA structural sheet affected by the elevated temperature, full embrittlement of the CSA steel is not expected due to insufficient aging time at temperature. No loss in ductility and no embrittlement of the CSA containment boundary will occur since its peak temperature remains well below the continuous use temperature of 316°C for the Alloy UNS S31803 stainless steel.

The significance of possible CSA steel embrittlement is further reduced by the fact that the fire test is the last hypothetical accident condition which is applicable per 10 CFR 71 (i.e., no post-fire drop events are considered plausible). As such, the only subsequent structural loads occurring for the package will arise from 1 g recovery operations. Therefore, even if a reduction in ductility does occur over the small portion of the structural shell affected by the puncture bar damage, no safety impact will result since sufficient package ductility will remain to allow recovery operations.

As demonstrated by the temperature response curves presented in Figure 3.4-3, the containment and sampling/vent port seals show only a limited temperature affect from the HAC fire event. The maximum temperature of 95 °C attained by the CSA debris shield is well below the intermittent use temperature for the silicone foam and porous polyethylene used in the debris shield. Therefore, while a potential failure of the debris shield poses no safety concern for the HAC fire event, the relatively low temperature attained also indicates that no out–gassing from this material which could lead to pressurization of the CSA cavity will occur.

The thermal protection afforded by the TRUPACT–III design is further illustrated by Figure 3.4-6 which illustrates the average temperature response within the balsa wood and polyurethane foam components. The fact that the average balsa wood temperature remains near or below 450 °C is significant in that temperatures in excess of this are required to reduce the wood structure to char. As such, while the outer layer of the balsa may be charred, it is expected that un-damaged balsa will exist below that. Further, the fact that the average temperature of the polyurethane foam in the package body and corner segments is below 190 °C indicates that the

bulk of the polyurethane foam will not experience any significant decomposition as the result of exposure to the HAC fire event since significant decomposition begins at approximately 354 °C (see Section 3.5.4, *'Last-A-Foam' Response under HAC Conditions*).

While the HAC evaluation assumes no air gaps between the balsa and polyurethane foam components and the metallic surfaces of the package, the peak predicted HAC temperatures are not seen as being affected by the presence or absence of air gaps between the modeled components. This conclusion is based on the fact that the peak CSA temperature occurs at the location of the puncture bar damage where the surface of the CSA is directly exposed to the HAC environment and not at locations that underlie the other model segments. Further, as demonstrated by the sensitivity analysis conducted under the NCT evaluations, the effect of the assumed air gaps for NCT had a thermally insignificant effect on the NCT results (i.e., less than 1 °C).

Table 3.4-1 summarizes the peak component temperatures expected during the HAC fire event. As seen from the table, with the exception of a limited surface area on the CSA structural sheet, all components exhibit large thermal margins between the noted peak temperatures and the associated maximum allowable temperatures for the component. As explained above, while a small region of the CSA structural sheet may experience a reduction in ductility due to being heated above 316 °C, full embrittlement of the steel is not expected due to the limited time at temperature and no significant impact is expected on post-accident handling or the ability of the CSA to maintain containment of the payload. Therefore, the TRUPACT–III Package design is seen as complying with the thermal limits established for operation under the short-term conditions existing for the HAC fire event. Further, given the conservative method of analysis, the pedigree of the thermal properties assumed for the various components, and the level of the thermal margins (as presented in Table 3.4-1), this conclusion is seen as being unaffected by any potential uncertainties in the method or basis of analysis.

Given the relative light weight structure of the TRUPACT–III package, the peak temperature results for the cold weather conditions will be similar to those seen for the HAC hot condition presented above. Further, since the thermal gradients that may exist within the package structure are very limited due to the thickness of the metal sheets used in its fabrication, no significant increase in thermal stresses will occur for the HAC cold condition from those observed under the evaluated HAC hot condition. As such, no specific analysis is presented for the HAC cold condition.

3.4.3.2 Maximum HAC Pressure

The maximum internal pressure within the CSA during the HAC event is determined in the same manner as for NCT (see Section 3.3.2, *Maximum Normal Operating Pressure*). Based on the conservative assumption that the TRUPACT–III package has reached its MNOP pressure of 172 kPa gauge due to gas generation just prior to the initiation of the fire, the predicted pressure increase within the CSA due to heat up from its pre-fire, steady-state level is computed via the ideal gas law as follows:

$$\text{pressure increase during fire} = \frac{p_{\text{Pre-fire}}\left(T_{\text{Void Volume Fire}} + 273.15\,\text{K}\right)}{\left(T_{\text{Void Volume Pre-fire}} + 273.15\,\text{K}\right)} - p_{\text{Pre-fire}}$$

$$\text{where, } T_{\text{Void Volume Fire}} = \frac{83 + 222}{2} = 153\ ^{\circ}\text{C}$$

$$T_{\text{Void Volume Pre-Fire}} = \frac{63+55}{2} = 59^{\circ}\text{C}$$

$$\text{and, } p_{\text{Pre-fire}} = 101.3+172 = 273.3\,\text{kPa}$$

As such, the maximum pressure increase during the fire transient is 77.3 kPa, yielding a peak HAC pressure of 249.3 kPa gauge. This pressure increase value is conservative in that the analysis is based on maximum of non-coincidental peak temperatures and the fact that the peak temperature of the CSA containment sheet is used as opposed to an area weighted average temperature.

The relatively low temperature attained within the CSA indicates that no significant out–gassing will occur from the silicone foam and porous polyethylene used for the debris shield or the plastic material used on the CSA's guide bars which could lead to pressurization of the CSA cavity. As explained in Section 3.3.2, *Maximum Normal Operating Pressure*, compliance with the limitation on the buildup of flammable mixtures within the package is ensured by administrative controls on the payloads that are permitted to be loaded. See Section 3.3.2 for more discussion.

3.4.4 Maximum Thermal Stresses

As shown in Section 3.4.3.2, *Maximum HAC Pressure*, the internal pressure within the payload cavity will increase by a maximum of 77.3 kPa, or +45% from its maximum pre-fire level, due to the HAC thermal event. As such, pressure stresses due to the HAC thermal event increase a corresponding maximum of 45%. This level of pressurization is within the capability of the CSA as demonstrated in Section 2.7.4.3, *Stress Calculations*. Further, since the TRUPACT–III package is fabricated principally of sheet metal and relatively thin structural steel shapes, the thermal stresses developed within any component during the HAC fire event will be low and not significant to the safety of the package.

Table 3.4-1 – HAC Temperatures w/ SLB2 Payload

Location / Component	Temperatures (°C)			
	Pre-fire [1,2]	End of Fire [2]	Peak [2]	Maximum Allowable [3]
Bounding Waste Box Payload				
- Maximum	162	163	177	230
- Bulk Avg.	90	92	107	230
Standard Large Box (SLB2) Payload				
- Maximum sidewall	62	83	89	230
- Minimum sidewall (coincident)	53	54	54	230
- Avg. sidewall	55	59	60	230
- Bulk Avg. (of void only)	55	59	76	230
- Bulk Avg. (of total volume) [4]	63	66	83	230
Containment O-ring Seal	52	63	95	204
Sampling/Vent Port O-ring Seal	51	53	80	204
Debris Shield	52	63	95	-
CaSi (Seal Protection) Insulation	61	688	688	982
CSA Structural Sheet (includes Lid outer sheet), - Peak/Avg. [5]	58 / 52	689 / 73	689 / 75	725 for < 1 hour / 316
CSA Containment Sheet (includes Lid inner sheet)				
- Maximum	55	216	222	316
- Minimum (coincident)	50	51	51	316
CSA Lid Bolts	53	187	187	316
Outer Skin				
- Package Body, Peak	71	800	800	1,370
- Package Cheek, Peak	69	800	800	1,370
- Package Cover, Peak	73	800	800	1,370
Last-a-Foam				
- Package Body, Peak/Avg.	66 / 52	684 / 75	684 / 96	-
- Package Corner, Peak/Avg.	60 / 55	797 / 189	797 / 189	-
- Package Cheek, Peak/Avg.	69 / 52	800 / 373	800 / 373	-
- Overpack Cover Outer Area, Peak/Avg.	73 / 52	792 / 168	792 / 169	-
- Overpack Cover Recess Area, Peak/Avg.	58 / 50	695 / 70	695 / 99	-
Balsa				
- Package Body, Peak/Avg.	73 / 54	793 / 455	793 / 455	-
- Overpack Cover, Peak/Avg.	64 / 51	784 / 449	784 / 449	-

Notes:

1) Initial temperatures based on SLB2 with 80 watt decay heat load at the 424 hour point in the transient NCT Hot analysis.
2) For conservatism, the decay heat is confined to a bounding minimum sub-volume within the SLB2. This sub-volume represents 23% of the total available volume. The remaining SLB2 volume is assumed to have zero decay heat and the thermal properties of air.
3) Maximum allowable temperatures are established in Section 3.2.2, *Technical Specifications of Components.*
4) Bulk average temperature computed assuming SLB2 internal volume of 7,394 liters and a bounding waste box volume of 1,609 liters.
5) The peak CSA structural sheet temperature occurs at the location of the puncture bar damage and lasts less than 1 hour. The peak temperature for the remaining portion of the structural sheet is substantially lower as demonstrated by the average temperature value.

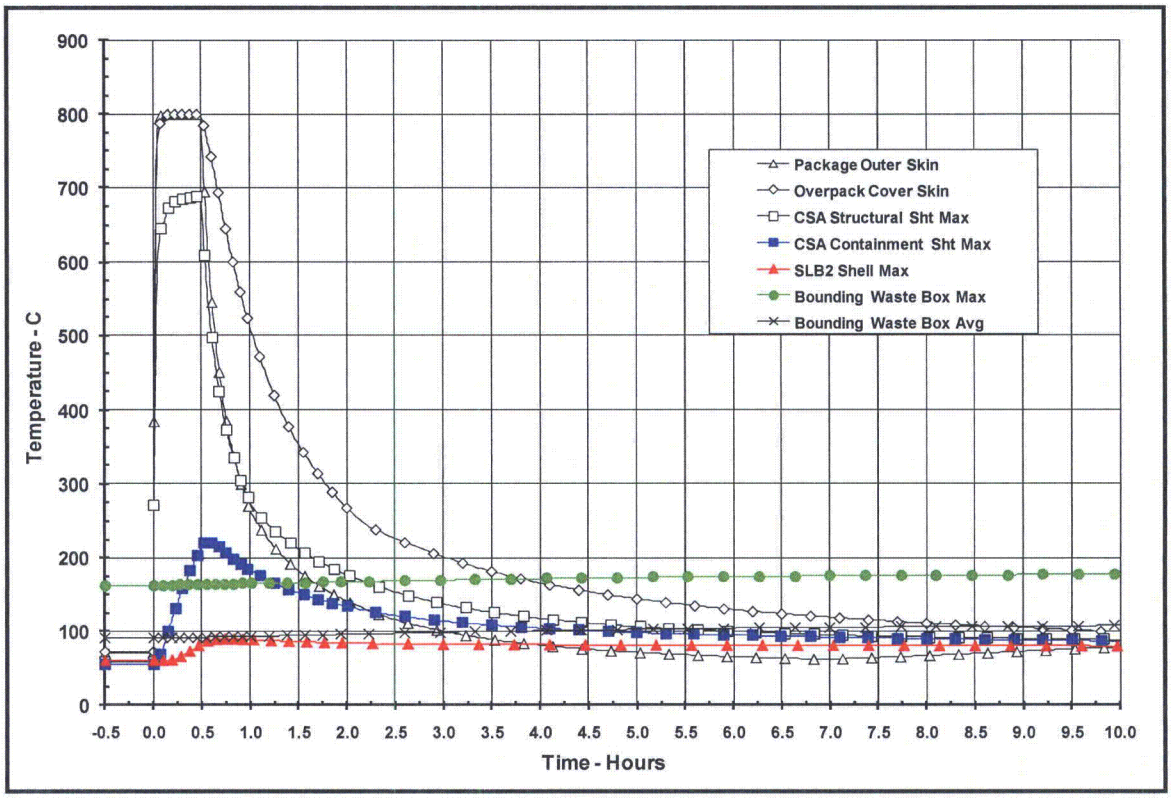

Figure 3.4-1 – TRUPACT–III Package HAC Temperature Response

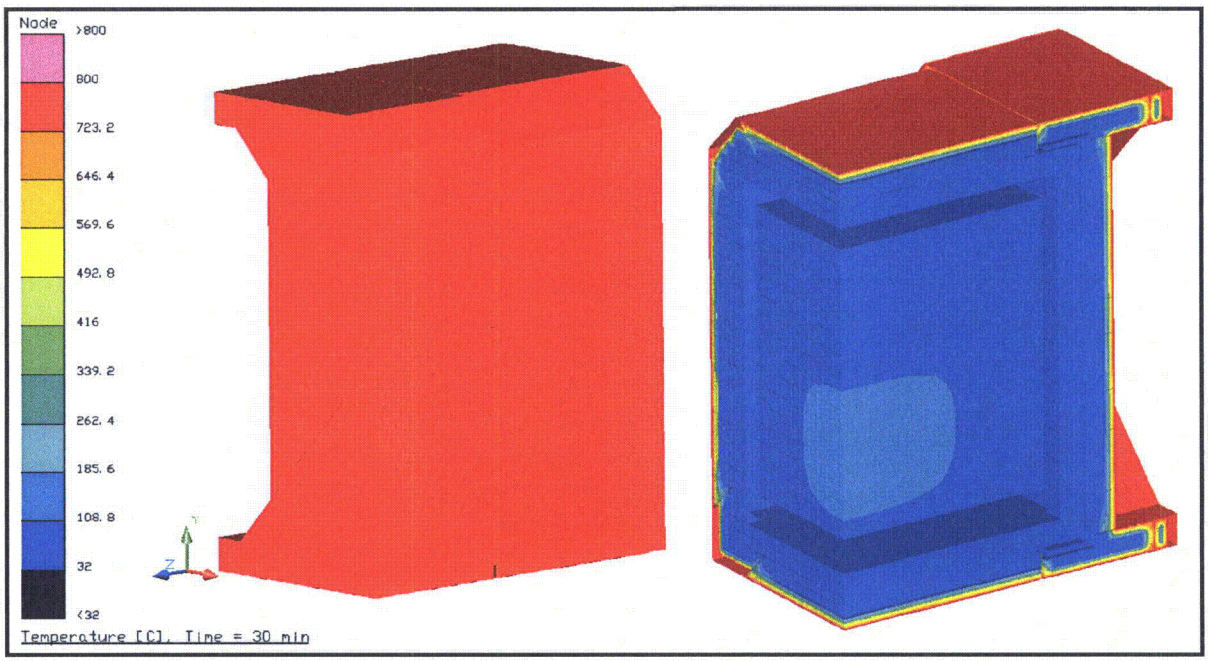

(Note: the positive y-axis is oriented towards the top of the package and the positive z-axis towards the package closure end)

Figure 3.4-2 – Temperature Distribution at End of 30 Minute Fire Event, Perspective and Reverse Perspective Views

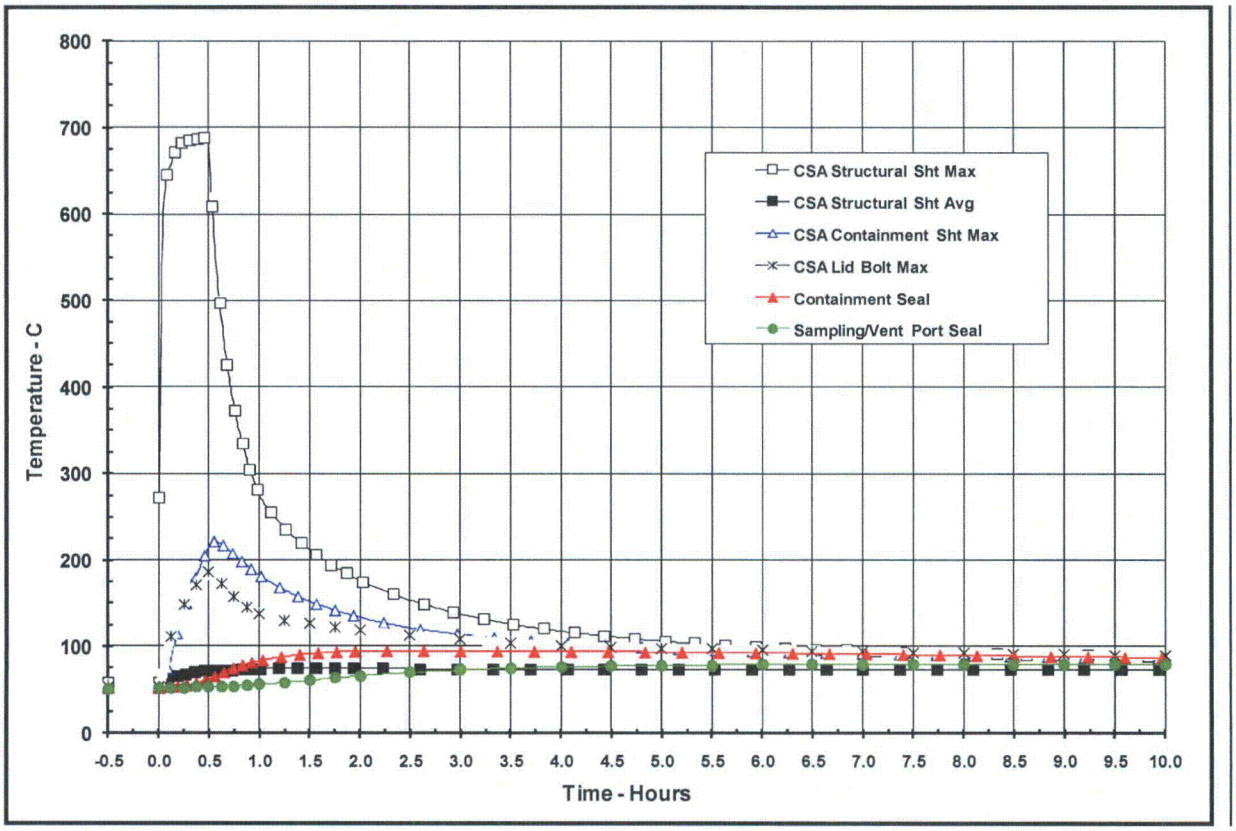

Figure 3.4-3 – Temperature Response of CSA to HAC Fire Event

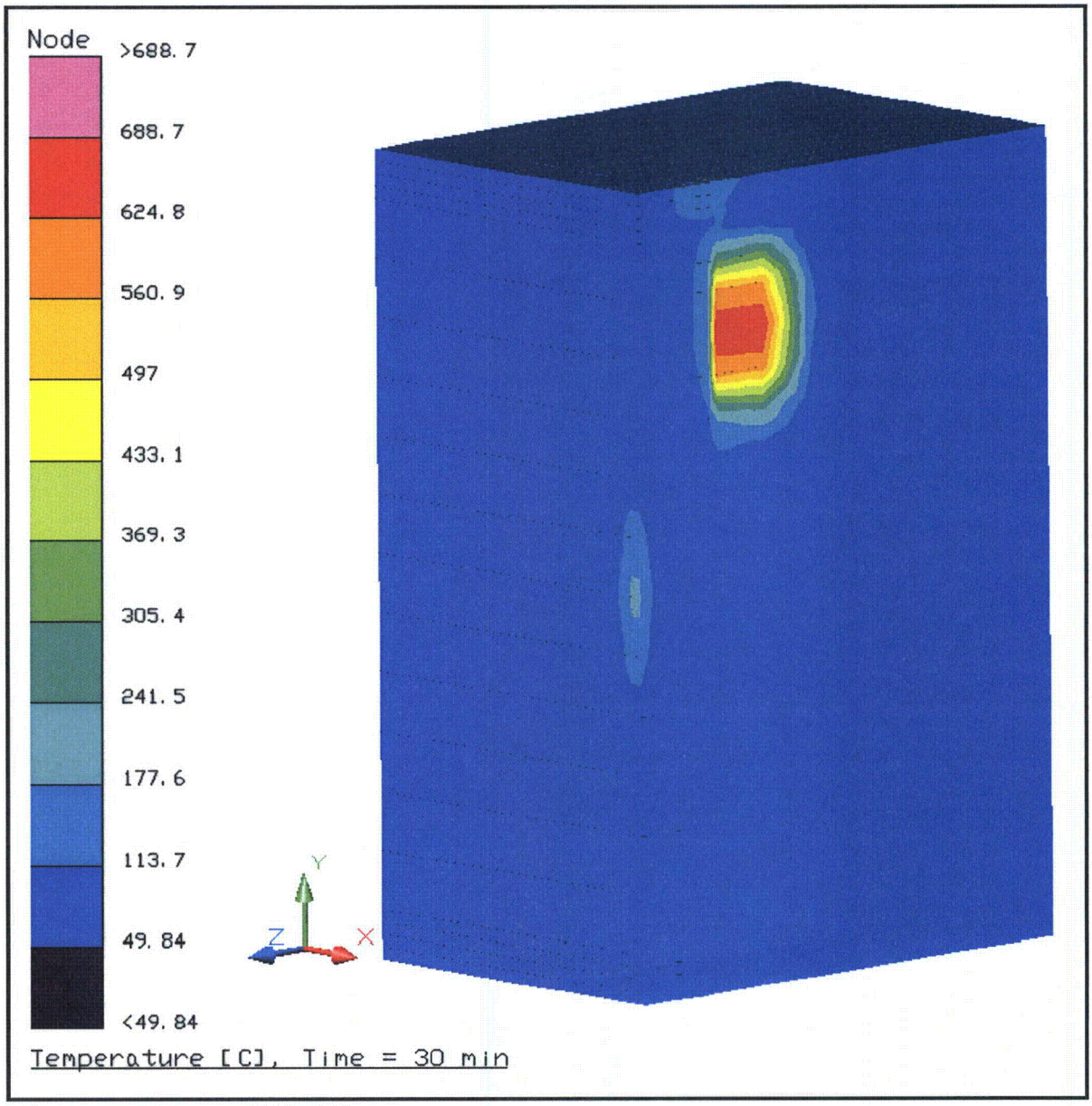

(Note: the positive y-axis is oriented towards the top of the package and the positive z-axis towards the package closure end)

Figure 3.4-4 – CSA Exterior Temperature Distribution at End of 30 Minute Fire Event

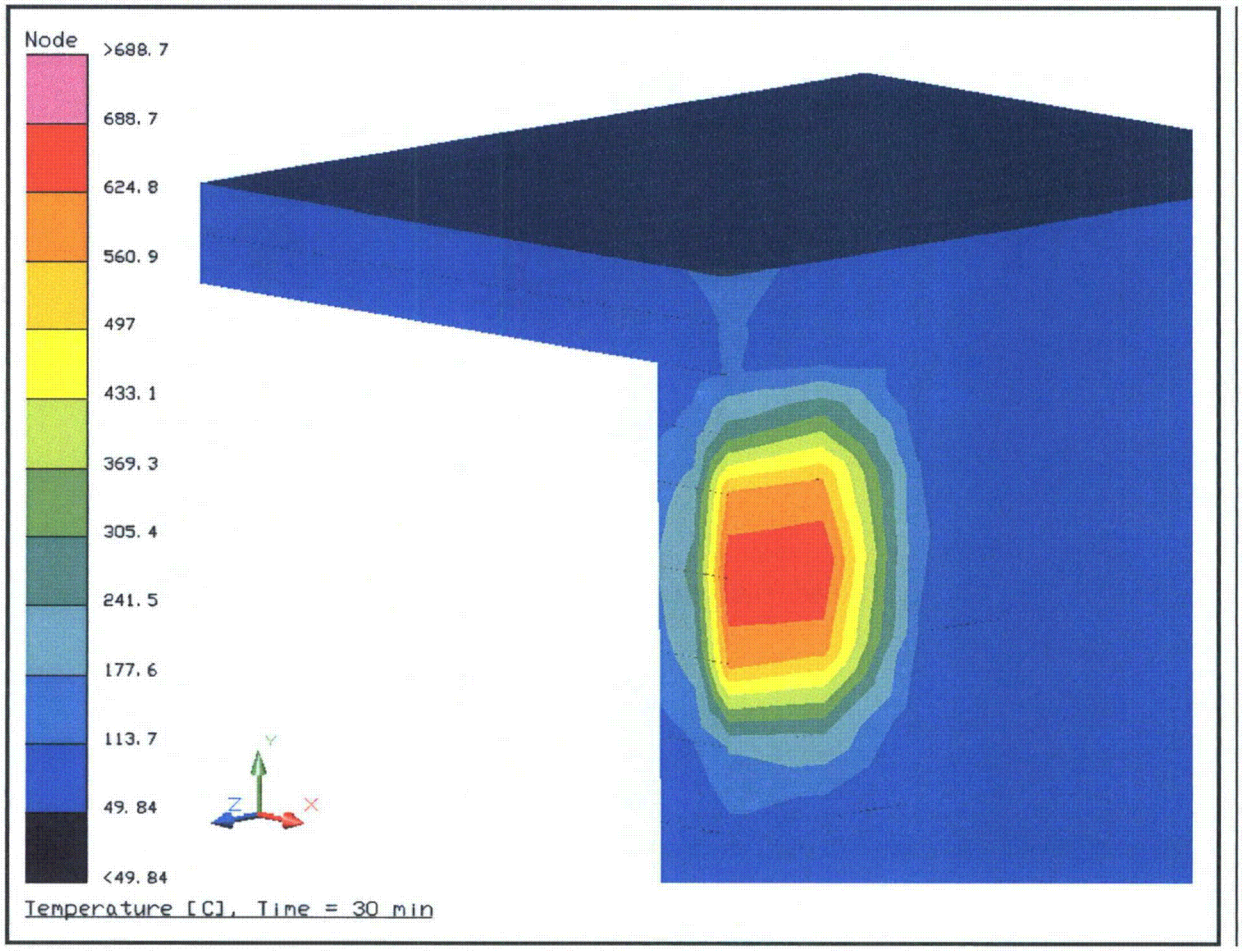

(Note: the positive y-axis is oriented towards the top of the package and the positive z-axis towards the package closure end)

Figure 3.4-5 – Temperature Distribution through CSA Wall at End of 30 Minute Fire Event

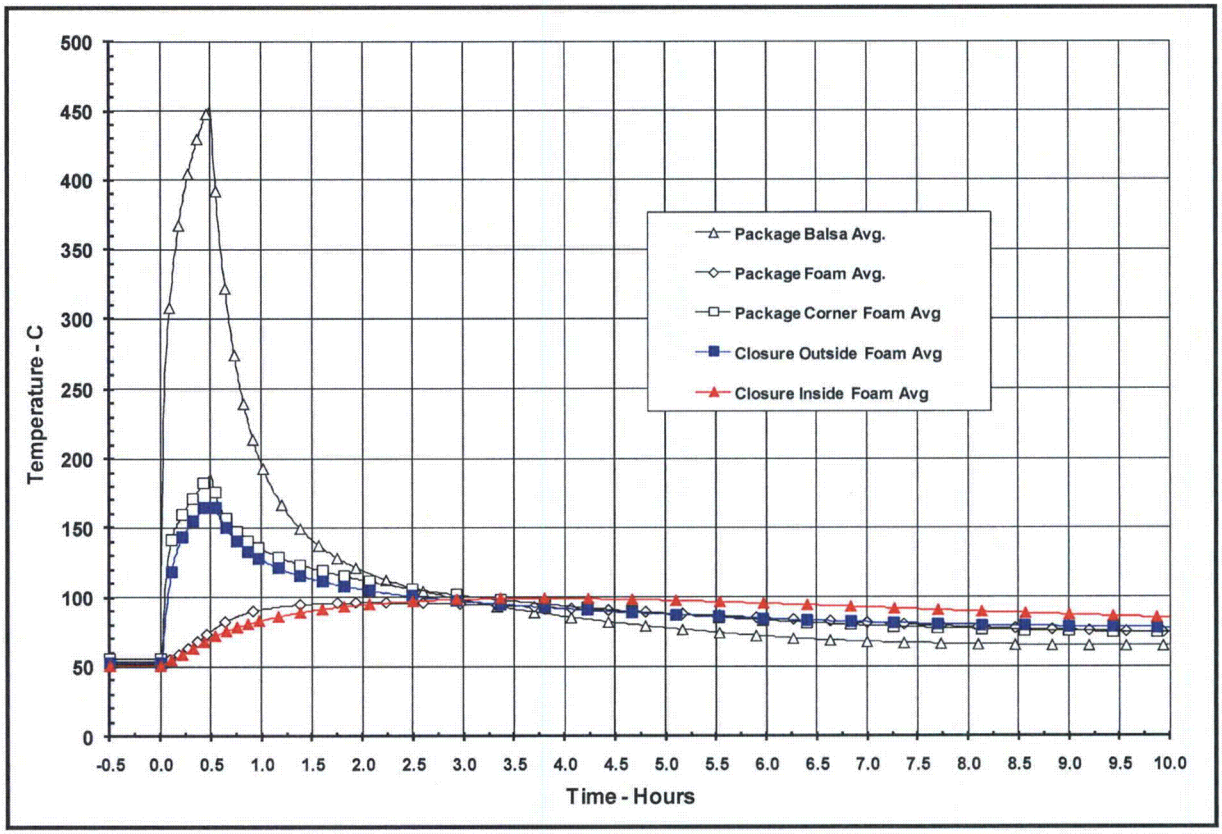

Figure 3.4-6 – Temperature Response of Package Polyurethane Foam and Balsa Wood Components to HAC Fire Event

3.5 Appendices

3.5.1 Computer Analysis Results

3.5.2 Thermal Model Details

3.5.3 Review of TRUPACT–III Package Full–Scale Drop Test Results

3.5.4 'Last-A-Foam' Response Under HAC Conditions

This page intentionally left blank.

3.5.1 Computer Analysis Results

Due to the size and number of the output files associated with each analyzed condition, results from the computer analysis are provided on a DVD–R.

This page left intentionally blank.

3.5.2 Thermal Model Details

The analytical thermal model of the TRUPACT–III package was developed for use with the Thermal Desktop®[1] and SINDA/FLUINT[2] computer programs. These programs are designed to function together to build, exercise, and post-process a thermal model. The Thermal Desktop® computer program is used to provide graphical input and output display function, as well as computing the radiation exchange conductors for the defined geometry and optical properties. Thermal Desktop® is designed to run as an AutoCAD® application. As such, all of the CAD tools available for generating geometry within AutoCAD® can be used for generating a thermal model. In addition, the use of the AutoCAD® layers tool presents a convenient means of segregating the thermal model into its various elements.

The SINDA/FLUINT computer program is a general purpose code that handles problems defined in finite difference (i.e., lumped parameter) and/or finite element terms and can be used to compute the steady-state and transient behavior of the modeled system. Although the code can be used to solve any physical problem governed by diffusion-type equations, specialized functions used to address the physics of heat transfer and fluid flow make the code primarily a thermal code.

The SINDA/FLUINT and Thermal Desktop® computer programs have been validated for safety basis calculations for nuclear related projects[3,4].

Together, the Thermal Desktop® and SINDA/FLUINT codes provide the capability to simulate steady-state and transient temperatures using temperature dependent material properties and heat transfer via conduction, convection, and radiation. Complex algorithms may be programmed into the solution process for the purposes of computing heat transfer coefficients as a function of the local geometry, gas thermal properties as a function of species content, temperature, and pressure, or, for example, to estimate the effects of buoyancy driven heat transfer as a function of density differences and flow geometry.

3.5.2.1 Description of Thermal Model for NCT Conditions

The thermal model of the TRUPACT–III package defines a quarter symmetry model of the package's closure end (i.e., symmetrical about the package axial axis and 180° symmetry about the package vertical axis). This modeling choice captures the thermally sensitive seal region at the package's closure lid and allows the incorporation of varying insolation loads that will occur at the top, sides, and ends of the package and the adiabatic conditions assumed to exist over the bottom surface of the package. Program features within the Thermal Desktop® computer program automatically compute the various areas, lengths, thermal conductors, and view factors involved in determining the individual elements that make up the thermal model of the complete

[1] Thermal Desktop®, Version 4.8/5.1, Cullimore & Ring Technologies, Inc., Littleton, CO, 2005/2008.

[2] SINDA/FLUINT, Systems Improved Numerical Differencing Analyzer and Fluid Integrator, Version 4.8/5.1, Cullimore & Ring Technologies, Inc., Littleton, CO, 2005/2008.

[3] Software Validation Test Report for Thermal Desktop® and SINDA/FLUINT, Version 4.8, Packaging Technology, Inc., File No. TR-VV-05-001, Rev. 1.

[4] AFS-TR-VV-006, Rev. 0, Thermal Desktop and SINDA/FLUINT Testing and Acceptance Report, V5.1, Windows XP, AREVA Federal Services LLC, September 2008.

assembly. The modeling assumes that the TRUPACT–III operations are conducted with the package in its normal, horizontal orientation.

Figure 3.5-1 illustrates a perspective view of the three dimensional thermal model developed for the purposes of this calculation. The origin of the thermal model axis is located at the center of the package, with the positive x-axis pointing towards the right side of the package (when facing the closure end), the positive y-axis pointing towards the top of the package and the positive z-axis pointing towards the closure end of the package. The model is composed of solid and plate type elements to represent the various package components. Thermal communication between the various components is via conduction, convection, radiation, and surface-to-surface contact. A total of approximately 14,700 thermal nodes, 9,300 planar elements, and 11,300 solids are used in the model to provide thermal resolution. One boundary node is used to represent the ambient environment for convection purposes and a second boundary node is used to represent the ambient temperature for the purpose of radiation heat transfer. An effective emissivity of 1.0 is assumed for the hypothetical fire.

The balsa wood, the polyurethane foam, and the calcium silicate insulation used in the packaging are installed as individual components. Therefore, direct contact between the various packaging layers may be relatively low, depending on the 'tightness' of the fit up. To reflect this situation, the interface with the components fabricated of these materials is treated as an air gap with conductance across the gap computed as a function of the thermal conductivity of air and an assumed gap thickness. Radiation heat transfer is ignored for conservatism. A nominal gap width of 0.5-mm is used between the layered components of the package side walls, with an assumed gap width of 0.5-mm to 1-mm used at the other various material interfaces.

A comparison of the thermal model configuration, illustrated by Figure 3.5-2 to Figure 3.5-9, with the TRUPACT–III package design, as defined by Figure 1.1-1 through Figure 1.1-6 from Section 1.1, *Introduction*, and Figure 3.1-1 to Figure 3.1-5, demonstrates that the placement and geometry of the major components of the package are individually captured in the thermal model. The design features captured include the recessed overpack cover, the puncture resistant sheets, and the calcium silicate insulation protection plates. In addition, the thermal connection between the structural shell of the CSA and the outer skin of the package via the 6-mm support ribs at the corners of the package is accurately represented in the model (see Figure 3.5-3). These support ribs provide a significant thermal bridge, in relation to the level of the payload decay heat load, between the CSA and the ambient.

Payload Container Thermal Model

As discussed in Section 3.1.1.2, *Payload Configuration*, the only payload form currently planned for the TRUPACT–III package is one (1) SLB2 container. Since the SLB2 containers may contain a variety of TRU waste and that waste may either be placed directly into the SLB2 container or be housed within other containers, the thermal model is set up to simulate either an SLB2 container completely filled with waste, or an SLB2 container containing waste that is confined within a small region of the SLB2 (i.e., 965-mm × 965-mm × 1,727-mm, or approximately 23% of the total SLB2 container volume) for the given decay heat loading. See Section 3.1.1.2, *Payload Configuration*, and Section 3.1.2, *Content's Decay Heat*, for a description and justification of this bounding waste form.

Figure 3.5-10 illustrates the 1/4-symmetry thermal modeling of the SLB2 container with its enclosed hypothetical bounding waste box form and the roller floor pallet system. The figure shows the external surface of the SLB2 container and the enclosed hypothetical bounding waste

box. While the decay heat is assumed to be evenly distributed over the volume of the bounding waste box form, it actually represents a non-uniform heat distribution within the SLB2 container since the bounding waste box form is only 23% of the available waste volume within the SLB2 container. Heat transfer within the bounding waste box volume is via conduction only, based on the thermal properties of air. Heat transfer between the surface of the bounding waste box form and the internal surfaces of the SLB2 container are assumed to be via conduction and radiation across the void air volume. The hypothetical waste box is assumed to be horizontally and axially centered within the SLB2 container and to be resting against the bottom of the SLB2 container. This placement yields the maximum expected separation distance between the payload and the interior of the TRUPACT–III.

The heat transfer between the exterior of the SLB2 container and the interior cavity of the TRUPACT–III is computed based on conduction and radiation across the void air volume. The SLB2 container may either be 'rolled' into the package via a roller floor pallet or slid into the package onto a floor pallet structure with similar dimensions and thermal resistance. The pallet structure is simulated as two 4.75-mm thick aluminum sheets separated by a 66.7-mm airspace. The thermal properties of Type 6061 aluminum are assumed. Conductance between the upper and lower sheets of the pallet structure is modeled via conductors which simulate the heat transfer through the air gap and the vertical metal 'legs' of the pallet structure. Credit is taken for direct contact heat transfer between the pallet structure and the bottom of the CSA interior, but only over that portion of the support rail surface area that actually makes contact with the CSA. No credit is taken for direct contact heat transfer between the SLB2 container and roller floor. Instead, the heat transfer is modeled as conduction and radiation across an approximately 130-mm airspace representing a conservative estimate of the standoff height of the SLB2 container above the roller floor, plus an allowance for the separation distance between the hypothetical waste box and the base of the SLB2 container.

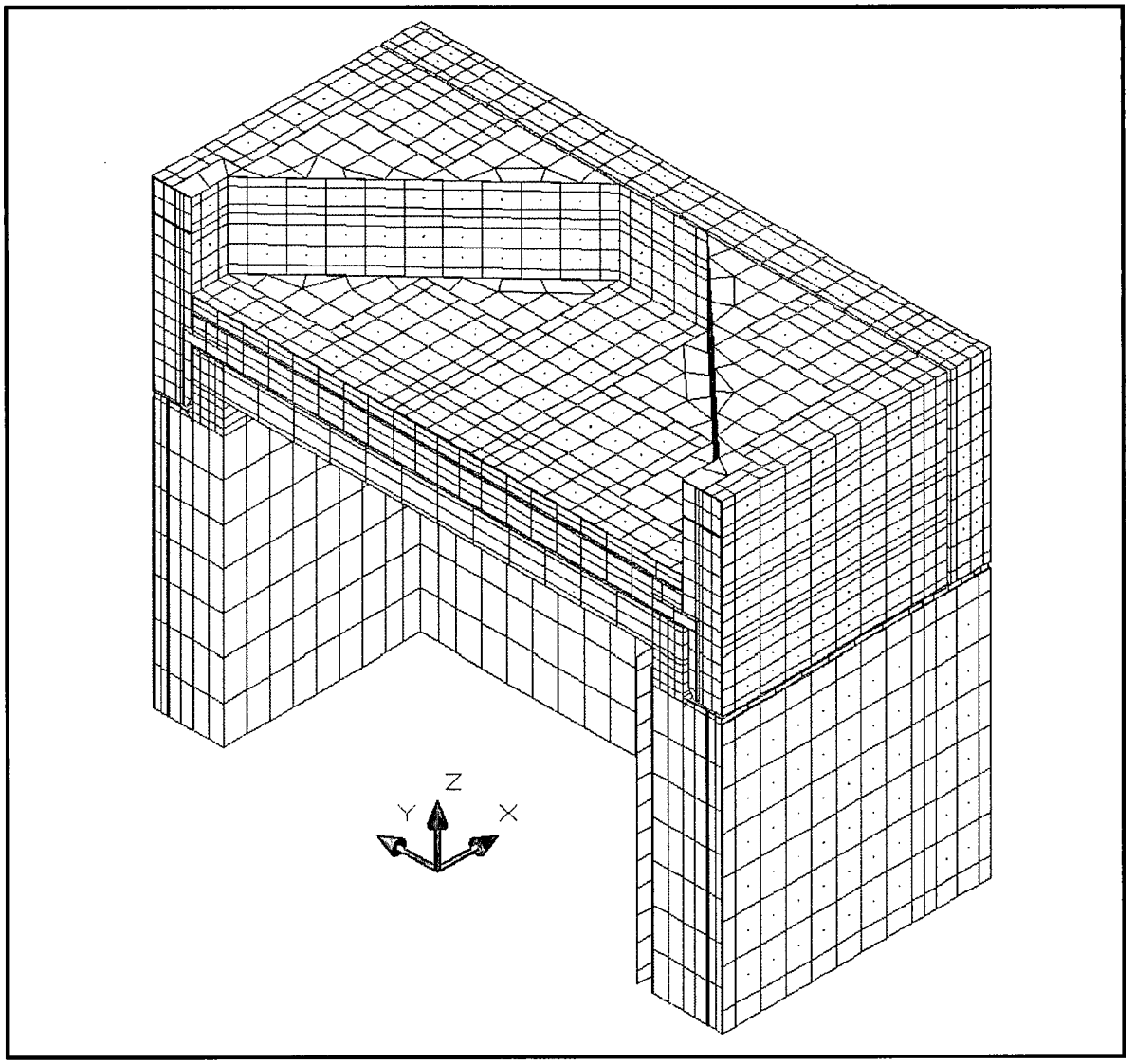

(Note: the positive y-axis is oriented towards the top of the package and the positive z-axis towards the package closure end)

Figure 3.5-1 – Perspective View of One-Quarter Symmetry TRUPACT–III Thermal Model

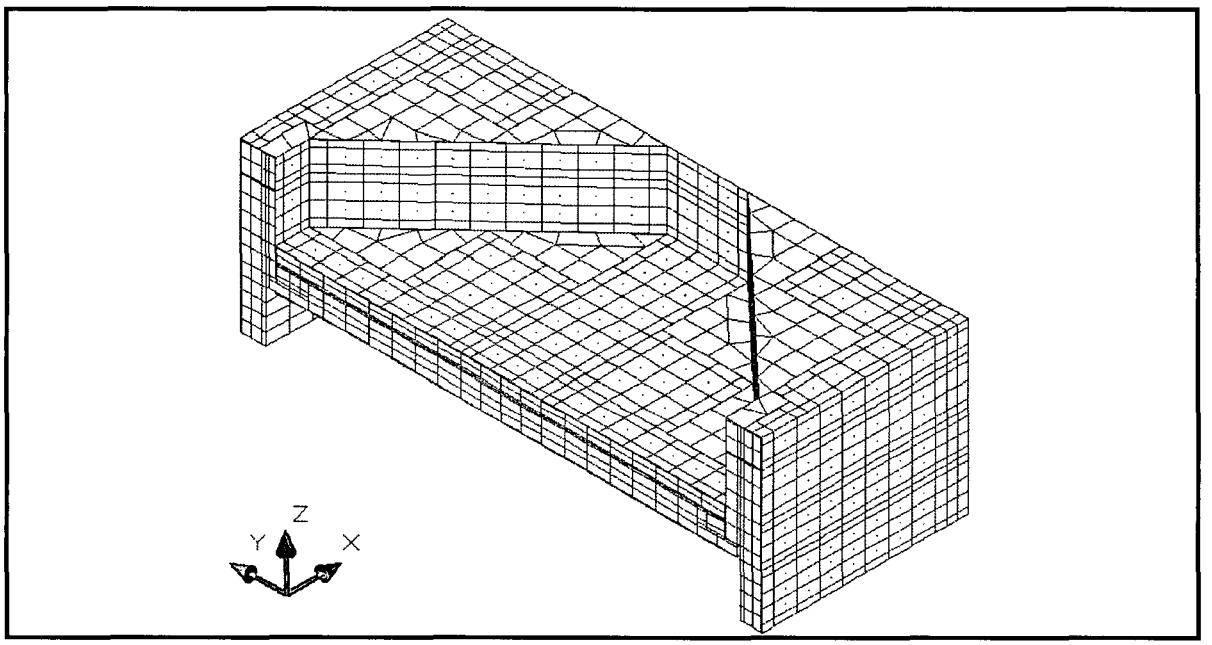

Figure 3.5-2 – Perspective View of Modeled Closure End

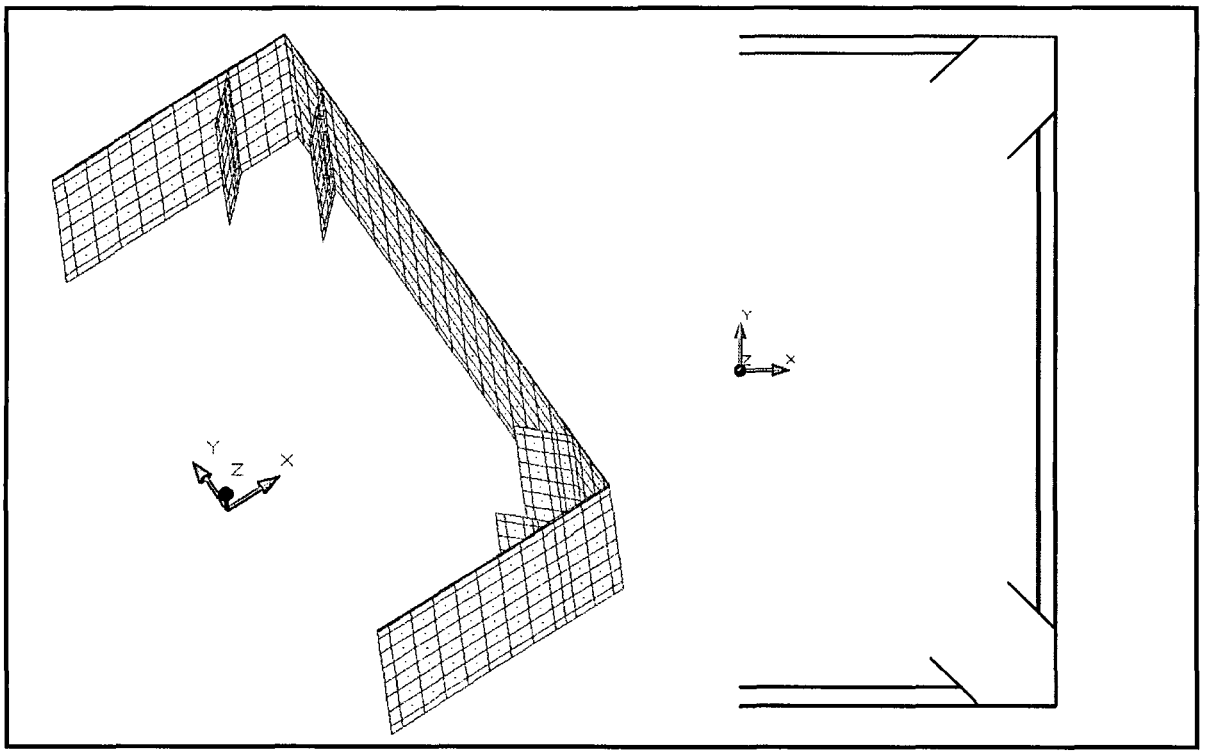

(Note: the positive y-axis is oriented towards the top of the package and the positive z-axis towards the package closure end)

Figure 3.5-3 – Perspective and Plan Views of Modeled Outer Skin, Puncture Protection Plate, and Corner Ribs

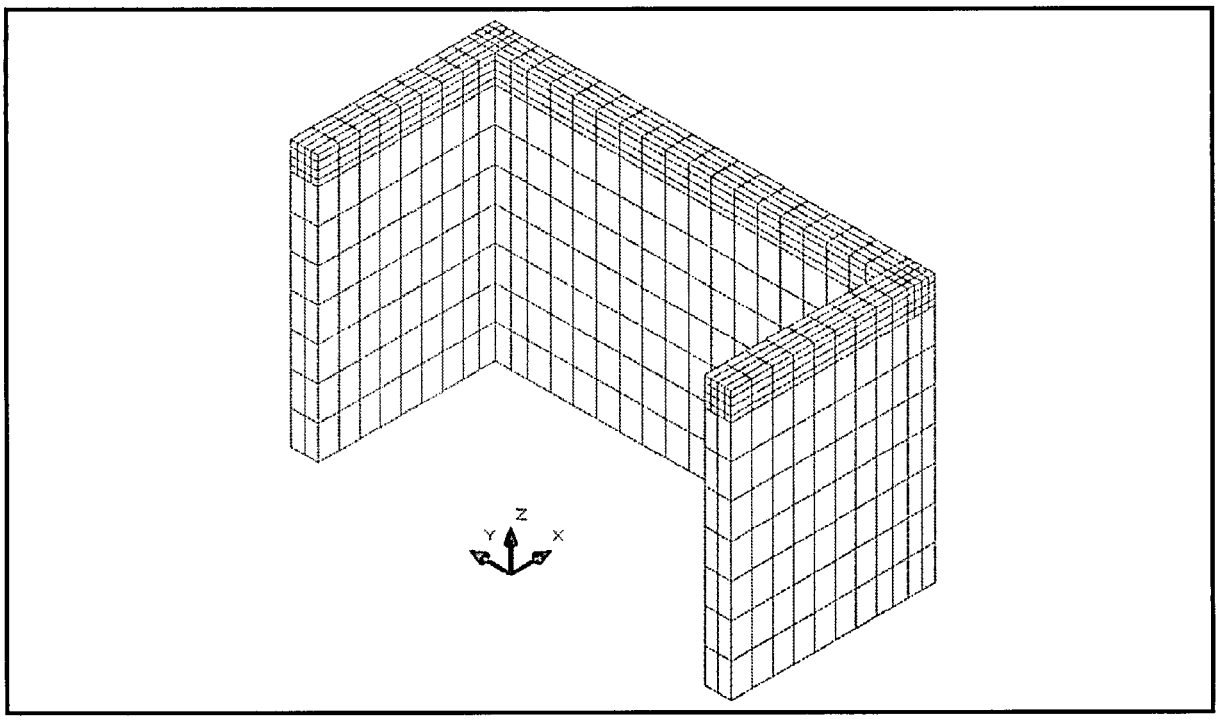

Note: the positive y-axis is oriented towards the top of the package and the positive z-axis towards the package closure end)

Figure 3.5-4 – Perspective View of CSA Thermal Model

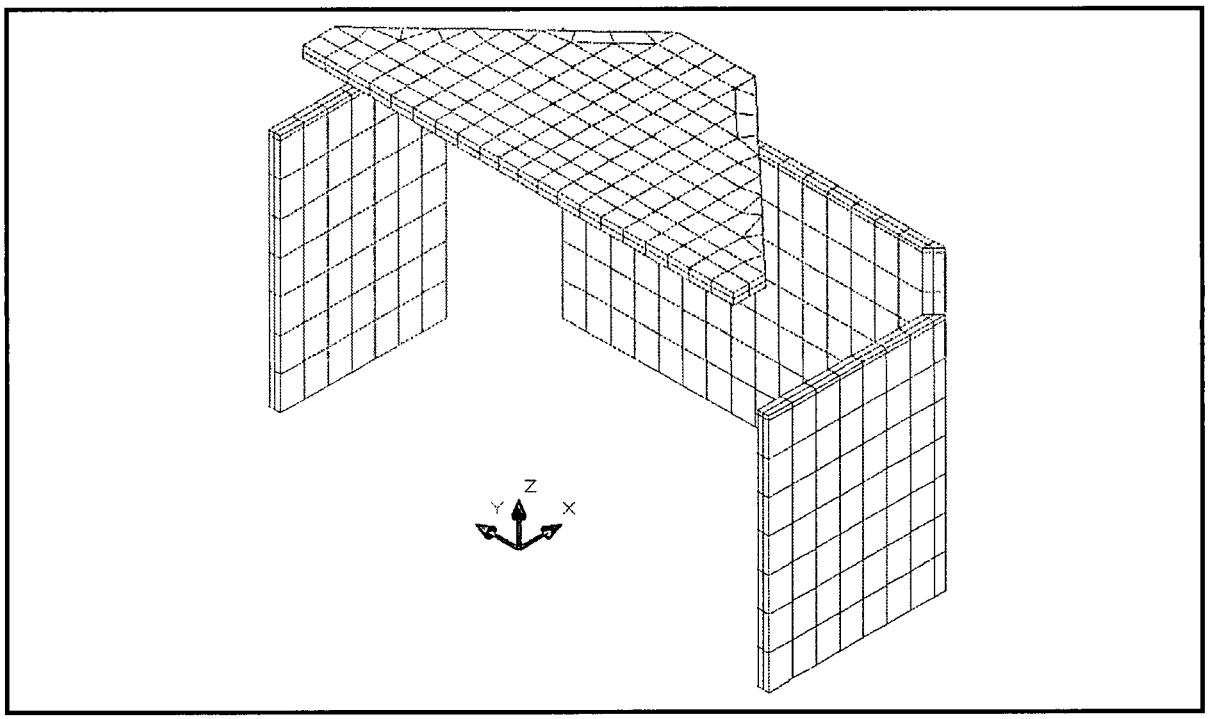

(Note: the positive y-axis is oriented towards the top of the package and the positive z-axis towards the package closure end)

Figure 3.5-5 – Perspective View of Modeled Balsa

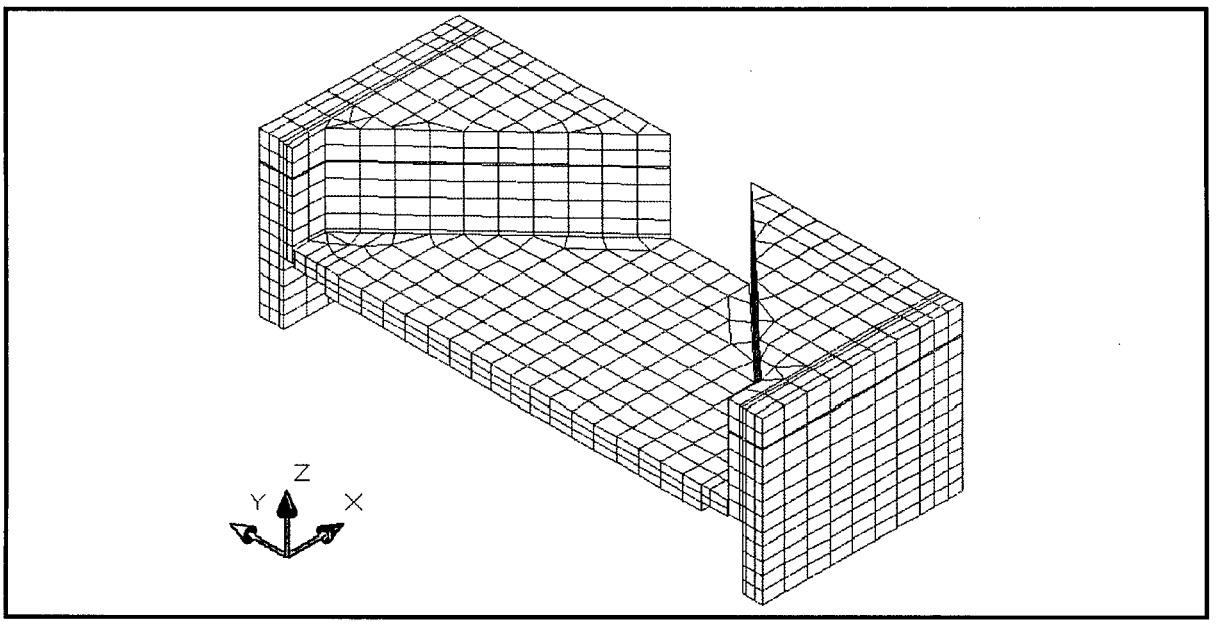

Note: the positive y-axis is oriented towards the top of the package and the positive z-axis towards the package closure end)

Figure 3.5-6 – Perspective View of Modeled Closure End Polyurethane Foam

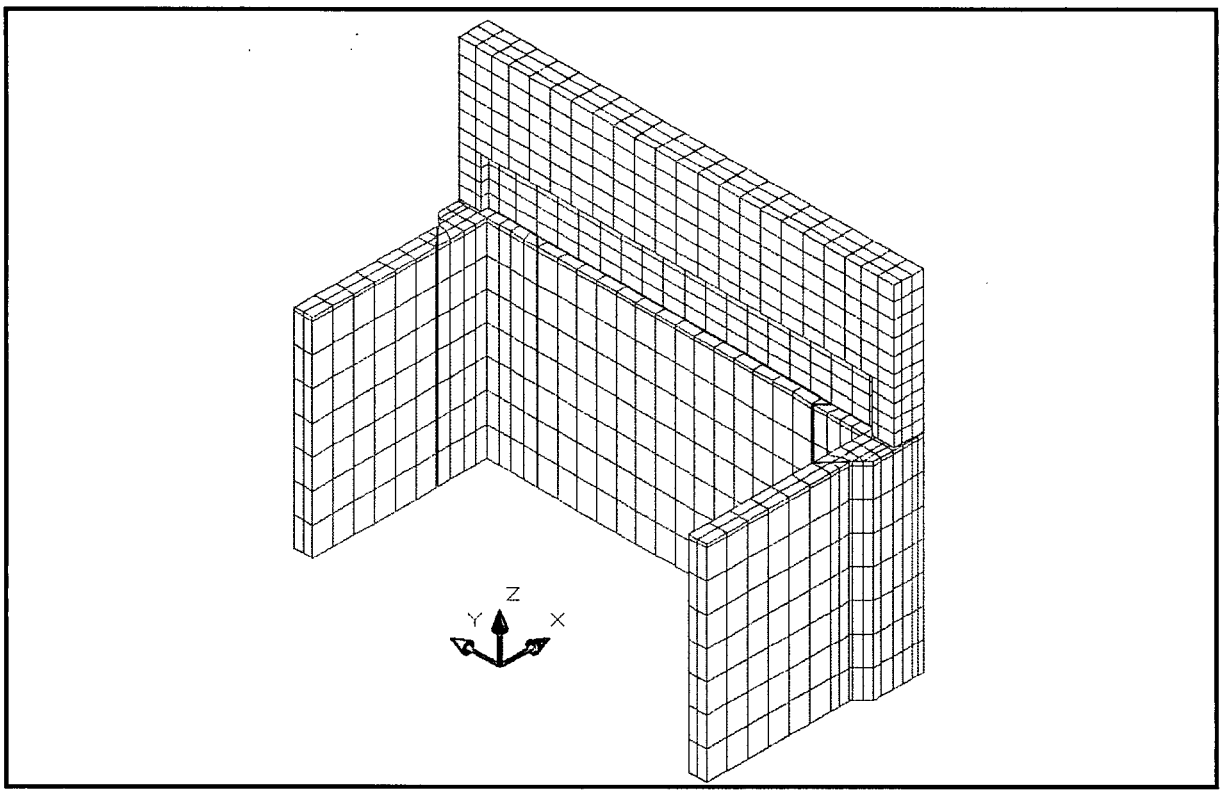

(Note: the positive y-axis is oriented towards the top of the package and the positive z-axis towards the package closure end)

Figure 3.5-7 – Perspective View of Modeled Package Polyurethane Foam

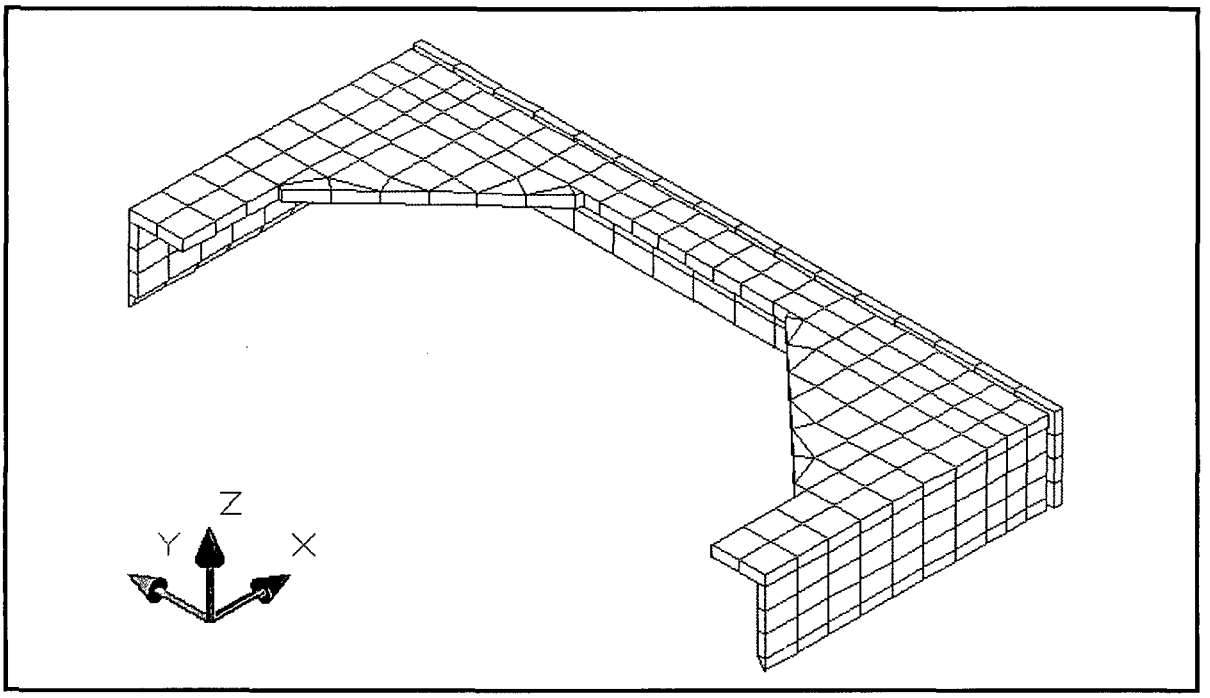

Note: the positive y-axis is oriented towards the top of the package and the positive z-axis towards the package closure end)

Figure 3.5-8 – Perspective View of Modeled Calcium Silicate Insulation

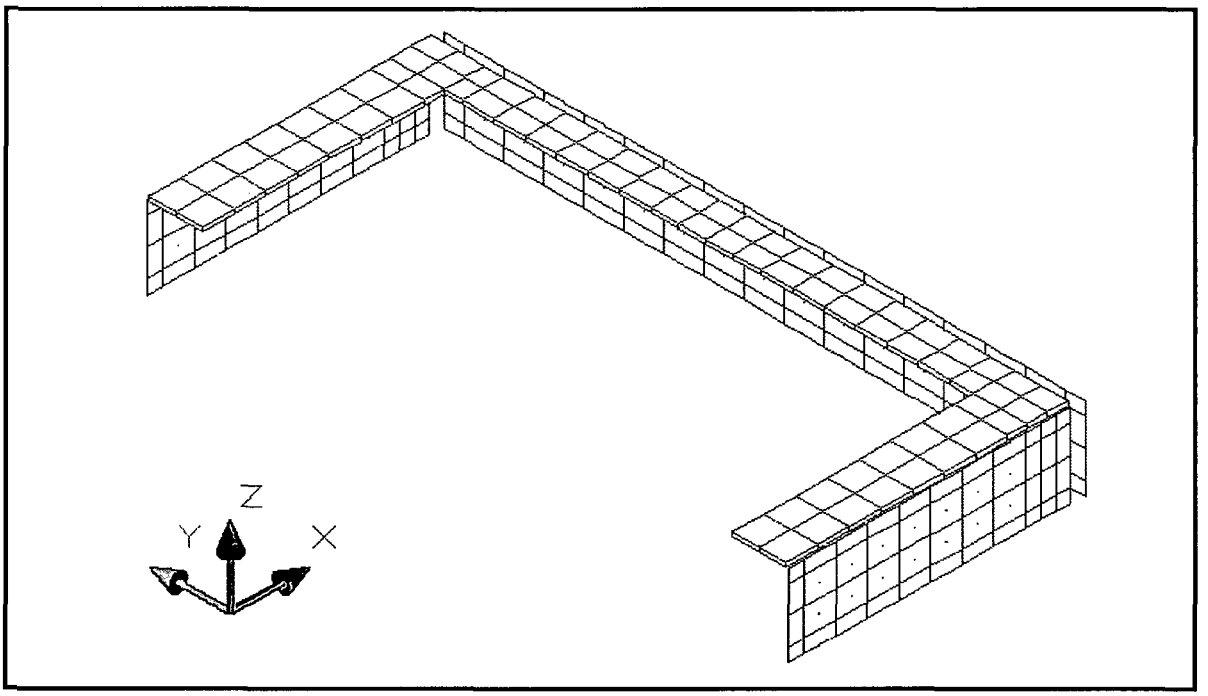

(Note: the positive y-axis is oriented towards the top of the package and the positive z-axis towards the package closure end.)

Figure 3.5-9 – Perspective View of Modeled 16-mm Protection Plates

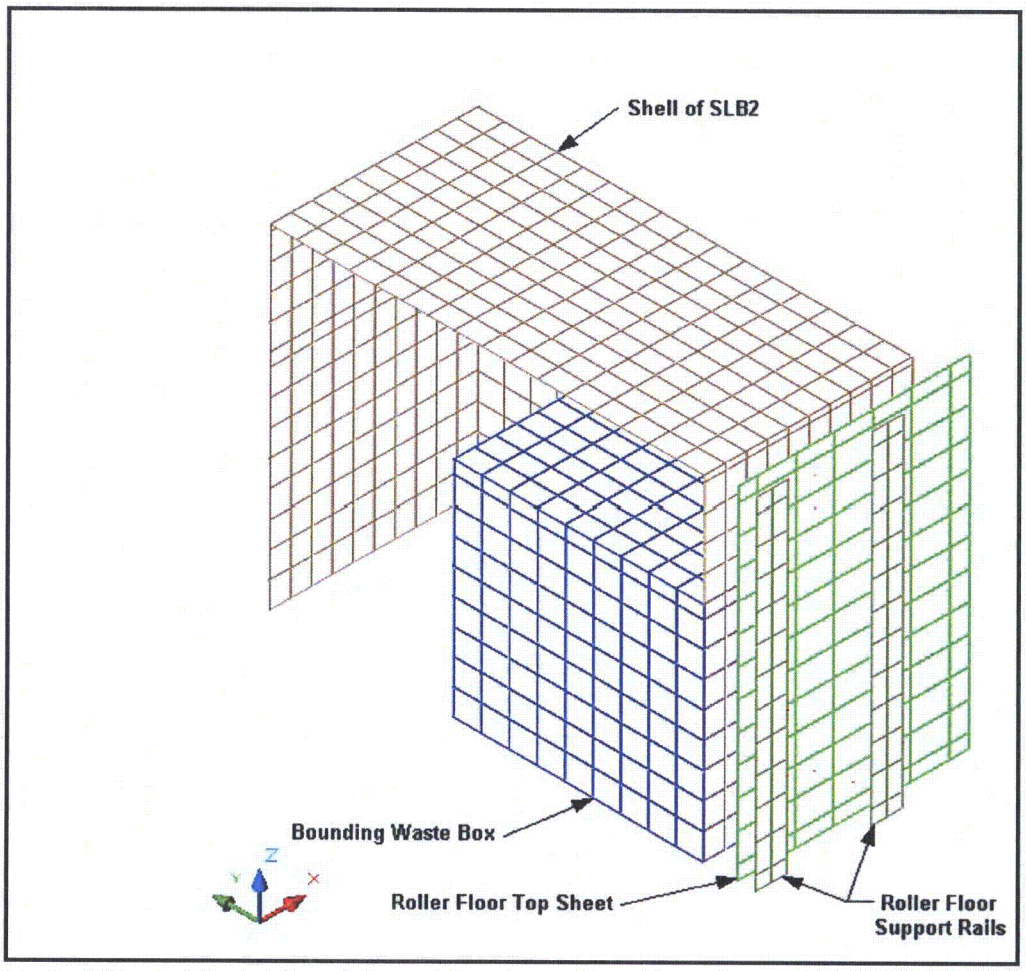

(Note: the positive y-axis is oriented towards the top of the package and the positive z-axis towards the package closure end)

Figure 3.5-10 – SLB2 Model (Shown with Hypothetical Bounding Waste Box Form and Roller Floor)

3.5.2.2 Convection Coefficient Calculation

The convective heat transfer coefficient, h_c, has a form of:

$$h_c = Nu\frac{k}{L}$$

where k is the thermal conductivity of the gas at the mean film temperature and L is the characteristic length of the vertical or horizontal surface.

Natural convection from each surface is computed based on semi-empirical relationships using the local Rayleigh number and the characteristic length for the surface. The Rayleigh number is defined as:

where $$Ra_L = \frac{\rho^2 g_c \beta L^3 \Delta T}{\mu^2} \times Pr$$

g_c = gravitational acceleration, 9.81 m/s^2

β = coefficient of thermal expansion, K^{-1}

ΔT = temperature difference, °C

ρ = density of air at the film temperature, g/m^3

μ = dynamic viscosity, N-s/m^2

Pr = Prandtl number = (c_p μ) / k

L = characteristic length, m

k = thermal conductivity of air film temperature, W/m-K

c_p = specific heat, J/g-°C

Ra_L = Rayleigh #, based on length 'L'

Note that k, c_p, and μ are each a function of air temperature as taken from Table 3.2-9. Values for ρ are computed using the ideal gas law, β for an ideal gas is simply the inverse of the absolute temperature of the gas, and Pr is computed using the values for k, c_p, and μ from Table 3.2-9. Unit conversion factors are used as required to reconcile the units for the various properties used.

The natural convection from a discrete vertical surface is computed using Equation 4-33 of Rohsenow, et. al. [5], which is applicable over the range 1 < Rayleigh number (Ra) < 10^{12}:

$$Nu^T = \overline{C}_L Ra^{1/4}$$

$$\overline{C}_L = \frac{0.671}{\left(1+(0.492/Pr)^{9/16}\right)^{4/9}}$$

$$Nu_L = \frac{2.0}{\ln\left(1+2.0/Nu^T\right)}$$

$$Nu_t = \frac{C_t^V Ra^{1/3}}{\left(1+1.4x10^9\ Pr/Ra\right)}$$

[5] Rohsenow, Hartnett, and Choi, *Handbook of Heat Transfer*, 3rd edition, McGraw-Hill Publishers, 1998.

$$C_t^V = \frac{0.13\,Pr^{0.22}}{\left(1+0.61\,Pr^{0.81}\right)^{0.42}}\left[1+0.78\left(\frac{T_{wall}}{T_\infty}-1\right)\right]$$

where T_{wall} and T_∞ are in terms of absolute temperature.

$$Nu = \frac{h_c L}{k} = \left[(Nu_L)^6 + (Nu_t)^6\right]^{1/6}$$

Natural convection from horizontal surfaces is computed from Equations 4.39 and 4.40 of Rohsenow, et. al.[5], and Equations 3.34 to 3.36 of Guyer [6], where the characteristic dimension (L) is equal to the plate surface area divided by the plate perimeter. For a heated surface facing upwards or a cooled surface facing downwards and Ra > 1:

$$Nu = \frac{h_c L}{k} = \left[(Nu_L)^{10} + (Nu_t)^{10}\right]^{1/10}$$

$$Nu_L = \frac{1.4}{\ln\left(1+1.677/\left(\overline{C_L}Ra^{1/4}\right)\right)}$$

$$\overline{C_L} = \frac{0.671}{\left[1+(0.492/Pr)^{9/16}\right]^{4/9}}$$

$$Nu_t = 0.14Ra^{1/3}$$

For a heated surface facing downwards or a cooled surface facing upwards and $10^3 < Ra < 10^{10}$, the correlation is as follows:

$$Nu = Nu_L = \frac{2.5}{\ln\left(1+2.5/Nu^T\right)}$$

$$Nu^T = \frac{0.527}{\left(1+(1.9/Pr)^{9/10}\right)^{2/9}}Ra^{1/5}$$

The forced convection coefficients applied during the HAC fire event are computed using the relationships in Table 6-5 of *Principles of Heat Transfer*[7] for flat surfaces where the characteristic dimension (L) is equal to the length along the surface. For Reynolds number (Re) < 5×10^5 and Prandtl number (Pr) > 0.1:

$$Nu = 0.664\,Re_L^{0.5}\,Pr^{0.33}$$

For Reynolds number (Re) > 5×10^5 and Prandtl number (Pr) > 0.5:

$$Nu = 0.036\,Pr^{0.33}[Re_L^{0.8} - 23{,}200]$$

[6] Guyer, E.C., *Handbook of Applied Thermal Design*, McGraw-Hill, Inc., 1989.

[7] Kreith, Frank, *Principles of Heat Transfer*, 3rd edition, Harper & Row, 1973.

3.5.2.3 Insolation Loads

The thermal loading on the TRUPACT–III during NCT arises from insolation on the outer skin of the package and, to a much lesser degree, from the decay heat of the payload. The 10CFR71.71(c)(1) insolation values represent the total insolation over a 12-hour period. The presence of the balsa wood and polyurethane foam in the package wall and shock absorbing structures will thermally isolate the interior of the package from the external environment. The presence of these materials and the relatively thin exterior skin of the package will result in the peak surface temperatures of the package responding rapidly to changes in the external environment. As such, transient modeling of the insolation loading provides the best means of capturing both the peak temperatures near the exterior of the package while not underestimating the peak payload temperatures and vice-versa.

A sine wave model is used to simulate the variation in the applied insolation on the surfaces of the package over a 24-hour period, except that when the sine function is negative, the insolation level is set to zero. The timing of the sine wave is set to achieve its peak at 12 pm and peak value of the curve is adjusted to ensure that the total energy delivered matched the values in 10 CFR §71.71(c)(1). As such, the total energy delivered in one day by the sine wave solar model is given by:

$$\int_{6\cdot hr}^{18\cdot hr} Q_{peak}\cdot\sin\left(\frac{\pi\cdot t}{12\cdot hr}-\frac{\pi}{2}\right)dt=\left(\frac{24\cdot hr}{\pi}\right)\cdot Q_{peak}$$

Using the expression above for the peak rate of insolation, the peak rates for top and side insolation may be calculated as follows:

$$Q_{top}=\left(800\frac{cal}{cm^2}\right)\cdot\left(\frac{\pi}{24\,hr}\right) \qquad Q_{top}=1.218\times10^{-3}\frac{W}{mm^2}$$

$$Q_{side}=\left(200\frac{cal}{cm^2}\right)\cdot\left(\frac{\pi}{24\,hr}\right) \qquad Q_{side}=3.045\times10^{-4}\frac{W}{mm^2}$$

Conversion factors of 1 cal/sec. = 4.1868 W and 1 cal/cm^2-hr = 1.163 x 10^{-5} W/mm^2 are used in the above calculation. These peak rates are multiplied by the sine function to create the top and side insolation values as a function of time of day.

3.5.2.4 Effective Thermal Properties for Corrugated Wall/Lid Structures

The walls and lid of the TRUPACT–III container are corrugated structures comprised of inner and outer plates separated by V-stiffeners on approximately 164-mm centers. The enclosed void volumes are filled with air at atmospheric pressure. Figure 1.1-5 from Section 1.1, *Introduction*, illustrates a typical cross-section of the container wall and closure lid. The overall 140-mm wall thickness of the container wall is comprised of two 8-mm sheets and 4-mm thick V-stiffeners inclined at an approximately 67 degree angle. The closure lid has a similar cross-section, except that the inner and outer plates are 12-mm thick and the V-stiffeners are on 165-mm centers.

Modeling the exact geometry of the container's wall and lid structures would be node intensive and unnecessary, given the relatively low temperature gradients expected. Instead, a set of effective thermal properties are developed which permits the walls and lid to be simulated as

homogeneous solids. The effective thermal properties, based on the temperature dependant properties for Alloy UNS S31803 stainless steel, consists of a set of anisotropic (i.e., direction dependant) thermal conductivities, an effective density value, and specific heat values. Figure 3.5-11 illustrates the thermal model segment used to develop the effective thermal properties for the prototypic wall section. A similar thermal model, but with the appropriate dimensional changes, is used to compute the effective thermal properties for the lid section.

The Figure 3.5-11 model segment represents a symmetrical section of the container wall that is 164-mm long × 164-mm wide × 140-mm thick (132-mm between the centerlines of the inner and outer walls). A total of approximately 300 nodes are used to represent the temperature distribution across the wall/rib surfaces and the enclosed air volume. A constant heat flux condition is assumed on the inner wall of the model segment, while a constant temperature condition is assumed on the outer wall. Adiabatic boundary conditions are assumed at the remaining four edges of the modeled segment. Perfect connection between the ends of the V-stiffeners and the containment sheet is assumed to simulate the continuous seam welds, while the plug welded connection between the flat of the V-stiffeners and the structural sheet is modeled using contact elements.

Computation of the effective thermal properties in the 'along' direction (i.e., into the page for the Figure 3.5-11 plan view) is based on an area weighted average of the material cross-sections. For the wall segments with 8-mm thick inner and outer plates the effective thermal conductivity is computed as:

$$\text{Area}_{\text{cross-section}} \times k_{\text{along-wall}} = \text{Area}_{\text{inner/outer plates}} \times k_{\text{318 Stainless steel}} + \text{Area}_{\text{ribs}} \times k_{\text{318 Stainless steel}}$$

$$(164\,\text{mm} \times 140\,\text{mm}) \times k_{\text{along-wall}} = (2 \times 164\,\text{mm} \times 8\,\text{mm}) \times k_{\text{318 Stainless steel}} + (2 \times 136.694\,\text{mm} + 35\,\text{mm}) \times 4\,\text{mm} \times k_{\text{318 Stainless steel}}$$

$$k_{\text{along-wall}} = 0.16801 \times k_{\text{318 Stainless steel}}$$

It should be noted that the 136.694 mm dimension in the above equation is obtained from the modeled length of the 'v' in the thermal model.

The contributions of the air and radiation are conservatively ignored. The effective thermal conductivity for the lid structure is higher due to the 50% greater thickness in the inner and outer plates. The effective thermal conductivity for the 'along' direction of the lid is:

$$(165\,\text{mm} \times 148\,\text{mm}) \times k_{\text{along-lid}} = (2 \times 165\,\text{mm} \times 12\,\text{mm}) \times k_{\text{318 Stainless steel}} + (2 \times 139.715\,\text{mm} + 39\,\text{mm}) \times 4\,\text{mm} \times k_{\text{318 Stainless steel}}$$

$$k_{\text{along-lid}} = 0.21432 \times k_{\text{318 Stainless steel}}$$

The 139.715 mm dimension in the above equation is obtained from the modeled length of the 'v' in the thermal model.

The effective thermal properties in the 'axial' direction of the container wall (i.e., across the Figure 3.5-11 plan view) is computed in a similar fashion via the following equation:

$$\text{Area}_{\text{cross-section}} \times k_{\text{axial-wall}} = \text{Area}_{\text{inner/outer plates}} \times k_{\text{318 Stainless steel}}$$

$$(\text{unit length} \times 140\,\text{mm}) \times k_{\text{axial-wall}} = 2 \times (\text{unit length} \times 8\,\text{mm}) \times k_{\text{318 Stainless steel}}$$

$$k_{\text{axial-wall}} = 0.114286 \times k_{\text{318 Stainless steel}}$$

Again, the effective thermal conductivity for the lid structure is higher due to the thicker inner and outer plates. The effective thermal conductivity for the 'axial' direction of the lid is:

$$(\text{unit length} \times 148\,\text{mm}) \times k_{\text{axial-lid}} = 2 \times (\text{unit length} \times 12\,\text{mm}) \times k_{\text{318 Stainless steel}}$$

$$k_{\text{axial-lid}} = 0.162162 \times k_{\text{318 Stainless steel}}$$

As seen, these formulations for the 'axial' thermal conductivity conservatively ignore the contribution of ribs in addition to the contributions of the air and radiation.

In contrast to the 'along' and 'axial' thermal conductivity, the contributions of heat transfer through the enclosed air and radiation exchange is more significant for the computation of the effective thermal conductivity through the wall/lid structures (i.e., between the inner and outer plates). Further, the interaction between the ribs and the inner and outer plates is complex. As such, the 'thru' thermal conductivity was evaluated using the lumped model depicted in Figure 3.5-11 and the Thermal Desktop™ and SINDA/FLUINT™ programs. A constant heat flux condition is assumed on the inner wall, while a constant temperature condition is assumed on the outer wall. The constant heat flux condition was determined assuming the maximum payload heat load of 80 watts and an even distribution over the surface area of the container's sides, top, and ends (the floor is conservatively ignored given the presence of the roller floor and pallet). The resulting heat flux is equal to 80 watts/(2 × 2.790 m × 2.0 m + 2.790 m × 1.840 m + 2 × 2.0 m × 1.840 m), or 3.3821 watts/m^2. The thermal model was exercised for a range of boundary temperature conditions and the temperature results used to compute the effective 'thru' thermal conductivity for the CSA wall via the equation:

$$Q_{\text{thru-wall}} = \text{Section Area/Section Thickness} \times k_{\text{thru}} \times \Delta T$$

$$3.3821 \frac{\text{watts}}{\text{m}^2} \times (0.164\,\text{m})^2 = (164\,\text{mm} \times 164\,\text{mm})/140\,\text{mm} \times k_{\text{thru-wall}} \times$$

$$(\text{Ave. Inner Wall Temp.} - \text{Ave. Outer Wall Temp.})$$

$$k_{\text{thru-wall}} = 0.090965\,\text{watts} \times 5.2052\,\text{m}^{-1} / (\text{Ave. Inner Wall Temp.} - \text{Ave. Outer Wall Temp.})$$

The 'thru' conductivity for the container lid is computed in a similar fashion, but with adjustment given its greater overall thickness, thicker inner and outer plates, and different rib geometry. The Figure 3.5-11 thermal model was modified for these geometry differences and the results of the Thermal Desktop™ and SINDA/FLUINT™ modeling used with the following equation:

$$k_{\text{thru-lid}} = 0.092078\,\text{watts} \times 5.4362\,\text{m}^{-1} / (\text{Ave. Inner Lid Temp.} - \text{Ave. Outer Lid Temp.})$$

Table 3.2-2 and Table 3.2-3 present the computed 'thru', 'along', and 'axial' thermal conductivity values for a range of temperatures based on the results of the Thermal Desktop® and SINDA/FLUINT modeling. The 'along' and 'axial' thermal conductivity values are computed using the thermal conductivity for Alloy UNS S31803 stainless steel (see Table 3.2-4) and the multiplication factors determined above. The effective densities of the container wall and lid sections are determined as volume weighted functions of the Alloy UNS S31803 stainless steel values where:

$$\text{Volume}_{\text{cross-section}} \times \rho_{\text{effective}} = \text{Volume}_{\text{inner/outer plates}} \times \rho_{\text{318 Stainless steel}} + \text{Volume}_{\text{ribs}} \times \rho_{\text{318 Stainless steel}}$$

Thus, $$\rho_{\text{wall-effective}} = 0.16801 \times \rho_{\text{318 Stainless steel}}$$

$$\rho_{\text{wall-effective}} = 1.33\ \text{kg/dm}^3$$

and $$\rho_{\text{lid-effective}} = 0.21432 \times \rho_{\text{318 Stainless steel}}$$

$$\rho_{\text{lid-effective}} = 1.69\ \text{kg/dm}^3$$

The specific heat of the container walls and lid are assumed to be the same as Alloy UNS S31803 stainless steel.

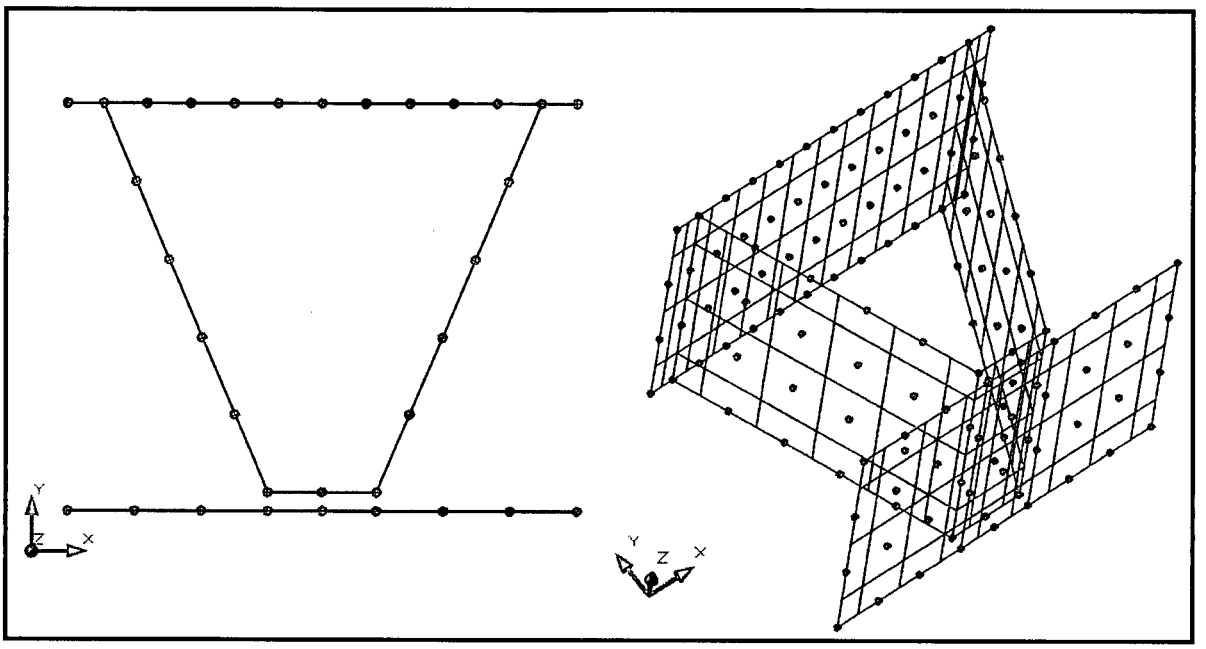

Figure 3.5-11 – Plan and Perspective Views of Container Wall Section Model for Effective Thermal Conductivity Calculation

3.5.2.5 Effective Thermal Properties for CSA End Detail & Lid Perimeter

CSA End Detail

The effective thermal properties for the walls of the CSA body developed in Section 3.5.2.4, *Effective Thermal Properties for Corrugated Wall/Lid structures*, are appropriate for defining the heat transfer through the CSA structure for all but the structural detail at the closure end. At this location, the structure is defined by a box beam structure as illustrated in Figure 3.5-12 and Figure 3.5-13. The design illustrated in these figures represents a slight modification from the preliminary design used to develop the thermal model (see Figure 3.5-14). The differences consist of a thickening of the front plate from 19 mm to 25 ± 5 mm and the elimination of the 35 mm lightening hole on the backside of the closure bolt bar stock. Since these design changes provide a greater thermal mass and a higher effective thermal conductance in the transverse direction, ignoring the design change is conservative for NCT conditions. The thermal gradients are low enough that a composite of the thermal properties for each location can be used to define the thermal performance of the structure around its entire circumference.

The effective thermal properties in the axial direction (i.e., along the z-axis of the package) in the segments not encompassing the closure bolt insertions can be defined on a per unit length as:

$$k_{axial} = \frac{\text{Actual Heat Transfer Area}}{\text{Full Area}} \times k_{318\,\text{Stainless steel}}$$

$$k_{axial} = \frac{(2 \times 15\,\text{mm}) \times 1\,\text{mm}}{140\,\text{mm} \times 1\,\text{mm}} \times k_{318\,\text{Stainless steel}}$$

$$k_{axial} = 0.2143 \times k_{318\,\text{Stainless steel}}$$

The bolt inserts are on 198 mm centers and are fabricated of 70 mm diameter bar stock with 35 mm diameter holes drilled from one direction. Therefore, the minimum axial heat transfer area of each bolt insert is:

$$\text{Area}_{insert} = \left[\left(\frac{70}{2}\right)^2 - \left(\frac{35}{2}\right)^2\right] \times \pi$$

$$\text{Area}_{insert} = 2{,}886.3\,\text{mm}^2$$

Therefore, the effective axial heat transfer, including the effect of the bolt inserts, is:

$$k_{axial} = \frac{(2 \times 15\,\text{mm} \times 198\,\text{mm} + 2{,}886.3\,\text{mm}^2)}{140\,\text{mm} \times 198\,\text{mm}} \times k_{318\,\text{Stainless steel}}$$

$$k_{axial} = 0.318 \times k_{318\,\text{Stainless steel}}$$

The effective thermal properties in the transverse direction (i.e., vertically, across the plane of Figure 3.5-12 or Figure 3.5-13) can be defined in a similar manner. Conservatively ignoring the thicker front plate provided by the latest design iteration and using the Figure 3.5-14 design layout, the transverse thermal conductivity is defined as:

$$k_{transverse} = \frac{\text{Actual Heat Transfer Area}}{\text{Full Area}} \times k_{318\,\text{Stainless steel}}$$

$$k_{transverse} = \frac{(19\,\text{mm} + 10\,\text{mm}) \times 198\,\text{mm}}{145\,\text{mm} \times 198\,\text{mm}} \times k_{318\,\text{Stainless steel}}$$

$$k_{transverse} = 0.20 \times k_{318\,\text{Stainless steel}}$$

Finally, the effective thermal properties along the CSA's structural end detail (i.e., into the plane of Figure 3.5-12 or Figure 3.5-13) can be defined in a similar manner. While the holes in the structure for the lid bolts will have only a local effect, it is simpler and conservative to reduce the heat transfer area by their diameter. Based on this approach, the effective thermal conductivity is computed as:

$$k_{along} = \frac{\text{Actual Heat Transfer Area}}{\text{Full Area}} \times k_{318\,\text{Stainless steel}}$$

$$k_{along} = \frac{(19\,\text{mm} + 10\,\text{mm}) \times (140\,\text{mm} - 35\,\text{mm for bolt holes}) + (2 \times 15\,\text{mm}) \times (145\,\text{mm} - 19\,\text{mm} - 10\,\text{mm})}{140\,\text{mm} \times 145\,\text{mm}} \times k_{318\,\text{Stainless steel}}$$

$$k_{along} = 0.321 \times k_{318\,\text{Stainless steel}}$$

The effective density of the CSA end detail is determined as a volume weighted function of the Alloy UNS S31803 stainless steel values where:

$$\text{Volume}_{section} \times \rho_{\text{CSA-effective}} = \text{Volume}_{\text{inner/outer plates}} \times \rho_{318\,\text{Stainless steel}} + \text{Volume}_{\text{bolt insert}} \times \rho_{318\,\text{Stainless steel}}$$

$$\rho_{\text{CSA-effective}} = [(19\,\text{mm} + 10\,\text{mm}) \times 140\,\text{mm} \times 198\,\text{mm} + (2 \times 15\,\text{mm} \times 116\,\text{mm}) \times 198\,\text{mm} + 2{,}886.3\,\text{mm}^2 \times 116\,\text{mm}] / (145\,\text{mm} \times 140\,\text{mm} \times 198\,\text{mm}) \times \rho_{318\,\text{Stainless steel}}$$

$$\rho_{\text{CSA-effective}} = 0.455 \times \rho_{318\,\text{Stainless steel}}$$

The specific heat is the same as Alloy UNS S31803 stainless steel.

Since ignoring the thicker front plate thickness is non-conservative for HAC conditions, the effective thermal properties used in the HAC modeling are re-computed based on the maximum dimensions depicted in Figure 3.5-12 and Figure 3.5-13.

$$k_{transverse} = \frac{((25 + 5)\,\text{mm} + 10\,\text{mm}) \times 198\,\text{mm}}{145\,\text{mm} \times 198\,\text{mm}} \times k_{318\,\text{Stainless steel}}$$

$$k_{transverse} = 0.276 \times k_{318\,\text{Stainless steel}}$$

$$k_{along} = \frac{(30\,\text{mm} + 10\,\text{mm}) \times (140\,\text{mm} - 35\,\text{mm for bolt hole}) + (2 \times 15\,\text{mm}) \times (145\,\text{mm} - 30\,\text{mm} - 10\,\text{mm})}{140\,\text{mm} \times 145\,\text{mm}} \times k_{318\,\text{Stainless steel}}$$

$$k_{along} = 0.362 \times k_{318\,\text{Stainless steel}}$$

The thermal conductivity in the axial direction is the same as used for NCT conditions. For conservatism, the effective density computed for NCT conditions is used.

Lid Perimeter

The perimeter of the CSA closure lid incorporates a box beam edge detail as depicted in Figure 3.5-15. The effective thermal properties for this portion of the lid are computed in the same manner as that presented above for the CSA end structure. The effective thermal properties in the axial direction (i.e., along the z-axis of the package) in the segments not encompassing the closure bolt insertions can be defined on a per unit length as:

$$k_{axial} = \frac{\text{Actual Heat Transfer Area}}{\text{Full Area}} \times k_{318\,\text{Stainless steel}}$$

$$k_{axial} = \frac{(2 \times 16\,\text{mm}) \times 1\,\text{mm}}{140\,\text{mm} \times 1\,\text{mm}} \times k_{318\,\text{Stainless steel}}$$

$$k_{axial} = 0.229 \times k_{318\,\text{Stainless steel}}$$

The bolt inserts are on 198 mm centers and are fabricated of 64 mm diameter bar stock with a 44 mm inner diameter. Therefore, the area of each bolt insert is:

$$\text{Area}_{insert} = \left[\left(\frac{64}{2}\right)^2 - \left(\frac{44}{2}\right)^2\right] \times \pi$$

$$\text{Area}_{insert} = 1{,}696.5\,\text{mm}^2$$

Therefore, the effective axial heat transfer, including the effect of the bolt inserts, is:

$$k_{axial} = \frac{(2 \times 16\,\text{mm} \times 198\,\text{mm} + 1{,}696.5\,\text{mm}^2)}{140\,\text{mm} \times 198\,\text{mm}} \times k_{318\,\text{Stainless steel}}$$

$$k_{axial} = 0.290 \times k_{318\,\text{Stainless steel}}$$

It should be noted that the thermal model assumes that $k_{axial} = 0.308 \times k_{318\,\text{Stainless steel}}$ based on earlier assumptions regarding the geometry of the bolt inserts. The 0.308 multiplier factor represents an approximately 6% higher value than the correct multiplier factor of 0.290. Since the principal heat transfer concern for this package arises during the HAC fire event when heat is moving into the package, the use of the higher multiplier factor will provide a conservative estimate of the peak temperature achieved in the package closure seal.

The effective thermal properties in the transverse direction (i.e., vertically, across the plane of Figure 3.5-15) can be defined in a similar manner as:

$$k_{transverse} = \frac{\text{Actual Heat Transfer Area}}{\text{Full Area}} \times k_{318\,\text{Stainless steel}}$$

$$k_{transverse} = \frac{(20\,\text{mm} + 20\,\text{mm}) \times 198\,\text{mm}}{148\,\text{mm} \times 198\,\text{mm}} \times k_{318\,\text{Stainless steel}}$$

$$k_{transverse} = 0.270 \times k_{318\,\text{Stainless steel}}$$

Finally, the effective thermal properties along the perimeter of the lid (i.e., into the plane of Figure 3.5-15) can be defined in a similar manner as:

$$k_{along} = \frac{\text{Actual Heat Transfer Area}}{\text{Full Area}} \times k_{318\,\text{Stainless steel}}$$

$$k_{along} = \frac{(20\,\text{mm} + 20\,\text{mm}) \times (140\,\text{mm} - 36\,\text{mm}) + (2 \times 16\,\text{mm}) \times (148\,\text{mm} - 2 \times 20\,\text{mm})}{140\,\text{mm} \times 148\,\text{mm}} \times k_{318\,\text{Stainless steel}}$$

$$k_{along} = 0.368 \times k_{318\,\text{Stainless steel}}$$

The effective density of the lid perimeter detail is determined as a volume weighted function of the Alloy UNS S31803 stainless steel values where:

$$\text{Volume}_{section} \times \rho_{\text{lid-effective}} = \text{Volume}_{\text{inner/outer plates}} \times \rho_{318\,\text{Stainless steel}} + \text{Volume}_{\text{bolt insert}} \times \rho_{318\,\text{Stainless steel}}$$

Thus,

$$\rho_{\text{lid-effective}} = [(2 \times 20\,\text{mm} \times 140\,\text{mm}) \times 198\,\text{mm} + (2 \times 16\,\text{mm} \times 108\,\text{mm}) \times 198\,\text{mm} + 2{,}199.1\,\text{mm}^2 \times 108\,\text{mm}] / (148\,\text{mm} \times 140\,\text{mm} \times 198\,\text{mm}) \times \rho_{318\,\text{Stainless steel}}$$

$$\rho_{\text{lid-effective}} = 0.495 \times \rho_{318\,\text{Stainless steel}}$$

The specific heat is the same as Alloy UNS S31803 stainless steel.

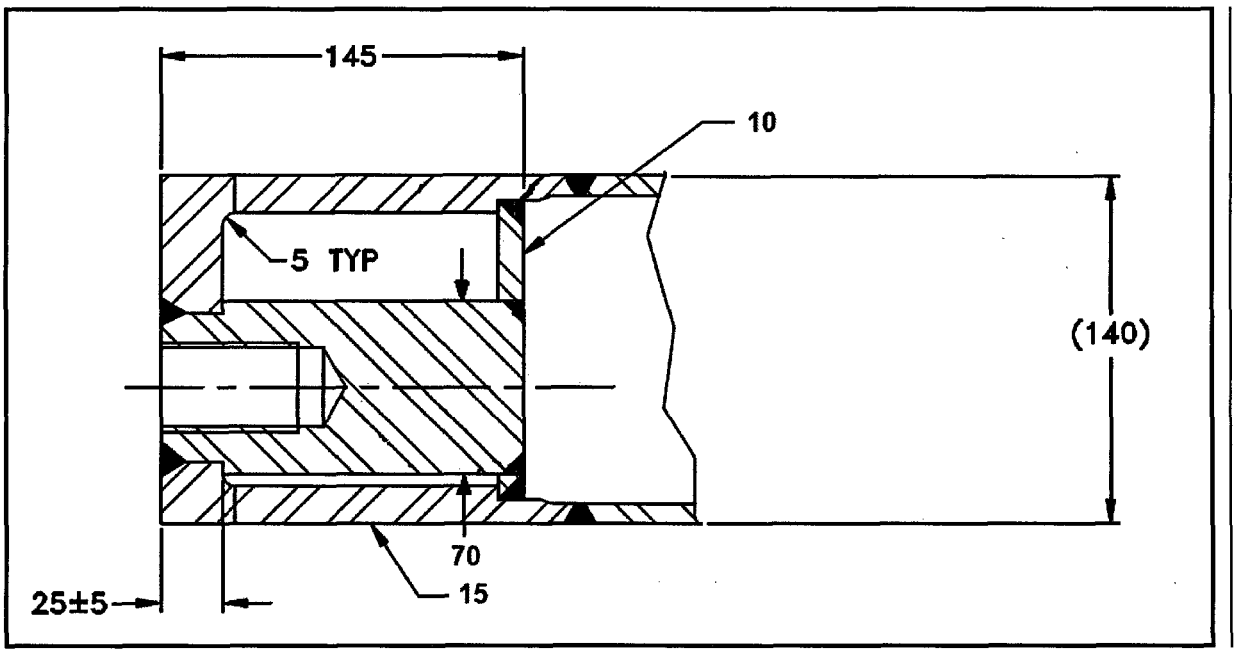

Figure 3.5-12 – CSA End Detail at Location of Closure Bolts

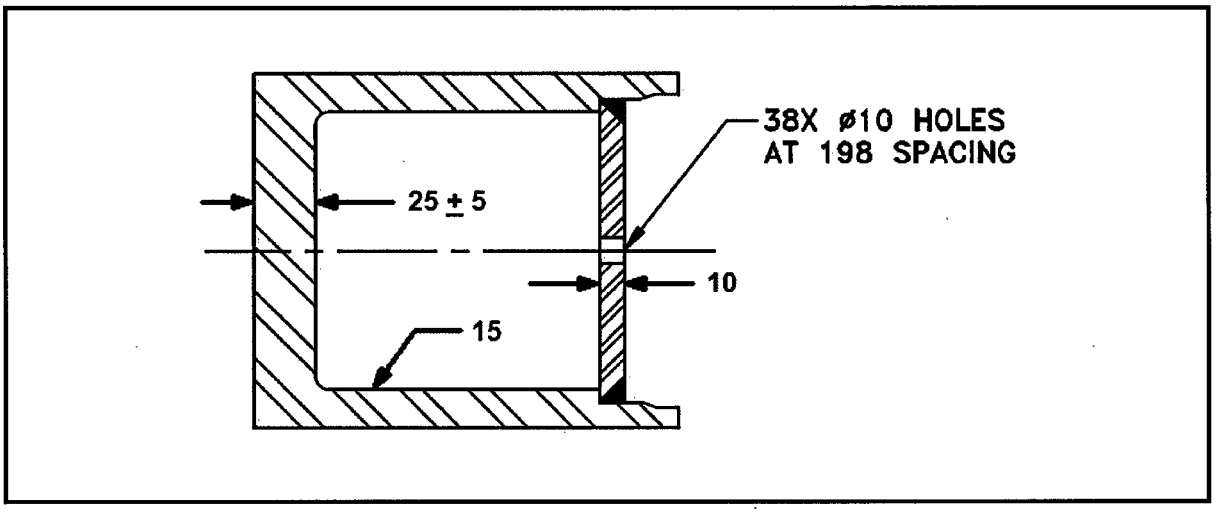

Figure 3.5-13 – CSA End Detail at Locations between Closure Bolts

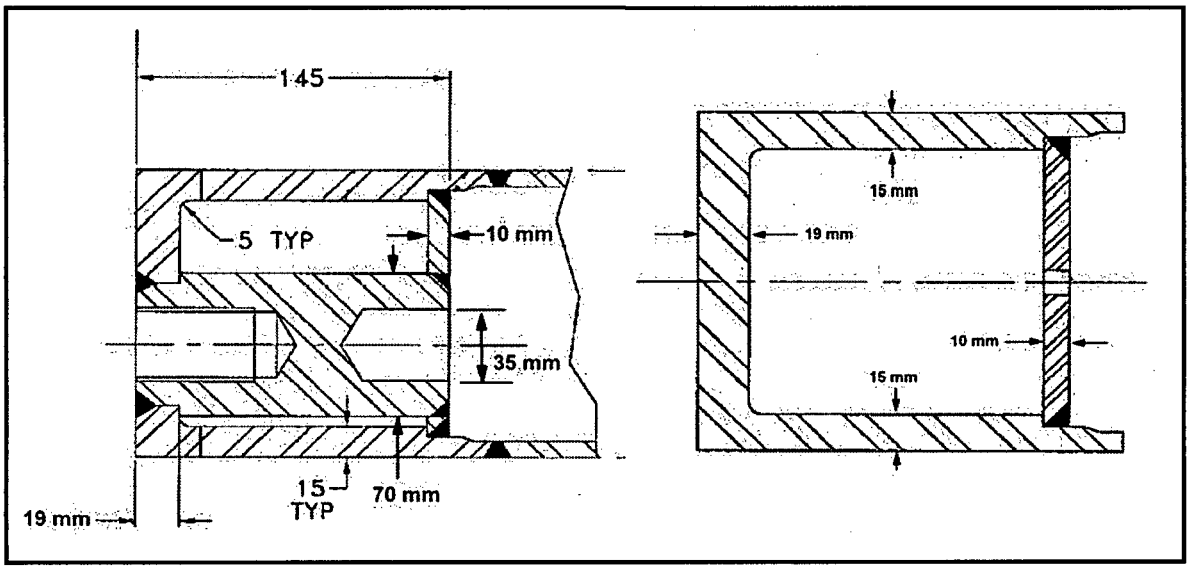

Figure 3.5-14 – Preliminary CSA End Detail as Modeled for NCT

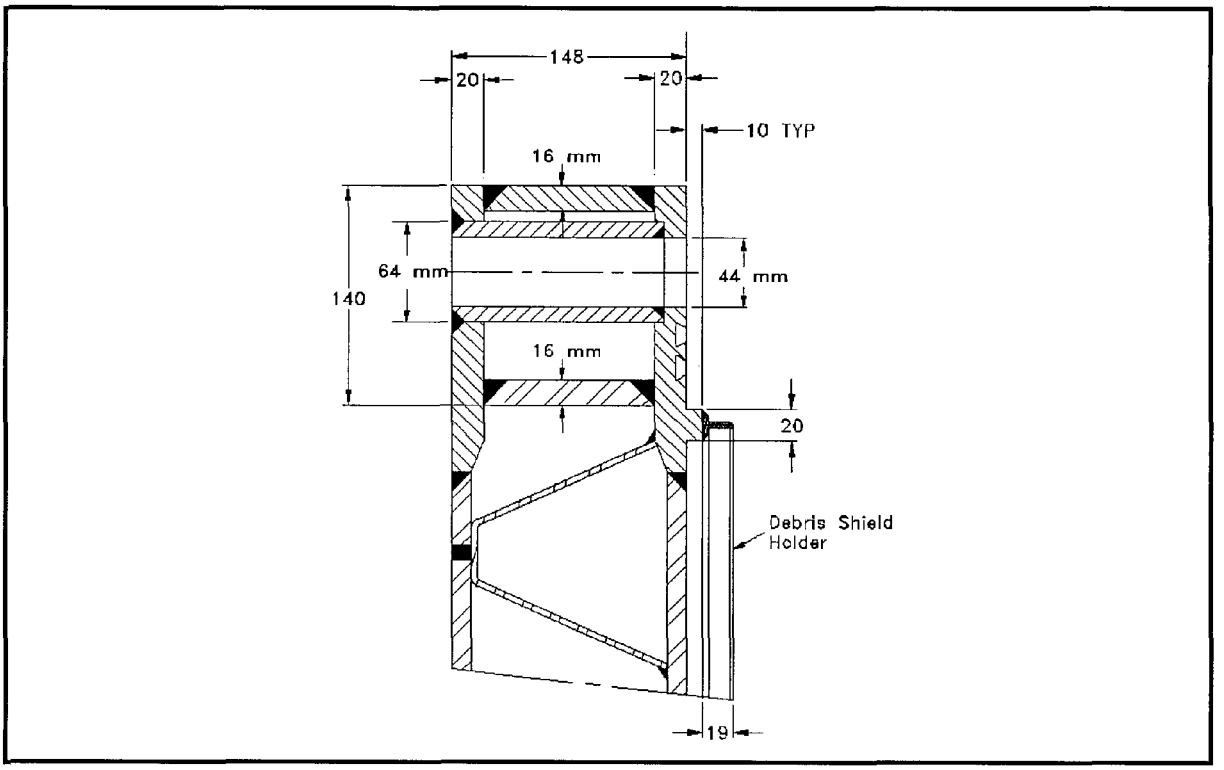

Figure 3.5-15 – Closure Lid Edge Detail

3.5.2.6 Description of Thermal Model for HAC Conditions

The analytical thermal model of the TRUPACT–III used for HAC conditions is a modified version of the quarter symmetry NCT model described in Section 3.5.2.1, *Description of Thermal Model for NCT Conditions*. This is appropriate since the use of a quarter symmetry model to simulate the non-symmetric damages arising from the HAC drop events is inherently conservative. The primary modifications made to the NCT model for the HAC modeling consist of the following:

- Simulated the worst-case HAC free and puncture drops consisting of an oblique side-edge drop and subsequent puncture bar damage adjacent to the side-edge damage and just aft of the cheek to body joint (see Figure 3.5-16 and the discussion below for details),
- Changed the thermal conductivity of the balsa wood from a value consistent with the low end of the observed range to a value that represents the high end of the range,
- Increased the emissivity of the external surfaces from 0.8 to 0.9 to account for possible soot accumulation on the surfaces,
- The balsa wood surfaces adjacent to undamaged portions of the outer skin will be charred from the HAC fire, but not consumed due to the lack of air. However, since the thermal conductivity of solid wood is greater than that for charred wood, the thermal properties of undamaged wood are assumed for computing the heat flow into the package,
- Replaced the assumed air gaps between the layered components of the package side wall with direct contact,
- Replaced the adiabatic boundary condition applied to the bottom of the package for NCT conditions with convective and radiation thermal conductors to the ambient,
- Apply convection heat transfer coefficients between the package and the ambient that are appropriate for gas velocities of 10 m/sec[8] during the 30-minute fire event. Convection coefficients based on still air are assumed following the 30-minute fire event,
- An 800 °C ambient condition with an effective emissivity of 1.0 is used to simulate the elevated temperature of the fire for convective and radiation heat transfer during the 30-minute fire event. The ambient condition is re-set at the end of the 30-minute fire to the pre-fire ambient condition of 38 °C with an effective emissivity of 1.0 and with the addition of insolation.

The presence of the outer skin, balsa, polyurethane foam, and calcium silicate insulation provides significant thermal protection to the TRUPACT–III package. The potential damage to these components arising from the hypothetical free drop and puncture bar accidents is established based on the results of a series of drop tests on a full-scale model of the TRUPACT–III package. A summary of the testing and the associated results is presented in Section 2.7, *Hypothetical Accident*

[8] Schneider, M.E and Kent, L.A., *Measurements Of Gas Velocities And Temperatures In A Large Open Pool Fire, Heat and Mass Transfer in Fire* - HTD Vol. 73, 1987, ASME, New York, NY.

Conditions. The drop tests covered a range of hypothetical free drop orientations and a series of puncture bar drops. Section 3.5.3, *Review of TRUPACT–III Package Full Scale Drop Test Results*, provides a further overview of the drop test results and justification for the selected bounding damage combination. Of the tested drop scenarios, the oblique drop on the side-edge of the package with a subsequent puncture bar attack just aft of the cheek to body joint (see Figure 3.5-24) is judged to be the most damaging to the thermally sensitive areas of the package. As discussed in Section 2.7.1.5.2, *Side-Edge Free Drop Extrapolation*, the oblique side-edge drop is expected to create a flattened region approximately 305 mm wide along the package length. The flattened region will be reduced to approximately 178 mm at the cheek areas due to the additional structure and the higher density polyurethane foam used in the cheeks. The minimum distance between the outer skin and the corner of the CSA is estimated to be 75 mm over the length of the package body and 65 mm between the outer skin and the corner of the protection plate enclosure (i.e., thermal shield) surrounding the calcium silicate insulation at the cheek areas. Additionally, the weld seam joining the outer skin of the front cheek with the outer skin of the package body is assumed to fail for a distance of approximately 914 mm creating an opening with a maximum width of 51 mm.

Consistent with the damage observed from the drop tests, the puncture bar is predicted to have penetrated both the outer skin and the underlying 10 mm thick puncture-resistant plate and to have opened a hole in the outer skin that is approximately 254 mm long by 178 mm wide. The hole in the underlying 10 mm thick puncture-resistant plate is approximately 178 mm in diameter. The puncture bar is conservatively assumed to have pulled out of the package prior to the start of the fire, thus fully exposing the damaged area to exposure to the fire environment. To maximize the potential effect on the package temperature, the simulated puncture drop damage is located directly below the chevron-shaped edge sheet and directly behind the cheek to package body junction. Locating the damage ahead of the joint would not be as thermally significant due to the presence of the 16-mm protection plate and the calcium silicate. Likewise, locating the puncture bar damage in the corner region would also not be as thermally significant since the higher foam density in this region would act to reduce penetration by the bar and the bar would contact the edge of the CSA obliquely and reduce the area of exposure.

Figure 3.5-16 presents an overview of the bounding damage inflicted on the package thermal model prior to the initiation of the HAC fire. To model the combined damage condition, the thermal model used for the NCT analysis was modified via the following steps:

a. the NCT thermal model was altered at one corner to reflect the flattening of the outer shell of the package expected to result from the 9 m free drop under NCT Hot conditions,
b. the underlying foam in the crushed corner regions is compressed by approximately 30% to yield an apparent density of 0.41 kg/dm^3. For conservatism, a lower bound density of 0.36 kg/dm^3 is used to estimate the recession depth of 42 mm within the foam under HAC conditions (see Section 3.5.4, *'Last-A-Foam' Response under HAC Condition*). Further, although the recession of the foam will occur over the 30 minute exposure to the HAC fire temperatures, for conservatism the full recession depth is assumed to occur at the start of the HAC fire event.
c. the foam at the undamaged corners of the package is likewise recessed at the start of the fire event to reflect the expected 60 mm of foam recession that is expected to occur over the entire HAC event for 0.25 kg/dm^3 density foam (representing the lower bound density for the corner region foam).

d. the foam in the cheek regions of the package is assumed to be crushed at the top and recessed at its exterior surfaces by 36 mm for the lower bound fabrication density of 0.41 kg/dm^3 for foam in this region. The remaining foam depth and recession depth are conservatively captured by the thermal model,

e. the 140 mm thick, 0.16 kg/dm^3 foam at the end of the closure overpack is assumed to have recessed by 60 mm,

f. the heat transfer between the ablated foam surfaces and the exterior skin of the package is modeled as a combination of radiation and conduction across an air filled gap

g. the puncture drop damage is simulated by fully exposing a surface area on the CSA measuring 179 mm wide by 239 mm directly to the HAC fire conditions. This surface area essentially matches the size of the damage noted to the outer skin from the puncture bar (i.e., 254 mm by 178 mm) and is nearly twice the size of the 178 mm diameter hole created in the 10 mm puncture-resistant sheet (see discussion of the puncture bar damage above). The 179 mm by 239 mm area was chosen for modeling since it matched the surface resolution available in the thermal model. No credit is taken for the potential shielding provided by the compacted foam, metal, etc. that may remain within the damaged area. This assumption, together with the larger hole assumed in the 10 mm puncture-resistant sheet, provides a significant level of conservatism on the effect of the HAC damage. Further, as discussed above, the surface area is located directly below the corner ribs and directly behind the cheek to package body junction. A view factor of 0.23 is assumed between the exposed CSA surface and the HAC fire based on a view factor calculation for parallel plates, the 179 mm by 239 mm dimensions of the hole, and the nominal 185 mm separation distance between the CSA surface and the outer sheet of the package skin,

h. the emissivity of the exterior surfaces of the package skin is increased to 0.90 (both sides),

i. the thermal conductivity of the balsa components is increased from the conservatively low value of 0.0415 W/m-K assumed for NCT conditions to a conservatively high value of 0.168 W/m-K,

j. given the package dimension, the package is assumed to be in its horizontal orientation during and the HAC event, and

k. the convection heat transfer coefficients are based on a gas velocity of 10 m/sec during the 30-minute fire event and still air afterwards. The elevated HAC convection heat transfer rate is conservatively applied to the surfaces of the CSA exposed by the puncture bar attack, even though convection will be significantly reduced within the recessed cavity created by the puncture bar attack.

l. the assumed air gaps between the layered balsa wood and polyurethane foam components and the metallic surfaces of the package side walls are replaced with direct contact.

Figure 3.5-17 presents an elevation view of the thermal model of the simulated damaged TRUPACT–III package along the package body. As seen from the figure, the model captures the flattened corner on the outer shell of the package that results from the oblique side-edge drop. In addition, the simulated ablation of the 0.29 kg/dm^3 polyurethane foam in the corners of the package is incorporated into the modeled geometry.

Figure 3.5-18 illustrates an elevation view through the HAC thermal model of the package cheek. The ablation of the 0.48 kg/dm^3 polyurethane foam used in the cheek is conservatively captured

using a lower bound foam density of 0.41 kg/dm^3 to yield a predicted 36 mm recession depth. The modeling also conservatively assumes that the 16-mm protection plate surrounding the calcium silicate insulation in the cheek has been uncovered by the foam ablation along its top surface. This assumption results in the top surface of the protection plate structure being exposed to conductive and radiation heat transfer with the outer skin of the cheek throughout the entire HAC fire event. In reality, this thermal exposure is not expected to occur or, if it did, only near the end of the 30-minute fire event.

Modeling of Balsa Wood Performance

Ignition of the balsa wood requires the wood to be subjected to sufficient heat and in an atmosphere with sufficient oxygen. The absence of either of these conditions will prevent the sustained combustion of the wood. Since the balsa wood components are encapsulated in metal, it will not ignite and it will not burn unless there is damage to the outer skin which allows the free passage of air. The openings created as the result of the melting of the plastic in the pressure relief fittings on the outer skin are not adequate to support active combustion of the wood. Likewise, with the exception of the failure of the weld seam joining the outer skin of the front cheek with the outer skin of the package body (see Figure 3.5-20), all other cracks or tears in the outer skin resulting from the HAC free drops are too small to support active combustion of the under lying wood.

The heat flux from the HAC fire through the outer skin will cause thermal decomposition of the exterior layers of the balsa wood components, resulting in the production of water vapor, carbon monoxide, and non-flammable and flammable volatiles. These gases will exit the package through the pressure relief fittings and may be ignited by the HAC fire. However, the absence of free air movement across the boundary formed by the outer skin will prevent combustion within the wood itself. As such, the pyrolysis process will remain endothermic, potentially resulting in a charred layer of wood, but no combustion. Further, since wood char has a lower thermal conductivity than virgin wood, the process will be self-limiting.

Therefore, the modeling approach used for the balsa wood contained within compartments whose boundaries have not been breached or where the level of breaching is considered insignificant is essentially the same as that used for NCT conditions. To bound the heat flux into the package, a thermal conductivity representing the high end of the observed range of values for balsa wood (see Table 3.2-8) is assumed. The density and specific heat values used for the NCT analyses are retained for the HAC analysis based on the assumptions that the wood will remain essentially intact and that any loss of wood density would also be accompanied by the endothermic process wherein the volatized material is expelled through the pressure relief ports in the outer skin, thus carrying with it a significant portion of the thermal energy passed into the wood. It is assumed for the purposes of this evaluation that this un-modeled mass transport of energy will offset the un-modeled reduction in density and change in specific heat values that would accompany the charring of the wood.

While the balsa wood contained within compartments whose boundaries have been breached could become involved in active combustion during the HAC fire event, the extent of the combustion will be severely restricted by the limited size of the openings. The largest breach noted from the drop tests was the failure of the weld seam joining the outer skin of the front cheek with the outer skin of the package body where the joint failed for a distance of approximately 914 mm creating an opening with a maximum width of 51 mm. The size of the

gap between the outer skin and the balsa wood reduced to zero approximately 150 to 175 mm from the edges of the tear. A revised weld joint design is expected to prevent this from occurring for the production units. However, for the purposes of the thermal modeling for the HAC evaluation this failure mode is conservatively assumed to exist and that the balsa wood contained in the affected compartment could ignite during the HAC fire.

However, given the limited free passage of air permitted by the size of the tear to the surface of the wood and the fact that the wood component exists as one, continuous block of balsa, it can be assumed that the balsa wood combustion in the vicinity of the weld failure would be limited to surface burning and that the extent of the balsa involved would extend no further than 250 mm from the edges of the tear. Any combustion and/or charring will be self-limiting since the developed char layer will insulate the underlying virgin wood and the presence of the sheetmetal encasement will protect the char layer. Further, even if active combustion were to occur, the thermally sensitive portion of the package (i.e., the CSA and the containment seals) are separated from the balsa wood in the package by a 10-mm thick puncture resistant sheet and a 109 to 114 mm thick layer of 0.10 kg/dm^3 polyurethane foam. As demonstrated by the discussion in Section 3.5.4, *'Last-A-Foam' Response under HAC Condition*, this combination of foam density and thickness is sufficient to protect the underlying CSA from excessive temperatures from a 30-minute fire event even if the balsa wood was not present and from any heat generated by the wood combustion. Therefore, when combined with the expected limited combustion of the balsa wood in the vicinity of the weld failure, the potential failure of the weld joint is not seen as having a significant impact on the peak temperatures within the thermally sensitive areas of the package. The same applies to the edges of the balsa wood exposed by the puncture bar attack.

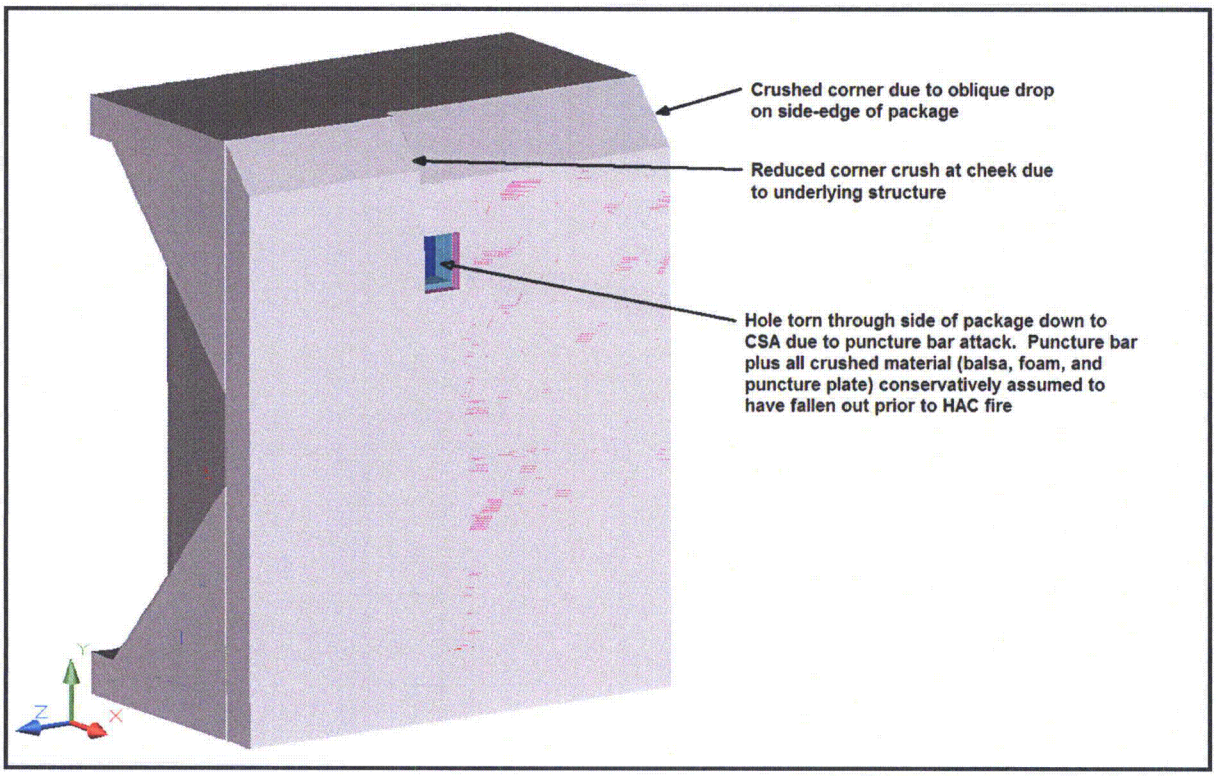

Figure 3.5-16 – Overview of Thermal Model of Damaged TRUPACT–III Package

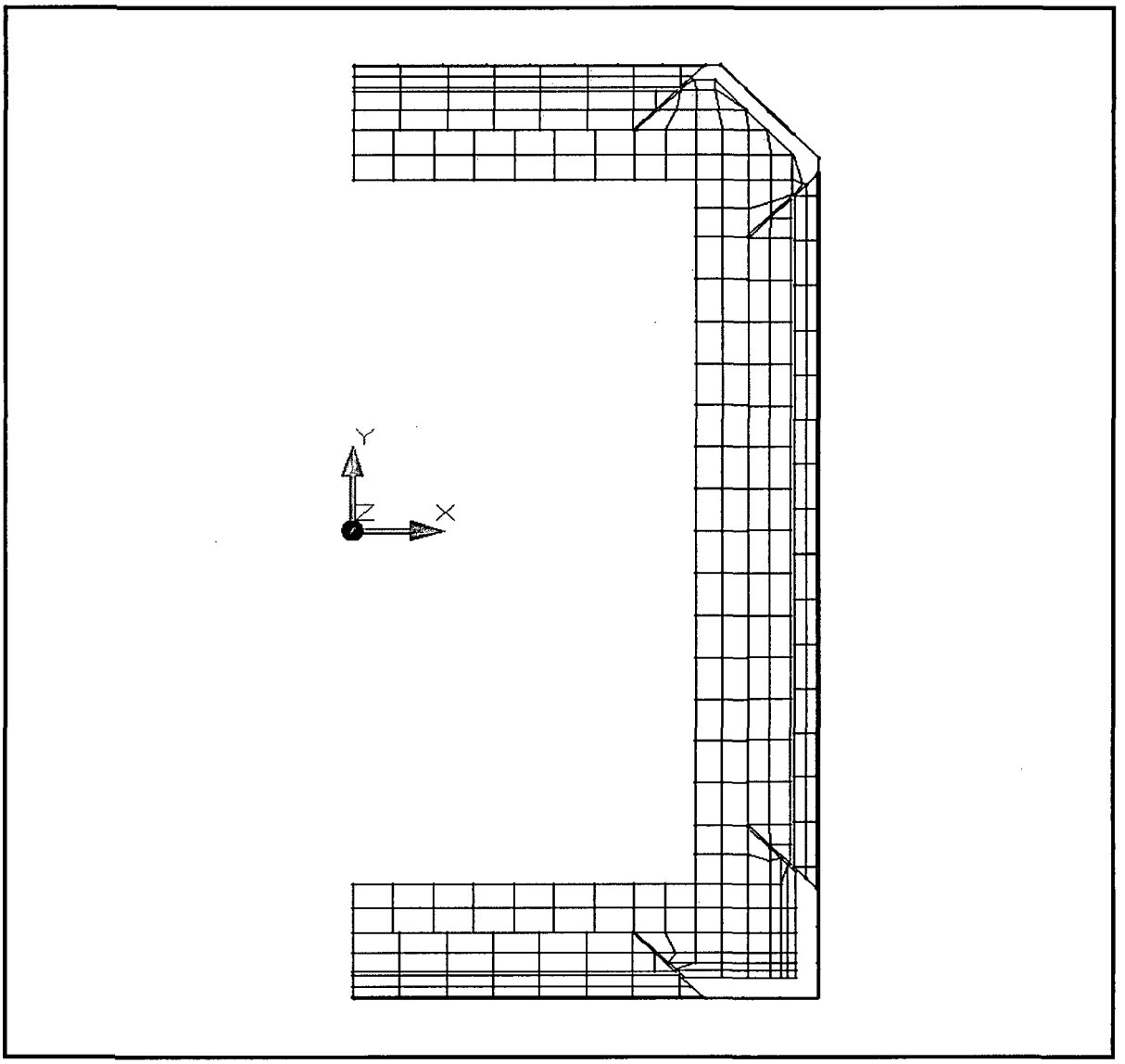

Figure 3.5-17 – Elevation View, Thermal Model of Damaged TRUPACT–III Package

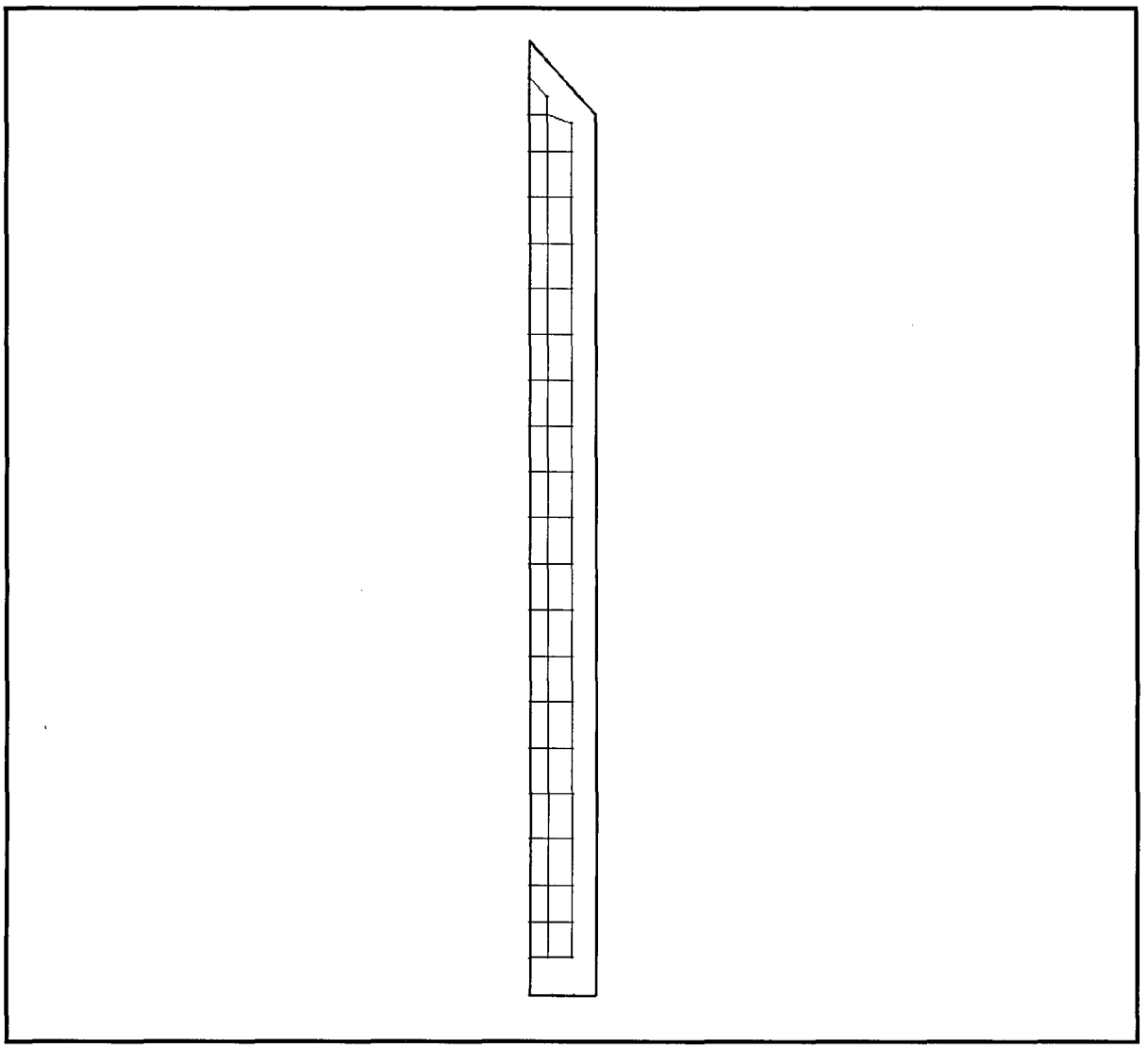

Figure 3.5-18 – Elevation View through Cheek of Damaged TRUPACT–III Thermal Model

This page intentionally left blank.

3.5.3 Review of TRUPACT–III Package Full–Scale Drop Test Results

The potential thermal damage to the TRUPACT–III package arising from the hypothetical free drop and puncture bar accidents is established based on the results of two series of drop tests on full-scale certification test units (i.e., CTU-1 and CTU-2) of the TRUPACT–III package, as described in Section 2.7, *Hypothetical Accident Conditions*. The following paragraphs examine the results of the tested drop scenarios from each test series and provide justification for the selected damage condition being bounding on the thermal performance of the package under HAC conditions.

NCT and HAC Free Drops

One (1) NCT and four (4) HAC free drops were carried out on the CTU-1 test unit. The NCT drop test was made from a height of 0.3 m (one foot) onto the overpack cover. Post-drop inspection indicated that the overpack cover, which had projected by approximately 22 mm beyond the end faces of the cheeks, had been crushed by approximately 7 mm. No other damage was noted. Based on exposed surface area, even less damage is expected for NCT free drops on the other faces of the package. As such, the NCT thermal model can conservatively assume un-damaged conditions as a basis of analysis.

The four (4) HAC free drop test scenarios consisted of: 1) vertical, overpack cover down (Ref. No. LD2), 2) horizontal, side of the package down (Ref. No. LD3), 3) CG-over-corner, overpack cover down (Ref. No. LD4), and 4) oblique side-edge of the package down (Ref. No. LD5). See the Section 2.7 for a full description of each drop orientation. Each free drop was from a height of 9 m (30 feet).

The LD2 test showed a total crush of 36 mm and cracks in the welds around the octagonal opening in the cover and at the ISO fittings of 51 mm to 152 mm long. In addition, the overpack body in the vicinity of the overpack bolts exhibited weld cracks of approximately 305 mm in length and a bulge in the outer skin of approximately 45 mm. This damage level is considered to be slight from a thermal point of view. The reduction in the depth of the foam insulation thickness is less than 7% (i.e., 36 mm vs. a total foam thickness of 140 + 380 = 520 mm, see Figure 3.1-3). Further, since the foam thickness is compacted and not physically lost, the principal thermal protection afforded by the foam under HAC conditions is essentially unaffected (see Section 3.5.4, *'Last-A-Foam' Response under HAC Condition*, for details). The noted cracks in the welds are too narrow to permit the hot gases from the fire event to penetrate the package boundary. As such, the package damage sustained under the vertical, overpack cover down (Ref. No. LD2) scenario is too limited to affect the HAC performance of the package.

The vertical, side of the package down (Ref. No. LD3) drop scenario resulted in the CSA moving towards the impact surface by approximately 7 mm. This movement is assumed to have occurred entirely via crushing of the polyurethane foam surrounding the package (see Figure 1.1-3 from Section 1.1, *Introduction*). In addition, the impact was noted as cracking the weld in the overpack outer skin at the joint between the cheek and the package body. The weld crack extended across the width of the chevron and had a maximum opening of approximately 25 mm. Both the reduction in the thickness of the polyurethane foam and the potential exposure of the polyurethane foam under the cracked weld are considered too minor to significantly affect the thermal performance of the package under HAC conditions.

The Ref. No. LD4 test scenario examined the potential damage arising from the CG-over-corner drop onto the overpack cover. While this drop scenario resulted in the greatest deflection from the original shell dimensions, the area of damage is limited and relatively remote from the thermally sensitive areas of the package. As documented in Section 2.7, *Hypothetical Accident Conditions*, the impact caused a triangular flattened region having a dimension of 1,054 mm diagonally across the overpack cover, 838 mm along the bottom, and 800 mm along the right side of the package. No significant weld seam failures were noted. Given this level of damage, no significant impact on the thermal performance of the package under HAC conditions is expected.

The final HAC free drop orientation examined using the CTU-1 test unit was the oblique side-edge of the package down (Ref. No. LD5). Except for the front and rear cheek areas, the impact caused a flattened region approximately 305 mm wide along the package length. The flattened region reduced to approximately 178 mm at the cheek areas. Figure 3.5-19 illustrates the damage caused by the Ref. No. LD5 free drop orientation. This degree of crush left a minimum distance of approximately 105 mm (as determined analytically, see Figure 3.5-21) between the outer skin and the corner of the CSA and approximately 95 mm (as measured during post-test disassembly, see Section 2.12.3.7.4, *Free Drop, Side-Edge HAC (Test LD5)*) between the outer skin and the corner of the protection plate enclosure surrounding the calcium silicate insulation. Additionally, as shown in Figure 3.5-20, the weld seam joining the outer skin of the front cheek with the outer skin of the package body failed for a distance of approximately 914 mm creating an opening with a maximum width of 51 mm. The gap developed between the outer skin and the balsa wood quickly decreased with distance from the tear until an essentially zero width gap was noted approximately 150 to 175 mm from the edges of the tear. Based on the level and extent of the damage and its proximity to the thermally sensitive areas of the package, the oblique side-edge of the package down drop scenario is seen as providing the bounding damage to the package resulting from the HAC free drop event.

The supplementary testing on CTU-2 repeated the LD4 CG-over-corner drop onto the overpack cover under the cold (i.e., -29 °C) foam temperature condition. The primary purpose of repeating this test scenario (test designation LD91) was to verify that the debris shield would exclude debris from entering the seal region during the package deflections occurring during the worst-case free drop event. The impact caused a triangular flat region having dimensions of 737 mm along the overpack cover, 864 mm along the bottom, and 787 mm along the left side of CTU-2. This level of damage is consistent with that seen from the LD4 test scenario for the testing on CTU-1 (see above). As with the original testing, no significant weld seam failures were noted from this supplementary testing and no significant impact on the thermal performance of the package under HAC conditions is expected.

HAC Puncture Drops

In addition to the free drops, the CTU-1 test article was subjected to four (4) puncture drop tests, all from a height of 1 meter. The drop orientations evaluated were 1) impact on the side damage, inclined at 20° from the horizontal (Ref. No. LP1), 2) impact on the recessed portion of the overpack cover, inclined at 25° from the vertical (Ref. No. LP2), 3) impact on the CG-over-corner damage (Ref. No. LP3), and 4) impact on the oblique side-edge damaged area, inclined at 30° from the horizontal (Ref. No. LP4).

The Ref. No. LP1 puncture drop resulted in penetration of both the outer skin and the underlying 10 mm thick puncture-resistant plate (see Figure 3.5-22 and Figure 3.5-23). The outer skin and balsa wood were 'cookie cut' and carried inward by the puncture bar. The cut section of balsa wood ended up as compressed disk, approximately 3 mm thick. The puncture-resistant plate was cut and then folded out of the way in a 'dog ear' fashion. The underlying foam was compressed and then shoved to the side as the package rotated after the puncture bar impacted with the CSA. While a dent approximately 51 mm deep was left in the CSA, there was no cutting or cracking of the CSA's outer skin. Post-impact rotation of the package resulted in enlarging the hole in the outer skin from approximately 178 mm in diameter to approximately 254 mm long by 178 mm wide. The hole in the 10 mm puncture-resistant plate was approximately 178 mm in diameter.

The Ref. No. LP2 puncture drop resulted in penetration of the outer skin and the balsa wood, but not the 15-mm puncture-resistant plate. A dent approximately 145 mm deep was left in the 15-mm puncture-resistant plate, with an associated dent of approximately 5 mm in the lid. Post-impact rotation of the package resulted in enlarging the original hole in the outer skin to approximately 360 mm long by 205 mm wide.

The third puncture bar drop scenario (Ref. No. LP3) attacked the CG-over-corner damage incurred from the LD4 free drop. The puncture bar struck near the center of the damage and created a further deformation over an area that is 178 mm in diameter and 102 mm deep. While the puncture bar locally compressed the material previously deformed by the LD4 free drop, it did not significantly increase the exposure of the underlying foam. As such, this puncture bar drop scenario was dropped from further consideration in determining the bounding damage scenario for the TRUPACT–III package.

The fourth puncture bar drop scenario (Ref. No. LP4) examined was the impact on the oblique side-edge damaged area. The bar penetrated the outer skin, creating a hole approximately 178 mm in diameter, and impacted the corner of the protection plate enclosure surrounding the calcium silicate insulation in the cheek. Post-impact inspection showed no damage to the calcium silicate insulation and only minor cracks in the protection plate welds.

The supplementary testing on CTU-2 repeated one puncture bar test from the test series on CTU-1 and addressed one additional scenario. The LP91 puncture test repeated the impact on the CG-over-corner damage addressed by the LP3 test in the CTU-1 test series. While the resultant damage loosened the lower quadrant of the overpack cover's outer sheet and a significant portion of the low density (0.16 kg/dm^3) foam fell out, little of the high density (0.48 kg/dm^3) foam was exposed and essentially none was lost. In addition, the corner of the puncture bar partially sheared into the 6-mm thick puncture resistant plate located between the low density and high density foam by 38 mm [1.5 inches]. Although the level of damage noted from the LP91 and LD91 drop combination is slightly worse than that seen for the original LP3 and LD4 drop combination on CTU-1, the level of remaining thermal protection is significant and no adverse affect on the TRUPACT–III seal region will occur.

The supplementary testing on CTU-2 added a puncture bar attack on the bottom side of the package that was not addressed by the original test series. Under the LP92 test, the puncture bar struck the package approximately 476 mm [18.7 inches] from the closed outer end of the package, with the package inclined 40° from the horizontal. The bar penetrated the outer skin and impacted the CSA outer structural sheet, creating a crack in the weld between the structural sheet and the rear diagonal corner stiffener of the CSA, and in some of the adjacent plug welds

which connect the outer structural sheet to the V-stiffener nearest the impact. However, there was no evidence of any dent or bulge in the CSA inner (containment) sheet at the puncture site and the containment boundary remained leak tight. Post-impact rotation of the package resulted in enlarging the hole in the outer skin from approximately 178 mm (7 inches) in diameter to approximately 318 mm (12.5 inches) long by 152 mm (6 inches) wide. The level of damage and the size of the CSA area exposed by the puncture bar is consistent with that seen for the LP1 test under the original testing on CTU-1. Given this and since the damage location is remote from the thermally sensitive area of the package (i.e., the containment seals), this puncture bar test was dropped from further consideration in determining the bounding damage scenario for the TRUPACT–III package.

Bounding Combined HAC Free and Puncture Drop Damage

Based on the above discussion, it is concluded that the bounding damage scenario for the TRUPACT–III package will consist of an oblique free drop on the side-edge of the package (Ref. No. LD5), followed by a puncture bar impact just aft of the cheek to body joint. The selected free drop and puncture drop damage scenarios will impart the most significant damage compared to the other free drop scenarios for the reasons described above.

Since the Ref. No. LD5 test was conducted at a corner foam temperature of approximately 7°C vs. the approximately 50°C average foam temperature expected under the NCT Hot condition of transportation and since the foam strength is a function of its temperature, post-test calculations (see Section 2.7.1.5.2, *Side-Edge Free Drop Extrapolation*) are used to extrapolate the package performance to the higher foam temperature. The maximum deformation at the NCT Hot condition is found by analysis to add an estimated 30 mm to the total crush depth. With this temperature correction, the minimum distance between the outer skin and the corner of the CSA is estimated to be 105 mm – 30 mm = 75 mm, while the distance between the outer skin and the corner of the protection plate enclosure surrounding the calcium silicate insulation will be 95 mm - 30 mm = 65 mm. The resulting level of crush in the underlying foam regions is estimated to be 30% along the CSA and 31.5% along the cheek. Figure 3.5-21 illustrates the crush lines as noted from the full-scale testing and as extrapolated for the foam temperatures predicted to occur at the NCT Hot conditions.

Of the puncture bar drop scenarios only two (Ref. No. LP1 and LP92) penetrated all the way through the package's thermal protection system. The others were stopped short by the puncture resistant plates and/or other package structures. However, it is noted that the location of both the Ref. No. LP1and LP92 impact damage are too far from the package closure seals to have any significant thermal effect beyond the localized heating of the CSA structural sheet. Instead, by hypothetically re-locating the impact location to just aft of the cheek to body joint on the package and just below the damage caused by the Ref. No. LD5 free drop damage scenario (see Figure 3.5-24), the combined damage would create the maximum thermal exposure of the package in the vicinity of the closure seals to the HAC fire environment that can be supported by observed results from the full-scale CTU drop tests. No temperature corrections are required for the puncture drop damage scenarios since the puncture resistance of the package is principally determined by the steel plates and not the polyurethane foam.

The bending of the puncture bar during the LP1 puncture attack (see Figure 3.5-22) did not lessen the damage to the package. The basis for this conclusion comes from the video record of the LP1

puncture event which shows that the package comes essentially to rest before beginning a relatively slow rotation off of the puncture bar. The video clearly shows that the package does not receive any support from the ground before the energy of the 1m free fall has been absorbed in the wall overpack/puncture-resistant structure. As the package rolled off of the bar, the package c.g. moved away from the bar axis, and the bar bent over. Once the bar begins to bend, the amount of damage to the package has reached its limit. This is also demonstrated in the video, where it is shown that no further damage is occurring to the package as the bar bends. Similarly, a longer bar would tend to bend sooner due to its longer moment arm and, as such, do less damage. For these reasons, a longer bar would have no effect on the puncture damage experienced in LP1. Review of the other punctures confirms that this conclusion is universally true of the puncture drop tests performed.

The observed damage resulting from the LP1 puncture bar attack is bounding for the damage that could be obtained by a similar puncture bar attack elsewhere on the side surface of the package and, as such, the simple transfer of the observed damage to the containment seal region provides a significant level of conservatism for the assumed HAC damage scenario for the containment seals. The basis for this conclusion is that the LP1 puncture bar attack was through the package's center of gravity to ensure that all of the energy from the 1m free fall was absorbed in the package structures and not partially dissipated via rotation of the package about the puncture bar impact point. Therefore, an actual puncture attack in the region of the containment seal would have exhibited less damage than seen for the LP1 puncture test, partly because the overpack wall structures are stiffer in the region of the containment seals, and partly because the axis of the puncture bar would not pass through the c.g. of the package since the package orientation would need to be on the order of 55° to the horizontal. An attack at such a steep angle would cause the puncture bar to either glance off of the surface, or simply bend out of the way and yield a significantly lower level of damage than observed for the LP1 puncture bar attack.

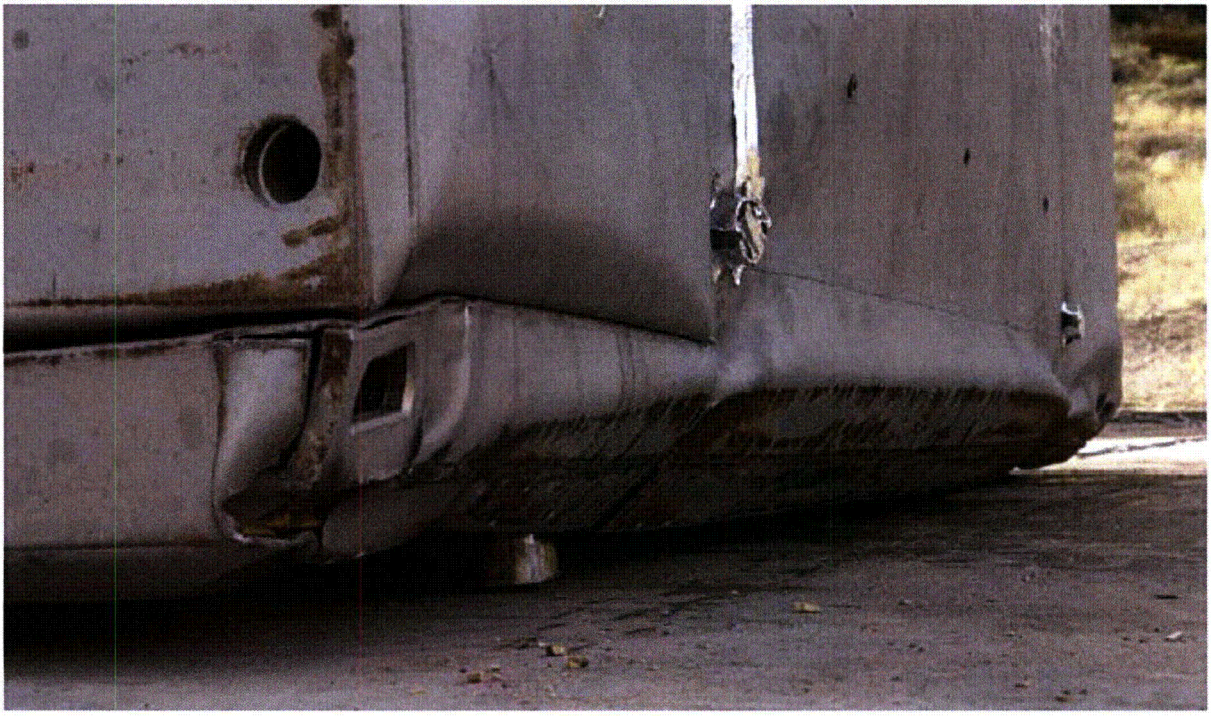

Figure 3.5-19 – Edge Deformation from LD-5 Free Drop Orientation

Figure 3.5-20 – Weld Tear from LD-5 Free Drop Orientation

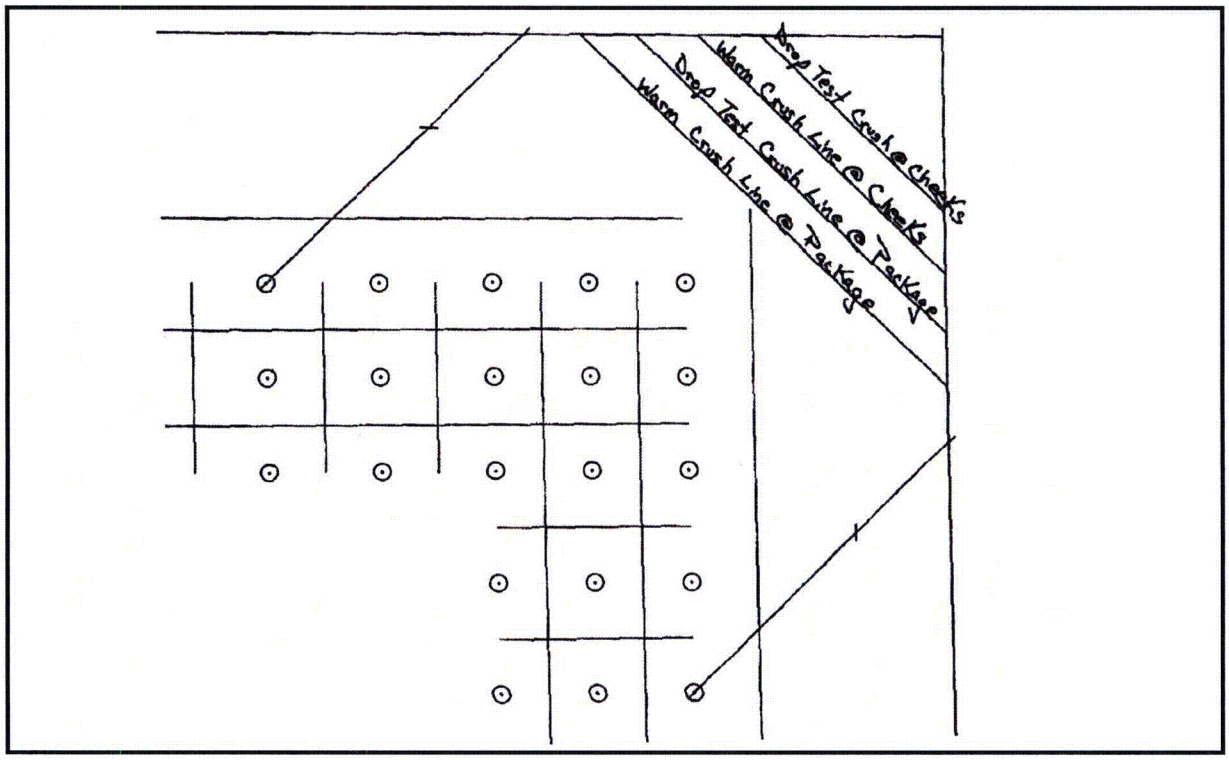

Figure 3.5-21 – Corner Crush Depths, Test and NCT Hot Conditions

Figure 3.5-22 – LP1 Puncture Bar Damage before Removal of Bar

Figure 3.5-23 – LP1 Puncture Bar Damage after Removal of Bar

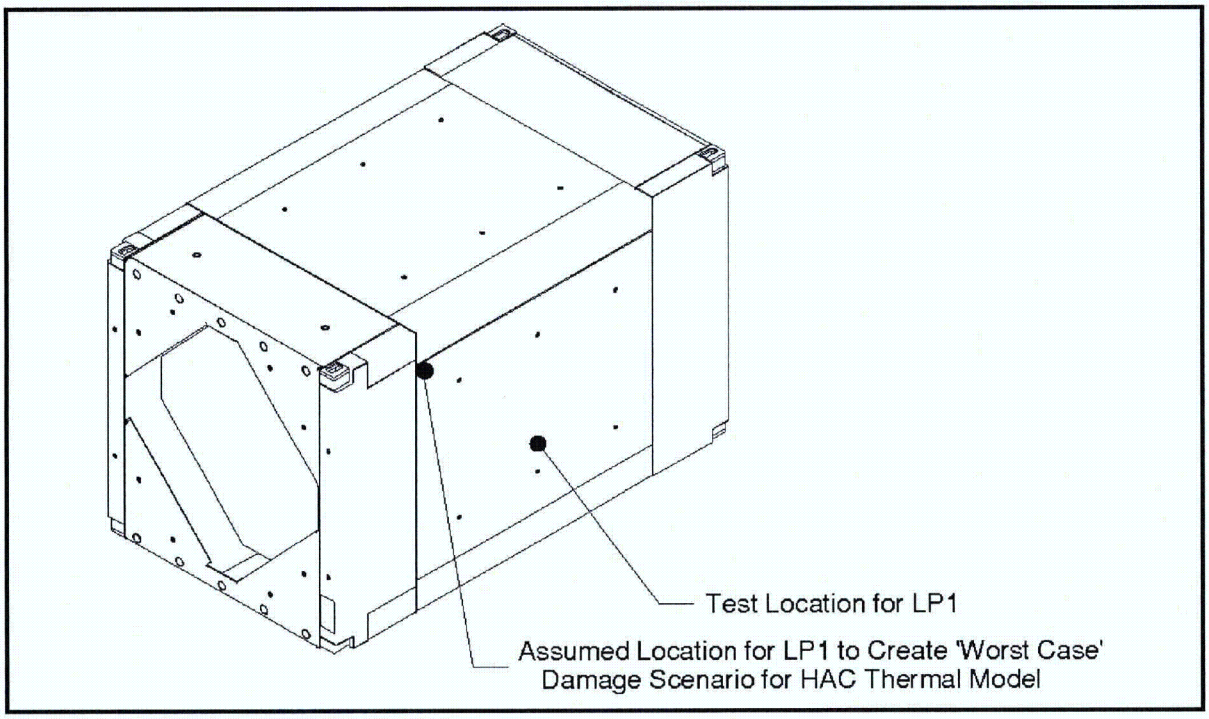

Figure 3.5-24 – Assumed Re-Location of LP1 Puncture Bar Damage

3.5.4 'Last-A-Foam' Response under HAC Conditions

The General Plastics LAST-A-FOAM® FR-3700 rigid polyurethane foam[1] has been used in numerous radioactive materials packages. The FR-3700 formulation is specially designed to allow predictable impact-absorption performance under dynamic loading, while also providing an intumescent char layer that insulates and protects the underlying materials, even when exposed to pool-fire conditions. Upon exposure to fire temperatures, this proprietary foam decomposes into an intumescent char that swells and tends to fill voids or gaps created by free drop or puncture bar damage. The thermal decomposition absorbs a significant amount of the heat transferred into the foam, which is then expelled from the package as a high temperature gas. At the same time, the resultant char layer shields the underlying undamaged foam from further direct exposure to the external high temperatures. This behavior has been observed in numerous fire tests of other packages.

Since the decomposition of the foam under elevated temperatures is an endothermic process, the foam is self-extinguishing and will not support a flame once the external fire is removed. However, the gases generated by the decomposition process are combustible and will burn under piloted conditions. Further, a portion of these generated gases could remain trapped within the charred layer of the foam for a period of time after the cessation of the HAC fire event and could support further combustion, although at a much reduced level, until a sufficient time has passed for their depletion from the cell structure.

The mechanisms behind the observed variations in the thermal properties and behavior of the FR-3700 foam at elevated temperatures are varied and complex and only limited research has been conducted in this area. As such, currently no definitive analytical model of the foam properties under HAC conditions exists. Instead, a combination of empirical data and modeling conservatism is used to simulate the thermal performance of the LAST-A-FOAM® FR-3700 polyurethane foam for this application.

A series of fire tests[2,3] conducted on 5-gallon cans filled with FR-3700 foam at densities from 0.107 to 0.412 kg/dm^3 helped define the expected performance of the foam under fire accident conditions. Under the fire tests, one end of the test articles (i.e., the "hot face" surface) was subjected to an open diesel fueled burner flame at temperatures of 980 to 1,200 °C for 30+ minutes. A thermal shield prevented direct exposure to the burner flame on any surface of the test article other than the hot face. Each test article was instrumented with thermocouples located at various depths in the foam. In addition, samples of the foam were subjected to thermogravimetric analysis (TGA) to determine the thermal decomposition vs. temperature. The exposure temperatures for the TGA tests varied from 21 to 816 °C and were conducted in both air and nitrogen atmospheres. The result for the nitrogen environment (see Figure 3.5-25) is more representative of the low oxygen environment existing within the enclosures encasing the foam components of the TRUPACT–III

---

[1] Last-A-Foam™ FR3700 On-line Data Sheet, www.generalplastics.com.

[2] "*Thermal Assault And Polyurethane Foam Evaluating Protective Mechanisms For Transport Containers*", C.L. Williamson, Z.L. Iams, General Plastics Manufacturing Company, Tacoma, WA, presented at Waste Management '05 Symposium, Tucson, AZ, 2005.

[3] "*Thermal Assault And Polyurethane Foam - Evaluating Protective Mechanisms*", C.L. Williamson, Z.L. Iams, General Plastics Manufacturing Company, Tacoma, WA, presented at PATRAM International Symposium, Berlin, Germany, 2004.

package. These test results indicate that the following steps occur in the thermal breakdown of the foam under the level of elevated temperatures reached during the HAC fire event:

- Below 120 °C, the variation in foam thermal properties with temperature are slight and reversible. As such, fixed values for specific heat and thermal conductivity are appropriate.
- Between 120 °C and 260 °C, small variations in foam thermal properties occur as water vapor and non-condensable gases are driven out of the foam. As such, fixed values for specific heat and thermal conductivity are also appropriate for this temperature range. Further, the observed changes are so slight that the same thermal properties used for temperatures below 120 °C may also be used to characterize the thermal performance of the foam between 120 °C and 260 °C.
- Irreversible thermal decomposition of the foam begins as the temperature rises above 260 °C and increases non-linearly with temperature. Based on the TGA testing (see Figure 3.5-25), approximately 2/3's of this decomposition occurs over a narrow temperature range centered about 354 °C.
- The decomposition is accompanied by vigorous out–gassing from the foam and an indeterminate amount of internal heat generation. The internal heat generation arises from the gases generated by the decomposition process that are combustible under piloted conditions. However, since the decomposition process is endothermic, the foam will not support combustion indefinitely. Further, the out gassing process removes a significant amount of heat from the package via mass transport.
- The weight loss due to out–gassing not only has direct affect on the heat flux into the remaining virgin foam, but changes the composition of the resulting foam char since the foam constituents are lost at different rates. This change in composition affects both the specific heat and the thermal conductivity of the foam char layer.
- As temperature continues to rise, the developing char layer begins to take on the characteristics of a gas-filled cellular structure where radiative interchange from one cell surface to another becomes the dominant portion of the overall heat transfer mechanism. This change in heat transfer mechanisms causes the apparent heat conductivity to take on a highly non-linear relationship with temperature.
- Finally, at temperatures above 675°C, the thermal breakdown of the foam is essentially completed and only about 5 to 10% of the original mass is left. In the absence of direct exposure to a flame or erosion by the channeling of the outgas products through the foam, the char layer will be the same or slightly thicker than the original foam depth. This char layer will continue to provide radiative shielding to the underlying foam material.

The sharp transition in the state of the foam noted in Figure 3.5-25 at or about 354 °C can be used to correlate the depth of the foam char and the occurrence of this temperature level within the foam. Figure 3.5-26 illustrates the relationship between foam recession (i.e., char depth) and foam density following exposure to a 30-minute fire as complied from a series of tests. The correlation between the foam recession depth and the foam density is expressed by the relation:

$$y = -0.94681 - 11.64 \times \log_{10}(x)$$

where, y = the recession depth, cm

x = foam density (g/cm^3)

Based on this correlation, the recession depth expected for the nominal 0.29 kg/dm^3 density foam used in the corner regions of the package is estimated to be 53 mm. Given that the fabrication tolerance for the foam density is ±15%, the actual foam density may range from 0.25 to 0.33 kg/dm^3. The recession depth associated with the lower bound foam density of 0.25 kg/dm^3 is estimated to be 60 mm.

The expected worst case crush of the corner region foam is estimated to be approximately 30% (see Section 3.5.3, *Review of TRUPACT–III Package Full Scale Drop Test Results*). Since the package deflection would be accommodated by the compression of the corner foam, the density of the foam would increase from a lower bound density of 0.25 kg/dm^3 to an apparent density of 0.36 kg/dm^3. Since the recession depth for the foam is a function of its density, the recession depth for the 'crushed' foam will be approximately 42 mm.

The foam in the cheek region of the package has a nominal density of 0.48 kg/dm^3, except for a region 140 mm thick at the end of the cheek which has a nominal density of 0.16 kg/dm^3. The higher foam density in the cheek will yield a much smaller expected recession depth during the fire event than that expected for the corner region foam. At the nominal density of 0.48 kg/dm^3 the estimated recession depth will be 28 mm. The recession depth will increase to 36 mm at the lower bound fabrication density (-15%) of 0.41 kg/dm^3. The regions of the cheek crushed by the side-edge down drop will see a 31.5% increase in the nominal foam density of 48 kg/dm^3, or increase in the apparent density to approximately 0.70 kg/dm^3. Extrapolation of the recession depth relationship in Figure 3.5-26 to this density would yield an expected foam recession depth of only 8.6 mm. Even after accounting for the lower bound fabrication density, the increase in the apparent density would go from 0.41 kg/dm^3 to approximately 0.60 kg/dm^3 with an associated recession depth of 16 mm.

The 0.10 kg/dm^3 foam surrounding the CSA is 109 to 114 mm thick. Based on the recession depth correlation presented in Figure 3.5-26, a thickness of 107 mm is sufficient for the 0.10 kg/dm^3 foam to withstand a 30-minute regulatory fire event, even without the benefit of the 10 mm puncture-resistant sheet and the 60 mm thick balsa wood that lie between it and the outer skin. As such, local combustion within the balsa wood due to openings in the outer shell created by the drop damage will not create a thermal issue for the CSA.

An additional correction to the expected recession is required to account for the fact that the thermal testing upon which the recession depth correlation is based used a flame temperature 980 to 1,200 °C, whereas the regulatory fire flame temperature is specified as 800 °C[4]. The lower flame temperature will have a significant effect on the recession depth noted in the various foam components since the rate of heat transfer is directly related to the temperature of the flame. For example, the recession depth estimated for the nominal 0.29 kg/dm^3 density foam would be reduced from the 53 mm estimated by the correlation to less than 38 mm. For conservatism, a correction for the regulatory flame temperature is not applied for the purposes of this application.

[4] Title 10, Code of Federal Regulations, Part 71 (10 CFR 71), *Packaging and Transportation of Radioactive Material*, 01–01–09 Edition.

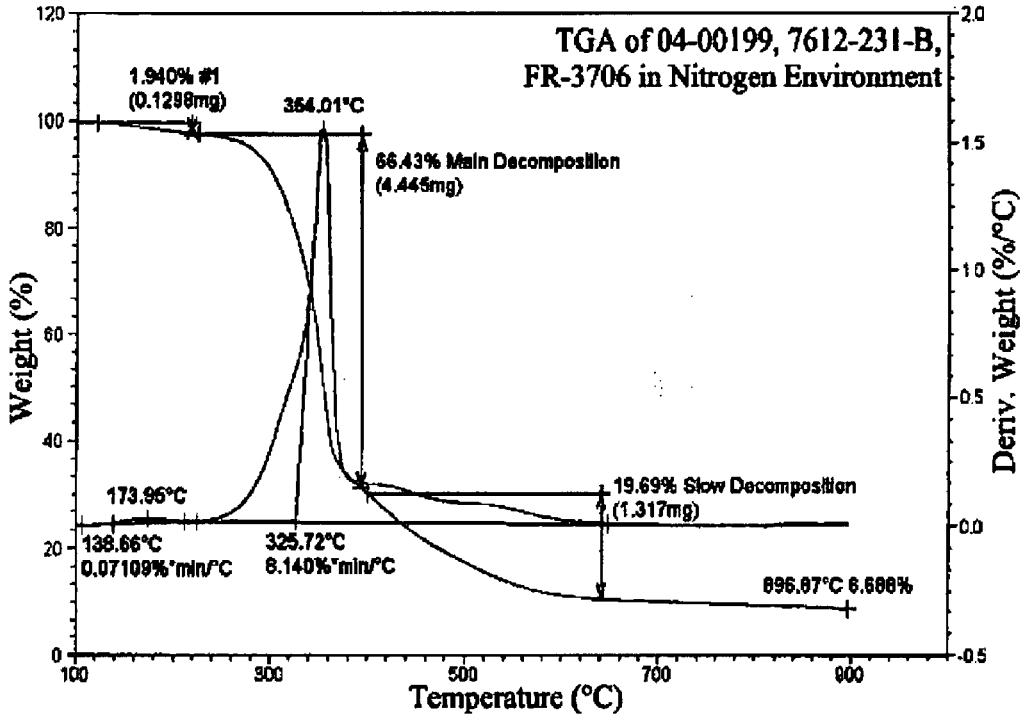

Figure 3.5-25 – TGA Analysis of Foam Decomposition in Nitrogen

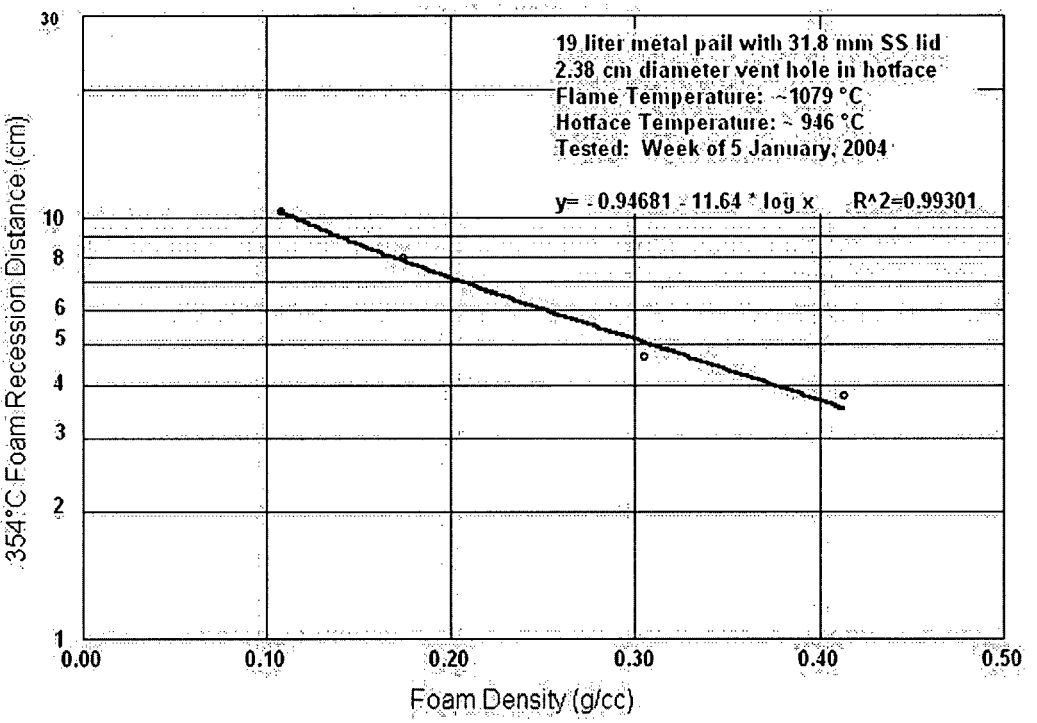

Figure 3.5-26 – Foam Recession vs. Density for 30-minute Fire

4.0 CONTAINMENT

4.1 Description of the Containment System

4.1.1 Containment Vessel

A single level of containment is established within the TRUPACT–III packaging. In general, the containment vessel is constructed primarily of Alloy UNS S31803 duplex stainless steel. The exceptions to the use of Alloy UNS S31803 stainless steel are so noted in the following detailed description.

The containment boundary of the TRUPACT–III packaging consists of the inner surfaces of the containment structural assembly (CSA). Specifically, the containment boundary is comprised of the inner rear wall, the inner side walls, the inner top and bottom walls, and the inner sheet of the closure lid. The containment boundary also includes those parts of the CSA body and closure lid flanges which are inboard of the containment (innermost) butyl O-ring seal. In addition, the containment boundary includes an aluminum bronze vent port insert with a mating inner butyl O-ring seal. A more detailed description of the containment boundary is provided in Section 1.2.1.1, *Body*, Section 1.2.1.2, *Closure Lid*, and in Appendix 1.3.1, *Packaging General Arrangement Drawings*.

4.1.2 Containment Penetrations

The only containment boundary penetrations into the containment vessel are the closure lid itself and the vent port. Each penetration is designed to demonstrate "leaktight" sealing integrity, i.e., a leakage rate not to exceed 1×10^{-8} Pa-m^3/s, air, as defined in ANSI N14.5[1].

4.1.3 Seals and Welds

4.1.3.1 Seals

The minimum and maximum compression for the TRUPACT–III containment O-ring seal are calculated based on the worst-case dimensions for the O-ring seal and groove as shown in Appendix 1.3.1, *Packaging General Arrangement Drawings*. The main closure lid containment O-ring seal has a diameter of 12 ± 0.15 mm. The groove into which the seal is placed has a depth of 8.27 ± 0.15 mm. The groove length, based on centerline dimensions of 1,888 × 2,048, with 50-mm corner radii, is:

$$L_G = 2(1{,}888 \text{ mm} + 2{,}048 \text{ mm}) - 8(50) + 2\pi\,(50 \text{ mm}) = 7{,}786 \text{ mm}$$

The inner diameter of the containment O-ring is 2,394 mm, or 2,394 + 12 = 2,406 mm on its centerline. The centerline length is therefore 2,406 × π = 7,559 mm, for a stretch of:

[1] ANSI N14.5–1997 (or later), *American National Standard for Radioactive Materials – Leakage Tests on Packages for Shipment,* American National Standards Institute, Inc. (ANSI).

$$S = \frac{(\text{Groove Length}) - (\text{O-ring Length})}{(\text{O-ring Length})} \times 100 = \frac{(7{,}786) - (7{,}559)}{(7{,}559)} \times 100 = 3.0\,\%$$

From Figure 3-3 for the calculated curve of the Parker O-ring Handbook[2], the resulting reduction in O-ring seal cross-sectional diameter is 1.5%. The reduced cross-sectional diameters, D_{Rmin} and D_{Rmax}, are therefore 1.5% less than the non-stretched diameters, ($D_{min} = 12 - 0.15 = 11.85$ mm) and ($D_{max} = 12 + 0.15 = 12.15$ mm), or:

$$D_{Rmin} = (1 - 0.015)D_{min} = 11.67 \text{ mm}$$

$$D_{Rmax} = (1 - 0.015)D_{max} = 11.97 \text{ mm}$$

The range of groove depths in the closure lid is:

minimum groove depth, $d_{min} = 8.27 - 0.15 = 8.12$ mm

maximum groove depth, $d_{max} = 8.27 + 0.15 = 8.42$ mm

Using these quantities, the maximum and minimum seal compression at ambient temperature, C_{seal}, is calculated as follows:

$$C_{seal} = \left[1 - \left(\frac{d}{D_R}\right)\right] \times 100$$

$$C_{seal\text{-}min} = \left[1 - \left(\frac{d_{max}}{D_{Rmin}}\right)\right] \times 100 = 27.8\%$$

$$C_{seal\text{-}max} = \left[1 - \left(\frac{d_{min}}{D_{Rmax}}\right)\right] \times 100 = 32.2\%$$

As shown in Section 2.12.2.6, *Test Results*, a room temperature compression of at least 19.8% is required to ensure that the minimum allowable compression of 18.5% exists at the minimum NCT temperature of -40 °C. The minimum room temperature compression of 27.8% is well in excess of this value.

A summary of seal testing prior to first use, during routine maintenance, and upon assembly for transportation is as follows.

4.1.3.1.1 Fabrication Leakage Rate Tests

During fabrication and following the pressure testing per Section 8.1.3.2, *Containment Vessel Pressure Testing*, the CSA shall be leakage rate tested as delineated in Section 8.1.4, *Fabrication Leakage Rate Tests*. The fabrication leakage rate tests are consistent with the guidelines of Section 7.3 of ANSI N14.5. This leakage rate test verifies the containment integrity of the TRUPACT–III packaging to a leakage rate not to exceed 1×10^{-8} Pa–m^3/s, air.

[2] ORD 5700, *Parker O-ring Handbook*, 2007, Parker Hannifin Corporation, Cleveland, OH.

4.1.3.1.2 Maintenance/Periodic Leakage Rate Tests

Annually, or at the time of damaged containment seal replacement or sealing surface repair, the O-ring seals shall be leakage rate tested as delineated in Section 8.2.2, *Maintenance/Periodic Leakage Rate Tests*. The maintenance/periodic leakage rate tests are consistent with the guidelines of Section 7.4 of ANSI N14.5. This test verifies the sealing integrity of the closure lid and vent port containment seals to a leakage rate not to exceed 1×10^{-8} Pa–m^3/s, air.

4.1.3.1.3 Preshipment Leakage Rate Tests

Prior to shipment of the loaded TRUPACT–III package, the main inner O-ring seal and vent port insert O-ring seal shall be leakage rate tested per Section 7.4, *Preshipment Leakage Rate Test*. The preshipment leakage rate tests are consistent with the guidelines of Section 7.6 of ANSI N14.5. This test verifies the sealing integrity of the closure lid and vent port insert containment seals to a leakage rate sensitivity of 1×10^{-4} Pa–m^3/s, air.

The maintenance/periodic leakage rate tests, delineated in Section 8.2.2, *Maintenance/Periodic Leakage Rate Tests*, may be performed as an option, in lieu of the preshipment leakage rate tests.

4.1.3.2 Welds

All containment vessel body welds are full penetration welds that have been radiographed to ensure structural and containment integrity. Non-radiographed, safety related welds such as those that attach the V-stiffeners to their respective containment plates are examined using liquid penetrant testing on the final pass. All containment boundary welds are confirmed to be leaktight as delineated in Section 8.1.4, *Fabrication Leakage Rate Tests*.

4.1.4 Closure

With reference to Figures 1.1-1 and 1.1-2 in Chapter 1.0, *General Information*, the closure lid is secured to the body via forty-four (44) M36 × 4 socket head cap screws tightened to a torque of 1,600 ±120 N-m. Thus, the closure lid is securely attached. After completing the installation of the closure lid, the overpack cover is installed over the closure lid, which completely covers the lid and the vent port. The overpack cover is secured with ten (10), M36 × 4 socket head cap screws tightened to a torque of 1,600 ±120 N-m. Thus, the closure lid and the vent port cannot be inadvertently opened.

This page intentionally left blank.

4.2 Containment Under Normal Conditions of Transport

4.2.1 Containment of Radioactive Material

The results of the normal conditions of transport (NCT) structural and thermal evaluations performed in Section 2.6, *Normal Conditions of Transport*, and Section 3.3, *Thermal Evaluation for Normal Conditions of Transport*, respectively, and the results of full-scale structural testing presented in Appendix 2.12.3, *Certification Tests on CTU-1* and Appendix 2.12.6, *Certification Tests on CTU-2*, verify that there will be no release of radioactive materials per the "leaktight" definition of ANSI N14.5[1] under any of the NCT tests described in 10 CFR §71.71[2].

4.2.2 Pressurization of Containment Vessel

The maximum normal operating pressure (MNOP) of the CSA is 172 kPa per Section 3.3.2, *Maximum Normal Operating Pressure*. The design pressure of the CSA is 172 kPa. Based on the structural evaluations performed in Chapter 2.0, *Structural Evaluation*, pressure increases to 172 kPa will not reduce the effectiveness of the TRUPACT–III package to maintain containment integrity per Section 4.2.1, *Containment of Radioactive Material.*

4.2.3 Containment Criterion

At the completion of fabrication, the CSA shall be leakage rate tested as described in Section 4.1.3.1.1, *Fabrication Leakage Rate Tests*. For annual maintenance, the CSA shall be leakage rate tested as described in Section 4.1.3.1.2, *Maintenance/Periodic Leakage Rate Tests*. In addition, at the time of a seal replacement if other than during routine maintenance (e.g., if damage during assembly necessitates seal replacement), maintenance/periodic leakage rate testing shall be performed for the seal that is replaced. For verification of proper assembly prior to shipment, the CSA shall be leakage rate tested as described in Section 4.1.3.1.3, *Preshipment Leakage Rate Tests.*

[1] ANSI N14.5–1997 (or later), *American National Standard for Radioactive Materials – Leakage Tests on Packages for Shipment,* American National Standards Institute, Inc. (ANSI).

[2] Title 10, Code of Federal Regulations, Part 71 (10 CFR 71), *Packaging and Transportation of Radioactive Material*, 01–01–09 Edition.

This page intentionally left blank.

4.3 Containment Under Hypothetical Accident Conditions

4.3.1 Fission Gas Products

There are no fission gas products in the TRUPACT–III package payload.

4.3.2 Containment of Radioactive Material

The results of the hypothetical accident condition (HAC) structural and thermal evaluations performed in Section 2.7, *Structural Evaluation for Hypothetical Accident Conditions*, and Section 3.4, *Thermal Evaluation for Hypothetical Accident Conditions*, respectively, and the results of full-scale structural testing presented in Appendix 2.12.3, *Certification Tests on CTU-1* and Appendix 2.12.6, *Certification Tests on CTU-2*, verify that there will be no release of radioactive materials per the "leaktight" definition of ANSI N14.5[1] under any of the HAC tests described in 10 CFR §71.73[2].

[1] ANSI N14.5–1997 (or later), *American National Standard for Radioactive Materials – Leakage Tests on Packages for Shipment,* American National Standards Institute, Inc. (ANSI).

[2] Title 10, Code of Federal Regulations, Part 71 (10 CFR 71), *Packaging and Transportation of Radioactive Material,* 01–01–09 Edition.

This page intentionally left blank.

4.4 Leakage Rate Tests for Type B Packages

The TRUPACT–III package is leakage rate tested as described in Section 4.1.3.1, *Seals*, to meet the "leaktight" definition of ANSI N14.5[1].

[1] ANSI N14.5–1997 (or later), *American National Standard for Radioactive Materials – Leakage Tests on Packages for Shipment,* American National Standards Institute, Inc. (ANSI).

This page intentionally left blank.

5.0 SHIELDING EVALUATION

The compliance evaluation of the TRUPACT–III packaging with respect to the dose rate limits established by 10 CFR §71.47(a)[1] for normal conditions of transport (NCT) or 10 CFR §71.51(a)(2) for hypothetical accident conditions (HAC) is based on limiting the dose rate of the payload container, not crediting the use of supplemental shielding within the payload container, and relying on the additional dose rate attenuation inherit in the structural design of the packaging to ensure that the package dose rate requirements are satisfied.

Each contact-handled transuranic (CH–TRU) waste payload container, i.e., SLB2, as prepared for transport in a TRUPACT–III package, is limited such that the external radiation field, both gamma and neutron, shall be less than or equal to 2 milliSieverts per hour (mSv/hr) at the surface of the payload container. This dose rate limit is for the payload container prior to addition of any lead, steel or other shielding material to the payload container for *as-low-as-reasonably-achievable* (ALARA) dose reduction purposes during non-transport handling operations.

The TRUPACT–III packaging is not designed to provide any significant gamma or neutron shielding. Five essentially concentric stainless steel sheets comprise the TRUPACT–III structure, providing an overall composite thickness of 36 mm. A minimum of 109 mm of polyurethane foam and 60 mm of balsa wood occupies the remaining spaces between the containment structural assembly and outer sheet.

Prior to transport, the TRUPACT–III package shall be monitored on the semi-trailer or railcar for both gamma and neutron radiation to demonstrate compliance with 10 CFR §71.47. Since the TRUPACT–III package is not significantly deformed under NCT, the package will meet the dose rate limits for NCT if the measurements demonstrate compliance with the allowable dose rate levels in 10 CFR §71.47. The shielding Transport Index (TI), as defined in 10 CFR §71.4, will be determined by measuring the dose rate at a distance of one meter from the package surface per the requirements of 49 CFR §173.403[2].

Shielding materials are not specifically provided by the TRUPACT–III packaging, and none are permitted in the payload containers to meet the dose rate limits of 10 CFR §71.47 for NCT. Therefore, shielding provided by the stainless steel shells and polyurethane foam of the packaging is not needed to meet the higher dose rate limits after the HAC tests delineated in 10 CFR §71.73. This ensures that the post-HAC, allowable dose rate of 10 mSv/hr a distance of one meter from the package surface per 10 CFR §71.51(a)(2) will be met.

Even if payload material is released from a payload container during a HAC event, the post-HAC dose rate limit of 10 mSv/hr at one meter from the package surface will always be met. This is because each CH-TRU waste payload container must have a dose rate less than or equal to 2 mSv/hr on contact prior to the addition of any ALARA dose reduction shielding for non-transport handling operations prior to being loaded into the TRUPACT–III packaging. Since shielding within the payload container is not permitted to meet the transportation dose rate limits

[1] Title 10, Code of Federal Regulations, Part 71 (10 CFR 71), *Packaging and Transportation of Radioactive Material*, 01–01–09 Edition.

[2] Title 49, Code of Federal Regulations, Part 173 (49 CFR 173), *Shippers – General Requirements for Shipments and Packagings*, 10–01–09 Edition.

for NCT, release of the materials from the payload container during a HAC event will not increase the dose rate significantly or cause it to exceed the dose rate limit for HAC.

6.0 CRITICALITY EVALUATION

The following analyses demonstrate that the TRUPACT–III package complies with the requirements of 10 CFR §71.55 and §71.59[1]. The analyses presented herein demonstrate that the criticality requirements are satisfied when limiting the TRUPACT–III package to the fissile gram equivalent (FGE) limits provided in Table 6.1-1 for the payloads described in the *TRUPACT–III TRU Waste Authorized Methods for Payload Control (TRUPACT–III TRAMPAC)*[2]. The contents are manually compacted (i.e., not machine compacted) waste contaminated with fissile materials containing less than or equal to 1% by weight quantities of special reflector materials

6.1 Description of Criticality Design

6.1.1 Design Features

No special features are required to maintain criticality safety for any number of TRUPACT–III packages for both normal conditions of transport (NCT) and hypothetical accident conditions (HAC). The presence and location of the stainless steel containment vessel sheets and adjoining concentric sheet and plate structures are all that are required to maintain criticality safety.

6.1.2 Summary Table of Criticality Evaluation

The maximum results of the TRUPACT–III criticality calculations are summarized in Table 6.1-1 for four assumed Pu-240 loadings (0, 5, 15, and 25 g). As Pu-240 behaves neutronically as a poison, the FGE limit increases with increasing Pu-240 mass.

For a single TRUPACT–III package under NCT or HAC conditions, the maximum calculated k_s ($k+2\sigma$) value is 0.9335 when optimally moderated and reflected with a mixture of 25% polyethylene, 74% water, and 1% beryllium (by volume). This value is below the USL of 0.9392. Therefore, the requirements of 10 CFR §71.55 are met when the contents of a single TRUPACT–III package are limited to the values provided in Table 6.1-1.

For an infinite array of TRUPACT–III packages under NCT or HAC conditions, the maximum calculated k_s value is 0.9335 for optimal internal moderation and reflection with a mixture of 25% polyethylene, 74% water, and 1% beryllium (by volume) and optimal external interspersed moderation by water. As with the single package case, the k_s is below the USL of 0.9392. This maximum value occurs when each of the packages in the array is fully reflected (internally) and therefore isolated from each other.

Results indicate that the maximum reactivity of the package arrays is identical to that of the single-unit. This occurs because:

[1] Title 10, Code of Federal Regulations, Part 71 (10 CFR 71), *Packaging and Transportation of Radioactive Material*, 01–01–09 Edition.

[2] *TRUPACT–III TRU Waste Authorized Methods for Payload Control (TRUPACT–III TRAMPAC)*, U.S. Department of Energy, Carlsbad Field Office, Carlsbad, New Mexico.

- When internally reflected to the maximum extent, the fissile material regions of the array of TRUPACT–III packages are essentially isolated from each other, and
- When the fissile material region of each damaged or undamaged TRUPACT–III package is internally unreflected, interaction between TRUPACT–III packages is maximized. However, for the array of TRUPACT–III packages, interactive effects are not as great as the effect of full internal reflection.

Therefore, the requirements of 10 CFR §71.59 are met for arrays of TRUPACT–III packages when the contents of a single TRUPACT–III package is limited to the values provided in Table 6.1-1. Furthermore, a Criticality Safety Index (CSI) of zero (0.0) is justified because an infinite array of packages is utilized.

6.1.3 Criticality Safety Index

As noted in Section 6.1.2, an infinite array of packages is modeled for both NCT and HAC conditions. Therefore, the CSI = $50/\infty = 0.0$.

Table 6.1-1 – Summary of Criticality Evaluation

FGE Limit	**325**	**340**	**360**	**380**
Pu-240 Content (g)	**0**	**5**	**15**	**25**
Normal Conditions of Transport (NCT)				
Number of undamaged packages calculated to be subcritical	∞	∞	∞	∞
Single Unit Maximum k_s	0.9333	0.9335	0.9317	0.9319
Infinite Array Maximum k_s	0.9333	0.9335	0.9317	0.9319
Hypothetical Accident Conditions (HAC)				
Number of damaged packages calculated to be subcritical	∞	∞	∞	∞
Single Unit Maximum k_s	0.9333	0.9335	0.9317	0.9319
Infinite Array Maximum k_s	0.9333	0.9335	0.9317	0.9319
Upper Subcritical Limit (USL)	0.9392			

6.2 Fissile Material Contents

6.2.1 General

The contents are manually compacted (i.e., not machine compacted) waste contaminated with fissile materials containing less than or equal to 1% by weight quantities of special reflector materials. The payload within each TRUPACT–III package is held within a Standard Large Box 2 (SLB2). The SLB2 overall size envelope consists of a 108" length, 69" width, and 73" height. A single TRUPACT–III can transport one SLB2. The SLB2 is not modeled in the criticality evaluation.

The typical isotopic distribution of the waste is provided in Table 6.2-1. In accordance with ANSI/ANS-8.1[1], the quantities of all fissile isotopes other than Pu-239 present in the CH-TRU waste material and other authorized payloads may be converted to a fissile gram equivalent (FGE) of the most restrictive isotope for criticality evaluations. As noted in Table 6.1-1, the mass of the fissile contents ranges from 325 FGE Pu-239 with no Pu-240 up to 380 FGE Pu-239 with 25 g Pu-240.

If no credit is taken for the poisoning effects of Pu-240, all fissile material present in the package is modeled as Pu-239. If credit is taken for the poisoning effects of Pu-240, the fissile material is modeled as a mixture of Pu-239 and Pu-240. When developing the total FGE for an actual package, Pu-240 should be conservatively included in the total FGE even if credit is taken for its poisoning effects. In addition, in accordance with ANSI/ANS-8.1, Pu-241 is considered to be Pu-239 when computing plutonium mass values provided the Pu-240 concentration exceeds the Pu-241 concentration.

No credit is taken for parasitic neutron absorption in contact-handled transuranic (CH-TRU) waste materials and other authorized payloads, dunnage, or package contents for the base case with no Pu-240, except to the extent that the elements present in the moderator absorb neutrons. For cases with variable amounts of Pu-240, credit is taken for parasitic neutron absorption in this material.

The CH-TRU waste material and other authorized payloads may contain plastic materials such as anti-contamination clothing, plastic bags, and other plastic refuse. Plastic items present in the payload will be present with a low packing density. Because polyethylene is a superior moderator to water and leads to higher reactivities, the volume fraction of polyethylene used in TRUPACT–III criticality analysis must bound the polyethylene volume fraction expected in the waste stream. The volume fraction of polyethylene was experimentally determined, using hand-packing of surrogate waste forms, to be 13.36%[2]. Therefore, in all TRUPACT–III criticality models, a bounding value of 25% polyethylene (by volume) is utilized.

A small amount of special reflecting materials may be present in the waste stream as a result of cross-contamination. To bound the presence of small (< 1% of the waste mass) amounts of special reflectors, models are developed with 1% by volume beryllium in the fissile and reflector regions. ("Reflector" in this context is the region outside the fissile mass but within the inner cavity of the package.) Due to the

[1] ANSI/ANS-8.1-1998, *Nuclear Criticality Safety in Operations with Fissionable Materials Outside Reactors*, American Nuclear Society, September 1998.

[2] WP 08-PT.09, *Test Plan to Determine the TRU Waste Polyethylene Packing Fraction*, Washington TRU Solutions, LLC., Revision 0, June 2003.

large volume of the package, 1% by volume bounds 1% by weight. Special reflectors are discussed further in Section 6.2.2, *Special Reflectors.*

Therefore, to bound the presence of both plastics and special reflectors in the waste stream, the fissile material is both moderated and reflected with a mixture of 25% polyethylene, 74% water, and 1% beryllium (by volume) for both NCT and HAC conditions.

6.2.2 Special Reflectors

As noted above, this analysis considers the potential presence of a limited quantity of "special reflectors," which are materials that can credibly provide better than 25% polyethylene/75% water equivalent reflection and are not authorized for shipment in quantities that exceed 1% by mass except in specific configurations discussed below. An extensive study of special reflectors has been documented in report SAIC-1322-001[3], which was developed for a reflected sphere of 325 g Pu-239 for the TRUPACT–II package. As the TRUPACT–II and TRUPACT–III are both large cavity packages with similar payloads for the general case, the conclusions from SAIC-1322-001 are also applicable to the TRUPACT–III. Based on the results from SAIC-1322-001, Be, BeO, C, D_2O, MgO, and depleted U (less than 0.72 wt.% and greater than or equal to 0.3 wt.% U-235) are the only materials that can provide reflection equivalent to a 2 ft thickness of 25% polyethylene and 75% water mixture under any of the following conditions:

- Less than 15.9-mm thick at 100% of theoretical density[4] in the form of large solids
- Less than 17.5-mm thick at 70% of theoretical density in the form of tightly-packed particulate solids
- Less than 20% packing fraction at 609.6-mm thick in the form of randomly dispersed particulate solids

SAIC-1322-001 found that beryllium is the bounding special reflector as it provides the best reflection of the system resulting in the highest reactivity. In the current analysis, the utilization of 1% by volume beryllium in the models bounds the presence of up to 1% by mass quantities of special reflectors that are dispersed in the waste matrix.

The reference study, SAIC-1322-001, found that, with the exception of Be, adding special reflector materials to the fissile region reduced the reactivity of a single 325 FGE, 25% polyethylene/75% water reflected sphere. Thus, if it can be shown that a candidate special reflector other than Be is chemically or mechanically bound to the fissile material, or otherwise in a form which would not provide better than a 25% polyethylene/75% water equivalent reflection, the FGE limits developed using an assumption of 1% Be by mass will apply even in the presence of greater than 1% by mass quantities of the special reflector.

---

[3] Neeley, G. W., D. L. Newell, S. L. Larson and R. J. Green, *Reactivity Effects of Moderator and Reflector Materials on a Finite Plutonium System*, SAIC-1322-001 Revision 1, Science Applications International Corporation, Oak Ridge, Tennessee, May 2004.

[4] Theoretical densities used in the study are 1.85 g/cm^3 for Be, 2.69 g/cm^3 for BeO, 2.1 g/cm^3 for C, 1.1054 g/cm^3 for D_2O, 3.22 g/cm^3 for MgO, and 19.05 g/cm^3 for U.

As further discussed below, a consideration of each candidate special reflector in CH-TRU waste has been made, leading to the conclusion that, with the exception of Be and BeO, none will provide better than a 25% polyethylene/75% water equivalent reflection. Therefore, the current analysis utilizes a mixture of 25% polyethylene, 74% water, and 1% beryllium (by volume) for both the moderator and reflector, which bounds a 25% polyethylene/75% water mix. In summary, except for limiting TRUPACT–III shipments to 1% by weight quantities of Be and BeO, no specific controls on candidate special reflectors are needed.

The only "special reflectors" applicable to CH-TRU waste criticality analysis are Be, BeO, C, D_2O, MgO, and depleted U, when present in quantities greater than 1% by weight. Each special reflector with regard to its possible presence in CH-TRU waste is discussed below.

Beryllium and Beryllium Oxide – Be and BeO may be present in CH-TRU waste in quantities which exceed 1% by weight. However, for transport in the TRUPACT–III, Be and BeO are specifically limited to quantities not exceeding 1% by weight.

Carbon – Carbon is present as a constituent in CH-TRU waste but not in forms that can reconfigure as a reflector. For example: (1) Carbon may be present as graphite molds or crucibles. In these forms the carbon will be chemically and irreversibly bound to the plutonium or other fissile material and cannot be separated. (2) Carbon may be present in filter media as spent or activated carbon. The plutonium or other fissile material would then be attached to the carbon filter media and would not be easily separated. (3) Granular activated carbon (GAC) pads may also be present in an enclosed bag for the purpose of absorbing volatile organic compounds. Once the GAC pad is placed inside the payload container, there is no method for the carbon to fully surround the fissile material and reconfigure as a reflector. (4) Carbon may also be present in alloys, which are by definition chemically and/or mechanically bound. In summary, there is no identified mechanism that could cause the carbon in CH-TRU waste to be separated from the fissile material and to be reconfigured as a reflector.

Deuterium – The presence of liquid waste in the payload containers, except for residual amounts, is prohibited. As specified by the TRUPACT–III TRAMPAC, the total volume of residual liquid in a payload container shall be less than 1 percent (volume) of the payload container. This limitation on the authorized contents is such that deuterium will not be present in concentrations of greater than 1% by weight.

Magnesium Oxide – Magnesium oxides used in temperature control applications may be present in solid inorganic waste forms such as glass, metal, and pyrochemical salts. If present, magnesium oxide will be bound to the fissile material and would not be easily separated. Magnesium oxide used for neutralization in solidified material cannot be separated out as it is chemically reacted in the waste generation process. There is no identified mechanism that could cause the magnesium oxide in CH-TRU waste to be reconfigured as a reflector.

Depleted Uranium – Depleted uranium may be present in CH-TRU waste, but it will be chemically and/or mechanically bound to the plutonium or physically inseparable because the densities of uranium and plutonium are similar. Separation by mechanical means or by leaching is extremely difficult and is considered highly unlikely in CH-TRU waste. Depleted uranium in CH-TRU waste will, therefore, not be separated from the fissile material and reconfigured as a reflector.

6.2.3 Fissile Material Modeling

It is assumed that when packaged, the fissile material is distributed throughout the waste volume. Under accident conditions, water in-leakage may cause some fissile material to migrate within the package interior. It is unlikely that a distributed volume of fissile material could coalesce into a single fuel lump, but such a scenario is conservatively assumed. Because the most conservative fissile geometry is a sphere, a spherical fissile geometry is utilized. Therefore, this geometry bounds the true NCT and HAC geometry of the fissile material, which would likely be highly distributed.

It is desired to compute the Pu number densities as a function of H/X, where X is the Pu-239 number density. To compute the number densities, the following gram densities are utilized: 1.0 g/cm^3 for water, 0.92 g/cm^3 for polyethylene, and 1.848 g/cm^3 for beryllium. As the H/X ratio becomes larger, the size of the fissile volume also becomes larger. The fissile material number densities are provided in Table 6.2-2 through **Error! Reference source not found.**Table 6.2-5 for a Pu-239 FGE limit of 325 g, 340 g, 360 g, and 380 g, respectively. Note that the number densities of the moderating elements (H, C, O, and Be) are not constant between the various cases**Error! Reference source not found.**. The reason for the slight variability in these number densities is that the volume displaced by the Pu (solid metal, density = 19.84 g/cm^3) is explicitly factored into the computations (e.g., the volume of Pu is subtracted from the total fissile volume, and the remaining volume is divided on a volume percentage between water, polyethylene, and beryllium.) However, because the Pu mass is relatively small, the moderator number densities are nearly constant**Error! Reference source not found.**.

Table 6.2-1 – Fissile Payload Composition (typical)

Nuclide	Weight-Percent
Pu-238	Trace
Pu-239	93.0
Pu-240	5.8
Pu-241	0.4
Pu-242	Trace
Am-241	Trace
All other fissile isotopes	0.7

Table 6.2-2 – Number Densities, 325 g Pu-239, 0 g Pu-240

H/X	Radius (cm)	Pu-239 (at/b-cm)	Pu-240 (at/b-cm)	H (at/b-cm)	Be (at/b-cm)	C (at/b-cm)	O (at/b-cm)
500	11.2286	1.3806E-04	0.0000E+00	6.9030E-02	1.2314E-03	9.8473E-03	2.4668E-02
600	11.9303	1.1510E-04	0.0000E+00	6.9062E-02	1.2320E-03	9.8518E-03	2.4679E-02
700	12.5580	9.8692E-05	0.0000E+00	6.9085E-02	1.2324E-03	9.8550E-03	2.4687E-02
800	13.1285	8.6377E-05	0.0000E+00	6.9102E-02	1.2327E-03	9.8575E-03	2.4693E-02
900	13.6533	7.6794E-05	0.0000E+00	6.9115E-02	1.2329E-03	9.8594E-03	2.4698E-02
1000	14.1406	6.9126E-05	0.0000E+00	6.9126E-02	1.2331E-03	9.8609E-03	2.4702E-02
1100	14.5965	6.2849E-05	0.0000E+00	6.9134E-02	1.2333E-03	9.8621E-03	2.4705E-02
1200	15.0255	5.7618E-05	0.0000E+00	6.9142E-02	1.2334E-03	9.8632E-03	2.4708E-02
1300	15.4313	5.3190E-05	0.0000E+00	6.9148E-02	1.2335E-03	9.8640E-03	2.4710E-02
1400	15.8169	4.9395E-05	0.0000E+00	6.9153E-02	1.2336E-03	9.8648E-03	2.4712E-02
1500	16.1845	4.6105E-05	0.0000E+00	6.9157E-02	1.2337E-03	9.8654E-03	2.4713E-02
1600	16.5361	4.3226E-05	0.0000E+00	6.9161E-02	1.2338E-03	9.8660E-03	2.4715E-02
1700	16.8734	4.0685E-05	0.0000E+00	6.9165E-02	1.2338E-03	9.8665E-03	2.4716E-02
1800	17.1977	3.8427E-05	0.0000E+00	6.9168E-02	1.2339E-03	9.8669E-03	2.4717E-02

Table 6.2-3 – Number Densities, 340 g Pu-239, 5 g Pu-240

H/X	Radius (cm)	Pu-239 (at/b-cm)	Pu-240 (at/b-cm)	H (at/b-cm)	Be (at/b-cm)	C (at/b-cm)	O (at/b-cm)
500	11.3989	1.3805E-04	2.0217E-06	6.9027E-02	1.2314E-03	9.8469E-03	2.4667E-02
600	12.1112	1.1510E-04	1.6856E-06	6.9060E-02	1.2320E-03	9.8515E-03	2.4678E-02
700	12.7484	9.8689E-05	1.4453E-06	6.9083E-02	1.2324E-03	9.8548E-03	2.4687E-02
800	13.3275	8.6375E-05	1.2649E-06	6.9100E-02	1.2327E-03	9.8572E-03	2.4693E-02
900	13.8603	7.6793E-05	1.1246E-06	6.9113E-02	1.2329E-03	9.8591E-03	2.4698E-02
1000	14.3550	6.9124E-05	1.0123E-06	6.9124E-02	1.2331E-03	9.8607E-03	2.4701E-02
1100	14.8177	6.2848E-05	9.2038E-07	6.9133E-02	1.2333E-03	9.8619E-03	2.4705E-02
1200	15.2533	5.7617E-05	8.4377E-07	6.9140E-02	1.2334E-03	9.8630E-03	2.4707E-02
1300	15.6652	5.3190E-05	7.7894E-07	6.9147E-02	1.2335E-03	9.8639E-03	2.4709E-02
1400	16.0566	4.9394E-05	7.2335E-07	6.9152E-02	1.2336E-03	9.8646E-03	2.4711E-02

Table 6.2-4 – Number Densities, 360 g Pu-239, 15 g Pu-240

H/X	Radius (cm)	Pu-239 (at/b-cm)	Pu-240 (at/b-cm)	H (at/b-cm)	Be (at/b-cm)	C (at/b-cm)	O (at/b-cm)
500	11.6184	1.3804E-04	5.7278E-06	6.9022E-02	1.2313E-03	9.8461E-03	2.4665E-02
600	12.3445	1.1509E-04	4.7755E-06	6.9055E-02	1.2319E-03	9.8509E-03	2.4677E-02
700	12.9939	9.8684E-05	4.0947E-06	6.9079E-02	1.2323E-03	9.8542E-03	2.4685E-02
800	13.5841	8.6371E-05	3.5838E-06	6.9097E-02	1.2326E-03	9.8568E-03	2.4692E-02
900	14.1271	7.6789E-05	3.1862E-06	6.9111E-02	1.2329E-03	9.8587E-03	2.4697E-02
1000	14.6313	6.9122E-05	2.8680E-06	6.9122E-02	1.2331E-03	9.8603E-03	2.4700E-02
1100	15.1029	6.2846E-05	2.6077E-06	6.9131E-02	1.2332E-03	9.8616E-03	2.4704E-02
1200	15.5468	5.7615E-05	2.3906E-06	6.9138E-02	1.2334E-03	9.8627E-03	2.4706E-02
1300	15.9667	5.3188E-05	2.2069E-06	6.9145E-02	1.2335E-03	9.8636E-03	2.4709E-02
1400	16.3656	4.9393E-05	2.0494E-06	6.9150E-02	1.2336E-03	9.8644E-03	2.4711E-02

Table 6.2-5 – Number Densities, 380 g Pu-239, 25 g Pu-240

H/X	Radius (cm)	Pu-239 (at/b-cm)	Pu-240 (at/b-cm)	H (at/b-cm)	Be (at/b-cm)	C (at/b-cm)	O (at/b-cm)
500	11.8300	1.3804E-04	9.0434E-06	6.9018E-02	1.2312E-03	9.8455E-03	2.4663E-02
600	12.5692	1.1509E-04	7.5398E-06	6.9051E-02	1.2318E-03	9.8503E-03	2.4675E-02
700	13.2304	9.8679E-05	6.4650E-06	6.9076E-02	1.2322E-03	9.8538E-03	2.4684E-02
800	13.8314	8.6367E-05	5.6583E-06	6.9094E-02	1.2326E-03	9.8564E-03	2.4691E-02
900	14.3842	7.6787E-05	5.0307E-06	6.9108E-02	1.2328E-03	9.8584E-03	2.4696E-02
1000	14.8975	6.9119E-05	4.5283E-06	6.9119E-02	1.2330E-03	9.8600E-03	2.4700E-02
1100	15.3778	6.2844E-05	4.1172E-06	6.9129E-02	1.2332E-03	9.8613E-03	2.4703E-02
1200	15.8297	5.7614E-05	3.7745E-06	6.9136E-02	1.2333E-03	9.8624E-03	2.4706E-02
1300	16.2572	5.3187E-05	3.4845E-06	6.9143E-02	1.2334E-03	9.8633E-03	2.4708E-02
1400	16.6634	4.9392E-05	3.2359E-06	6.9148E-02	1.2335E-03	9.8641E-03	2.4710E-02

6.3 General Considerations

Criticality calculations for the TRUPACT–III package are performed using the three-dimensional MCNP5 Monte Carlo program[1]. Descriptions of the packaging geometric models are given in Section 6.3.1, *Model Configuration.* The material properties for all non-fissile materials used in the models are provided in Section 6.3.2, *Material Properties.* The computer code and cross section libraries used are provided in Section 6.3.3, *Computer Codes and Cross-Section Libraries.* Finally, the most reactive configuration is discussed in Section 6.3.4, *Demonstration of Maximum Reactivity.*

6.3.1 Model Configuration

All relevant features of the TRUPACT–III package are modeled in MCNP. The key dimensions used in the MCNP models are summarized in Table 6.3-1 and discussed in the following paragraphs. The NCT single package model geometry is illustrated in Figure 6.3-1 and Figure 6.3-2.

The inner dimensions of the containment structural assembly (CSA) are 184 cm x 200 cm x 279 cm. The outer dimensions (width and height) of the CSA are 212 cm x 228 cm, with a modeled length of 308.6 cm. The CSA is comprised of two layers of 0.8 cm thick steel plate separated by corrugated steel. For the closure lid, the plates are 1.2 cm thick, with an overall lid thickness of 14.8 cm. The corrugated steel has a negligible impact on reactivity and is omitted from the MCNP models.

The CSA is protected by layers of foam and balsa on the top, bottom, and sides of the package. The foam is 10.9 cm thick on the top and bottom, and 11.4 cm thick on the sides. The foam and balsa are separated by a layer of steel 1.0 cm thick. The balsa is 6 cm thick on each of the four sides. The outer skin of the package is 0.6 cm thick steel. The overall width (x) and height (y) of the package are 250 cm and 265 cm.

On each end of the package is an overpack cover. The inner boundary of each overpack cover is hexagonal in shape, while the outer boundary is approximately square in shape. Through the centerline of the closure lid end overpack cover are layers of steel (0.6 cm), foam (12.0 cm), steel (1.5 cm), balsa (6.0 cm), and steel (0.6 cm). Through the edge of the closure lid end overpack cover are layers of steel (0.6 cm), calcium silicate (4.2 cm), steel (1.6 cm), foam (38.4 cm), steel (0.6 cm), foam (14.0 cm), and steel (0.8 cm). For simplicity, the "cheeks" of the front end are not modeled explicitly. Rather, the x and y dimensions of the main portion of the overpack cover are extended to fill this region. This simplification has a negligible impact on the results.

The rear end is similar to the closure lid end overpack cover, although it is integral to the package. Through the centerline of the rear end, the material thicknesses are the same, although the innermost layer of steel is absent. Through the edge of the rear end impact limiter are layers of foam (44.8 cm), steel (0.6 cm), foam (14.0 cm), and steel (0.8 cm). The 44.8 cm thickness for the foam is approximate and selected to give the correct overall package length (z) of 428.8 cm. Also, the cheeks are modeled in the same manner as the closure lid end overpack cover.

The dimensions listed in the preceding paragraph are consistent with the NCT models, for which crush damage is assumed to be negligible. For the HAC models, all foam and balsa are conservatively

[1] MCNP5, *MCNP – A General Monte Carlo N-Particle Transport Code, Version 5; Volume II: User's Guide*, LA-CP-03-0245, Los Alamos National Laboratory, April 2003.

replaced with water of variable density, see Figure 6.3-3. Also, although at most only one side of the package would exhibit crush, 2.54 cm of crush is applied to the top, bottom, and sides of the package, and 7.62 cm of crush is applied to the ends of the package. This crush is applied to the thickness of the balsa region in the HAC models. Note that the modeled crush depth bounds the results of the actual drop tests, which demonstrated little deflection. Refer to Section 2.7.1, *Free Drop.*

Note that foam of several different densities is utilized in the package design, ranging from a low density of 0.096 g/cm^3 (6 pcf) to a high density of 0.480 g/cm^3 (30 pcf). To be conservative and to maximize reflection in the single package cases, all foam is modeled with a density of 0.480 g/cm^3, which maximizes the hydrogen density in the foam. In addition, for simplicity the calcium silicate is simply modeled as foam in the NCT cases (variable density water in the HAC cases).

All single package models are reflected with 30.48 cm (12 inches) of water.

6.3.2 Material Properties

The TRUPACT–III is constructed primarily from UNS S31803 stainless steel plate, balsa wood, and polyurethane foam of several different densities.

MCNP accepts material input in a variety of formats. The method of input for each material has been selected both to be consistent with the source of the data and for computational convenience. For foam and stainless steel, elemental compositions are input as weight percents and the gram density is input on the MCNP cell cards. For water and balsa wood, elemental compositions are input as atoms per molecule and the gram density is input on the MCNP cell cards. For the source and internal reflector, number densities are explicitly computed and the total atom density is input on the MCNP cell cards. (The number densities for the source are provided in Section 6.2.3.)

Most of the steel plate used in the package is UNS S31803. The composition and density of S31803 are provided in Table 6.3-2 and is obtained from the Allegheny Ludlum Corporation[3].

Balsa wood is modeled with a density of 0.125 g/cm^3 and the chemical formula $C_6H_{10}O_5$. The S(α,β) card POLY.60T is used to simulate hydrogen bound to carbon. The standard composition for balsa is obtained from the SCALE material library[4].

Water is modeled with a density ranging up to 1.0 g/cm^3 and the chemical formula H_2O. The S(α,β) card LWTR.60T is used to simulate hydrogen bound to oxygen in water.

Polyurethane foam of several different densities is present in the package. The density ranges from a low density of 0.096 g/cm^3 (6 pcf) to a high density of 0.480 g/cm^3 (30 pcf). To be conservative, the NCT models utilize a density of 0.480 g/cm^3 for all foam. A high density bounds a low density because increasing the hydrogen concentration increases neutron reflection and hence reactivity, as demonstrated in Section 6.6. The foam composition is provided in Table 6.3-3. Because the composition is provided as ranges, the composition used in the analysis is

[3] Technical Data Blue Sheet for Stainless Steel AL 2205™ Alloy (UNS Designation S31803), Allegheny Ludlum Corporation, Pittsburgh, PA.

[4] *Standard Composition Library*, NUREG/CR-0200, Rev. 6, Volume 3, Section M8, ORNL/NUREG/CSD-2/V3/R6, September 1998.

selected to maximize the weight percent of hydrogen. The S(α,β) card POLY.60T is used to simulate hydrogen bound to carbon.

The internal reflector is a mixture of 25% polyethylene, 74% water, and 1% beryllium by volume. Because MCNP does not have a convenient method to input volume fractions, number densities are computed explicitly and are provided in Table 6.3-4. To compute the number densities, the following densities are utilized: 1.0 g/cm^3 for water, 0.92 g/cm^3 for polyethylene, and 1.848 g/cm^3 for beryllium. The S(α,β) card BE.60T is used to simulate metallic beryllium. Note that the hydrogen in the internal reflector may be bound to either carbon or oxygen. However, MCNP does not have the capability to utilize the two different S(α,β) cards for hydrogen bound to water and hydrogen bound to polyethylene in the same material. It is demonstrated in Section 6.4.1.1 that using either the card LWTR.60T or POLY.60T yields essentially identical results. LWTR.60T is used with the internal reflector (and source) for the models.

6.3.3 Computer Codes and Cross-Section Libraries

MCNP5 v1.30 is used for the criticality analysis. All cross sections utilized are at room temperature (293.6 K). The most recent cross sections available are used for each isotope. Most isotopes utilize ENDF/B-VI cross sections. ENDF/B-V elemental cross sections are utilized only when ENDF/B-VI elemental cross sections are not available. The Pu-239 cross sections are a preliminary version of ENDF/B-VII cross section set. Although the ENDF/B-VII cross section set had not been formally released with MCNP5 v1.30, LANL included this Pu-239 cross section because it showed significant improvements compared to the latest ENDF/B-VI Pu-239 cross section for certain LANL benchmark models. Titles of the cross sections utilized in the models have been extracted from the MCNP output and provided in Table 6.3-5. As discussed in Section 6.3.2, the S(α,β) cards LWTR.60T, POLY.60T, and BE.60T are utilized, as appropriate.

All cases are run with 1000 neutrons per generation for 510 generations, skipping the first 10, except as otherwise noted. The 1-sigma uncertainty is approximately 0.001 for all cases.

6.3.4 Demonstration of Maximum Reactivity

The fissile material in the limiting cases is both moderated and internally reflected with a mixture of 25% polyethylene, 74% water, and 1% beryllium (by volume). This composition is more reactive than simply moderating and internally reflecting with water.

The HAC array analysis demonstrates that reducing internal reflection reduces the reactivity, although neutronic interaction between packages may increase. Therefore, the most reactive condition is achieved by simply infinitely reflecting the most reactive single package geometry.

Although the package is leaktight, full inleakage of water is modeled in both the NCT and HAC cases. In the NCT cases, the foam and balsa are modeled explicitly, while in the HAC cases, foam and balsa are replaced with variable density water, and crush is modeled on all six sides to reduce the distance between fissile spheres in adjacent packages. Because the package is large and the NCT and HAC models are quite similar, there is no difference in reactivity between the NCT and HAC cases.

In the HAC array cases, various combinations of fissile sphere location and reflector density are used to maximize the reactivity, although the most reactive case is simply with a fully-reflected

fissile sphere at the center of the cavity. Because the cavity is large, the fissile material in each package is completely isolated from adjacent packages, and there is no difference in reactivity between the most reactive single package and array cases. The maximum reactivities of the four combinations of Pu-239/Pu-240 mass are also similar.

Table 6.3-1 – Key NCT As-Modeled Dimensions

Parameter	Value (cm)
Overall package width (x)	250.0
Overall package height (y)	265.0
Overall package length (z)	428.8
CSA cavity inner width (x)	184.0
CSA cavity inner height (y)	200.0
CSA cavity inner length (z)	279.0
CSA outer width (x)	212.0
CSA outer height (y)	228.0
CSA inner plate thickness	0.8
CSA outer plate thickness	0.8
Closure lid thickness	14.8
Closure lid plate thickness	1.2
Top/Bottom foam thickness	10.9
Side foam thickness	11.4
Steel thickness between foam and balsa	1.0
Top/Bottom/Side balsa thickness	6.0
Top/bottom/side outer steel thickness	0.6

(continued)

Table 6.3-1 – Key NCT As-Modeled Dimensions (concluded)

Parameter	Value (cm)
Closure Lid End Overpack Cover (centerline)	
Steel thickness	0.6
Foam thickness	12.0
Steel thickness	1.5
Balsa thickness	6.0
Steel thickness	0.6
Rear End Overpack Cover (centerline)	
Foam thickness	12.0
Steel thickness	1.5
Balsa thickness	6.0
Steel thickness	0.6
Closure Lid End Overpack Cover (outer edge)	
Steel thickness	0.6
Calcium silicate thickness	4.2
Steel thickness	1.6
Foam thickness	38.2
Steel thickness	0.6
Foam thickness	14.0
Steel thickness	0.8
Rear End Overpack Cover (outer edge)	
Foam thickness (from end of CSA) (Selected to give package length of 428.8 cm)	44.8
Steel thickness	0.6
Foam thickness	14.0
Steel thickness	0.8

Table 6.3-2 – UNS S31803 Composition

Component	UNS S31803 (Wt.%, Typical)
C	0.02
Si	0.4
P	0.025
Cr	22.4
Mn	0.70
Fe	67.194
Ni	5.8
N	0.16
S	0.001
Mo	3.3
Density (g/cm^3)	7.89

Table 6.3-3 – Polyurethane Foam Composition

Component	Wt.% Range	Modeled Wt.%
C	50 – 70	70
O	14 – 34	14
N	4 – 12	6
H	4 – 10	10
P	0 – 2	0
Si	< 1	0
Cl	< 0.18	0
Other	< 1	0
Maximum Density = 0.480 g/cm^3		

Table 6.3-4 – Internal Reflector Composition

Component	Number Density (atoms/b-cm)
H	6.9221E-02
Be	1.2348E-03
C	9.8745E-03
O	2.4736E-02
Total	1.0507E-01

Table 6.3-5 – Cross Section Libraries Utilized

Isotope/Element	Cross Section Label (from MCNP output)
1001.62c	1-h-1 at 293.6K from endf-vi.8 njoy99.50
4009.62c	4-be-9 at 293.6K from endf/b-vi.8 njoy99.50
6000.66c	6-c-0 at 293.6K from endf-vi.6 njoy99.50
7014.62c	7-n-14 at 293.6K from endf-vi.8 njoy99.50
8016.62c	8-o-16 at 293.6K from endf-vi.8 njoy99.50
14000.60c	14-si-nat from endf/b-vi
15031.66c	15-p-31 at 293.6K from endf-vi.6 njoy99.50
16000.62c	16-s-0 at 293.6K from endf/b-vi.8 njoy99.50
25055.62c	25-mn-55 at 293.6K from endf/b-vi.8 njoy99.50
24000.50c	njoy
26000.55c	njoy
28000.50c	njoy
42000.66c	42-mo-0 at 293.6K from endf-vi.0 njoy99.50
94239.69c	94-pu-239 at 293.6K from t16 pu239la7d njoy99.50
94240.66c	94-pu-240 at 293.6K from endf-vi.2 njoy99.50

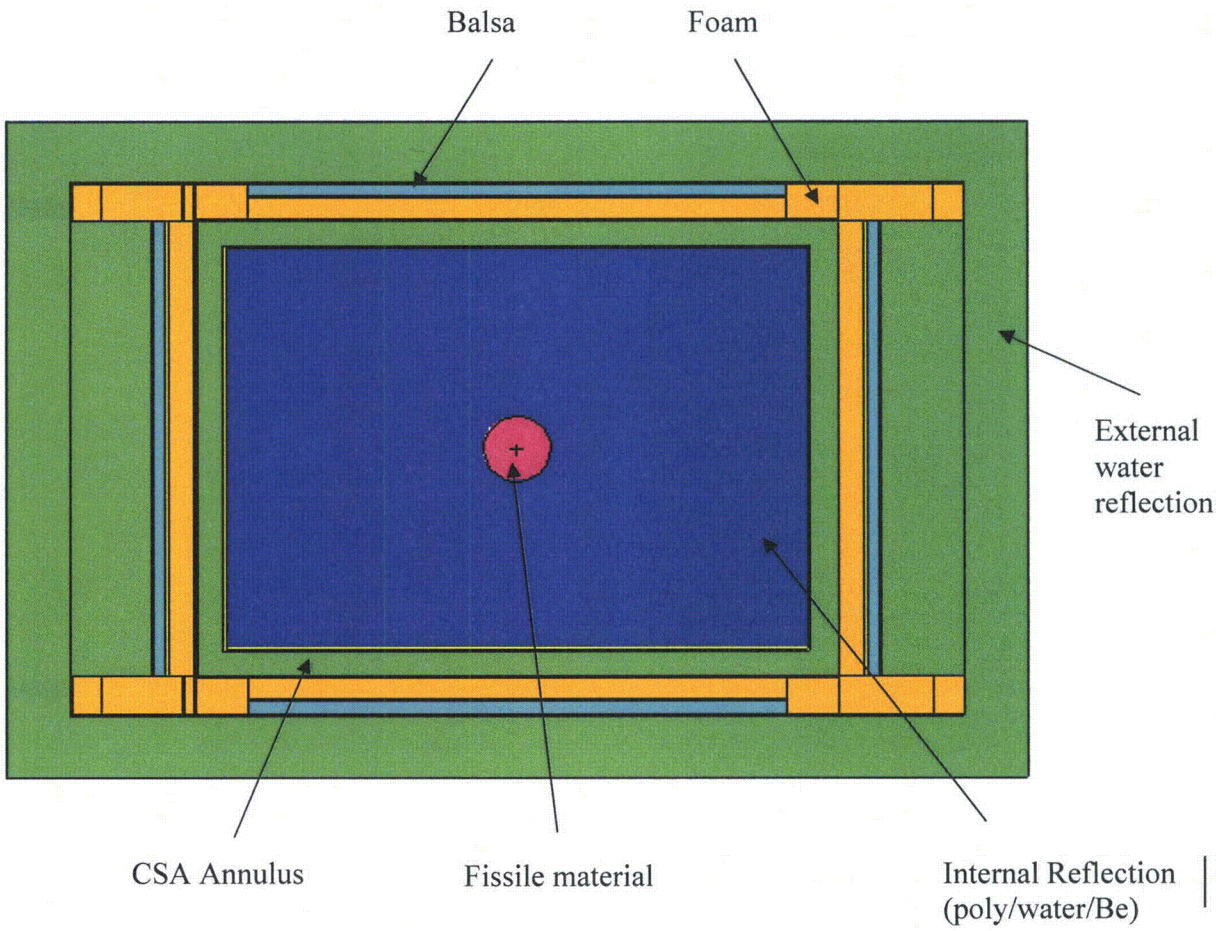

Figure 6.3-1 – NCT Single Package Model (z-y view)

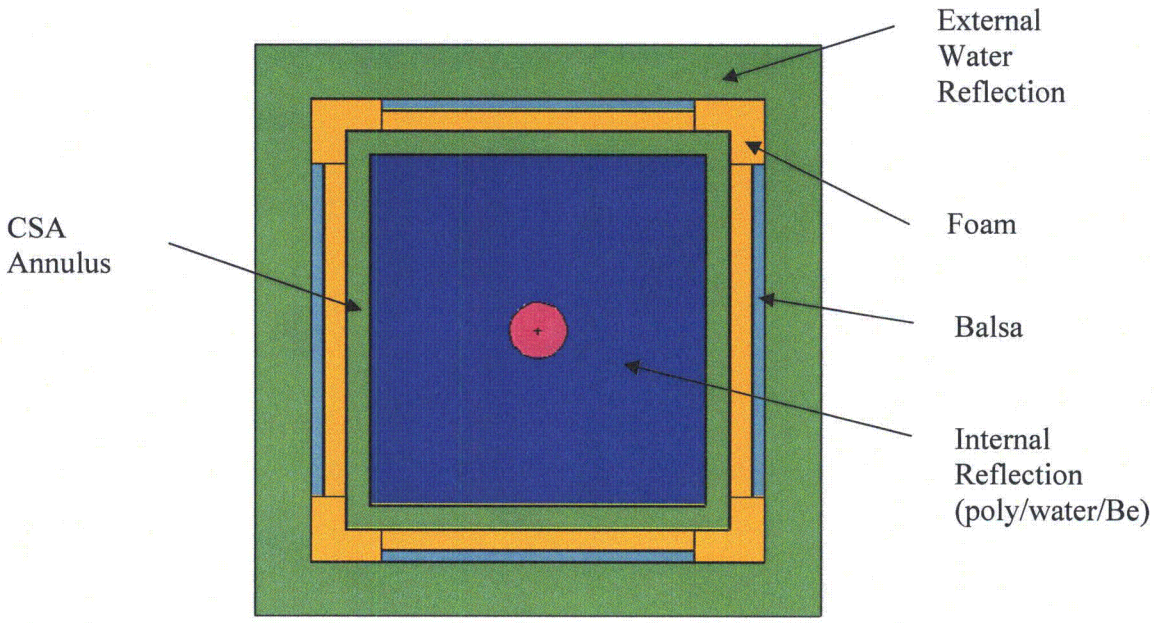

x-y view through center of package

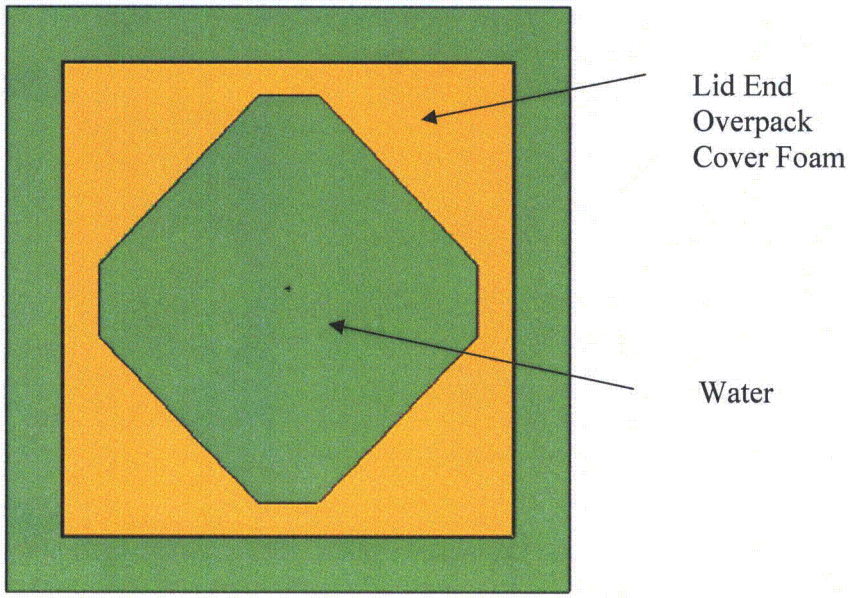

x-y view through lid end overpack cover

Figure 6.3-2 – NCT Single Package Model (x-y views)

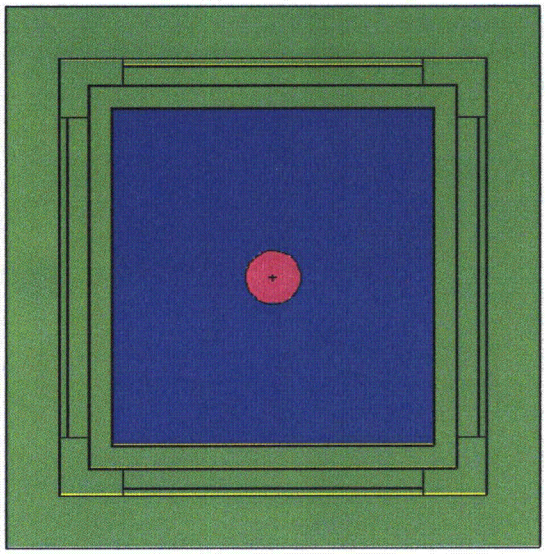

x-y view

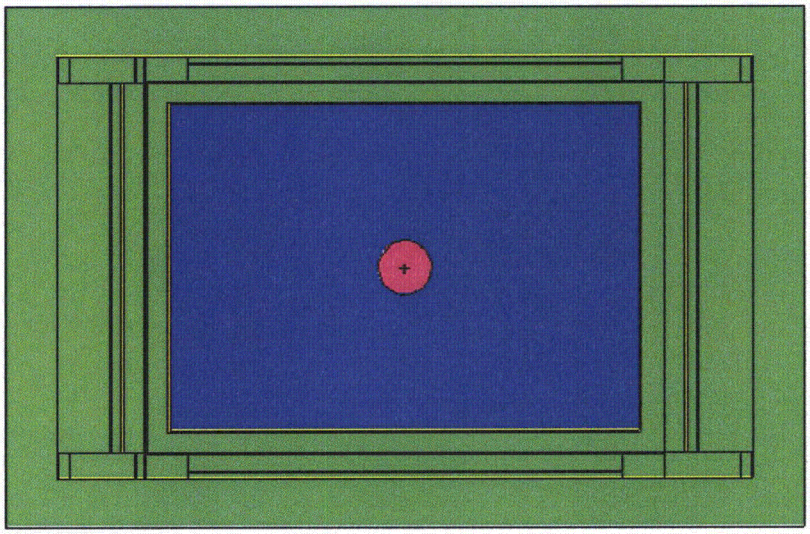

z-y view

Note: Foam and balsa have been replaced with water when compared to the NCT models. The package has also been crushed 2.54 cm on the top, bottom, and sides, and 7.62 cm on each end.

Figure 6.3-3 – HAC Single Package Model

6.4 Single Package Evaluation

Compliance with the requirements of 10 CFR 71 is demonstrated by analyzing optimally moderated damaged and undamaged, single-unit TRUPACT–III packages. The figures and descriptions provided in Section 6.3.1, *Model Configuration*, describe the basic geometry of the single-unit models.

6.4.1 Configuration

6.4.1.1 NCT Single Package Configuration

The geometry of the NCT single package configuration is discussed in Section 6.3.1. All relevant design features of the TRUPACT–III are modeled. The package is externally reflected with 30.48 cm of water. Although the package is leaktight, it is conservatively assumed that the package is also internally flooded with water, which is assumed to fill the CSA annulus as well as the cavity. Within the cavity itself, the internal reflector is modeled as a mixture of 25% polyethylene, 74% water, and 1% beryllium (by volume). This composition is also used to moderate the fissile material.

The fissile material is modeled as a sphere, which is the most reactive geometry possible. To maximize reflection, the sphere is modeled at the center of the cavity. The H/X ratio is varied between 500 and 1400 by adjusting the radius of the fissile sphere. Calculations are performed for four different FGE loadings and Pu-240 content: (1) 325 g Pu-239/0 g Pu-240, (2) 340 g Pu-239/5 g Pu-240, (3) 360 g Pu-239/15 g Pu-240, and (4) 380 g Pu-239/25 g Pu-240. The results are summarized in Table 6.4-1.

The proper use of S(α,β) cards is investigated for the 325 FGE series. By default, MCNP uses free gas treatment cross sections for all nuclides unless an S(α,β) card is specified to correct for the effects of binding the target atom to a specific molecule. For instance, BE.60T is used in the models to simulate metallic beryllium, and LWTR.60T is used in the pure water regions of the models. However, because the moderator and internal reflector are a mixture of both water and polyethylene, ~75% of the hydrogen atoms are bound to oxygen and ~25% of the hydrogen atoms are bound to carbon. For this reason, cases are run using the S(α,β) treatment for either water or polyethylene for the moderator/internal reflector, and the most reactive S(α,β) treatment is selected, as discussed in the following paragraph.

In Cases A1 through A10, the S(α,β) card LWTR.60T is used for both the fissile material and internal reflector. It is not possible to specify the S(α,β) cards LWTR.60T and POLY.60T in the same material. Therefore, additional cases are developed to investigate the impact on the reactivity of using these two S(α,β) cards individually. In Case A11, Case A5 is rerun with the POLY.60T card for the fissile material and internal reflector. K_s is lower (0.92900 vs. 0.93329), although the difference may be simply statistical fluctuation. To reduce the statistical uncertainty, Cases A11 and A5 are rerun as Cases A12 and A13, respectively, although the number of neutrons per cycle is increased by a factor of five. K_s values between Cases A12 and A13 are almost identical when the statistical uncertainty is reduced (0.92892 vs. 0.92901), and it is concluded that either LWTR.60T or POLY.60T may be used in the material cards for the fissile sphere and reflector. In the remaining cases (both HAC and NCT), LWTR.60T is used for fissile sphere and reflector materials.

Case A25 is the most reactive, with H/X=900 and k_s = 0.93354. This case has 340 g Pu-239 and 5 g Pu-240, although the maximum reactivities of the other FGE limits are similar. This result is below the USL of 0.9392.

6.4.1.2 HAC Single Package Configuration

The geometry of the HAC single package configuration is discussed in Section 6.3.1. It is essentially the same as the NCT configuration except that all foam and balsa components have been replaced with water, and the overall package dimensions have been crushed 2.54 cm on the top, bottom, and sides, and 7.62 cm on each end.

The single package HAC analysis is performed for 325, 340, 360, and 380 FGE. Results are provided in Table 6.4-2. The results are identical to the NCT single package results in all cases, indicating that the fissile sphere is so well reflected that essentially no neutrons are interacting with the package boundary. Case B15 is the most reactive, with H/X = 900 and k_s = 0.93354. This result is below the USL of 0.9392.

6.4.2 Results

Following are the tabulated results for the single package cases. The most reactive configuration in each table is listed in boldface.

Table 6.4-1 – NCT Single Package Results

Case ID	Filename	H/X	k	σ	k_s (k+2σ)
325 g Pu-239, 0 g Pu-240					
A1	ns_0g240_x0500	500	0.89611	0.00125	0.89861
A2	ns_0g240_x0600	600	0.91240	0.00126	0.91492
A3	ns_0g240_x0700	700	0.92548	0.00111	0.92770
A4	ns_0g240_x0800	800	0.93000	0.00124	0.93248
A5	**ns_0g240_x0900**	**900**	**0.93101**	**0.00114**	**0.93329**
A6	ns_0g240_x1000	1000	0.92669	0.00112	0.92893
A7	ns_0g240_x1100	1100	0.92192	0.00110	0.92412
A8	ns_0g240_x1200	1200	0.91987	0.00103	0.92193
A9	ns_0g240_x1300	1300	0.91286	0.00105	0.91496
A10	ns_0g240_x1400	1400	0.90661	0.00098	0.90857
A11	ns_0g240_x0900p	900	0.92674	0.00113	0.92900
A12	ns_0g240_x0900p_long	900	0.92786	0.00053	0.92892
A13	ns_0g240_x0900_long	900	0.92801	0.00050	0.92901
340 g Pu-239, 5 g Pu-240					
A21	ns_5g240_x0500	500	0.89458	0.00124	0.89706
A22	ns_5g240_x0600	600	0.91409	0.00122	0.91653
A23	ns_5g240_x0700	700	0.92270	0.00124	0.92518
A24	ns_5g240_x0800	800	0.92997	0.00116	0.93229
A25	**ns_5g240_x0900**	**900**	**0.93136**	**0.00109**	**0.93354**
A26	ns_5g240_x1000	1000	0.92922	0.00111	0.93144
A27	ns_5g240_x1100	1100	0.92648	0.00114	0.92876
A28	ns_5g240_x1200	1200	0.92055	0.00107	0.92269
A29	ns_5g240_x1300	1300	0.91337	0.00111	0.91559
A30	ns_5g240_x1400	1400	0.90735	0.00104	0.90943
360 g Pu-239, 15 g Pu-240					
A31	ns_15g240_x0500	500	0.89349	0.00126	0.89601
A32	ns_15g240_x0600	600	0.91135	0.00117	0.91369
A33	ns_15g240_x0700	700	0.92150	0.00123	0.92396
A34	ns_15g240_x0800	800	0.92647	0.00118	0.92883
A35	**ns_15g240_x0900**	**900**	**0.92943**	**0.00111**	**0.93165**
A36	ns_15g240_x1000	1000	0.92865	0.00113	0.93091
A37	ns_15g240_x1100	1100	0.92556	0.00111	0.92778
A38	ns_15g240_x1200	1200	0.92121	0.00109	0.92339
A39	ns_15g240_x1300	1300	0.91752	0.00099	0.91950
A40	ns_15g240_x1400	1400	0.91014	0.00100	0.91214

(continued)

Table 6.4-1 – NCT Single Package Results (concluded)

Case ID	Filename	H/X	k	σ	k_s (k+2σ)
380 g Pu-239, 25 g Pu-240					
A41	ns_25g240_x0500	500	0.89015	0.00128	0.89271
A42	ns_25g240_x0600	600	0.90726	0.00123	0.90972
A43	ns_25g240_x0700	700	0.92172	0.00116	0.92404
A44	ns_25g240_x0800	800	0.92644	0.00117	0.92878
A45	**ns_25g240_x0900**	**900**	**0.92966**	**0.00112**	**0.93190**
A46	ns_25g240_x1000	1000	0.92686	0.00118	0.92922
A47	ns_25g240_x1100	1100	0.92833	0.00110	0.93053
A48	ns_25g240_x1200	1200	0.92250	0.00105	0.92460
A49	ns_25g240_x1300	1300	0.91759	0.00104	0.91967
A50	ns_25g240_x1400	1400	0.91194	0.00106	0.91406

Table 6.4-2 – HAC Single Package Results

Case ID	Filename	H/X	k	σ	k_s (k+2σ)
325 g Pu-239, 0 g Pu-240					
B1	hs_0g240_x0500	500	0.89611	0.00125	0.89861
B2	hs_0g240_x0600	600	0.91240	0.00126	0.91492
B3	hs_0g240_x0700	700	0.92548	0.00111	0.92770
B4	hs_0g240_x0800	800	0.93000	0.00124	0.93248
B5	**hs_0g240_x0900**	**900**	**0.93101**	**0.00114**	**0.93329**
B6	hs_0g240_x1000	1000	0.92669	0.00112	0.92893
B7	hs_0g240_x1100	1100	0.92192	0.00110	0.92412
B8	hs_0g240_x1200	1200	0.91987	0.00103	0.92193
B9	hs_0g240_x1300	1300	0.91286	0.00105	0.91496
B10	hs_0g240_x1400	1400	0.90661	0.00098	0.90857
340 g Pu-239, 5 g Pu-240					
B11	hs_5g240_x0500	500	0.89458	0.00124	0.89706
B12	hs_5g240_x0600	600	0.91409	0.00122	0.91653
B13	hs_5g240_x0700	700	0.92270	0.00124	0.92518
B14	hs_5g240_x0800	800	0.92997	0.00116	0.93229
B15	**hs_5g240_x0900**	**900**	**0.93136**	**0.00109**	**0.93354**
B16	hs_5g240_x1000	1000	0.92922	0.00111	0.93144
B17	hs_5g240_x1100	1100	0.92648	0.00114	0.92876
B18	hs_5g240_x1200	1200	0.92055	0.00107	0.92269
B19	hs_5g240_x1300	1300	0.91337	0.00111	0.91559
B20	hs_5g240_x1400	1400	0.90735	0.00104	0.90943
360 g Pu-239, 15 g Pu-240					
B21	hs_15g240_x0500	500	0.89349	0.00126	0.89601
B22	hs_15g240_x0600	600	0.91135	0.00117	0.91369
B23	hs_15g240_x0700	700	0.92150	0.00123	0.92396
B24	hs_15g240_x0800	800	0.92647	0.00118	0.92883
B25	**hs_15g240_x0900**	**900**	**0.92943**	**0.00111**	**0.93165**
B26	hs_15g240_x1000	1000	0.92865	0.00113	0.93091
B27	hs_15g240_x1100	1100	0.92556	0.00111	0.92778
B28	hs_15g240_x1200	1200	0.92121	0.00109	0.92339
B29	hs_15g240_x1300	1300	0.91752	0.00099	0.91950
B30	hs_15g240_x1400	1400	0.91014	0.00100	0.91214
380 g Pu-239, 25 g Pu-240					
B31	hs_25g240_x0500	500	0.89015	0.00128	0.89271
B32	hs_25g240_x0600	600	0.90726	0.00123	0.90972
B33	hs_25g240_x0700	700	0.92172	0.00116	0.92404
B34	hs_25g240_x0800	800	0.92644	0.00117	0.92878
B35	**hs_25g240_x0900**	**900**	**0.92966**	**0.00112**	**0.93190**
B36	hs_25g240_x1000	1000	0.92686	0.00118	0.92922
B37	hs_25g240_x1100	1100	0.92833	0.00110	0.93053
B38	hs_25g240_x1200	1200	0.92250	0.00105	0.92460
B39	hs_25g240_x1300	1300	0.91759	0.00104	0.91967
B40	hs_25g240_x1400	1400	0.91194	0.00106	0.91406

This page intentionally left blank.

6.5 Evaluation of Package Arrays under Normal Conditions of Transport

6.5.1 Configuration

It is established in the HAC array analysis (Section 6.6) that the most reactive array configuration is with full density internal reflector and the fissile sphere in the center of the cavity. This configuration minimizes neutronic communication between packages. Because the NCT and HAC package geometry is very similar, this conclusion is also valid for the NCT array configuration. Therefore, it is sufficient to simply infinitely reflect the NCT single package models by removing the external water reflection and changing the six outer package surfaces to be reflective (i.e., mirror boundary condition). A series of cases is executed for each of the four FGE limits of interest over a range of H/X from 500 through 1400.

The results are provided in Table 6.5-1. The results are identical to the single package results, indicating that each package is essentially isolated from adjacent packages. Case C15 is the most reactive case, with $k_s = 0.93354$. This result is below the USL of 0.9392.

6.5.2 Results

The results for the NCT array cases are provided in the following table. The most reactive configurations are listed in boldface.

Table 6.5-1 – NCT Array Results

Case ID	Filename	H/X	k	σ	k_s (k+2σ)
325 g Pu-239, 0 g Pu-240					
C1	na_0g240_x0500	500	0.89611	0.00125	0.89861
C2	na_0g240_x0600	600	0.91240	0.00126	0.91492
C3	na_0g240_x0700	700	0.92548	0.00111	0.92770
C4	na_0g240_x0800	800	0.93000	0.00124	0.93248
C5	**na_0g240_x0900**	**900**	**0.93101**	**0.00114**	**0.93329**
C6	na_0g240_x1000	1000	0.92669	0.00112	0.92893
C7	na_0g240_x1100	1100	0.92192	0.00110	0.92412
C8	na_0g240_x1200	1200	0.91987	0.00103	0.92193
C9	na_0g240_x1300	1300	0.91286	0.00105	0.91496
C10	na_0g240_x1400	1400	0.90661	0.00098	0.90857
340 g Pu-239, 5 g Pu-240					
C11	na_5g240_x0500	500	0.89458	0.00124	0.89706
C12	na_5g240_x0600	600	0.91409	0.00122	0.91653
C13	na_5g240_x0700	700	0.92270	0.00124	0.92518
C14	na_5g240_x0800	800	0.92997	0.00116	0.93229
C15	**na_5g240_x0900**	**900**	**0.93136**	**0.00109**	**0.93354**
C16	na_5g240_x1000	1000	0.92922	0.00111	0.93144
C17	na_5g240_x1100	1100	0.92648	0.00114	0.92876
C18	na_5g240_x1200	1200	0.92055	0.00107	0.92269
C19	na_5g240_x1300	1300	0.91337	0.00111	0.91559
C20	na_5g240_x1400	1400	0.90735	0.00104	0.90943
360 g Pu-239, 15 g Pu-240					
C21	na_15g240_x0500	500	0.89349	0.00126	0.89601
C22	na_15g240_x0600	600	0.91135	0.00117	0.91369
C23	na_15g240_x0700	700	0.92150	0.00123	0.92396
C24	na_15g240_x0800	800	0.92647	0.00118	0.92883
C25	**na_15g240_x0900**	**900**	**0.92943**	**0.00111**	**0.93165**
C26	na_15g240_x1000	1000	0.92865	0.00113	0.93091
C27	na_15g240_x1100	1100	0.92556	0.00111	0.92778
C28	na_15g240_x1200	1200	0.92121	0.00109	0.92339
C29	na_15g240_x1300	1300	0.91752	0.00099	0.91950
C30	na_15g240_x1400	1400	0.91014	0.00100	0.91214
380 g Pu-239, 25 g Pu-240					
C31	na_25g240_x0500	500	0.89015	0.00128	0.89271
C32	na_25g240_x0600	600	0.90726	0.00123	0.90972
C33	na_25g240_x0700	700	0.92172	0.00116	0.92404
C34	na_25g240_x0800	800	0.92644	0.00117	0.92878
C35	**na_25g240_x0900**	**900**	**0.92966**	**0.00112**	**0.93190**
C36	na_25g240_x1000	1000	0.92686	0.00118	0.92922
C37	na_25g240_x1100	1100	0.92833	0.00110	0.93053
C38	na_25g240_x1200	1200	0.92250	0.00105	0.92460
C39	na_25g240_x1300	1300	0.91759	0.00104	0.91967
C40	na_25g240_x1400	1400	0.91194	0.00106	0.91406

6.6 Package Arrays under Hypothetical Accident Conditions

6.6.1 Configuration

The basic HAC infinite array model is developed by removing the external water reflector from the HAC single package model and changing the six outer package surfaces to be reflective. For the HAC configuration, all of the foam and balsa is replaced with variable density water.

When the package internal reflector is at maximum density, neutronic communication between packages is minimized. If the density of the internal reflector is reduced, more neutrons may escape to interact with fissile material in adjacent packages, although this condition may or may not be more reactive. Reactivity is also influenced by the location of the fissile sphere. If the fissile sphere is in the center of the package, it is unlikely the fissile sphere will interact with the fissile spheres in adjacent packages. Likewise, package to package interactions should be maximized if the fissile sphere is placed in the corner of the cavity, as this configuration effectively models eight fissile spheres in the closest possible proximity. However, placing the fissile sphere closer to the package walls increases parasitic absorption in the steel walls of the package, which tends to reduce the reactivity.

To investigate the effects of reduced internal reflector density and fissile sphere location, nine computational series are performed for the 325 FGE case. The results of the nine computational series are provided in Table 6.6-1 and are summarized below. The most reactive configuration is then utilized for the 340, 360, and 380 FGE analyses.

Series 1 (Cases D1 through D10): Series 1 is simply the infinitely reflected HAC single package case. The fissile sphere is in the center of the package, and all reflecting materials are at full density, including the internal reflector, all water within the package between the steel plates, and the water at the ends of the overpack covers (inside the octagonal regions).

Series 2 (Cases D11 through D20): Series 2 is the same as Series 1, except the water between the steel plates (including the CSA annulus) and water at the ends of the overpack covers are replaced with void. The internal reflector remains at full density. The purpose of this series is to investigate if reducing the hydrogenated material between the packages will increase reactivity by increasing interactions between packages.

Series 3 (Cases D21 through D30): Series 3 is the same as Series 1, except all hydrogenous reflector materials are voided, including the internal reflector. Therefore, the only hydrogenous materials are in the fissile sphere itself. This configuration would maximize package to package interactions.

Comparing Series 1, 2, and 3, the reactivites of Series 1 and 2 are identical. This indicates that the fissile sphere is fully reflected within the CSA cavity, and no neutrons at the package boundary are reflecting back into the fissile sphere. Series 3 is significantly less reactive than Series 1 or 2, although all hydrogenous materials are absent and neutrons are able to interact between adjacent packages.

Series 4 (Cases D31 through D40): Series 4 is the same as Series 1, except the fissile sphere is placed in the corner of the package, near the lid.

Series 5 (Cases D41 through D50): Series 5 is the same as Series 2, except the fissile sphere is placed in the corner of the package, near the lid.

Series 6 (Cases D51 through D60): Series 6 is the same as Series 3, except the fissile sphere is placed in the corner of the package, near the lid.

Comparing Series 4, 5, and 6, Series 4 and 5 are much more reactive than Series 6. Series 4 is slightly more reactive than Series 5, indicating that reflection outweighs package to package interactions when maximizing the reactivity. Series 4 is less reactive than Series 1, indicating that the center of the package is a more reactive location for the fissile sphere than the corner. It is expected that placing the fissile sphere in the corner may increase package to package interactions, but parasitic absorption in the steel components reduces the reactivity.

In Series 7, 8, and 9, a variety of hydrogenous material densities are examined with the fissile sphere in the center of the cavity.

Series 7 (Cases D61 through D70): Series 7 is the same as Series 1, but the densities of all cells containing hydrogenous reflector material are multiplied by 0.1.

Series 8 (Cases D71 through D80): Series 8 is the same as Series 1, but the densities of all cells containing hydrogenous reflector material are multiplied by 0.5.

Series 9 (Cases D81 through D90): Series 9 is the same as Series 1, but the densities of all cells containing hydrogenous reflector material are multiplied by 0.9.

The reactivities of Series 7, 8, and 9 are less than Series 1, although the reduced densities would presumably lead to greater package to package interactions. The reactivity becomes smaller as the density of hydrogenous materials decreases. This result again demonstrates that full-reflection rather than increased package to package interactions maximizes the reactivity.

An additional three miscellaneous cases (Cases D91, D92, and D93) are developed to examine scenarios in which the fissile sphere is in other locations. Full-reflection and H/X = 900 are utilized in these cases. In Case D91, the fissile sphere is placed midway between the corner and the center. K_s is identical between Cases D91 and D5, indicating that the fissile sphere does not need to be in the center of the cavity to be isolated from adjacent packages. In Case D92, the fissile sphere is located in a bottom end corner rather than a lid end corner, although the results are essentially identical (compare with Case D35). In Case D93, the fissile sphere is placed along an edge at the midplane of the package (z = 0), which effectively places four fissile spheres in close proximity. The results are essentially identical to cases with the fissile sphere in a corner.

The most reactive 325 FGE case is Series 1, Case D5, with $k_s = 0.93329$. This result is identical to the single package NCT result (Case A5), single package HAC result (Case B5), and NCT array result (Case C5) for 325 FGE. Although these cases all have slightly different package geometries and boundary conditions, neutronically the cases behave simply as a fissile sphere surrounded by a large reflector.

The Series 1 configuration is repeated for 340, 360, and 380 FGE, and the results are provided in Table 6.6-2. As with the 325 FGE cases, the results are identical to those obtained for the single package and NCT array cases.

Case E5 is the most reactive of all the HAC array cases, with $k_s = 0.93354$. This value is below the USL of 0.9392.

6.6.2 Results

Following are the tabulated results for the HAC array cases. The most reactive configurations in each table are listed in boldface.

Table 6.6-1 – HAC Array Results, 325 FGE

Case ID	Filename	H/X	k	σ	k_s (k+2σ)
Series 1: All hydrogenous materials are at full density, fissile sphere in center.					
D1	ha1_0g240_x0500	500	0.89611	0.00125	0.89861
D2	ha1_0g240_x0600	600	0.91240	0.00126	0.91492
D3	ha1_0g240_x0700	700	0.92548	0.00111	0.92770
D4	ha1_0g240_x0800	800	0.93000	0.00124	0.93248
D5	**ha1_0g240_x0900**	**900**	**0.93101**	**0.00114**	**0.93329**
D6	ha1_0g240_x1000	1000	0.92669	0.00112	0.92893
D7	ha1_0g240_x1100	1100	0.92192	0.00110	0.92412
D8	ha1_0g240_x1200	1200	0.91987	0.00103	0.92193
D9	ha1_0g240_x1300	1300	0.91286	0.00105	0.91496
D10	ha1_0g240_x1400	1400	0.90661	0.00098	0.90857
Series 2: The internal reflector is at full density, but the water between the steel plates (including the CSA annulus) and water at the ends of the overpack covers are replaced with void, fissile sphere in center.					
D11	ha2_0g240_x0500	500	0.89611	0.00125	0.89861
D12	ha2_0g240_x0600	600	0.91240	0.00126	0.91492
D13	ha2_0g240_x0700	700	0.92548	0.00111	0.92770
D14	ha2_0g240_x0800	800	0.93000	0.00124	0.93248
D15	**ha2_0g240_x0900**	**900**	**0.93101**	**0.00114**	**0.93329**
D16	ha2_0g240_x1000	1000	0.92669	0.00112	0.92893
D17	ha2_0g240_x1100	1100	0.92192	0.00110	0.92412
D18	ha2_0g240_x1200	1200	0.91987	0.00103	0.92193
D19	ha2_0g240_x1300	1300	0.91286	0.00105	0.91496
D20	ha2_0g240_x1400	1400	0.90661	0.00098	0.90857
Series 3: All hydrogenous reflector materials are voided, including the internal reflector, fissile sphere in center.					
D21	ha3_0g240_x0900	900	0.78658	0.00125	0.78908
D22	ha3_0g240_x1000	1000	0.79330	0.00115	0.79560
D23	ha3_0g240_x1100	1100	0.79903	0.00115	0.80133
D24	ha3_0g240_x1200	1200	0.80269	0.00114	0.80497
D25	**ha3_0g240_x1300**	**1300**	**0.80333**	**0.00111**	**0.80555**
D26	ha3_0g240_x1400	1400	0.80259	0.00107	0.80473
D27	ha3_0g240_x1500	1500	0.80154	0.00110	0.80374
D28	ha3_0g240_x1600	1600	0.79811	0.00101	0.80013
D29	ha3_0g240_x1700	1700	0.79598	0.00102	0.79802
D30	ha3_0g240_x1800	1800	0.79243	0.00097	0.79437

(continued)

Table 6.6-1 – HAC Array Results, 325 FGE

Case ID	Filename	H/X	k	σ	k_s (k+2σ)
Series 4: Same as Series 1, but with the fissile sphere in the corner.					
D31	ha4_0g240_x0500	500	0.88528	0.00124	0.88776
D32	ha4_0g240_x0600	600	0.90186	0.00120	0.90426
D33	ha4_0g240_x0700	700	0.91165	0.00118	0.91401
D34	ha4_0g240_x0800	800	0.91947	0.00118	0.92183
D35	**ha4_0g240_x0900**	**900**	**0.92013**	**0.00122**	**0.92257**
D36	ha4_0g240_x1000	1000	0.91989	0.00107	0.92203
D37	ha4_0g240_x1100	1100	0.91593	0.00106	0.91805
D38	ha4_0g240_x1200	1200	0.91322	0.00106	0.91534
D39	ha4_0g240_x1300	1300	0.90792	0.00111	0.91014
D40	ha4_0g240_x1400	1400	0.90049	0.00103	0.90255
Series 5: Same as Series 2, but with the fissile sphere in the corner.					
D41	ha5_0g240_x0500	500	0.86906	0.00124	0.87154
D42	ha5_0g240_x0600	600	0.89055	0.00126	0.89307
D43	ha5_0g240_x0700	700	0.90030	0.00118	0.90266
D44	ha5_0g240_x0800	800	0.90891	0.00122	0.91135
D45	ha5_0g240_x0900	900	0.91227	0.00115	0.91457
D46	**ha5_0g240_x1000**	**1000**	**0.91320**	**0.00116**	**0.91552**
D47	ha5_0g240_x1100	1100	0.91099	0.00109	0.91317
D48	ha5_0g240_x1200	1200	0.90539	0.00115	0.90769
D49	ha5_0g240_x1300	1300	0.90191	0.00108	0.90407
D50	ha5_0g240_x1400	1400	0.89597	0.00095	0.89787
Series 6: Same as Series 3, but with the fissile sphere in the corner.					
D51	ha6_0g240_x0900	900	0.81255	0.00121	0.81497
D52	ha6_0g240_x1000	1000	0.81993	0.00114	0.82221
D53	ha6_0g240_x1100	1100	0.82386	0.00120	0.82626
D54	ha6_0g240_x1200	1200	0.82417	0.00109	0.82635
D55	**ha6_0g240_x1300**	**1300**	**0.82757**	**0.00107**	**0.82971**
D56	ha6_0g240_x1400	1400	0.82444	0.00107	0.82658
D57	ha6_0g240_x1500	1500	0.82249	0.00110	0.82469
D58	ha6_0g240_x1600	1600	0.81590	0.00101	0.81792
D59	ha6_0g240_x1700	1700	0.81477	0.00097	0.81671
D60	ha6_0g240_x1800	1800	0.80818	0.00097	0.81012

(continued)

Table 6.6-1 – HAC Array Results, 325 FGE (concluded)

Case ID	Filename	H/X	k	σ	k_s (k+2σ)
Series 7: Same as Series 1, but the densities of all cells containing hydrogenous reflector material are multiplied by 0.1.					
D61	ha7_0g240_x0900	900	0.79687	0.00117	0.79921
D62	ha7_0g240_x1000	1000	0.80488	0.00125	0.80738
D63	ha7_0g240_x1100	1100	0.80883	0.00118	0.81119
D64	**ha7_0g240_x1200**	**1200**	**0.81085**	**0.00121**	**0.81327**
D65	ha7_0g240_x1300	1300	0.81091	0.00110	0.81311
D66	ha7_0g240_x1400	1400	0.80962	0.00113	0.81188
D67	ha7_0g240_x1500	1500	0.80756	0.00107	0.80970
D68	ha7_0g240_x1600	1600	0.80840	0.00103	0.81046
D69	ha7_0g240_x1700	1700	0.80257	0.00104	0.80465
D70	ha7_0g240_x1800	1800	0.79840	0.00100	0.80040
Series 8: Same as Series 1, but the densities of all cells containing hydrogenous reflector material are multiplied by 0.5.					
D71	ha8_0g240_x0500	500	0.83681	0.00135	0.83951
D72	ha8_0g240_x0600	600	0.85899	0.00120	0.86139
D73	ha8_0g240_x0700	700	0.87490	0.00123	0.87736
D74	ha8_0g240_x0800	800	0.88071	0.00120	0.88311
D75	ha8_0g240_x0900	900	0.88630	0.00124	0.88878
D76	ha8_0g240_x1000	1000	0.89035	0.00117	0.89269
D77	**ha8_0g240_x1100**	**1100**	**0.89127**	**0.00109**	**0.89345**
D78	ha8_0g240_x1200	1200	0.88734	0.00106	0.88946
D79	ha8_0g240_x1300	1300	0.88319	0.00107	0.88533
D80	ha8_0g240_x1400	1400	0.88007	0.00108	0.88223
Series 9: Same as Series 1, but the densities of all cells containing hydrogenous reflector material are multiplied by 0.9.					
D81	ha9_0g240_x0500	500	0.88810	0.00120	0.89050
D82	ha9_0g240_x0600	600	0.90529	0.00122	0.90773
D83	ha9_0g240_x0700	700	0.91734	0.00118	0.91970
D84	ha9_0g240_x0800	800	0.92253	0.00116	0.92485
D85	**ha9_0g240_x0900**	**900**	**0.92303**	**0.00117**	**0.92537**
D86	ha9_0g240_x1000	1000	0.92118	0.00109	0.92336
D87	ha9_0g240_x1100	1100	0.91848	0.00108	0.92064
D88	ha9_0g240_x1200	1200	0.91604	0.00109	0.91822
D89	ha9_0g240_x1300	1300	0.90980	0.00104	0.91188
D90	ha9_0g240_x1400	1400	0.90314	0.00103	0.90520
Miscellaneous					
D91	ha10_0g240_x0900_p1	900	0.93101	0.00114	0.93329
D92	ha10_0g240_x0900_p2	900	0.92125	0.00118	0.92361
D93	ha10_0g240_x0900_p3	900	0.92221	0.00109	0.92439

Table 6.6-2 – HAC Array Results (340, 360, 380 FGE)

Case ID	Filename	H/X	k	σ	k_s (k+2σ)
340 g Pu-239, 5 g Pu-240					
E1	ha_5g240_x0500	500	0.89458	0.00124	0.89706
E2	ha_5g240_x0600	600	0.91409	0.00122	0.91653
E3	ha_5g240_x0700	700	0.92270	0.00124	0.92518
E4	ha_5g240_x0800	800	0.92997	0.00116	0.93229
E5	**ha_5g240_x0900**	**900**	**0.93136**	**0.00109**	**0.93354**
E6	ha_5g240_x1000	1000	0.92922	0.00111	0.93144
E7	ha_5g240_x1100	1100	0.92648	0.00114	0.92876
E8	ha_5g240_x1200	1200	0.92055	0.00107	0.92269
E9	ha_5g240_x1300	1300	0.91337	0.00111	0.91559
E10	ha_5g240_x1400	1400	0.90735	0.00104	0.90943
360 g Pu-239, 15 g Pu-240					
E11	ha_15g240_x0500	500	0.89349	0.00126	0.89601
E12	ha_15g240_x0600	600	0.91135	0.00117	0.91369
E13	ha_15g240_x0700	700	0.92150	0.00123	0.92396
E14	ha_15g240_x0800	800	0.92647	0.00118	0.92883
E15	**ha_15g240_x0900**	**900**	**0.92943**	**0.00111**	**0.93165**
E16	ha_15g240_x1000	1000	0.92865	0.00113	0.93091
E17	ha_15g240_x1100	1100	0.92556	0.00111	0.92778
E18	ha_15g240_x1200	1200	0.92121	0.00109	0.92339
E19	ha_15g240_x1300	1300	0.91752	0.00099	0.91950
E20	ha_15g240_x1400	1400	0.91014	0.00100	0.91214
380 g Pu-239, 25 g Pu-240					
E21	ha_25g240_x0500	500	0.89015	0.00128	0.89271
E22	ha_25g240_x0600	600	0.90726	0.00123	0.90972
E23	ha_25g240_x0700	700	0.92172	0.00116	0.92404
E24	ha_25g240_x0800	800	0.92644	0.00117	0.92878
E25	**ha_25g240_x0900**	**900**	**0.92966**	**0.00112**	**0.93190**
E26	ha_25g240_x1000	1000	0.92686	0.00118	0.92922
E27	ha_25g240_x1100	1100	0.92833	0.00110	0.93053
E28	ha_25g240_x1200	1200	0.92250	0.00105	0.92460
E29	ha_25g240_x1300	1300	0.91759	0.00104	0.91967
E30	ha_25g240_x1400	1400	0.91194	0.00106	0.91406

6.7 Fissile Material Packages for Air Transport

This section does not apply for the TRUPACT–III package, because air transport is not claimed.

This page intentionally left blank.

6.8 Benchmark Evaluations

The Monte Carlo computer program MCNP5 v1.30 is utilized for this benchmark analysis. MCNP has been used extensively in criticality evaluations for several decades and is considered a standard in the industry.

ENDF/B-VI cross sections are used for most isotopes, although ENDF/B-V elemental cross sections are utilized when ENDF/B-VI elemental cross sections are not available. Also, the Pu-239 cross sections represent a preliminary version of the ENDF/B-VII cross section set. Although the ENDF/B-VII cross section set had not been formally released with MCNP5 v1.30, LANL included this Pu-239 cross section because it showed significant improvements compared to the latest ENDF/B-VI Pu-239 cross section for certain LANL benchmark models. All cross sections utilized are at room temperature. A listing of the cross section libraries used in the TRUPACT–III analysis is provided in Table 6.3-5. These cross sections are consistent with the cross sections utilized in the benchmarks.

The ORNL USLSTATS code[1] is used to establish a USL for the analysis. USLSTATS provides a simple means of evaluating and combining the statistical error of the calculation, code biases and benchmark uncertainties. The USLSTATS calculation uses the combined uncertainties and data to provide a linear trend and an overall uncertainty. Computed multiplication factors, k_{eff}, for the package are deemed to be adequately subcritical if the computed value of k_s is less than or equal to the USL as follows:

$$k_s = k_{eff} + 2\sigma \leq USL$$

The USL includes the combined effects of code bias, uncertainty in the benchmark experiments, uncertainty in the computational evaluation of the benchmark experiments, and an administrative margin. This methodology has accepted precedence in establishing criticality safety limits for transportation packages complying with 10 CFR 71.

6.8.1 Applicability of Benchmark Experiments

The critical experiment benchmarks are selected from the International Handbook of Evaluated Criticality Safety Benchmark Experiments[2] based upon their similarity to the TRUPACT–III package and contents. The important parameters of the package configuration are homogeneous mixtures of plutonium, water and/or polyethylene. Benchmark experiments that utilize plutonium solutions with beryllium reflectors are also desired because the TRUPACT–III may contain up to 1% beryllium by weight.

Two-hundred (200) plutonium solution benchmarks are selected from the Handbook[3]. No thermal benchmarks that utilize plutonium with beryllium reflectors are available, although U-233/beryllium benchmarks are described in U233-SOL-THERM-015. Note that four of the 31

---

[1] USLSTATS, *USLSTATS: A Utility To Calculate Upper Subcritical Limits For Criticality Safety Applications,* Version 1.4.2, Oak Ridge National Laboratory, April 23, 2003.

[2] *International Handbook of Evaluated Criticality Safety Benchmark Experiments*, Nuclear Energy Agency, NEA/NSC/DOC(95)03, September 2004.

[3] Note that PU–SOL–THERM–024, Case 6, is not included in the benchmark evaluation because the EALF for this case is an order of magnitude higher than the other plutonium cases.

U-233 benchmarks from U233-SOL-THERM-015 are rejected because there is no beryllium present in these cases. Therefore, twenty-seven (27) U-233 benchmarks are selected that utilize beryllium reflectors, for a total of 227 benchmark experiments. The titles for all utilized experiments are listed in Table 6.8-1.

Care must be exercised in the application of the U-233/beryllium benchmarks because the introduction of U-233 cross sections introduces a new source of uncertainty. The uncertainties added by including the U-233 benchmarks are evaluated by examining 70 U-233 benchmarks that do not use beryllium reflectors. These additional benchmarks, however, are not considered part of the TRUPACT–III benchmark set. Note that the four benchmarks rejected from U233-SOL-THERM-015 because they did not contain beryllium are included in this set. The titles for all U-233 experiments that do not utilize beryllium are also included in Table 6.8-1.

6.8.2 Bias Determination

The USL is calculated by application of the USLSTATS computer program. USLSTATS receives as input the k_{eff} as calculated by MCNP, the total 1-σ uncertainty (combined benchmark and MCNP uncertainties), and a trending parameter. Three trending parameters have been selected: (1) H/fissile atom ratio (abbreviated as H/X), (2) Pu240/Pu ratio, and (3) Energy of the Average neutron Lethargy causing Fission (EALF).

The only trending parameter used for both the plutonium and U-233 benchmarks is EALF. The U-233 benchmarks are not considered when trending with respect to H/X as the optimum H/X range will be significantly different for a U-233 system vs. a plutonium system. Also, the U-233 benchmarks are not considered when trending with the Pu240/Pu parameter, as this parameter has no meaning for the U-233 benchmarks.

The uncertainty value, σ_{total}, assigned to each case is a combination of the benchmark uncertainty for each experiment, σ_{bench}, and the Monte Carlo uncertainty associated with the particular computational evaluation of the case, σ_{MCNP}, or:

$$\sigma_{total} = (\sigma_{bench}^2 + \sigma_{MCNP}^2)^{½}$$

These values are input into the USLSTATS program in addition to the following parameters, which are the values recommended by the USLSTATS user's manual[4]:

- P, proportion of population falling above lower tolerance level = 0.995 (note that this parameter is required input but is not utilized in the calculation of USL Method 1)
- α, confidence on proportion P = 0.95 (note that this parameter is required input but is not utilized in the calculation of USL Method 1)
- 1-γ, confidence on fit = 0.95
- Δk_m, administrative margin used to ensure subcriticality = 0.05.

These data are followed by triplets of trending parameter value, computed k_{eff}, and uncertainty for each case. The USL Method 1 performs a confidence band analysis on the data for the

[4] USLSTATS is described in Appendix C, *User's Manual for USLSTATS V1.0*, in NUREG/CR-6361 *Criticality Benchmark Guide for Light-Water-Reactor Fuel in Transportation and Storage Packages*, March 1997.

trending parameter. The USL generated for each of the three trending parameters utilized is provided in Table 6.8-2. Note that several different trending analyses are performed for the EALF parameter in order to determine which benchmarks are dominating the USL computation for this parameter. The application of these equations in the determination of the USL is discussed in the following section. All benchmark data used as input to USLSTATS are reported in Table 6.8-3 for the plutonium benchmarks, Table 6.8-4 for the U-233/Be benchmarks, and Table 6.8-5 for the U-233/no Be benchmarks.

H/X

The ratio of the hydrogen number density (H) to the fissile number density (X) is used as the first trending parameter. Only the 200 plutonium benchmarks are utilized for this parameter. Both Pu-239 and Pu-241 are summed to determine the value of X for each experiment, although the Pu-241 number densities in the experiments are negligible. The USL1 value is a constant value of 0.9392 over the entire range. When the data is plotted, as shown in Figure 6.8-1, $R^2 = 0.0368$, indicating essentially no correlation between this variable and the calculated benchmark results.

The TRUPACT–III cases have an H/X range from 500 to 1800, which is within the range of the benchmark experiments.

Pu-240/Pu

Pu-240 weight fraction within the Pu is used as the second trending parameter. Only the 200 plutonium benchmarks are utilized for this parameter. The USL1 value is a constant value of 0.9396 over the entire range. When the data is plotted, as shown in Figure 6.8-2, $R^2 = 0.0038$, indicating essentially no correlation between this variable and the calculated benchmark results.

The TRUPACT–III cases utilize three discreet Pu-240/Pu ratios, 5/345 = 0.014, 15/375 = 0.04, and 25/405 = 0.062. These three ratios fall within the range of the benchmark experiments.

Energy of Average Lethargy of Fission (EALF)

The EALF is used as the third trending parameter for the benchmark cases. The EALF comparison provides a means to observe neutron spectral dependencies or trends. This parameter is examined for several different combinations of benchmark experiments to determine which benchmarks are dominating the USL computation for this parameter.

All 227 benchmark experiments are utilized in the first study (EALF1). When the data is plotted, as shown in Figure 6.8-3, $R^2 = 0.5319$, indicating high correlation between this variable and the calculated benchmark results. However, this correlation exists only for EALF values above 3.5×10^{-7} MeV. At the high end of the energy range, the USL = 0.9171, which is a low result. However, for EALF values below 3.5×10^{-7} MeV, the USL is a constant value of 0.9385. Examining the EALF data shown in Table 6.8-3 and Table 6.8-4, it is apparent that many of the U-233 benchmarks have a higher EALF than the plutonium benchmarks. Also, as several of the U-233 benchmarks have k_{eff} as low as ~0.97, the U-233 benchmarks depress the USL at the higher energy range.

When the EALF trending is performed for only the 200 plutonium benchmarks (EALF2), the USL over the entire energy range is a constant 0.9396. Conversely, when the EALF trending is performed for only the 27 U-233 benchmarks (EALF3), the trending is again poor, with a minimum USL of 0.9136.

Clearly, the U-233/Be benchmarks are distorting the EALF results. There may be a number of reasons for the poor U-233/Be benchmark results, including: (1) uncertainties in the U-233 cross sections, (2) uncertainties in the beryllium cross sections, or (3) experimental errors. To examine the bias in the U-233 cross sections, an additional 70 U-233 benchmark experiments are developed that do not use beryllium. These cases are summarized in Table 6.8-5. Note that six of these benchmarks are intermediate spectrum benchmarks rather than thermal benchmarks, which is desirable because the experiments with harder spectra tend to have more inaccurate results. The percentages of fissions caused by thermal, intermediate, and fast neutrons are also included in the tables to further demonstrate the different spectrum of the U-233 cases.

When the EALF trending is performed for the 70 U-233 benchmarks without beryllium (EALF4), the trending is worse than case EALF1, with a minimum USL of 0.9028. Based on these results, it may be concluded that the U-233 cross sections have large uncertainties in the intermediate energy range that result in low values of k_{eff} for many of these benchmarks. In the thermal energy range, the U-233 cross sections appear to be acceptable.

Because the EALF1 result is biased by poor U-233 cross sections unrelated to the TRUPACT–III analysis, the U-233/Be benchmarks are screened to exclude any benchmark experiment with an EALF > 5×10^{-7} MeV, which excludes 15 of the U-233/Be cases with a harder spectra. When the EALF trending is performed for this reduced set of 212 "highly thermalized" benchmarks (EALF5), the USL is a constant value of 0.9393 over the entire energy range. When the data is plotted, as shown in Figure 6.8-4, $R^2 = 0.0096$, indicating essentially no correlation between EALF and the calculated benchmark results for the "highly thermalized" data set.

The TRUPACT–III models have EALF values of approximately 5×10^{-8} MeV, which is within the range of the benchmark experiments.

Recommended USL

The USL for H/X is a constant value of 0.9392, and the USL for Pu240/Pu is a constant value of 0.9396. For the EALF parameter, only the EALF2 (0.9396) and EALF5 (0.9393) results are applicable because the EALF1 and EALF3 results are biased by poor U-233 cross sections. Comparing these USL values, the minimum USL of 0.9392 is selected for the analysis. The selected USL is applicable over the parameter ranges of 4.1×10^{-8} MeV $\leq$ EALF $\leq 4.7 \times 10^{-7}$ MeV, $91 \leq$ H/X ≤ 2800, and $0.005 \leq$ Pu240/Pu ≤ 0.23.

Table 6.8-1 – Benchmark Experiments Utilized

Series	Title
Pu Benchmarks (including U-233 Benchmarks with Beryllium)	
PU-SOL-THERM-001	Water-Reflected 11.5-Inch Diameter Spheres Of Plutonium Nitrate Solutions
PU-SOL-THERM-002	Water-Reflected 12-Inch Diameter Spheres Of Plutonium Nitrate Solutions
PU-SOL-THERM-003	Water-Reflected 13-Inch Diameter Spheres Of Plutonium Nitrate Solutions
PU-SOL-THERM-004	Water-Reflected 14-Inch Diameter Spheres Of Plutonium Nitrate Solutions 0.54% To 3.43% Pu240
PU-SOL-THERM-005	Water-Reflected 14-Inch Diameter Spheres Of Plutonium Nitrate Solutions 4.05% And 4.40% Pu240
PU-SOL-THERM-006	Water-Reflected 15-Inch Diameter Spheres Of Plutonium Nitrate Solutions
PU-SOL-THERM-007	Water-Reflected 11.5-Inch Diameter Spheres Partly Filled with Plutonium Nitrate Solutions
PU-SOL-THERM-009	Unreflected 48-Inch-Diameter Sphere Of Plutonium Nitrate Solution
PU-SOL-THERM-010	Water-Reflected 9-, 10-, 11-, And 12-Inch-Diameter Cylinders Of Plutonium Nitrate Solutions
PU-SOL-THERM-011	Bare 16- And 18-Inch-Diameter Spheres Of Plutonium Nitrate Solutions
PU-SOL-THERM-014	Interacting Cylinders of 300-mm Diameter Spheres of Plutonium Nitrate Solution (115.1gPu/L) in Air
PU-SOL-THERM-015	Interacting Cylinders of 300-mm Diameter with Plutonium Nitrate Solution (152.5gPu/L) in Air
PU-SOL-THERM-016	Interacting Cylinders of 300-mm and 256-mm Diameters with Plutonium Nitrate Solution (152.5 and 115.1 gPu/L) and Nitric Acid (2n) in Air
PU-SOL-THERM-017	Interacting Cylinders of 256-mm and 300-mm Diameters with Plutonium Nitrate Solution (115.1 gPu/L) in Air
PU-SOL-THERM-020	Water-Reflected and Water-Cadmium Reflected 14-inch Diameter Spheres of Plutonium Nitrate Solutions
PU-SOL-THERM-021	Water-Reflected and Bare 15.2-inch Diameter Spheres of Plutonium Nitrate Solutions
PU-SOL-THERM-024	Slabs of Plutonium Nitrate Solutions Reflected by 1-inch Thick Plexiglas
U233-SOL-THERM-015	Uranyl-Fluoride (^{233}U) Solutions in Spherical Stainless Steel Vessels with Reflectors of Be, CH_2, and Be-CH_2 Composites – Part II (Excluding Cases 7, 10, 17, and 25)
U-233 Benchmarks Without Beryllium	
U233-SOL-THERM-001	Unreflected Spheres of ^{233}U Nitrate Solutions
U233-SOL-THERM-003	Paraffin-Reflected 5-, 5.4-, 6-, 6.6-, 7.5-, 8-, 8.5-, 9-, and 12-inch Diameter Cylinders of ^{233}U Uranyl Fluoride Solutions
U233-SOL-THERM-012	Water-Reflected Spherical Vessels Partially Filled or Filled with $^{233}UO_2(NO_3)_2$ Solution
U233-SOL-THERM-013	Unreflected Spherical Vessels Partially Filled or Filled with $^{233}UO_2(NO_3)_2$ Solution
U233-SOL-THERM-014	Lucite-Moderated and Unmoderated, Reflected and Non-Reflected Arrays of Bottles Containing Uranyl Nitrate (98.2 wt.% ^{233}U) solution.
U233-SOL-THERM-015	Uranyl-Fluoride (^{233}U) Solutions in Spherical Stainless Steel Vessels with Reflectors of Be, CH_2, and Be-CH_2 Composites – Part II (Cases 7, 10, 17, and 25)
U233-SOL-INTER-001	Uranyl-Fluoride (^{233}U) Solutions in Spherical Stainless Steel Vessels with Reflectors of Be, CH_2, and Be-CH_2 Composites – Part I

Table 6.8-2 – USL Trending Equations

Trending Parameter (P)	USL equation	Minimum USL Over Range of Applicability	Range of Applicability
H/X (200 Pu benchmarks)	0.9392	0.9392	$90.899 \leq P \leq 2800.6$
Pu240/Pu (200 Pu benchmarks)	0.9396	0.9396	$4.95000E\text{-}3 \leq P \leq 0.23200$
EALF1 (200 Pu and 27 U-233/Be benchmarks)	0.9385 0.9449 - 1.8443E+4*P	0.9385 0.9171	$4.07630E\text{-}8 \leq P \leq 3.49827E\text{-}7$ $3.49827E\text{-}7 < P \leq 1.51290E\text{-}6$
EALF2 (200 Pu benchmarks)	0.9396	0.9396	$4.07630E\text{-}8 \leq P \leq 4.65100E\text{-}7$
EALF3 (27 U-233/Be benchmarks)	0.9355 - 1.4523E+4*P	0.9136	$1.27400E\text{-}7 \leq P \leq 1.51290E\text{-}6$
EALF4 (70 U-233/no Be benchmarks)	0.9273 0.9330 - 6.3995E+3*P	0.9273 0.9028	$3.94770E\text{-}8 \leq P \leq 8.83898E\text{-}7$ $8.83898E\text{-}7 < P \leq 4.70670E\text{-}6$
EALF5 (212 highly thermal Pu and U-233/Be benchmarks)	0.9393	0.9393	$4.07630E\text{-}8 \leq P \leq 4.69400E\text{-}7$

Table 6.8-3 – Plutonium Benchmark Experiment Data

No.	Filename	Thermal (<0.635 eV)	Inter (>0.635 eV, <100 KeV)	Fast (>100 KeV)	EALF (MeV)	H/X	Pu240/Pu	k_{eff}	σ MCNP	σ bench	σ total
1	pust001_c01	94.32%	5.02%	0.66%	8.736E-08	370.2	0.0465	1.00368	0.00103	0.0050	0.0051
2	pust001_c02	92.56%	6.53%	0.91%	1.107E-07	270.7	0.0465	1.00549	0.00103	0.0050	0.0051
3	pust001_c03	91.08%	7.81%	1.12%	1.335E-07	215.2	0.0465	1.00707	0.00102	0.0050	0.0051
4	pust001_c04	89.99%	8.77%	1.24%	1.503E-07	189.8	0.0465	0.99970	0.00098	0.0050	0.0051
5	pust001_c05	89.56%	9.13%	1.32%	1.582E-07	179.6	0.0465	1.00317	0.00103	0.0050	0.0051
6	pust001_c06	81.77%	15.69%	2.54%	3.464E-07	90.9	0.0465	1.00610	0.00099	0.0050	0.0051
7	pust002_c01	95.71%	3.81%	0.48%	7.080E-08	524.3	0.0311	1.00302	0.00098	0.0047	0.0048
8	pust002_c02	95.55%	3.96%	0.49%	7.236E-08	504.9	0.0311	1.00363	0.00096	0.0047	0.0048
9	pust002_c03	95.15%	4.30%	0.55%	7.730E-08	451.3	0.0311	1.00146	0.00099	0.0047	0.0048
10	pust002_c04	94.90%	4.51%	0.59%	8.064E-08	420.5	0.0311	1.00434	0.00097	0.0047	0.0048
11	pust002_c05	94.59%	4.78%	0.62%	8.432E-08	392.8	0.0311	1.00539	0.00103	0.0047	0.0048
12	pust002_c06	93.95%	5.35%	0.71%	9.228E-08	344.2	0.0311	1.00264	0.00097	0.0047	0.0048
13	pust002_c07	93.38%	5.84%	0.78%	9.965E-08	308.9	0.0311	1.00594	0.00098	0.0047	0.0048
14	pust003_c01	96.92%	2.75%	0.32%	5.778E-08	788.0	0.0175	1.00219	0.00091	0.0047	0.0048
15	pust003_c02	96.80%	2.85%	0.35%	5.905E-08	756.0	0.0175	1.00360	0.00090	0.0047	0.0048
16	pust003_c03	96.57%	3.05%	0.38%	6.149E-08	698.9	0.0311	1.00496	0.00088	0.0047	0.0048
17	pust003_c04	96.53%	3.09%	0.38%	6.226E-08	681.7	0.0311	1.00090	0.00094	0.0047	0.0048
18	pust003_c05	96.26%	3.33%	0.41%	6.484E-08	626.6	0.0311	1.00589	0.00094	0.0047	0.0048
19	pust003_c06	95.99%	3.57%	0.45%	6.861E-08	562.8	0.0311	1.00609	0.00095	0.0047	0.0048
20	pust003_c07	96.81%	2.83%	0.35%	5.877E-08	737.8	0.0311	1.00456	0.00094	0.0047	0.0048
21	pust003_c08	96.73%	2.91%	0.36%	5.950E-08	714.3	0.0311	1.00608	0.00095	0.0047	0.0048
22	pust004_c01	97.37%	2.36%	0.27%	5.309E-08	987.0	0.0054	1.00304	0.00087	0.0047	0.0048
23	pust004_c02	97.36%	2.36%	0.28%	5.329E-08	976.9	0.0418	0.99783	0.00084	0.0047	0.0048
24	pust004_c03	97.31%	2.41%	0.28%	5.415E-08	934.6	0.0450	0.99976	0.00091	0.0047	0.0048
25	pust004_c04	97.19%	2.52%	0.29%	5.528E-08	888.9	0.0326	0.99814	0.00090	0.0047	0.0048
26	pust004_c05	97.28%	2.44%	0.29%	5.408E-08	942.0	0.0363	0.99932	0.00089	0.0047	0.0048
27	pust004_c06	97.23%	2.48%	0.29%	5.436E-08	927.4	0.0050	1.00092	0.00084	0.0047	0.0048
28	pust004_c07	97.18%	2.52%	0.30%	5.530E-08	891.7	0.0050	1.00542	0.00085	0.0047	0.0048

No.	Filename	Thermal (<0.635 eV)	Inter (>0.635 eV, <100 KeV)	Fast (>100 KeV)	EALF (MeV)	H/X	Pu240/Pu	k_{eff}	σ MCNP	σ bench	σ total
29	pust004_c08	97.12%	2.57%	0.31%	5.596E-08	869.0	0.0050	1.00027	0.00091	0.0047	0.0048
30	pust004_c09	96.87%	2.80%	0.33%	5.822E-08	805.2	0.0153	1.00040	0.00091	0.0047	0.0048
31	pust004_c10	96.49%	3.14%	0.37%	6.260E-08	689.4	0.0251	0.99994	0.00091	0.0047	0.0048
32	pust004_c11	96.00%	3.57%	0.43%	6.794E-08	591.7	0.0233	0.99886	0.00090	0.0047	0.0048
33	pust004_c12	97.13%	2.56%	0.31%	5.550E-08	892.7	0.0316	1.00298	0.00089	0.0047	0.0048
34	pust004_c13	97.20%	2.49%	0.31%	5.502E-08	903.1	0.0335	0.99956	0.00089	0.0047	0.0048
35	pust005_c01	97.17%	2.53%	0.30%	5.501E-08	902.8	0.0403	1.00299	0.00088	0.0047	0.0048
36	pust005_c02	97.06%	2.62%	0.32%	5.635E-08	867.7	0.0403	1.00224	0.00091	0.0047	0.0048
37	pust005_c03	96.98%	2.69%	0.33%	5.714E-08	834.4	0.0403	1.00371	0.00085	0.0047	0.0048
38	pust005_c04	96.76%	2.89%	0.35%	5.937E-08	765.2	0.0403	1.00515	0.00086	0.0047	0.0048
39	pust005_c05	96.49%	3.13%	0.38%	6.242E-08	694.1	0.0403	1.00753	0.00090	0.0047	0.0048
40	pust005_c06	96.22%	3.37%	0.41%	6.536E-08	633.4	0.0403	1.00320	0.00090	0.0047	0.0048
41	pust005_c07	95.93%	3.62%	0.45%	6.871E-08	580.6	0.0403	1.00422	0.00092	0.0047	0.0048
42	pust005_c08	97.04%	2.65%	0.32%	5.620E-08	868.7	0.0403	0.99760	0.00089	0.0047	0.0048
43	pust005_c09	96.96%	2.71%	0.33%	5.743E-08	825.1	0.0403	1.00355	0.00087	0.0047	0.0048
44	pust006_c01	97.46%	2.28%	0.26%	5.194E-08	1061.1	0.0311	1.00032	0.00081	0.0035	0.0036
45	pust006_c02	97.42%	2.32%	0.27%	5.272E-08	1017.8	0.0311	1.00193	0.00085	0.0035	0.0036
46	pust006_c03	97.21%	2.49%	0.30%	5.489E-08	940.1	0.0311	1.00163	0.00086	0.0035	0.0036
47	pust007_c02	84.19%	13.67%	2.14%	2.753E-07	109.2	0.0457	1.00653	0.00108	0.0047	0.0048
48	pust007_c03	84.77%	13.16%	2.06%	2.617E-07	113.6	0.0457	1.00156	0.00101	0.0047	0.0048
49	pust007_c05	92.46%	6.62%	0.91%	1.120E-07	266.7	0.0457	1.00731	0.00105	0.0047	0.0048
50	pust007_c06	92.35%	6.71%	0.94%	1.135E-07	261.2	0.0457	1.00177	0.00105	0.0047	0.0048
51	pust007_c07	92.47%	6.61%	0.92%	1.121E-07	264.9	0.0457	1.00239	0.00101	0.0047	0.0048
52	pust007_c08	92.26%	6.79%	0.94%	1.147E-07	257.6	0.0457	0.99838	0.00103	0.0047	0.0048
53	pust007_c09	92.27%	6.78%	0.95%	1.142E-07	258.9	0.0457	0.99579	0.00103	0.0047	0.0048
54	pust007_c10	92.93%	6.21%	0.86%	1.055E-07	284.1	0.0457	0.99814	0.00102	0.0047	0.0048
55	pust009_c01	98.61%	1.25%	0.14%	4.129E-08	2646.2	0.0251	1.01561	0.00046	0.0033	0.0033
56	pust009_c02	98.67%	1.21%	0.13%	4.076E-08	2776.7	0.0251	1.01905	0.00044	0.0033	0.0033
57	pust009_c03	98.66%	1.21%	0.13%	4.091E-08	2800.6	0.0251	1.01843	0.00043	0.0033	0.0033
58	pust010_c1.09	92.62%	6.49%	0.89%	1.102E-07	266.9	0.0284	1.01699	0.00104	0.0048	0.0049

No.	Filename	Thermal (<0.635 eV)	Inter (>0.635 eV, <100 KeV)	Fast (>100 KeV)	EALF (MeV)	H/X	Pu240/Pu	k_{eff}	σ MCNP	σ bench	σ total
59	pust010_c1.11	95.43%	4.06%	0.51%	7.478E-08	485.0	0.0284	1.01117	0.00103	0.0048	0.0049
60	pust010_c1.12	95.90%	3.63%	0.46%	6.913E-08	543.4	0.0289	1.00888	0.00094	0.0048	0.0049
61	pust010_c2.09	94.21%	5.11%	0.68%	8.887E-08	356.9	0.0284	1.01255	0.00104	0.0048	0.0049
62	pust010_c2.11	95.88%	3.66%	0.46%	6.925E-08	558.1	0.0284	1.00903	0.00093	0.0048	0.0049
63	pust010_c2.12	96.28%	3.31%	0.42%	6.485E-08	618.3	0.0289	1.00885	0.00097	0.0048	0.0049
64	pust010_c3.09	95.47%	4.03%	0.50%	7.349E-08	484.2	0.0284	1.00708	0.00095	0.0048	0.0049
65	pust010_c3.11	95.94%	3.60%	0.46%	6.866E-08	558.1	0.0284	1.00814	0.00098	0.0048	0.0049
66	pust010_c3.12	96.71%	2.93%	0.36%	6.013E-08	728.1	0.0289	1.01223	0.00092	0.0048	0.0049
67	pust010_c4.11	96.16%	3.42%	0.42%	6.607E-08	605.9	0.0284	1.00125	0.00095	0.0048	0.0049
68	pust010_c4.12	97.08%	2.61%	0.31%	5.633E-08	849.7	0.0289	1.01133	0.00090	0.0048	0.0049
69	pust010_c5.11	96.42%	3.19%	0.39%	6.370E-08	665.4	0.0284	1.00383	0.00095	0.0048	0.0049
70	pust010_c6.11	94.88%	4.53%	0.59%	8.074E-08	414.3	0.0289	1.01311	0.00102	0.0048	0.0049
71	pust010_c7.11	95.80%	3.73%	0.47%	6.991E-08	535.2	0.0289	1.00202	0.00095	0.0048	0.0049
72	pust011_c1.16	96.47%	3.14%	0.39%	6.287E-08	764.8	0.0415	1.01190	0.00104	0.0052	0.0053
73	pust011_c1.18	97.55%	2.19%	0.26%	5.143E-08	1207.8	0.0418	0.99465	0.00089	0.0052	0.0053
74	pust011_c2.16	96.37%	3.23%	0.40%	6.398E-08	736.0	0.0415	1.01659	0.00105	0.0052	0.0053
75	pust011_c2.18	97.45%	2.28%	0.27%	5.232E-08	1151.4	0.0418	1.00113	0.00090	0.0052	0.0053
76	pust011_c3.16	96.20%	3.38%	0.42%	6.611E-08	691.5	0.0415	1.01758	0.00101	0.0052	0.0053
77	pust011_c3.18	97.46%	2.27%	0.27%	5.245E-08	1158.2	0.0418	0.99814	0.00089	0.0052	0.0053
78	pust011_c4.16	96.08%	3.48%	0.44%	6.716E-08	681.7	0.0415	1.01174	0.00102	0.0052	0.0053
79	pust011_c4.18	97.30%	2.41%	0.29%	5.385E-08	1099.7	0.0418	0.99478	0.00090	0.0052	0.0053
80	pust011_c5.16	95.47%	4.02%	0.51%	7.446E-08	574.5	0.0415	1.01009	0.00102	0.0052	0.0053
81	pust011_c5.18	97.20%	2.50%	0.30%	5.498E-08	1038.9	0.0418	1.00372	0.00089	0.0052	0.0053
82	pust011_c6.18	96.88%	2.79%	0.33%	5.857E-08	908.4	0.0418	1.00169	0.00095	0.0052	0.0053
83	pust011_c7.18	97.34%	2.38%	0.28%	5.345E-08	1102.6	0.0418	1.00119	0.00089	0.0052	0.0053
84	pust014_c01	89.53%	9.18%	1.29%	1.650E-07	219.5	0.0423	1.00488	0.00097	0.0032	0.0033
85	pust014_c02	89.57%	9.15%	1.28%	1.657E-07	219.5	0.0423	1.00463	0.00103	0.0032	0.0034
86	pust014_c03	89.61%	9.10%	1.29%	1.647E-07	219.5	0.0423	1.00539	0.00102	0.0032	0.0034
87	pust014_c04	89.63%	9.09%	1.28%	1.644E-07	219.5	0.0423	1.00613	0.00100	0.0032	0.0034
88	pust014_c05	89.54%	9.16%	1.30%	1.655E-07	219.5	0.0423	1.00581	0.00097	0.0032	0.0033

No.	Filename	*Thermal* (<0.635 eV)	*Inter* (>0.635 eV, <100 KeV)	*Fast* (>100 KeV)	EALF (MeV)	H/X	Pu240/Pu	k_{eff}	σ MCNP	σ bench	σ total
89	pust014_c06	89.51%	9.21%	1.29%	1.654E-07	219.5	0.0423	1.00398	0.00105	0.0032	0.0034
90	pust014_c07	89.49%	9.21%	1.30%	1.660E-07	219.5	0.0423	1.00741	0.00103	0.0043	0.0044
91	pust014_c08	89.48%	9.22%	1.30%	1.666E-07	219.5	0.0423	1.00259	0.00103	0.0032	0.0034
92	pust014_c09	89.51%	9.19%	1.30%	1.661E-07	219.5	0.0423	1.00220	0.00101	0.0032	0.0034
93	pust014_c10	89.56%	9.15%	1.29%	1.649E-07	219.5	0.0423	1.00385	0.00100	0.0032	0.0034
94	pust014_c11	89.55%	9.16%	1.28%	1.656E-07	219.5	0.0423	1.00190	0.00099	0.0032	0.0033
95	pust014_c12	89.63%	9.08%	1.29%	1.646E-07	219.5	0.0423	1.00429	0.00103	0.0032	0.0034
96	pust014_c13	89.51%	9.20%	1.29%	1.666E-07	219.5	0.0423	1.00489	0.00101	0.0043	0.0044
97	pust014_c14	89.49%	9.21%	1.30%	1.663E-07	219.5	0.0423	1.00222	0.00097	0.0043	0.0044
98	pust014_c15	89.55%	9.16%	1.29%	1.650E-07	219.5	0.0423	1.00438	0.00102	0.0043	0.0044
99	pust014_c16	89.53%	9.18%	1.28%	1.651E-07	219.5	0.0423	1.00480	0.00099	0.0043	0.0044
100	pust014_c17	89.62%	9.09%	1.29%	1.650E-07	219.5	0.0423	1.00566	0.00100	0.0043	0.0044
101	pust014_c18	89.52%	9.18%	1.31%	1.670E-07	219.5	0.0423	1.00697	0.00099	0.0043	0.0044
102	pust014_c19	89.49%	9.22%	1.29%	1.663E-07	219.5	0.0423	1.00308	0.00101	0.0043	0.0044
103	pust014_c20	89.61%	9.11%	1.29%	1.647E-07	219.5	0.0423	1.00522	0.00102	0.0043	0.0044
104	pust014_c21	89.51%	9.20%	1.29%	1.659E-07	219.5	0.0423	1.00065	0.00102	0.0043	0.0044
105	pust014_c22	89.58%	9.12%	1.29%	1.651E-07	219.5	0.0423	1.00489	0.00105	0.0043	0.0044
106	pust014_c23	89.57%	9.13%	1.30%	1.648E-07	219.5	0.0423	1.00311	0.00095	0.0043	0.0044
107	pust014_c24	89.48%	9.24%	1.28%	1.667E-07	219.5	0.0423	1.00655	0.00100	0.0043	0.0044
108	pust014_c25	89.55%	9.16%	1.29%	1.659E-07	219.5	0.0423	1.00300	0.00099	0.0043	0.0044
109	pust014_c26	89.55%	9.19%	1.27%	1.652E-07	219.5	0.0423	1.00375	0.00100	0.0043	0.0044
110	pust014_c27	89.57%	9.14%	1.29%	1.653E-07	219.5	0.0423	1.00333	0.00103	0.0043	0.0044
111	pust014_c28	89.54%	9.16%	1.30%	1.654E-07	219.5	0.0423	1.00272	0.00103	0.0043	0.0044
112	pust014_c29	89.57%	9.15%	1.29%	1.650E-07	219.5	0.0423	1.00411	0.00096	0.0043	0.0044
113	pust014_c30	89.47%	9.22%	1.31%	1.677E-07	219.5	0.0423	1.00449	0.00092	0.0043	0.0044
114	pust014_c31	89.49%	9.21%	1.29%	1.667E-07	219.5	0.0423	1.00232	0.00098	0.0043	0.0044
115	pust014_c32	89.45%	9.25%	1.29%	1.662E-07	219.5	0.0423	1.00402	0.00103	0.0043	0.0044
116	pust014_c33	89.49%	9.20%	1.31%	1.664E-07	219.5	0.0423	1.00139	0.00102	0.0043	0.0044
117	pust014_c34	89.54%	9.16%	1.30%	1.660E-07	219.5	0.0423	1.00232	0.00101	0.0043	0.0044
118	pust014_c35	89.53%	9.19%	1.29%	1.652E-07	219.5	0.0423	1.00100	0.00103	0.0043	0.0044

No.	Filename	Thermal (<0.635 eV)	Inter (>0.635 eV, <100 KeV)	Fast (>100 KeV)	EALF (MeV)	H/X	Pu240/Pu	k_{eff}	σ MCNP	σ bench	σ total
119	pust015_c01	86.45%	11.82%	1.73%	2.345E-07	162.1	0.0423	1.00710	0.00100	0.0038	0.0039
120	pust015_c02	86.45%	11.82%	1.73%	2.344E-07	162.1	0.0423	1.00682	0.00107	0.0038	0.0039
121	pust015_c03	86.42%	11.85%	1.73%	2.344E-07	162.1	0.0423	1.00433	0.00102	0.0038	0.0039
122	pust015_c04	86.44%	11.82%	1.74%	2.348E-07	162.1	0.0423	1.00335	0.00101	0.0038	0.0039
123	pust015_c05	86.45%	11.82%	1.73%	2.342E-07	162.1	0.0423	1.00464	0.00102	0.0038	0.0039
124	pust015_c06	86.57%	11.71%	1.72%	2.324E-07	162.1	0.0423	1.00569	0.00104	0.0038	0.0039
125	pust015_c07	86.39%	11.88%	1.74%	2.360E-07	162.1	0.0423	1.00606	0.00102	0.0047	0.0048
126	pust015_c08	86.36%	11.90%	1.74%	2.361E-07	162.1	0.0423	1.00472	0.00100	0.0047	0.0048
127	pust015_c09	86.40%	11.87%	1.74%	2.351E-07	162.1	0.0423	1.00390	0.00100	0.0047	0.0048
128	pust015_c10	86.44%	11.85%	1.71%	2.342E-07	162.1	0.0423	1.00324	0.00096	0.0047	0.0048
129	pust015_c11	86.35%	11.92%	1.73%	2.366E-07	162.1	0.0423	1.00305	0.00098	0.0047	0.0048
130	pust015_c12	86.41%	11.85%	1.74%	2.350E-07	162.1	0.0423	1.00363	0.00101	0.0047	0.0048
131	pust015_c13	86.41%	11.85%	1.74%	2.341E-07	162.1	0.0423	1.00516	0.00102	0.0047	0.0048
132	pust015_c14	86.46%	11.81%	1.73%	2.331E-07	162.1	0.0423	1.00479	0.00103	0.0047	0.0048
133	pust015_c15	86.44%	11.82%	1.74%	2.350E-07	162.1	0.0423	1.00633	0.00100	0.0047	0.0048
134	pust015_c16	86.33%	11.91%	1.76%	2.359E-07	162.1	0.0423	1.00369	0.00095	0.0047	0.0048
135	pust015_c17	86.45%	11.82%	1.73%	2.336E-07	162.1	0.0423	1.00491	0.00101	0.0047	0.0048
136	pust016_c01	86.45%	11.81%	1.74%	2.350E-07	162.1	0.0423	1.00255	0.00100	0.0043	0.0044
137	pust016_c02	86.46%	11.81%	1.73%	2.345E-07	162.1	0.0423	1.00330	0.00100	0.0043	0.0044
138	pust016_c03	86.50%	11.77%	1.73%	2.331E-07	162.1	0.0423	1.00691	0.00102	0.0043	0.0044
139	pust016_c04	86.41%	11.86%	1.74%	2.349E-07	162.1	0.0423	1.00516	0.00099	0.0043	0.0044
140	pust016_c05	89.48%	9.22%	1.30%	1.669E-07	219.5	0.0423	1.00269	0.00102	0.0038	0.0039
141	pust016_c06	89.53%	9.18%	1.30%	1.658E-07	219.5	0.0423	1.00380	0.00098	0.0038	0.0039
142	pust016_c07	89.57%	9.15%	1.28%	1.646E-07	219.5	0.0423	1.00446	0.00097	0.0038	0.0039
143	pust016_c08	89.59%	9.12%	1.30%	1.648E-07	219.5	0.0423	1.00486	0.00098	0.0038	0.0039
144	pust016_c09	89.54%	9.17%	1.29%	1.657E-07	219.5	0.0423	0.99743	0.00097	0.0033	0.0034
145	pust016_c10	89.56%	9.15%	1.29%	1.648E-07	219.5	0.0423	1.00293	0.00108	0.0033	0.0035
146	pust016_c11	89.54%	9.17%	1.30%	1.658E-07	219.5	0.0423	1.00495	0.00101	0.0033	0.0035
147	pust017_c01	89.56%	9.14%	1.30%	1.652E-07	219.5	0.0423	1.00226	0.00099	0.0038	0.0039
148	pust017_c02	89.55%	9.17%	1.28%	1.647E-07	219.5	0.0423	1.00284	0.00102	0.0038	0.0039

No.	Filename	Thermal (<0.635 eV)	Inter (>0.635 eV, <100 KeV)	Fast (>100 KeV)	EALF (MeV)	H/X	Pu240/Pu	k_{eff}	σ MCNP	σ bench	σ total
149	pust017_c03	89.60%	9.11%	1.29%	1.648E-07	219.5	0.0423	1.00406	0.00103	0.0038	0.0039
150	pust017_c04	89.64%	9.07%	1.29%	1.644E-07	219.5	0.0423	1.00493	0.00103	0.0038	0.0039
151	pust017_c05	89.55%	9.14%	1.31%	1.659E-07	219.5	0.0423	1.00075	0.00102	0.0038	0.0039
152	pust017_c06	89.49%	9.22%	1.30%	1.664E-07	219.5	0.0423	1.00415	0.00105	0.0038	0.0039
153	pust017_c07	89.58%	9.13%	1.29%	1.648E-07	219.5	0.0423	1.00166	0.00099	0.0038	0.0039
154	pust017_c08	89.49%	9.22%	1.29%	1.659E-07	219.5	0.0423	1.00606	0.00099	0.0038	0.0039
155	pust017_c09	89.61%	9.11%	1.28%	1.650E-07	219.5	0.0423	1.00394	0.00102	0.0038	0.0039
156	pust017_c10	89.55%	9.15%	1.30%	1.657E-07	219.5	0.0423	1.00505	0.00103	0.0038	0.0039
157	pust017_c11	89.58%	9.14%	1.28%	1.647E-07	219.5	0.0423	1.00530	0.00105	0.0038	0.0039
158	pust017_c12	89.62%	9.09%	1.28%	1.644E-07	219.5	0.0423	1.00372	0.00100	0.0038	0.0039
159	pust017_c13	89.51%	9.20%	1.29%	1.659E-07	219.5	0.0423	1.00392	0.00107	0.0038	0.0039
160	pust017_c14	89.47%	9.22%	1.30%	1.660E-07	219.5	0.0423	1.00446	0.00105	0.0038	0.0039
161	pust017_c15	89.54%	9.17%	1.29%	1.654E-07	219.5	0.0423	1.00542	0.00098	0.0038	0.0039
162	pust017_c16	89.54%	9.17%	1.29%	1.649E-07	219.5	0.0423	1.00437	0.00103	0.0038	0.0039
163	pust017_c17	89.58%	9.12%	1.29%	1.652E-07	219.5	0.0423	1.00435	0.00104	0.0038	0.0039
164	pust017_c18	89.58%	9.13%	1.30%	1.653E-07	219.5	0.0423	1.00637	0.00099	0.0038	0.0039
165	pust020_c01	96.20%	3.39%	0.41%	6.535E-08	633.1	0.0457	1.00313	0.00092	0.0059	0.0060
166	pust020_c02	96.35%	3.25%	0.40%	6.407E-08	651.5	0.0457	1.00550	0.00090	0.0059	0.0060
167	pust020_c03	96.82%	2.85%	0.34%	5.876E-08	783.7	0.0457	1.00118	0.00092	0.0059	0.0060
168	pust020_c05	95.32%	4.15%	0.53%	7.572E-08	485.1	0.0457	1.00201	0.00096	0.0059	0.0060
169	pust020_c06	95.10%	4.36%	0.54%	7.870E-08	474.0	0.0457	1.00549	0.00096	0.0059	0.0060
170	pust020_c07	96.68%	2.96%	0.36%	6.028E-08	759.3	0.0457	0.99646	0.00095	0.0059	0.0060
171	pust020_c08	93.12%	6.10%	0.77%	1.052E-07	359.7	0.0457	1.00363	0.00102	0.0059	0.0060
172	pust020_c09	95.33%	4.17%	0.51%	7.554E-08	566.5	0.0457	0.99706	0.00104	0.0059	0.0060
173	pust021_c01	96.18%	3.40%	0.43%	6.578E-08	699.6	0.0457	1.00682	0.00105	0.0032	0.0034
174	pust021_c02	96.51%	3.12%	0.37%	6.181E-08	795.3	0.0457	1.00906	0.00102	0.0032	0.0034
175	pust021_c03	83.73%	14.16%	2.11%	3.081E-07	131.4	0.0457	1.00651	0.00114	0.0065	0.0066
176	pust021_c04	97.44%	2.30%	0.26%	5.229E-08	1082.3	0.0457	1.00045	0.00084	0.0025	0.0026
177	pust021_c05	97.57%	2.18%	0.25%	5.094E-08	1120.9	0.0457	1.00528	0.00080	0.0025	0.0026
178	pust021_c06	95.86%	3.69%	0.45%	6.992E-08	579.4	0.0457	1.00634	0.00098	0.0044	0.0045

No.	Filename	Thermal (<0.635 eV)	Inter (>0.635 eV, <100 KeV)	Fast (>100 KeV)	EALF (MeV)	H/X	Pu240/Pu	k_{eff}	σ MCNP	σ bench	σ total
179	pust024_c01	78.85%	18.26%	2.89%	4.651E-07	108.9	0.1840	1.00026	0.00105	0.0062	0.0063
180	pust024_c02	78.95%	18.16%	2.89%	4.600E-07	108.9	0.1840	1.00056	0.00106	0.0062	0.0063
181	pust024_c03	78.99%	18.15%	2.86%	4.561E-07	108.9	0.1840	0.99979	0.00103	0.0062	0.0063
182	pust024_c04	79.09%	18.04%	2.87%	4.546E-07	108.9	0.1840	1.00131	0.00104	0.0062	0.0063
183	pust024_c05	79.16%	17.97%	2.87%	4.507E-07	108.9	0.1840	1.00011	0.00106	0.0062	0.0063
184	pust024_c07	86.15%	12.05%	1.80%	2.276E-07	179.2	0.1840	1.00906	0.0011	0.0053	0.0054
185	pust024_c08	86.18%	12.02%	1.79%	2.275E-07	179.2	0.1840	1.00681	0.00102	0.0053	0.0054
186	pust024_c09	86.20%	12.03%	1.76%	2.247E-07	179.2	0.1840	1.00898	0.00107	0.0053	0.0054
187	pust024_c10	86.33%	11.91%	1.76%	2.235E-07	179.2	0.1840	1.00715	0.00103	0.0053	0.0054
188	pust024_c11	86.34%	11.91%	1.75%	2.219E-07	179.2	0.1840	1.00898	0.00104	0.0053	0.0054
189	pust024_c12	86.45%	11.80%	1.75%	2.202E-07	179.2	0.1840	1.00713	0.00101	0.0053	0.0054
190	pust024_c13	86.37%	11.89%	1.74%	2.214E-07	179.2	0.1840	1.00657	0.00104	0.0053	0.0054
191	pust024_c14	83.56%	14.18%	2.27%	2.980E-07	152.9	0.2320	0.99988	0.00107	0.0053	0.0054
192	pust024_c15	83.60%	14.17%	2.23%	2.962E-07	152.9	0.2320	0.99923	0.00108	0.0053	0.0054
193	pust024_c16	83.68%	14.09%	2.23%	2.934E-07	152.9	0.2320	0.99979	0.0011	0.0053	0.0054
194	pust024_c17	83.84%	13.93%	2.22%	2.905E-07	152.9	0.2320	1.00347	0.00111	0.0053	0.0054
195	pust024_c18	93.94%	5.33%	0.73%	8.982E-08	457.4	0.1840	1.00364	0.00107	0.0051	0.0052
196	pust024_c19	93.95%	5.32%	0.72%	8.957E-08	457.4	0.1840	1.00523	0.00105	0.0051	0.0052
197	pust024_c20	93.97%	5.30%	0.73%	8.921E-08	457.4	0.1840	1.00623	0.00101	0.0051	0.0052
198	pust024_c21	93.98%	5.30%	0.72%	8.910E-08	457.4	0.1840	1.00463	0.00102	0.0051	0.0052
199	pust024_c22	94.03%	5.26%	0.71%	8.875E-08	457.4	0.1840	1.00530	0.00098	0.0051	0.0052
200	pust024_c23	94.00%	5.28%	0.72%	8.869E-08	457.4	0.1840	1.00358	0.00099	0.0051	0.0052

Table 6.8-4 – U-233 Benchmark Experiment Data (with Beryllium)

No.	Filename	Thermal (<0.635 eV)	Inter (>0.635 eV, <100 KeV)	Fast (>100 KeV)	EALF (MeV)	k_{eff}	σ MCNP	σ bench	σ total
201	ust015_c01	51.61%	45.08%	3.31%	1.114E-06	0.99327	0.00101	0.0075	0.0076
202	ust015_c02	50.16%	46.32%	3.51%	1.247E-06	0.98695	0.00102	0.0069	0.0070
203	ust015_c03	49.68%	46.68%	3.64%	1.314E-06	0.98732	0.00105	0.0055	0.0056
204	ust015_c04	58.25%	38.43%	3.32%	7.298E-07	0.98992	0.00095	0.0066	0.0067
205	ust015_c05	49.10%	47.11%	3.79%	1.385E-06	0.98658	0.00104	0.0063	0.0064
206	ust015_c06	48.70%	47.40%	3.90%	1.435E-06	0.97847	0.00103	0.0058	0.0059
207	ust015_c08	48.53%	47.41%	4.06%	1.488E-06	0.97451	0.00102	0.0048	0.0049
208	ust015_c09	48.38%	47.48%	4.15%	1.513E-06	0.96798	0.00102	0.0055	0.0056
209	ust015_c11	57.24%	40.07%	2.69%	7.003E-07	0.99395	0.00100	0.0068	0.0069
210	ust015_c12	56.02%	41.15%	2.83%	7.747E-07	0.99488	0.00102	0.0041	0.0042
211	ust015_c13	55.49%	41.57%	2.94%	8.148E-07	0.99382	0.00099	0.0055	0.0056
212	ust015_c14	63.58%	33.74%	2.68%	4.694E-07	0.99780	0.00095	0.0099	0.0099
213	ust015_c15	54.97%	41.97%	3.06%	8.520E-07	0.99208	0.00104	0.0070	0.0071
214	ust015_c16	54.76%	42.05%	3.19%	8.768E-07	0.99101	0.00102	0.0067	0.0068
215	ust015_c18	54.47%	42.23%	3.30%	9.073E-07	0.97410	0.00102	0.0051	0.0052
216	ust015_c19	54.43%	42.22%	3.36%	9.141E-07	0.97675	0.00106	0.0075	0.0076
217	ust015_c20	68.57%	29.72%	1.71%	2.920E-07	0.99786	0.00093	0.0069	0.0070
218	ust015_c21	67.50%	30.70%	1.81%	3.167E-07	1.00066	0.00102	0.0036	0.0037
219	ust015_c22	66.72%	31.40%	1.88%	3.340E-07	0.99732	0.00101	0.0060	0.0061
220	ust015_c23	66.32%	31.71%	1.97%	3.478E-07	0.99508	0.00100	0.0043	0.0044
221	ust015_c24	66.02%	31.96%	2.02%	3.566E-07	0.99074	0.00102	0.0029	0.0031
222	ust015_c26	79.37%	19.65%	0.98%	1.274E-07	0.99630	0.00092	0.0052	0.0053
223	ust015_c27	78.94%	20.04%	1.02%	1.314E-07	0.99994	0.00094	0.0079	0.0080
224	ust015_c28	78.68%	20.28%	1.05%	1.343E-07	0.99846	0.00089	0.0070	0.0071
225	ust015_c29	78.53%	20.39%	1.08%	1.361E-07	0.99818	0.00096	0.0062	0.0063
226	ust015_c30	78.41%	20.48%	1.11%	1.377E-07	0.99753	0.00097	0.0051	0.0052
227	ust015_c31	78.41%	20.43%	1.16%	1.379E-07	0.99385	0.00105	0.0023	0.0025

Table 6.8-5 – U-233 Benchmark Experiment Data (without Beryllium)

No.	Filename	Thermal (<0.635 eV)	Inter (>0.635 eV, <100 KeV)	Fast (>100 KeV)	EALF (MeV)	k_{eff}	σ MCNP	σ bench	σ total
228	ust015_c07	57.08%	39.48%	3.44%	8.016E-07	0.98486	0.00098	0.0051	0.0052
229	ust015_c10	52.16%	44.00%	3.84%	1.149E-06	0.98968	0.00110	0.0070	0.0071
230	ust015_c17	62.55%	34.65%	2.80%	5.116E-07	0.99702	0.00099	0.0050	0.0051
231	ust015_c25	72.66%	25.57%	1.78%	2.263E-07	0.99647	0.00096	0.0056	0.0057
232	ust001_c01	94.71%	5.08%	0.21%	3.948E-08	1.00136	0.00060	0.0031	0.0032
233	ust001_c02	94.53%	5.25%	0.22%	4.000E-08	1.00045	0.00060	0.0033	0.0034
234	ust001_c03	94.36%	5.41%	0.23%	4.060E-08	1.00082	0.00061	0.0033	0.0034
235	ust001_c04	94.16%	5.61%	0.23%	4.116E-08	1.00026	0.00062	0.0033	0.0034
236	ust001_c05	93.98%	5.78%	0.24%	4.172E-08	1.00013	0.00065	0.0033	0.0034
237	ust003_c40	69.08%	28.67%	2.25%	3.101E-07	1.00873	0.00112	0.0087	0.0088
238	ust003_c41	67.65%	30.05%	2.30%	3.427E-07	1.02347	0.00112	0.0151	0.0152
239	ust003_c42	68.08%	29.61%	2.31%	3.341E-07	1.00305	0.00118	0.0087	0.0088
240	ust003_c45	58.35%	38.09%	3.56%	7.600E-07	1.01077	0.00115	0.0126	0.0126
241	ust003_c55	55.20%	40.75%	4.05%	1.008E-06	1.01743	0.00111	0.0122	0.0123
242	ust003_c57	79.78%	19.01%	1.21%	1.294E-07	1.02347	0.00114	0.0087	0.0088
243	ust003_c58	85.19%	14.01%	0.81%	8.460E-08	1.01795	0.00107	0.0087	0.0088
244	ust003_c61	87.62%	11.74%	0.64%	6.949E-08	1.01112	0.00104	0.0087	0.0088
245	ust003_c62	89.03%	10.42%	0.56%	6.202E-08	1.01319	0.00098	0.0087	0.0088
246	ust003_c65	92.74%	6.92%	0.34%	4.633E-08	1.00900	0.00086	0.0087	0.0088
247	ust012_c01	75.96%	22.52%	1.52%	1.743E-07	0.99683	0.00117	0.0028	0.0030
248	ust012_c02	76.79%	21.74%	1.47%	1.643E-07	0.99704	0.00118	0.0025	0.0028
249	ust012_c03	78.26%	20.42%	1.32%	1.460E-07	1.00807	0.00114	0.0023	0.0026
250	ust012_c04	82.01%	16.96%	1.02%	1.078E-07	1.00021	0.00114	0.0015	0.0019
251	ust012_c05	84.03%	15.10%	0.87%	9.191E-08	1.00309	0.00112	0.0071	0.0072
252	ust012_c06	85.66%	13.58%	0.75%	8.082E-08	1.00495	0.00113	0.0010	0.0015
253	ust012_c07	90.87%	8.70%	0.43%	5.350E-08	1.00366	0.00101	0.0038	0.0039
254	ust012_c08	90.89%	8.67%	0.43%	5.351E-08	0.99846	0.00100	0.0048	0.0049
255	ust013_c01	76.82%	21.84%	1.34%	1.576E-07	1.00497	0.00106	0.0073	0.0074

No.	Filename	Thermal (<0.635 eV)	Inter (>0.635 eV, <100 KeV)	Fast (>100 KeV)	EALF (MeV)	k_{eff}	σ MCNP	σ bench	σ total
256	ust013_c02	76.77%	21.89%	1.34%	1.584E-07	1.00562	0.00103	0.0070	0.0071
257	ust013_c03	76.68%	21.99%	1.33%	1.585E-07	1.00512	0.00107	0.0069	0.0070
258	ust013_c04	76.86%	21.80%	1.34%	1.579E-07	1.00454	0.00107	0.0073	0.0074
259	ust013_c05	76.80%	21.86%	1.35%	1.578E-07	1.00773	0.00105	0.0067	0.0068
260	ust013_c06	77.32%	21.38%	1.31%	1.519E-07	1.00653	0.00099	0.0050	0.0051
261	ust013_c07	77.37%	21.33%	1.30%	1.512E-07	1.00837	0.00103	0.0054	0.0055
262	ust013_c08	77.43%	21.28%	1.29%	1.507E-07	1.00761	0.00101	0.0050	0.0051
263	ust013_c09	77.29%	21.40%	1.30%	1.519E-07	1.00543	0.00108	0.0045	0.0046
264	ust013_c10	77.38%	21.33%	1.29%	1.508E-07	1.00653	0.00106	0.0046	0.0047
265	ust013_c11	77.41%	21.29%	1.30%	1.513E-07	1.00482	0.00107	0.0054	0.0055
266	ust013_c12	77.40%	21.31%	1.30%	1.511E-07	1.00530	0.00101	0.0050	0.0051
267	ust013_c13	77.38%	21.32%	1.30%	1.519E-07	1.00384	0.00105	0.0062	0.0063
268	ust013_c14	77.28%	21.42%	1.30%	1.522E-07	1.00613	0.00101	0.0051	0.0052
269	ust013_c15	81.99%	17.04%	0.96%	1.056E-07	1.01973	0.00102	0.0077	0.0078
270	ust013_c16	84.13%	15.04%	0.82%	8.930E-08	0.99337	0.00102	0.0069	0.0070
271	ust013_c17	84.74%	14.47%	0.79%	8.566E-08	0.99574	0.00096	0.0052	0.0053
272	ust013_c18	85.50%	13.75%	0.76%	8.073E-08	0.99987	0.00097	0.0020	0.0022
273	ust013_c19	85.42%	13.83%	0.75%	8.095E-08	0.99661	0.00099	0.0089	0.0090
274	ust013_c20	88.95%	10.52%	0.53%	6.188E-08	0.99872	0.00092	0.0056	0.0057
275	ust013_c21	90.00%	9.53%	0.47%	5.686E-08	1.00412	0.00088	0.0034	0.0035
276	ust014_c01	59.84%	37.21%	2.95%	6.126E-07	0.97859	0.00104	0.0112	0.0112
277	ust014_c02	59.02%	37.94%	3.03%	6.516E-07	0.99304	0.00102	0.0112	0.0112
278	ust014_c03	69.43%	28.29%	2.27%	3.060E-07	1.01601	0.00092	0.0074	0.0075
279	ust014_c04	69.67%	28.08%	2.25%	3.002E-07	1.01238	0.00094	0.0089	0.0089
280	ust014_c05	71.04%	26.80%	2.16%	2.721E-07	1.01603	0.00091	0.0089	0.0089
281	ust014_c06	71.62%	26.25%	2.13%	2.618E-07	1.01415	0.00093	0.0089	0.0089
282	ust014_c07	72.11%	25.77%	2.12%	2.534E-07	1.00820	0.00089	0.0088	0.0088
283	ust014_c08	72.63%	25.30%	2.08%	2.437E-07	1.01384	0.00087	0.0091	0.0091
284	ust014_c09	69.60%	28.09%	2.31%	3.043E-07	1.01718	0.00093	0.0054	0.0055
285	ust014_c10	67.23%	30.34%	2.43%	3.602E-07	0.99953	0.00102	0.0108	0.0108

No.	Filename	Thermal (<0.635 eV)	Inter (>0.635 eV, <100 KeV)	Fast (>100 KeV)	EALF (MeV)	k_{eff}	σ MCNP	σ bench	σ total
286	ust014_c11	64.17%	33.24%	2.59%	4.441E-07	1.00298	0.00106	0.0126	0.0126
287	ust014_c12	69.34%	28.35%	2.30%	3.095E-07	1.01041	0.00099	0.0097	0.0098
288	ust014_c13	69.91%	27.80%	2.29%	2.981E-07	1.00589	0.00101	0.0104	0.0104
289	ust014_c14	70.28%	27.42%	2.31%	2.939E-07	1.00416	0.00098	0.0095	0.0096
290	ust014_c15	69.00%	28.62%	2.38%	3.217E-07	1.00117	0.00100	0.0098	0.0099
291	ust014_c16	61.16%	36.01%	2.83%	5.528E-07	0.98220	0.00106	0.0109	0.0110
292	usi001_c08	38.39%	54.72%	6.89%	4.520E-06	0.98014	0.00099	0.0056	0.0057
293	usi001_c16	49.52%	45.17%	5.31%	1.768E-06	0.97951	0.00099	0.0028	0.0030
294	usi001_c20	42.28%	51.78%	5.94%	3.021E-06	0.97843	0.00104	0.0056	0.0057
295	usi001_c23	36.51%	56.96%	6.54%	4.707E-06	0.98906	0.00103	0.0047	0.0048
296	usi001_c30	49.99%	45.54%	4.47%	1.471E-06	0.97677	0.00104	0.0053	0.0054
297	usi001_c33	45.08%	50.04%	4.88%	2.104E-06	0.99285	0.00105	0.0046	0.0047

This page intentionally left blank.

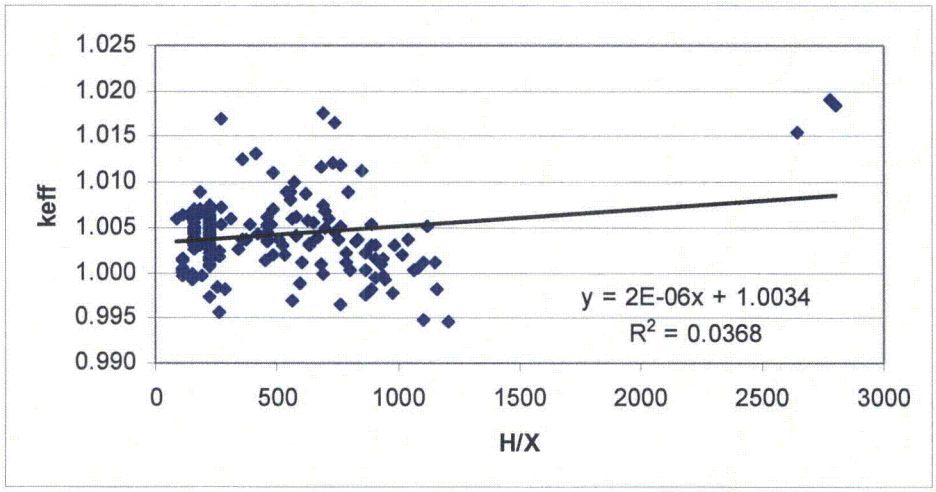

Figure 6.8-1 – Benchmark Data Trend for H/X

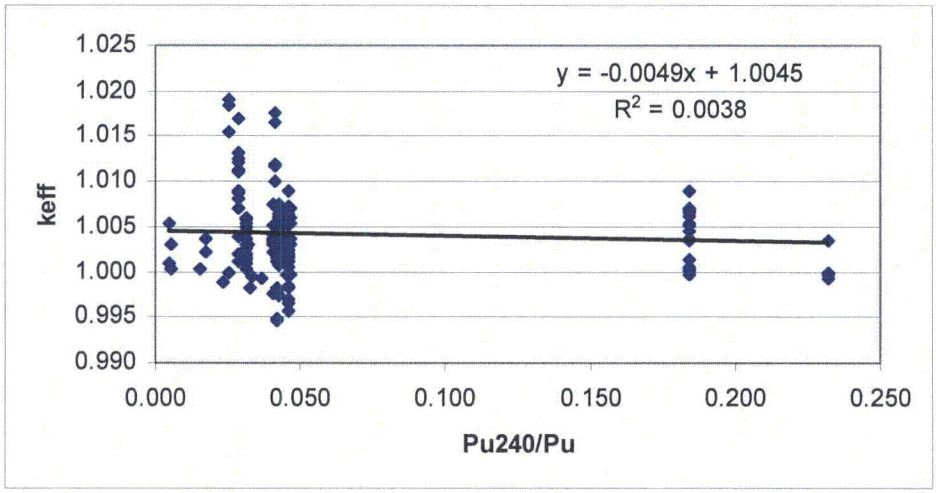

Figure 6.8-2 – Benchmark Data Trend for Pu240/Pu

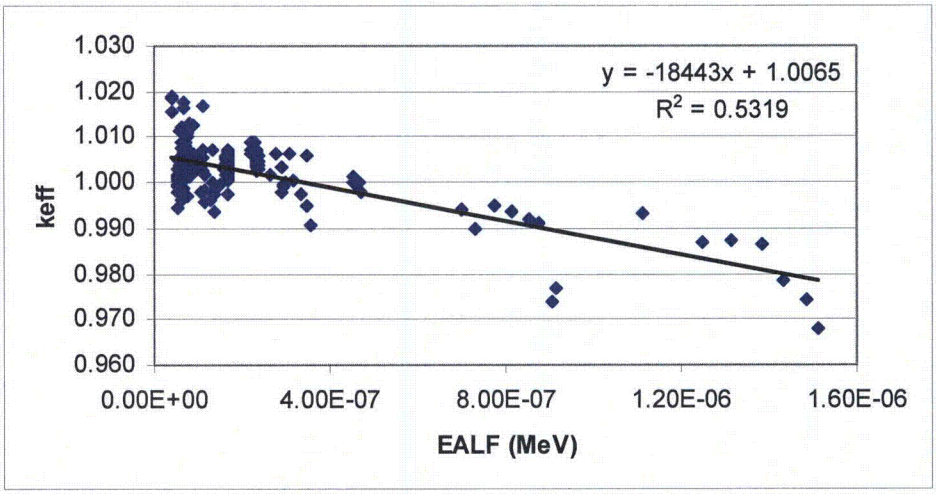

Figure 6.8-3 – Benchmark Data Trend for EALF1

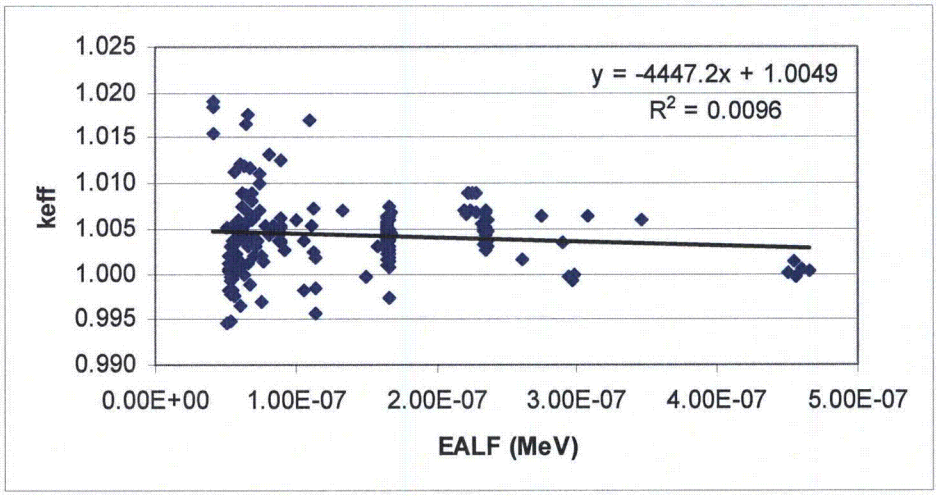

Figure 6.8-4 – Benchmark Data Trend for EALF5

6.9 Appendix

6.9.1 Sample Input File

A sample input file (filename ha_5g240_x0900) is provided for the most reactive HAC array case (Case E5 in Table 6.6-2).

ha_5g240_x0900

```
TRUPACT-III HA, H/X =  900 Pu239(g)= 340 Pu240(g)= 5
10      1 1.0498E-01 -5                                imp:n=1 $ source
11      2 1.0507E-01   10 -11 12 -13 14 -15 5                 imp:n=1 $ CSA cavity
12      3 -7.89  (-10:11:-12:13:-14:15) 20 -21 22 -23 24 -25 imp:n=1 $ inner CSA steel
13      4 -1.0   (-20:21:-22:23:-24:25) 30 -31 32 -33 34 -35 imp:n=1 $ CSA annulus
14      3 -7.89  (-30:31:-32:33:-34:35) 40 -41 42 -43 44 -45 imp:n=1 $ outer CSA steel
20      4 -1.0   90 -91 43 -53 46 -47                        imp:n=1 $ side foam
21      4 -1.0   90 -91 52 -42 46 -47                        imp:n=1 $ side foam
22      4 -1.0   92 -93 50 -40 46 -47                        imp:n=1 $ side foam
23      4 -1.0   92 -93 41 -51 46 -47                        imp:n=1 $ side foam
30      3 -7.89  90 -91 53 -63 46 -47                        imp:n=1 $ foam/balsa steel
31      3 -7.89  90 -91 62 -52 46 -47                        imp:n=1 $ foam/balsa steel
32      3 -7.89  92 -93 60 -50 46 -47                        imp:n=1 $ foam/balsa steel
33      3 -7.89  92 -93 51 -61 46 -47                        imp:n=1 $ foam/balsa steel
40      4 -1.0   90 -91 63 -73 46 -47                        imp:n=1 $ balsa
41      4 -1.0   90 -91 72 -62 46 -47                        imp:n=1 $ balsa
42      4 -1.0   92 -93 70 -60 46 -47                        imp:n=1 $ balsa
43      4 -1.0   92 -93 61 -71 46 -47                        imp:n=1 $ balsa
50      4 -1.0   (91 -41 43 -73 46 -47):(41 -71 93 -73 46 -47) imp:n=1 $ corner foam
51      4 -1.0   (40 -90 43 -73 46 -47):(70 -40 93 -73 46 -47) imp:n=1 $ corner foam
52      4 -1.0   (91 -41 72 -42 46 -47):(41 -71 72 -92 46 -47) imp:n=1 $ corner foam
53      4 -1.0   (40 -90 72 -42 46 -47):(70 -40 72 -92 46 -47) imp:n=1 $ corner foam
54      4 -1.0   (-40:41:-42:43) 70 -71 72 -73 44 -46         imp:n=1 $ corner foam
55      4 -1.0   (-40:41:-42:43) 70 -71 72 -73 47 -45         imp:n=1 $ corner foam
56      3 -7.89  (-70:71:-72:73) 80 -81 82 -83 135 -213       imp:n=1 $ outer steel
c
c       Front Impact Limiter
c
100     3 -7.89  70 -71 72 -73 120 -44                          imp:n=1 $ 6 mm steel
101     4 -1.0   116 -112 114 -110 -111 -113 -115 -117 121 -120 imp:n=1 $ 120 mm foam
102     3 -7.89  116 -112 114 -110 -111 -113 -115 -117 122 -121 imp:n=1 $ 15 mm steel
103     4 -1.0   116 -112 114 -110 -111 -113 -115 -117 123 -122 imp:n=1 $ 60 mm balsa
104     3 -7.89  116 -112 114 -110 -111 -113 -115 -117 124 -123 imp:n=1 $ 6 mm steel
105     4 -1.0   116 -112 114 -110 -111 -113 -115 -117 135 -124 imp:n=1 $ water
106     4 -1.0   (-116:112:-114:110:111:113:115:117)
                  70 -71 72 -73 130 -120 imp:n=1 $ calcium silicate outer
107     3 -7.89  (-116:112:-114:110:111:113:115:117)
                  70 -71 72 -73 131 -130 imp:n=1 $ steel outer
108     4 -1.0   (-116:112:-114:110:111:113:115:117)
                  70 -71 72 -73 132 -131 imp:n=1 $ foam outer
109     3 -7.89  (-116:112:-114:110:111:113:115:117)
                  70 -71 72 -73 133 -132 imp:n=1 $ steel outer
110     4 -1.0   (-116:112:-114:110:111:113:115:117)
                  70 -71 72 -73 134 -133 imp:n=1 $ foam outer
111     3 -7.89  (-116:112:-114:110:111:113:115:117)
                  70 -71 72 -73 135 -134 imp:n=1 $ steel outer
c
c       Rear Impact Limiter
c
200     4 -1.0   116 -112 114 -110 -111 -113 -115 -117 45  -200 imp:n=1 $ 120 mm foam
201     3 -7.89  116 -112 114 -110 -111 -113 -115 -117 200 -201 imp:n=1 $ 15 mm steel
202     4 -1.0   116 -112 114 -110 -111 -113 -115 -117 201 -202 imp:n=1 $ 60 mm balsa
203     3 -7.89  116 -112 114 -110 -111 -113 -115 -117 202 -203 imp:n=1 $ 6 mm steel
204     4 -1.0   116 -112 114 -110 -111 -113 -115 -117 203 -213 imp:n=1 $ water
205     4 -1.0   (-116:112:-114:110:111:113:115:117)
```

```
                 70 -71 72 -73 45  -210 imp:n=1 $ foam outer
206     3 -7.89  (-116:112:-114:110:111:113:115:117)
                 70 -71 72 -73 210 -211 imp:n=1 $ steel outer
207     4 -1.0   (-116:112:-114:110:111:113:115:117)
                 70 -71 72 -73 211 -212 imp:n=1 $ foam outer
208     3 -7.89  (-116:112:-114:110:111:113:115:117)
                 70 -71 72 -73 212 -213 imp:n=1 $ steel outer
c
c       Reflection
c
999     0   -80:81:-82:83:-135:213 imp:n=0

5     so 13.8603     $ source
c
10    px -92 $ CSA inner cavity
11    px  92
12    py -100
13    py  100
14    pz -139.5
15    pz  139.5
c
20    px -92.8  $ CSA inner wall (8 mm)
21    px  92.8  $ 8 mm
22    py -100.8 $ 8 mm
23    py  100.8 $ 8 mm
24    pz -140.7 $ 12 mm
25    pz  140.3 $ 8 mm
c
30    px -105.2 $ CSA annulus
31    px  105.2
32    py -113.2
33    py  113.2
34    pz -153.1 $ CSA lid annulus
35    pz  153.5
c
40    px -106   $ CSA outer
41    px  106
42    py -114
43    py  114
44    pz -154.3 $ CSA lid
45    pz  154.3
46    pz -128.7 $ side balsa/foam extent
47    pz  128.7
c
50    px -117.4 $ 114 mm foam
51    px  117.4 $ 114 mm foam
52    py -124.9 $ 109 mm foam
53    py  124.9 $ 109 mm foam
c
60    px -118.4 $ 10 mm steel
61    px  118.4
62    py -125.9
63    py  125.9
c
70    px -121.86 $ 60 mm balsa with 1" crush
71    px  121.86 $ 1" crush
72    py -129.36 $ 1" crush
73    py  129.36 $ 1" crush
c
*80    px -122.46 $ 6 mm steel (outer)
*81    px  122.46
*82    py -129.96
*83    py  129.96
c
90    px -86.35  $ picked to match steel width
91    px  86.35
92    py -94.9
```

```
93    py  94.9
c
c      Front Impact Limiter Surfaces
c
110    px  104.8
111    p   104.8  19.95 0  16.2  113.7 0  16.2  113.7 1
112    py  113.7
113    p  -104.8  19.95 0 -16.2  113.7 0 -16.2  113.7 1
114    px -104.8
115    p  -104.8 -19.95 0 -16.2 -113.7 0 -16.2 -113.7 1
116    py -113.7
117    p   104.8 -19.95 0  16.2 -113.7 0  16.2 -113.7 1
c
120    pz  -154.9 $ 6 mm steel
121    pz  -166.9 $ 120 mm foam
122    pz  -168.4 $ 15 mm steel
123    pz  -174.4 $ 60 mm balsa
124    pz  -175.0 $ 6 mm plate
130    pz  -159.1 $ 42 mm calcium silicate outer
131    pz  -160.7 $ 16 mm steel outer
132    pz  -198.9 $ 382 mm foam outer
133    pz  -199.5 $ 6 mm steel
134    pz  -205.88 $ 140 mm foam (crushed 3")
*135    pz  -206.68 $ 8 mm steel
c
c      Rear Impact Limiter Surfaces
c
200    pz  166.3 $ 120 mm foam
201    pz  167.8 $ 15 mm steel
202    pz  173.8 $ 60 mm balsa
203    pz  174.4 $ 6 mm steel
210    pz  199.1 $ 448 mm foam outer (gives overall length of 4288 mm)
211    pz  199.7 $ 6 mm steel outer
212    pz  206.08 $ 140 mm foam (crushed 3")
*213    pz  206.88 $ 8 mm steel outer

mode  n
sdef pos=0 0 0 rad=d1
si1 13.8603
kcode 1000 1.0 10 510
m1      94239.69c 7.6793E-05 $ fuel
        94240.66c 1.1246E-06
        1001.62c 6.9113E-02
        4009.62c 1.2329E-03
        6000.66c 9.8591E-03
        8016.62c 2.4698E-02
c        total 1.0498E-01
mt1   lwtr.60t be.60t
m2    1001.62c  6.9221E-02 $ reflector
      4009.62c  1.2348E-03
      6000.66c  9.8745E-03
      8016.62c  2.4736E-02
c     total     1.0507E-01
mt2   lwtr.60t be.60t
m3    6000.66c  -0.02      $ S31803 steel
      14000.60c -0.4
      15031.66c -0.025
      24000.50c -22.4
      25055.62c -0.7
      26000.55c -67.194
      28000.50c -5.8
      16000.62c -0.001
      42000.66c -3.3
      7014.62c  -0.16
m4    1001.62c   2         $ water
      8016.62c   1
mt4   lwtr.60t
```

```
m5     6000.66c   6          $ balsa
       1001.62c   10
       8016.62c   5
mt5    poly.60t
m6     6000.66c   -70        $ foam
       8016.62c   -14
       7014.62c   -6
       1001.62c   -10
mt6    poly.60t
```

7.0 OPERATING PROCEDURES

7.1 Procedures for Loading the Package

This section delineates the procedures for loading a payload into the TRUPACT–III packaging, and leakage rate testing of the containment boundary O–ring seals. Hereafter, reference to specific TRUPACT–III packaging components may be found in Appendix 1.3.1, *Packaging General Arrangement Drawings.*

The loading operation shall be performed in a dry environment. In the event of precipitation during outdoor loading operations, precautions, such as covering the payload cavity opening shall be implemented to prevent water or precipitation from entering. If precipitation enters the cavity, the free–standing water shall be removed prior to loading the payload.

7.1.1 Removal of the TRUPACT–III Package from the Transport Trailer/Railcar

1. Remove any devices covering the four (4) ISO fittings located at the upper corners of the body as necessary to allow engagement of a lifting device with the ISO fittings.
2. Disengage the straps, tie–rods, or equivalent on the transport trailer or railcar, and if necessary or desired, remove the tie–down assembly from the package.

   CAUTION: Failure to disengage the straps or tie–rods may cause damage to the packaging and/or transport trailer/railcar.
3. Rig an overhead crane, or equivalent, with an appropriate lift fixture capable of handling the TRUPACT–III package.
4. Lower the lift fixture onto the package and engage each ISO corner fitting.
5. Lift the package from the transport trailer or railcar and move the package to the loading station.
6. Place the package in the loading station, disengage from the four (4) ISO corner fittings, and remove the lift fixture.

7.1.2 Overpack Cover Removal

1. Open the two (2) M36 threaded holes in the top of the overpack cover.
2. Install two (2) M36 lifting rings or eyes into the threaded holes.
3. Rig an overhead crane, or equivalent, with an appropriate lift fixture capable of handling the overpack cover. Lower the lift fixture onto the overpack cover.
4. Remove the two (2) tamper–indicating seals (if installed) and the ten (10) M36 attachment bolts (socket head cap screws) from the overpack cover.
5. Raise the lift fixture and remove the overpack cover from the body. Store the overpack cover vertically to minimize potential damage.

7.1.3 Closure Lid Removal

1. Remove the vent port locking ring and vent port dust plug. Open the vent port to allow the payload cavity to vent to atmosphere.
2. Install two (2) M36 lifting rings or eyes into the threaded holes in the top of the closure lid. Rig an overhead crane, or equivalent, with an appropriate lift fixture capable of handling the closure lid via the two lifting rings or eyes.
3. Remove the forty–four (44) M36 closure bolts (socket head cap screws) from the closure lid.
4. Engage the lift fixture and remove the closure lid from the body. If necessary, separate the closure lid from the body using the four special M36 jacking threaded holes. Store the closure lid in a manner such that potential damage to the closure lid's sealing surface is minimized.

7.1.4 Loading the Payload into the TRUPACT–III Package

The following loading sequence requires that the payload has been properly prepared per the requirements of the *TRUPACT–III TRU Waste Authorized Methods for Payload Control (TRUPACT–III TRAMPAC)*[1].

1. Install sealing surface protectors onto the sealing flange of the body.
2. If not previously installed, install the roller floor (or equivalent payload loading system) in the payload cavity.
3. Connect an appropriate moving device to the loaded payload pallet.
4. Move the loaded payload pallet into the cavity until the payload is fully inserted into the payload cavity.
5. Ensure that a minimum of 2 mm axial clearance is present between any part of the SLB2 end face and the plane of the TRUPACT–III closure flange.

7.1.5 Closure Lid Installation

1. Visually inspect the closure bolts for wear or damage that could impair their function and, if necessary, replace or repair per the requirements of the drawings in Appendix 1.3.1, *Packaging General Arrangement Drawings*.
2. Visually inspect both closure lid main O–ring seals. If necessary, remove the O–ring seal(s) and clean the seal(s) and the sealing surface(s) on the closure lid and body to remove contamination. If, during the visual examination, it is determined that damage to the O–ring seal(s) and/or sealing surface(s) is sufficient to impair containment integrity, replace the damaged seal(s) and/or repair the damaged sealing surface(s) per Section 8.2.3.2.1, *Seal Area Routine Inspection and Repair*.
3. Visually inspect the O–ring seals on the vent port insert. If necessary, remove the O–ring seals, and clean the seals and sealing surfaces on the vent port insert and in the vent port to

[1] U.S. Department of Energy (DOE), *TRUPACT–III TRU Waste Authorized Methods for Payload Control (TRUPACT–III TRAMPAC)*, U.S. Department of Energy, Carlsbad Field Office, Carlsbad, New Mexico.

remove contamination. If, during the visual examination, it is determined that damage to the O–ring seal(s) and/or sealing surface is sufficient to impair containment integrity, replace the damaged seal(s) and/or repair the damaged sealing surface per Section 8.2.3.2.1, *Seal Area Routine Inspection and Repair*.

4. Visually inspect the debris shield foam insert and the eight (8) polyethylene filters for wear or damage that could impair their function and, if necessary, replace or repair per the requirements of the drawings in Appendix 1.3.1, *Packaging General Arrangement Drawings*.
5. As an option, remove and sparingly apply vacuum grease to the O–ring seals and/or sealing surfaces. Reinstall O–ring seals into the appropriate seal grooves in the closure lid and the vent port insert.
6. As an option, apply a silicone lubricant to the debris shield silicone foam insert.
7. If not previously installed, install two (2) M36 lifting rings or eyes into the threaded holes in the top of the closure lid.
8. Remove the sealing surface protectors from the sealing flange of the body.
9. Visually inspect the guide pins and the threaded holes for the closure bolts on the body sealing flange for wear or damage that could impair their function and, if necessary, replace or repair per the requirements of the drawings in Appendix 1.3.1, *Packaging General Arrangement Drawings*.
10. Rig an overhead crane, or equivalent, with an appropriate lift fixture capable of handling the closure lid. Engage the lift fixture and install the closure lid onto the body.
11. Install the forty–four (44) M36 × 205 mm closure bolts (socket head cap screws) through the access tubes in the closure lid to secure the lid to the body. Tighten the closure bolts to 1,480 – 1,720 N–m (1,092 – 1,269 lb_f–ft) torque (lubricated).
12. Remove the lift fixture and the lifting rings or eyes.
13. If not previously installed, install the vent port retaining ring/insert assembly; tighten to 370 – 430 N–m (273 – 317 lb_f–ft) torque.
14. Leakage rate testing of the main containment O–ring seal and the vent port insert O–ring seal shall be performed based on the following criteria:
    a. If the inner main O–ring seal (containment) and/or vent port insert inner O–ring is replaced, or the corresponding sealing surface(s) were repaired, then perform the maintenance/periodic leakage rate test per Section 8.2.2.2, *Helium Leakage Rate Testing the Main Containment O–ring Seal*, or Section 8.2.2.3, *Helium Leakage Rate Testing the Vent Port Insert O–ring Seal* as appropriate.
    b. If there are no changes to the inner main O–ring seal (containment) or the vent port insert inner O–ring, and no repairs made to the corresponding sealing surfaces, then perform preshipment leakage rate testing per Section 7.4, *Preshipment Leakage Rate Test*, or per Section 8.2.2.2, *Helium Leakage Rate Testing the Main Containment O–ring Seal*, or Section 8.2.2.3, *Helium Leakage Rate Testing the Vent Port Insert O–ring Seal* as appropriate.

13. If not previously installed, install the seal test port plug; tighten to 90 – 110 N–m (66 – 81 lb_f–ft) torque.
14. Install the vent port locking ring; tighten to 370 – 430 N–m (273 – 317 lb_f–ft) torque.
15. Install the vent port dust plug; tighten to 90 – 110 N–m (66 – 81 lb_f–ft) torque.

7.1.6 Overpack Cover Installation

1. Visually inspect the M36 attachment bolts (socket head cap screws) for wear or damage that could impair their function and, if necessary, replace or repair per the requirements of the drawings in Appendix 1.3.1, *Packaging General Arrangement Drawings*.
2. If not previously installed, install two (2) M36 lifting rings or eyes into the threaded holes in the top of the overpack cover.
3. Rig an overhead crane, or equivalent, with an appropriate lift fixture capable of handling the overpack cover. Engage the lift fixture and install the overpack cover onto the body.
4. Install ten, M36 × 60 mm attachment bolts (socket head cap screws) in the overpack cover; tighten to 1,480 – 1,720 N–m (1,092 – 1,269 lb_f–ft) torque (lubricated).
5. Remove the lift fixture and lifting rings or eyes, and install bolts or protective covers in the threaded holes.

7.1.7 Final Package Preparations for Transport (Loaded)

1. Install the two tamper–indicating devices (security seals) in the two overpack cover attachment bolt access tubes.
2. If the TRUPACT–III package is not already loaded onto and secured to the transport trailer or railcar, perform the following steps, as appropriate:
   a. Using an overhead crane, or equivalent, with a lift fixture of appropriate size, position the lift fixture on the top of the TRUPACT–III package and engage the ISO corner fittings. If the design of the tie–down frame allows, it may be pre–positioned on top of the TRUPACT–III package prior to positioning the lift fixture.
   b. Lift the loaded TRUPACT–III package, aligning the packaging over the tie–down points on the transport trailer or railcar.
   c. Disengage and remove the lift fixture from the top of the TRUPACT–III package.
   d. If not previously pre–positioned, install the tie–down assembly on top of the TRUPACT–III package. Install covers as/if necessary to disable the ISO fittings for use as a tie–down point.
   e. Secure the loaded TRUPACT–III package to the transport trailer or railcar using straps, tie–rods, or equivalent.

3. Monitor external radiation for each loaded TRUPACT–III package per the guidelines of 49 CFR §173.441[2].
4. Determine that surface contamination levels for each loaded TRUPACT–III package is per the guidelines of 49 CFR §173.443.
5. Determine the transport index for each loaded TRUPACT–III package per the guidelines of 49 CFR §173.403.
6. Complete all necessary shipping papers in accordance with Subpart C of 49 CFR 172[3].
7. TRUPACT–III package marking shall be in accordance with 10 CFR §71.85(c)[4] and Subpart D of 49 CFR 172. Package labeling shall be in accordance with Subpart E of 49 CFR 172. Package placarding shall be in accordance with Subpart F of 49 CFR 172.

[2] Title 49, Code of Federal Regulations, Part 173 (49 CFR 173), *Shippers–General Requirements for Shipments and Packagings*, 10–01–09 Edition.

[3] Title 49, Code of Federal Regulations, Part 172 (49 CFR 172), *Hazardous Materials Tables and Hazardous Communications Regulations*, 10–01–09 Edition.

[4] Title 10, Code of Federal Regulations, Part 71 (10 CFR 71), *Packaging and Transportation of Radioactive Material*, 01–01–09 Edition.

This page intentionally left blank.

7.2 Procedures for Unloading the Package

This section delineates the procedures for unloading a payload from the TRUPACT–III packaging. Hereafter, reference to specific TRUPACT–III packaging components may be found in Appendix 1.3.1, *Packaging General Arrangement Drawings.*

The unloading operation shall be performed in a dry environment. In the event of precipitation during outdoor unloading operations, precautions, such as covering the payload cavity shall be implemented to prevent water or precipitation from entering the cavity. If precipitation enters the cavity, the free–standing water shall be removed prior to installing the closure lid.

If the TRUPACT–III package will be unloaded while on the transport trailer or railcar, proceed directly to Section 7.2.2, *Overpack Cover Removal.*

7.2.1 Removal of the TRUPACT–III Package from the Transport Trailer/Railcar

1. Remove any devices covering the four (4) ISO fittings located at the upper corners of the body as necessary to allow engagement of a lifting device with the ISO fittings.
2. Disengage the straps, tie–rods, or equivalent on the transport trailer or railcar, and if necessary or desired, remove the tie–down assembly from the package.

   CAUTION: Failure to disengage the straps or tie–rods may cause damage to the packaging and/or transport trailer/railcar.
3. Rig an overhead crane, or equivalent, with an appropriate lift fixture capable of handling the TRUPACT–III package.
4. Lower the lift fixture onto the package and engage each ISO corner fitting.
5. Lift the package from the transport trailer or railcar and move the package to the unloading station.
6. Place the package in the unloading station, disengage from the four (4) ISO corner fittings, and remove the lift fixture.

7.2.2 Overpack Cover Removal

1. Open the two (2) M36 threaded holes in the top of the overpack cover.
2. Install two (2) M36 lifting rings or eyes into the threaded holes in the top of the overpack cover.
3. Rig an overhead crane, or equivalent, with an appropriate lift fixture capable of handling the overpack cover. Lower the lift fixture onto the overpack cover.
4. Remove the two (2) tamper indicating seals, and then the ten (10) M36 attachment bolts (socket head cap screws) from the overpack cover.
5. Raise the lift fixture and remove the overpack cover from the body. Store the overpack cover vertically to minimize potential damage.

7.2.3 Closure Lid Removal

1. Remove the vent port locking ring and vent port dust plug. Open the vent port to allow the payload cavity to vent to atmosphere.
2. Install two (2) M36 lifting rings or eyes into the threaded holes in the top of the closure lid. Rig an overhead crane, or equivalent, with an appropriate lift fixture capable of handling the closure lid.
3. Remove the forty–four (44) M36 closure bolts (socket head cap screws) from the closure lid.
4. Engage the lift fixture and remove the closure lid from the body. If necessary, separate the closure lid from the body using the four special M36 jacking threaded holes. Store the closure lid in a manner such that potential damage to the closure lid's sealing surface is minimized.

7.2.4 Unloading the Payload from the TRUPACT–III Package

1. Install sealing surface protectors to the sealing flange of the body.
2. Connect an appropriate moving device to the payload pallet.
3. Remove the loaded payload pallet from the payload cavity.

7.2.5 Closure Lid Installation

1. Visually inspect the closure bolts for wear or damage that could impair their function and, if necessary, replace or repair per the requirements of the drawings in Appendix 1.3.1, *Packaging General Arrangement Drawings.*
2. Visually inspect both closure lid main O–ring seals. If necessary, remove the O–ring seal(s) and clean the seal(s) and the sealing surface(s) on the closure lid and body to remove contamination. If, during the visual examination, it is determined that damage to the O–ring seal(s) and/or sealing surface(s) is sufficient to impair containment integrity, replace the damaged seal(s) and/or repair the damaged sealing surface(s) per Section 8.2.3.2.1, *Seal Area Routine Inspection and Repair.*
3. Visually inspect the O–ring seals on the vent port insert. If necessary, remove the O–ring seals, and clean the seals and sealing surfaces on the vent port insert and in the vent port to remove contamination. If, during the visual examination, it is determined that damage to the O–ring seal(s) and/or sealing surface is sufficient to impair containment integrity, replace the damaged seal(s) and/or repair the damaged sealing surface per Section 8.2.3.2.1, *Seal Area Routine Inspection and Repair.*
4. Visually inspect the debris shield foam insert and the eight polyethylene filters for wear or damage that could impair their function and, if necessary, replace or repair per the requirements of the drawings in Appendix 1.3.1, *Packaging General Arrangement Drawings.*
5. As an option, remove and sparingly apply vacuum grease to the O–ring seals and/or sealing surfaces. Reinstall O–ring seals into the appropriate seal grooves in the closure lid and the vent port insert.
6. As an option, apply a silicone lubricant to the debris shield silicone foam insert.

7. If not previously installed, install two (2) M36 lifting rings or eyes into the threaded holes in the top of the closure lid.
8. Remove the sealing surface protectors from the sealing flange of the body.
9. Visually inspect the guide pins and the threaded holes for the closure bolts on the body sealing flange for wear or damage that could impair their function and, if necessary, replace or repair per the requirements of the drawings in Appendix 1.3.1, *Packaging General Arrangement Drawings.*
10. Rig an overhead crane, or equivalent, with an appropriate lift fixture capable of handling the closure lid. Engage the lift fixture and install the closure lid onto the body.
11. Install the forty–four (44) M36 × 205 mm closure bolts (socket head cap screws) through the access tubes in the closure lid to secure the lid to the body. Tighten the closure bolts to at least 800 N–m [590 lb_f–ft], but no more than 1,480 – 1,720 N–m [1,092 – 1,269 lb_f–ft] torque (lubricated).
12. If not previously installed, install the vent port retaining ring/insert assembly; tighten to 370 – 430 N–m (273 – 317 lb_f–ft) torque.
13. Install the vent port locking ring; tighten to 370 – 430 N–m (273 – 317 lb_f–ft) torque.
14. Install the vent port dust plug; tighten to 90 – 110 N–m (66 – 81 lb_f–ft) torque.
15. Remove the lift fixture and two (2) M36 lifting rings or eyes from the threaded holes in the top of the closure lid.

7.2.6 Overpack Cover Installation

1. Visually inspect the M36 attachment bolts (socket head cap screws) for wear or damage that could impair their function and, if necessary, replace or repair per the requirements of the drawings in Appendix 1.3.1, *Packaging General Arrangement Drawings.*
2. If not previously installed, install two (2) M36 lifting rings or rings or eyes into the threaded holes in the top of the overpack cover.
3. Rig an overhead crane, or equivalent, with an appropriate lift fixture capable of handling the overpack cover. Engage the lift fixture and install the overpack cover onto the body.
4. Install ten, M36 × 60 mm attachment bolts (socket head cap screws) in the overpack cover; tighten to at least 800 N–m [590 lb_f–ft], but no more than 1,480 – 1,720 N–m [1,092 – 1,269 lb_f–ft] torque (lubricated).
5. Remove the lift fixture and lifting rings or eyes, and install bolts or protective covers in the threaded holes.

7.2.7 Final Package Preparations for Transport (Unloaded)

1. If the TRUPACT–III packaging is not already loaded onto and secured to the transport trailer or railcar, perform the following steps, as appropriate:
   a. Using an overhead crane, or equivalent, with a lift fixture of appropriate size, position the lift fixture on the top of the TRUPACT–III packaging and engage the ISO corner fittings.

If the design of the tie–down frame allows, it may be pre–positioned on top of the TRUPACT–III packaging prior to positioning the lift fixture.

b. Lift the TRUPACT–III packaging, aligning the packaging over the tie–down points on the transport trailer or railcar.

c. Disengage and remove the lift fixture from the top of the TRUPACT–III packaging.

d. If not previously pre–positioned, install the tie–down assembly on top of the TRUPACT–III packaging. Install covers as/if necessary to disable the ISO fittings for use as a tie–down point.

e. Secure the TRUPACT–III packaging to the transport trailer or railcar using straps, tie–rods, or equivalent.

2. Transport the TRUPACT–III packaging in accordance with Section 7.3, *Preparation of an Empty Package for Transport.*

7.3 Preparation of an Empty Package for Transport

Previously used and empty TRUPACT–III packagings shall be prepared and transported per the requirements of 49 CFR §173.428[1].

[1] Title 49, Code of Federal Regulations, Part 173 (49 CFR 173), *Shippers–General Requirements for Shipments and Packagings*, 10–01–09 Edition.

This page intentionally left blank.

7.4 Preshipment Leakage Rate Test

After the TRUPACT–III package is assembled and prior to shipment, leakage rate testing shall be performed to confirm proper assembly of the package following the guidelines of Section 7.6, *Preshipment Leakage Rate Test*, and Appendix A.5.2, *Gas Pressure Rise*, of ANSI N14.5[1].

7.4.1 Gas Pressure Rise Leakage Rate Test Acceptance Criteria

In order to demonstrate containment integrity in preparation for shipment, no leakage shall be detected when tested to a sensitivity of 1×10^{-4} reference Pascals – cubic meters per second (ref–Pa–m^3/s) [1×10^{-3} reference cubic centimeters per second (ref–cm^3/s)] air, or less, per Section 7.6, *Preshipment Leakage Rate Test*, of ANSI N14.5.

7.4.2 Determining the Test Volume and Test Time

1. Assemble a leakage rate test apparatus that consists of, at a minimum, the components illustrated in Figure 7.4–1, using a calibrated volume with a range of 100 – 500 cubic centimeters (6 – 31 cubic inches), and a calibrated pressure transducer with a minimum sensitivity of 0.013 kPa (100 millitorr). Connect the test apparatus to the test volume (i.e., the seal test port, or vent port insert, as appropriate).
2. Set the indicated sensitivity on the digital readout of the calibrated pressure transducer, ΔP, to, at a minimum, the resolution (i.e., sensitivity) of the calibrated pressure transducer (e.g., ΔP = 0.00013, 0.0013, or 0.013 kPa [1, 10, or 100 millitorr] sensitivity).
3. Open all valves (i.e., the vent valve, calibration valve, and vacuum pump isolation valve), and record ambient atmospheric pressure, P_{atm}.
4. Isolate the calibrated volume by closing the vent and calibration valves.
5. Evacuate the test volume to a pressure less than the indicated sensitivity on the digital readout of the calibrated pressure transducer or 0.10 kPa [0.76 torr], whichever is less.
6. Isolate the vacuum pump from the test volume by closing the vacuum pump isolation valve. Allow the test volume pressure to stabilize and record the test volume pressure, P_{test} (e.g., $P_{test} < 0.00013$ kPa [1 millitorr] for an indicated sensitivity of 0.00013 kPa [1 millitorr]).
7. Open the calibration valve and, after allowing the system to stabilize, record the total volume pressure, P_{total}.
8. Knowing the calibrated volume, V_c, calculate and record the test volume, V_t, using the following equation:

$$V_t = V_c\left(\frac{P_{atm} - P_{total}}{P_{total} - P_{test}}\right)$$

[1] ANSI N14.5–1997 (or later), *American National Standard for Radioactive Materials – Leakage Tests on Packages for Shipment,* American National Standards Institute, Inc. (ANSI).

9. Knowing the indicated sensitivity on the digital readout of the calibrated pressure transducer, ΔP, calculate and record the test time, t, using the following equation:

$$t = \Delta P(1.32)V_t$$

7.4.3 Performing the Gas Pressure Rise Leakage Rate Test

1. Isolate the calibrated volume by closing the calibration valve.
2. Open the vacuum pump isolation valve and evacuate the test volume to a pressure less than the test volume pressure, P_{test}, determined in Step 6 of Section 7.4.2, *Determining the Test Volume and Test Time*.
3. Isolate the vacuum pump from the test volume by closing the vacuum pump isolation valve. Allow the test volume pressure to stabilize and record the beginning test pressure, P_1. After a period of time equal to "t" seconds, determined in Step 9 of Section 7.4.2, *Determining the Test Volume and Test Time*, record the ending test pressure, P_2. To be acceptable, there shall be no difference between the final and initial pressures such that the requirements of Section 7.4.1, *Gas Pressure Rise Leakage Rate Test Acceptance Criteria*, are met.
4. If, after repeated attempts, the O–ring seal fails to pass the leakage rate test, replace the damaged seal and/or repair the damaged sealing surfaces per Section 8.2.3.2.1, *Seal Area Routine Inspection and Repair*. Perform verification leakage rate test per the applicable procedure delineated in Section 8.2.2, *Maintenance/Periodic Leakage Rate Tests*.

7.4.4 Optional Preshipment Leakage Rate Test

As an option to Section 7.4.3, *Performing the Gas Pressure Rise Leakage Rate Test*, Section 8.2.2, *Maintenance/Periodic Leakage Rate Tests*, may be performed.

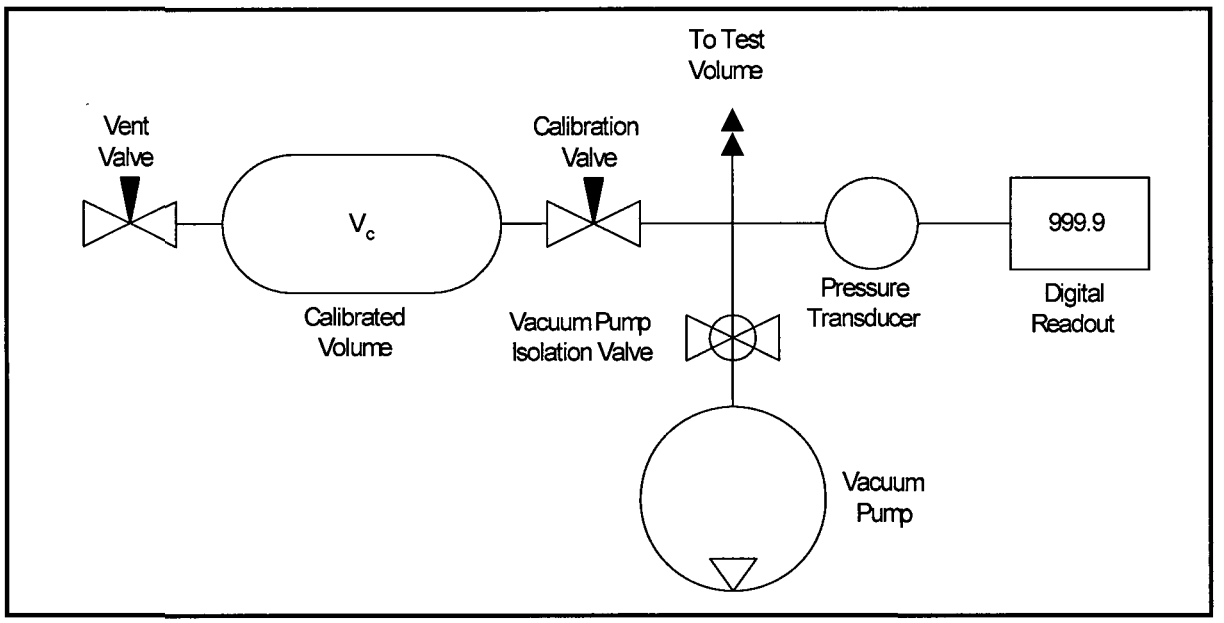

Figure 7.4-1 – Pressure Rise Leakage Rate Test Schematic

8.0 ACCEPTANCE TESTS AND MAINTENANCE PROGRAM

8.1 Acceptance Tests

Per the requirements of 10 CFR §71.85[1], this section discusses the inspections and tests to be performed prior to first use of the TRUPACT–III packaging. Acceptance criteria for all inspections and tests are found either on the drawings in Appendix 1.3.1, *Packaging General Arrangement Drawings,* or in the sections that follow. Deviations from requirements will be recorded and dispositioned in accordance with the cognizant quality assurance program.

8.1.1 Visual Inspections and Measurements

Each TRUPACT–III will be visually inspected and measured to ensure that all of the requirements delineated on the drawings in Appendix 1.3.1, *Packaging General Arrangement Drawings*, including but not limited to such items as materials, physical arrangement of components, quantities, dimensions, welds, and measurements, are satisfied.

8.1.2 Weld Examinations

The locations, types, and sizes of all welds will be identified and recorded to ensure compliance with the drawings in Appendix 1.3.1, *Packaging General Arrangement Drawings*. All welds in each TRUPACT–III packaging will be visually examined. With the exception of seal and specific non–structural welds, all welds will be liquid penetrant examined. In addition, all welds in the containment boundary will be radiograph examined. The type of inspection techniques and the acceptance criteria specific to each weld are identified on the drawings. Visual examination is performed according to AWS Specification D1.6[2]. Liquid penetrant and radiograph examinations are performed according to the relevant sections of the ASME code, as specified for each weld on the drawings.

8.1.3 Structural and Pressure Tests

8.1.3.1 Lifting Device Load Testing

From Section 2.1.3, *Weights and Center of Gravity*, the maximum weight of the TRUPACT–III is 25,000 kilograms (55,116 pounds). Each upper ISO corner fitting is designed to carry approximately 59% of the maximum lifted load, or 14,650 kg (32,298 lb). Each ISO corner fitting shall be load tested to 150% of the maximum working load, or at least 21,975 kg (48,447 lb), per ANSI N14.6[3].

Following load testing of the ISO corner fittings, all welds and adjacent base metal (minimum 13 mm [0.5 in.] on each side of the weld) directly related to the load testing of the fitting shall be visually

---

[1] Title 10, Code of Federal Regulations, Part 71 (10 CFR 71), *Packaging and Transportation of Radioactive Material*, 01–01–09 Edition.

[2] ANSI/AWS D1.6:1999, *Structural Welding Code – Stainless Steel*, American Welding Society (AWS).

[3] ANSI N14.6–1993, *American National Standard for Radioactive Materials – Special Lifting Devices for Shipping Containers Weighing 10,000 Pounds (4,500 kg) or More*, American National Standard Institute, Inc. (ANSI).

inspected for plastic deformation or cracking in accordance with AWS D1.6, and liquid penetrant inspected per ASME B & PV Code, Section III[4], Division 1, Subsection NF, Article NF–5000, and Section V[5], Article 6, as delineated on the drawings in Appendix 1.3.1, *Packaging General Arrangement Drawings*. Indications of cracking or distortion shall be recorded and evaluated in accordance with the cognizant quality assurance program.

8.1.3.2 Containment Vessel Pressure Testing

Per the requirements of 10 CFR §71.85(b), the containment structural assembly (CSA) shall be pressure tested to 150% of the maximum normal operating pressure (MNOP) to verify structural integrity. The MNOP of the TRUPACT–III package is equal to 172 kPa (25 psig). Thus, the CSA shall be pressure tested to at least 172 × 1.5 = 258 kPa (37.5 psig).

Following pressure testing of the CSA, accessible base material and welds directly related to the pressure testing of the containment boundary sheets of the CSA shall be visually inspected for plastic deformation or cracking in accordance with AWS D.1.6, and liquid penetrant inspected per ASME B & PV Code, Section III, Division 1, Subsection NB, Article NB–5000, and Section V, Article 6, as delineated on the drawings in Appendix 1.3.1, *Packaging General Arrangement Drawings*. Indications of cracking or distortion shall be recorded and evaluated in accordance with the cognizant quality assurance program.

Leakage rate testing per Section 8.1.4, *Fabrication Leakage Rate Tests*, shall be performed after completion of pressure testing to verify package configuration and performance to design criteria.

8.1.4 Fabrication Leakage Rate Tests

This section provides the generalized procedure for fabrication leakage rate testing of the containment vessel boundaries and penetrations following the completion of fabrication. Fabrication leakage rate testing shall follow the guidelines of Section 7.3, *Fabrication Leakage Rate Test*, of ANSI N14.5[6].

Prior to leakage rate testing, internal components that are not permanently affixed to the containment plate, such as the payload, roller floor, and payload pallet, shall be removed. For ease of leakage rate testing, the interior surfaces of the CSA should be thoroughly cleaned. As an option, the debris shield insert may be omitted from the assembly for fabrication leakage rate tests.

Fabrication leakage rate testing shall be performed on the CSA. Three separate tests comprise the series. Each test shall meet the acceptance criteria delineated in Section 8.1.4.1, *Fabrication Leakage Rate Test Acceptance Criteria*.

---

[4] American Society of Mechanical Engineers (ASME) Boiler and Pressure Vessel Code, Section III, *Rules for Construction of Nuclear Power Plant Components*, 2004 Edition, 2005 and 2006 Addenda.

[5] American Society of Mechanical Engineers (ASME) Boiler and Pressure Vessel Code, Section V, *Nondestructive Examination*, 2004 Edition, 2005 and 2006 Addenda.

[6] ANSI N14.5–1997 (or later), *American National Standard for Radioactive Materials – Leakage Tests on Packages for Shipment*, American National Standards Institute, Inc. (ANSI).

8.1.4.1 Fabrication Leakage Rate Test Acceptance Criteria

1. To be acceptable, each leakage rate test shall demonstrate a leakage rate of 1×10^{-8} reference Pascals – cubic meter per second (Pa–m^3/s) [1×10^{-7} ref cm^3/s], air, or less, per Section 6.3, *Application of Referenced Air Leakage Rate (L_R)*, of ANSI N14.5.
2. In order to adequately demonstrate this leakage rate, the sensitivity of the leakage rate test procedure shall be 5×10^{-9} Pa–m^3/s (5×10^{-8} cm^3/s), air, or less, per Section 8.4, *Sensitivity*, of ANSI N14.5.
3. Failure to meet the stated leakage rate shall be recorded and evaluated in accordance with the cognizant quality assurance program.

8.1.4.2 Helium Leakage Rate Testing the Containment Structure Integrity

1. The fabrication leakage rate test of the containment structure shall be performed following the guidelines of Section A.5.3, *Gas Filled Envelope – Gas Detector*, of ANSI N14.5.
2. Remove the body helium fill access plugs (inner and outer) in the closure lid and the body helium fill port plug in the body.
3. The CSA shall be assembled with both main O–ring seals installed into the closure lid, and the O–ring identified for the B1 groove installed in the closure lid. Tighten the closure bolts to 1,480 – 1,720 N–m (1,092 – 1,269 lb_f–ft) torque as shown in Appendix 1.3.1, *Packaging General Arrangement Drawings.*
4. Remove the vent port locking ring, and back–off or remove the vent port retaining ring and vent port insert. Install an adapter to the vent port to allow gas flow to and from the cavity.
5. Install a helium mass spectrometer leak detector to the adapter on the vent port. Evacuate the payload cavity through the vent port until the vacuum is sufficient to operate the helium mass spectrometer leak detector.
6. Connect a vacuum pump to the outer body helium fill access port in the closure lid and evacuate the annulus (defined as the space within the sandwich construction of the CSA body and lid walls) to 90% vacuum or better (i.e., ≤10% ambient atmospheric pressure).
7. Provide a helium atmosphere inside the annulus by backfilling with helium gas to a pressure slightly greater than atmospheric pressure, i.e., +7, -0 kPa (+1, -0 psig).
8. Perform the helium leakage rate test to the requirements of Section 8.1.4.1, *Fabrication Leakage Rate Test Acceptance Criteria.* If, after repeated attempts, the CSA structure fails to pass the leakage rate test, isolate the leak path and, prior to repairing the leak path and repeating the leakage rate test, record on a nonconformance report and disposition prior to final acceptance in accordance with the governing quality assurance program.

8.1.4.3 Helium Leakage Rate Testing the Main Containment O–ring Seal

1. The fabrication leakage rate test of the main containment O–ring seal (inner) shall be performed following the guidelines of Section A.5.4, *Evacuated Envelope – Gas Detector*, of ANSI N14.5.
2. The CSA shall be assembled with both main O–ring seals installed into the closure lid. If not previously tightened, tighten the closure bolts to 1,480 – 1,720 N–m (1,092 – 1,269 lb_f–ft) torque as shown in Appendix 1.3.1, *Packaging General Arrangement Drawings*.
3. Remove the vent port locking ring, and back–off or remove the vent port retaining ring and vent port insert. Install an adapter to the vent port to allow gas flow to and from the cavity.
4. Connect a vacuum pump to the adapter on the vent port, and evacuate the payload cavity to 90% vacuum or better (i.e., ≤10% ambient atmospheric pressure).
5. Remove the seal test port plug in the closure lid. Install an adapter to the seal test port.
6. Install a helium mass spectrometer leak detector to the adapter on the seal test port. Evacuate through the seal test port until the vacuum is sufficient to operate the helium mass spectrometer leak detector.
7. Provide a helium atmosphere inside the payload cavity by backfilling with helium gas to a pressure slightly greater than atmospheric pressure, i.e., +7, -0 kPa (+1, -0 psig).
8. Perform the helium leakage rate test to the requirements of Section 8.1.4.1, *Fabrication Leakage Rate Test Acceptance Criteria*. If, after repeated attempts, the main containment O–ring seal fails to pass the leakage rate test, isolate the leak path and, prior to repairing the leak path and repeating the leakage rate test, record on a nonconformance report and disposition prior to final acceptance in accordance with the governing quality assurance program.

8.1.4.4 Helium Leakage Rate Testing the Vent Port Insert O–ring Seal

1. The fabrication leakage rate test of the vent port insert O–ring seal shall be performed following the guidelines of Section A.5.4, *Evacuated Envelope – Gas Detector*, of ANSI N14.5.
2. The closure lid shall be assembled with both main O–ring seals installed into the vent port insert. Assembly is as shown in Appendix 1.3.1, *Packaging General Arrangement Drawings*.
3. Remove the vent port locking ring and vent port dust plug. Ensure that the vent port retaining ring is tightened to 370 – 430 N–m (273 – 317 lb_f–ft) torque.
4. Install an adapter to the internal threads of the vent port insert.
5. Install a helium mass spectrometer leak detector to the adapter on the vent port. Evacuate through the vent port until the vacuum is sufficient to operate the helium mass spectrometer leak detector.
6. Install an evacuation envelope over the ∅50–mm vent port on the inside surface of the closure lid. If desired, the TRUPACT–III body may be utilized as the envelope.
7. Connect a vacuum pump to the evacuation envelope and evacuate the envelope to 90% vacuum or better (i.e., ≤10% ambient atmospheric pressure).
8. Provide a helium atmosphere inside the evacuation envelope by backfilling with helium gas to a pressure slightly greater than atmospheric pressure, i.e., +7, -0 kPa (+1, -0 psig).

9. Perform the helium leakage rate test to the requirements of Section 8.1.4.1, *Fabrication Leakage Rate Test Acceptance Criteria.* If, after repeated attempts, the vent port insert O–ring seal fails to pass the leakage rate test, isolate the leak path and, prior to repairing the leak path and repeating the leakage rate test, record on a nonconformance report and disposition prior to final acceptance in accordance with the governing quality assurance program.

8.1.5 Component Tests

8.1.5.1 Polyurethane Foam

This section establishes the requirements and acceptance criteria for installation, inspection, and testing of the rigid, closed–cell, polyurethane foam utilized within the TRUPACT–III packaging.

8.1.5.1.1 Introduction and General Requirements

The polyurethane foam used within the TRUPACT–III packaging is comprised of a specific "formulation" of foam constituents that, when properly apportioned, mixed, and reacted, produce a polyurethane foam material with physical characteristics consistent with the requirements given in this section. In practice, the chemical constituents are batched into multiple parts (e.g., parts A and B) for later mixing in accordance with a formulation. Therefore, a foam "batch" is considered to be a specific grouping and apportionment of chemical constituents into separate and controlled vats or bins for each foam formulation part. Portions from each batch part are combined in accordance with the foam formulation requirements to produce the liquid foam material for pouring into a component or box. Thus, a foam "pour" is defined as apportioning and mixing the batch parts into a desired quantity for subsequent installation (pouring). Finally, all contiguous pours into a single mold are termed a "bun".

The following sections describe the general requirements for constituent storage, and foam pour and test data records.

8.1.5.1.1.1 Polyurethane Foam Constituent Storage

The foam supplier shall certify that the polyurethane foam constituents have been properly stored prior to use, and that the polyurethane foam constituents have been used within their shelf life.

8.1.5.1.1.2 Polyurethane Foam Pour and Test Data Records

A production pour and testing record shall be compiled by the foam supplier during the foam pouring operation and subsequent physical testing. Upon completion of production and testing, the foam supplier shall issue a certification referencing the production record data and test data pertaining to each foamed component. At a minimum, relevant pour and test data shall include:

- formulation, batch, and pour numbers, with foam material traceability, and pour date,
- instrumentation description, serial number, and calibration due date,
- pour and test data (e.g., date, temperature, dimensional, and/or weight measurements, compressive stress, etc., as applicable), and
- technician and Quality Assurance/Quality Control (QA/QC) sign–off.

8.1.5.1.2 Physical Characteristics

The following subsections define the required physical characteristics of the polyurethane foam material used for the TRUPACT–III packaging design.

Testing for the various polyurethane foam physical characteristics is based on a "formulation", "batch", or "pour", as appropriate, as defined in Section 8.1.5.1.1, *Introduction and General Requirements*. The physical characteristics determined for a specific foam formulation are relatively insensitive to small variations in chemical constituents and/or environmental conditions, and therefore include physical testing only for leachable chlorides, thermal conductivity, and specific heat. Similarly, the physical characteristics determined for a batch are only slightly sensitive to small changes in formulation and/or environmental conditions during batch mixing, and therefore include physical testing only for flame retardancy. Finally, the physical characteristics determined for a pour are also only slightly sensitive to small changes in formulation and slightly more sensitive to variations in environmental conditions during pour mixing, and therefore include physical testing for density and compressive stress.

8.1.5.1.2.1 Physical Characteristics Determined for a Foam Formulation

8.1.5.1.2.1.1 Leachable Chlorides

Polyurethane foam material physical characteristic for leachable chlorides shall be determined once for a particular foam formulation. If multiple components are to utilize a specific foam formulation, then additional physical testing, as defined below, need not be performed.

1. The leachable chlorides test shall be performed using an ion chromatograph (IC) apparatus. The IC measures inorganic anions of interest (i.e., chlorides) in water. Description of a typical IC is provided in EPA Method 300.0[7]. The IC shall be calibrated against a traceable reference specimen per the IC manufacturer's operating instructions.
2. One test sample shall be taken from a pour for each foam formulation. The test sample shall be a cube with dimensions of 50 ±1 mm (2.00 ±0.03 in).
3. Place the test sample in a room (ambient) temperature environment (i.e., 20 °C to 30 °C [68 °F to 86 °F]) for sufficient time to thermally stabilize the test sample. Measure and record the room temperature to an accuracy of ±1 °C (±2 °F).
4. Obtain a minimum of 550 ml of distilled or de–ionized water for testing. The test water shall be from a single source to ensure consistent anionic properties for testing control.
5. Obtain a 400 ml, or larger, contaminant free container that is capable of being sealed. Fill the container with 250 ±3 ml of test water. Fully immerse the test sample inside the container for a duration of 72 ±3 hours. If necessary, use an inert standoff to ensure the test sample is completely immersed for the full test duration. Seal the container prior to the 72–hour duration.
6. Obtain a second, identical container to use as a "control". Fill the control container with 250 ±3 ml of the same test water. Seal the control container prior to the 72–hour duration.

[7] EPA Method 300.0, Revision 2.2 (October 1999), *Determination of Inorganic Anions by Ion Chromatography*, U.S. Environmental Protection Agency.

7. At the end of the test period, measure and record the leachable chlorides in the test water per the IC manufacturer's operating instructions. The leachable chlorides in the test water shall not exceed one part per million (1 ppm).
8. Should leachable chlorides in the test water exceed 1 ppm, measure and record the leachable chlorides in the test water from the "control" container. The difference in leachable chlorides from the test water and "control" water sample shall not exceed 1 ppm.

8.1.5.1.2.1.2 Thermal Conductivity

1. The thermal conductivity test shall be performed using a heat flow meter (HFM) apparatus. The HFM establishes steady state unidirectional heat flux through a test specimen between two parallel plates at constant but different temperatures. By measurement of the plate temperatures and plate separation, Fourier's law of heat conduction is used by the HFM to automatically calculate thermal conductivity. Description of a typical HFM test method is provided in ASTM C518[8]. The HFM shall be calibrated against a traceable reference specimen per the HFM manufacturer's operating instructions.
2. Three test samples shall be taken from the sample pour. Each test sample shall be of sufficient size to enable testing per the HFM manufacturer's operating instructions.
3. Place the test samples in a room (ambient) temperature environment (i.e., 20 °C to 30 °C [68 °F to 86 °F]) for sufficient time to thermally stabilize the test samples.
4. Measure and record the necessary test sample parameters as input data to the HFM apparatus per the HFM manufacturer's operating instructions.
5. Perform thermal conductivity testing and record the measured thermal conductivity for each test sample following the HFM manufacturer's operating instructions.
6. Determine and record the average thermal conductivity of the three test samples. The numerically averaged thermal conductivity of the three test samples shall lie within the ranges shown by Table 8.1–1.

8.1.5.1.2.1.3 Specific Heat

1. The specific heat test shall be performed using a differential scanning calorimeter (DSC) apparatus. The DSC establishes a constant heating rate and measures the differential heat flow into both a test specimen and a reference specimen. The DSC shall be calibrated against a traceable reference specimen per the DSC manufacturer's operating instructions.
2. Three test samples shall be taken from the sample pour. Each test sample shall be of sufficient size to enable testing per the DSC manufacturer's operating instructions.
3. Place the test samples in a room (ambient) temperature environment (i.e., 20 °C to 30 °C [68 °F to 86 °F]) for sufficient time to thermally stabilize the test samples.

[8] ASTM C518–04, *Standard Test Method for Steady–State Thermal Transmission Properties by Means of the Heat Flow Meter Apparatus*, American Society for Testing and Materials (ASTM).

4. Measure and record the necessary test sample parameters as input data to the DSC per the DSC manufacturer's operating instructions.
5. Perform specific heat testing and record the measured specific heat for each test sample following the DSC manufacturer's operating instructions.
6. Determine and record the average specific heat of the three test specimens. The numerically averaged specific heat of the three test samples shall be within the range between 1.12 and 1.86 J/g–°C (0.27 and 0.44 Btu/lb–°F).

8.1.5.1.2.2 Physical Characteristics Determined for a Foam Batch

Polyurethane foam material physical characteristics for flame retardancy shall be determined once for a particular foam batch based on the batch definition in Section 8.1.5.1.1, *Introduction and General Requirements*. If single or multiple components are to utilize a single foam batch, then additional flame retardancy testing, as defined below, need not be performed for each foam pour.

Polyurethane foam shall be tested for flame retardancy as follows:

1. Three test samples shall be taken from a pour from each foam batch. Each test sample shall be a rectangular prism with nominal dimensions of 13 mm (0.5 in) thick, 75 mm (3.0 in) wide, and a minimum length of 178 mm (7.0 in). In addition, individual sample lengths must not be less than the total burn length observed for the sample when tested.
2. Place the test samples in a room (ambient) temperature environment (i.e., 20 °C to 30 °C [68 °F to 86 °F]) for sufficient time to thermally stabilize the test samples. Measure and record the room temperature to an accuracy of ±1 °C (±2 °F).
3. Measure and record the length of each test sample to an accuracy of ±3 mm (±0.1 in).
4. Install an approximately 10–mm [3/8 in], or larger, Bunsen or Tirrill burner inside an enclosure of sufficient size to perform flame retardancy testing. Adjust the burner flame height to 38 ±5 mm (1½ ±1/8 in). Verify that the burner flame temperature is 850 °C (1,562 °F), minimum.
5. Support the test sample with the long axis oriented vertically within the enclosure such that the test sample's bottom edge will be 19 ±2 mm (3/4 ±1/16 in, see adjacent figure) above the top edge of the burner.

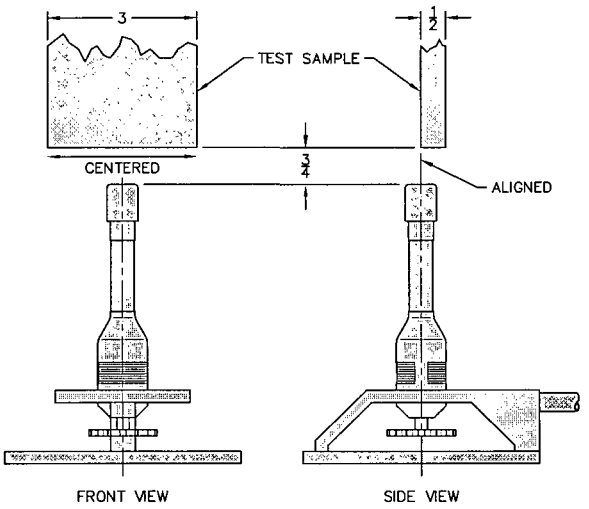

6. Move the burner flame under the test sample for an elapsed time of 60 ±3 seconds. As illustrated, align the burner flame with the front edge of the test sample thickness and the center of the test sample width.
7. Immediately after removal of the test sample from the burner flame, measure and record the following data:

a. Measure and record, to the nearest second, the elapsed time until flames from the test sample extinguish.

b. Measure and record, to the nearest second, the elapsed time from the occurrence of drips, if any, until drips from the test sample extinguish.

c. Measure and record, to the nearest 3 mm, the burn length following cessation of all visible burning and smoking.

8. Flame retardancy testing acceptance is based on the following criteria:

a. The numerically averaged flame extinguishment time of the three test samples shall not exceed fifteen seconds.

b. The numerically averaged flame extinguishment time of drips from the three test samples shall not exceed three seconds.

c. The numerically averaged burn length of the three test samples shall not exceed 150 mm (6.0 in).

8.1.5.1.2.3 Physical Characteristics Determined for a Foam Pour

8.1.5.1.2.3.1 Density

Polyurethane foam material physical characteristic for density shall be determined for each foam pour based on the pour definition in Section 8.1.5.1.1, *Introduction and General Requirements.*

1. Three test samples shall be taken from the foam pour. Each test sample shall be a rectangular prism with minimum nominal dimensions of 25 mm (1.0 in) thick (T) × 25 mm (1.0 in) wide (W) × 25 mm (1.0 in) long (L).
2. Place the test samples in a room (ambient) temperature environment (i.e., 20 °C to 30 °C [68 °F to 86 °F]) for sufficient time to thermally stabilize the test samples. Measure and record the room temperature to an accuracy of ±1 °C (±2 °F).
3. Measure and record the weight of each test sample to an accuracy of ±1 gram (±0.03 oz).
4. Measure and record the thickness, width, and length of each test sample to an accuracy of ±0.04 mm (±0.002 in).
5. Determine and record the room temperature density of each test sample utilizing the following formula:

$$\rho_{foam} = \frac{\text{Weight, g}}{\text{T} \times \text{W} \times \text{L, mm}^3} \times \frac{10^6 \text{ mm}^3/\text{dm}^3}{10^3 \text{ g/kg}}, \text{ kg/dm}^3$$

6. Determine and record the average density of the three test samples. The numerically averaged density of the three test samples shall be within ±15% of the specified nominal foam density.

8.1.5.1.2.3.2 Compressive Stress

1. Three test samples shall be taken from each foam pour. Each test sample shall be a rectangular prism with minimum nominal dimensions of 25 mm (1.0 in) thick (T) × 25 mm (1.0 in) wide (W) × 25 mm (1.0 in) long (L). The thickness dimension shall be the parallel–to–rise direction (for the perpendicular–to–rise direction, see below).
2. Place the test samples in a room (ambient) temperature environment (i.e., 20 °C to 30 °C [68 °F to 86 °F]) for sufficient time to thermally stabilize the test samples. Measure and record the room temperature to an accuracy of ±1 °C (±2 °F).
3. Measure and record the thickness, width, and length of each test sample to an accuracy of ±0.04 mm (±0.002 in).
4. Compute and record the surface area of each test sample by multiplying the width by the length (i.e., W × L).
5. Place a test sample in a Universal Testing Machine. Lower the machine's crosshead until it touches the test sample. Set the machine's parameters for the thickness of the test sample.
6. Determine and record the average parallel–to–rise compressive stress of the three test samples from each batch pour for each foam density. As shown in Table 8.1-2, the average parallel–to–rise compressive stress for each foam pour shall be the nominal compressive stress ±15% at strains of 10%, 40%, and 70% (60% for 0.48 kg/dm^3 [30 lb/ft^3] foam).
7. Determine and record the average parallel–to–rise compressive stress of all test samples from each foamed component. As shown in Table 8.1-2, the average parallel–to–rise compressive stress for all foam pours used in a single bun shall be the nominal compressive stress ±10% at strains of 10%, 40%, and 70% (60% for 0.48 kg/dm^3 [30 lb/ft^3] foam).
8. Data for compressive stress in the perpendicular–to–rise direction shall be obtained in an identical manner, using three additional test samples, except that the thickness dimension of the test samples shall be perpendicular to the foam rise direction. As shown in Table 8.1-3, the average perpendicular–to–rise compressive stress for each foam pour shall be the nominal compressive stress ±15% at strains of 10%, 40%, and 70% (60% for 0.48 kg/dm^3 [30 lb/ft^3] foam). As further shown in Table 8.1-3, the average perpendicular–to–rise compressive stress for all foam pours used in a single bun shall be the nominal compressive stress ±10% at strains of 10%, 40%, and 70% (60% for 0.48 kg/dm^3 [30 lb/ft^3] foam).

8.1.5.2 Balsa Wood

Balsa wood material physical characteristics for the following parameters shall be determined for each lot based on the following acceptance tests. All wood shall be free of gross defects and knots. Acceptable panel defects are as follows:

1. Cracks less than 1.5 mm (0.06 in) wide and less than 120 mm (4.72 in) long
2. A maximum of 4 cracks from 1.5 mm to 8 mm (0.06 in to 0.32 in) wide and less than 150 mm (6 in) long per panel.

8.1.5.2.1 Density

The density of each wood lot shall be determined in accordance with ASTM D2395[9], Method A. At least three test samples shall be taken from each lot of wood. The numerically averaged density of the test samples shall be within the range 0.11 ± 0.03 kg/dm³ (6.9 ±1.9 lb_m/ft^3).

8.1.5.2.2 Moisture Content

The moisture content of each wood lot shall be determined in accordance with ASTM D4442[10] or ASTM D4444[11]. At least three test samples shall be taken from each lot of wood. The moisture content shall be determined within 12 hours prior to being installed into the packaging. The moisture content for all wood samples shall not exceed 12%.

8.1.5.3 Butyl Rubber O–rings

Physical characteristics of butyl rubber containment O–ring seals for the following parameters shall be determined for each lot based on the following acceptance tests.

8.1.5.3.1 Durometer

The durometer of each lot of the butyl rubber material shall be determined in accordance with ASTM D2240[12]. Each lot of butyl rubber material shall have a hardness of 70 ±5 Shore A durometer (i.e., within the range of 65 to 75 Shore A durometer).

8.1.5.3.2 Tensile Strength and Elongation

The tensile strength of each lot of the butyl rubber material shall be determined in accordance with ASTM D412[13]. Each lot of butyl rubber material shall have a minimum tensile strength of 10 MPa (1,450 psi) and a minimum elongation of 250%.

8.1.5.3.3 Heat Resistance

The heat resistance of each lot of the butyl rubber material shall be determined in accordance with ASTM D573[14]. Each lot of butyl rubber material shall experience a maximum 10 Shore A durometer hardness increase, a maximum reduction in tensile strength of 25%, and a maximum reduction in ultimate elongation of 25%, when tested at 70 °C (158 °F).

---

[9] ASTM D2395–02, *Standard Test Methods for Specific Gravity of Wood and Wood–Based Materials*, American Society for Testing and Materials (ASTM).

[10] ASTM D4442–92(2003), *Standard Tests Methods for Direct Moisture Content Measurement of Wood and Wood–Based Materials*, American Society for Testing and Materials (ASTM).

[11] ASTM D4444–92(1998)e1, *Standard Tests Methods for Use and Calibration of Hand–Held Moisture Meters*, American Society for Testing and Materials (ASTM).

[12] ASTM D2240–05, *Standard Test Method for Rubber Property – Durometer Hardness*, American Society for Testing and Materials (ASTM).

[13] ASTM D412–98a(2002)e1, *Standard Test Methods for Vulcanized Rubber and Thermoplastic Rubbers and Thermoplastic Elastomers – Tension*, American Society for Testing and Materials (ASTM).

[14] ASTM D573–04, *Standard Test Method for Rubber – Deterioration in an Air Oven*, American Society for Testing and Materials (ASTM).

8.1.5.3.4 Compression Set

The compression set of each lot of the butyl rubber material shall be determined in accordance with Method B of ASTM D395[15]. After 22 hours at 70 °C (158 °F), each lot of butyl rubber material shall have a maximum compression set of 25%.

8.1.5.3.5 Cold Temperature Resistance

The cold temperature resistance of each lot of the butyl rubber material shall be determined in accordance with Method A, 9.3.2 of ASTM D2137[16]. After 3 minutes at -40 °C (-40 °F), each lot of butyl rubber material shall be non–brittle.

8.1.5.3.6 Cold Temperature Resiliency

The cold temperature resiliency of each lot of the butyl rubber material shall be determined in accordance with the TR–10 test of ASTM D1329[17]. Each lot of butyl rubber material shall be resilient at a test temperature of -50 °C (-58 °F) or less.

8.1.5.4 Calcium Silicate Insulation Board

This section establishes the requirements and acceptance criteria for inspection and testing of calcium silicate insulation board utilized within the TRUPACT–III packaging.

8.1.5.4.1 Composition

The insulation board supplier shall certify that the composition of the calcium silicate insulation board has a minimum fiber content of 95% mineral fibers.

8.1.5.4.2 Density

1. Three test samples shall be taken from each lot of calcium silicate insulation board. Each test sample shall be a rectangular prism with nominal dimensions of the sheet thickness (T) × 50 mm (2.0 in) wide (W) × 50 mm (2.0 in) long (L).
2. Place the test samples in a room (ambient) temperature environment (i.e., 20 °C to 30 °C [68 °F to 86 °F]) for sufficient time to thermally stabilize the test samples. Measure and record the room temperature to an accuracy of ±1 °C (±2 °F).
3. Measure and record the weight of each test sample to an accuracy of ±1 gram (±0.03 oz).
4. Measure and record the thickness, width, and length of each test sample to an accuracy of ±1 mm (0.04 in).

---

[15] ASTM D395–03, *Standard Test Methods for Rubber Property – Compression Set,* American Society for Testing and Materials (ASTM).

[16] ASTM D2137–94(2000), *Standard Test Methods for Rubber Property – Brittleness Point of Flexible Polymers and Coated Fabrics,* American Society for Testing and Materials (ASTM).

[17] ASTM D1329–02, *Standard Test Method for Evaluating Rubber Property – Retraction at Lower Temperatures (TR Test),* American Society for Testing and Materials (ASTM).

5. Determine and record the room temperature density of each test sample utilizing the following formula:

$$\rho_{cal\ sil} = \frac{\text{Weight, g}}{T \times W \times L,\ \text{mm}^3} \times \frac{10^6\ \text{mm}^3/\text{dm}^3}{10^3\ \text{g/kg}},\ \text{kg/dm}^3$$

6. Determine and record the average density of the three test samples. The numerically averaged density of the three test samples shall be 0.45 ±0.10 kg/dm^3 (28 ±6 lb$_m$/ft^3) (i.e., within the range of 0.35 to 0.55 kg/dm^3 [22 to 34 lb$_m$/ft^3]).

8.1.5.4.3 Thermal Conductivity

1. The thermal conductivity test shall be performed using a heat flow meter (HFM) apparatus. The HFM establishes steady state unidirectional heat flux through a test specimen between two parallel plates at constant but different temperatures. By measurement of the plate temperatures and plate separation, Fourier's law of heat conduction is used by the HFM to automatically calculate thermal conductivity. Description of a typical HFM test method is provided in ASTM C518. The HFM shall be calibrated against a traceable reference specimen per the HFM manufacturer's operating instructions.
2. Three test samples shall be taken from each lot of calcium silicate insulation board. Each test sample shall be of sufficient size to enable testing per the HFM manufacturer's operating instructions.
3. Place the test samples in a room (ambient) temperature environment (i.e., 20 °C to 30 °C [68 °F to 86 °F]) for sufficient time to thermally stabilize the test samples.
4. Measure and record the necessary test sample parameters as input data to the HFM apparatus per the HFM manufacturer's operating instructions.
5. Perform thermal conductivity testing and record the measured thermal conductivity for each test sample following the HFM manufacturer's operating instructions.
6. Determine and record the average thermal conductivity of the three test samples. The numerically averaged thermal conductivity of the three test samples shall be 0.085 ±0.017 W/m–K (0.59 ±0.12 Btu–in/hr–ft^2–°F) (i.e., within the range of 0.068 to 0.102 W/m–K [0.47 to 0.71 Btu–in/(hr–ft^2–°F)]).

8.1.6 Tests for Shielding Integrity

The TRUPACT–III packaging does not contain any biological shielding.

8.1.7 Thermal Acceptance Test

Material properties utilized in Chapter 3.0, *Thermal Evaluation*, are consistently conservative for the normal conditions of transport (NCT) and hypothetical accident condition (HAC) thermal analyses performed. With the exception of the tests required for polyurethane foam, wood, and calcium silicate insulation board, as shown in Section 8.1.5, *Component Tests*, specific acceptance tests for material thermal properties are not performed.

Table 8.1-1 – Foam Thermal Conductivity at 20 °C to 30 °C [68 °F to 86 °F]

Thermal Conductivity			
Density	**Nominal –20%**	**Nominal**	**Nominal +20%**
Kg/dm^3	**W/(m–K)**	**W/(m–K)**	**W/(m–K)**
0.10	0.024	0.030	0.036
0.16	0.025	0.031	0.037
0.29	0.038	0.047	0.056
0.48	0.055	0.069	0.083

Table 8.1-2 – Foam Compressive Strength, Parallel–to–Rise, at 20 °C to 30 °C [68 °F to 86 °F]

	Minimum		Nominal	Maximum	
	Nom. -15%	Nom. -10%		Nom. +10%	Nom. +15%
Strain	Crush Strength, MPa (psi) (Note: Metric units govern)				
Density 0.10 kg/dm^3 (6 lb/ft^3)					
10%	0.83 (120)	0.88 (128)	0.98 (142)	1.08 (157)	1.13 (164)
40%	0.89 (129)	0.95 (138)	1.05 (152)	1.16 (168)	1.21 (175)
70%	1.83 (265)	1.94 (281)	2.15 (312)	2.37 (344)	2.47 (358)
Density 0.16 kg/dm^3 (10 lb/ft^3)					
10%	1.96 (284)	2.07 (300)	2.30 (334)	2.53 (367)	2.65 (384)
40%	2.15 (312)	2.28 (331)	2.53 (367)	2.78 (403)	2.91 (422)
70%	5.59 (811)	5.92 (858)	6.58 (954)	7.24 (1,050)	7.57 (1,098)
Density 0.29 kg/dm^3 (18 lb/ft^3)					
10%	5.85 (848)	6.19 (898)	6.88 (998)	7.57 (1,098)	7.91 (1,147)
40%	7.16 (1,038)	7.58 (1,099)	8.42 (1,221)	9.26 (1,343)	9.68 (1,404)
70%	21.11 (3,061)	22.35 (3,241)	24.83 (3,600)	27.31 (3,560)	28.55 (4,140)
Density 0.48 kg/dm^3 (30 lb/ft^3)					
10%	15.27 (2,214)	16.17 (2,345)	17.97 (2,606)	19.77 (2,867)	20.67 (2,997)
40%	20.67 (2,997)	21.89 (3,174)	24.32 (3,526)	26.75 (3,879)	27.97 (4,056)
60%	38.16 (5,533)	40.40 (5,858)	44.89 (6,509)	49.38 (7,160)	51.62 (7,485)

Table 8.1-3 – Foam Compressive Strength, Perpendicular–to–Rise, at 20 °C to 30 °C [68 °F to 86 °F]

Strain	Minimum		Nominal	Maximum	
	Nom. -15%	Nom. -10%		Nom. +10%	Nom. +15%
	Crush Strength, MPa (psi) (Note: Metric units govern)				
Density 0.10 kg/dm^3 (6 lb/ft^3)					
10%	0.82 (119)	0.86 (125)	0.96 (139)	1.06 (154)	1.10 (160)
40%	0.86 (125)	0.91 (132)	1.01 (146)	1.11 (161)	1.16 (168)
70%	1.83 (265)	1.94 (281)	2.15 (312)	2.37 (344)	2.47 (358)
Density 0.16 kg/dm^3 (10 lb/ft^3)					
10%	1.96 (284)	2.07 (300)	2.30 (334)	2.53 (367)	2.65 (384)
40%	2.15 (312)	2.28 (331)	2.53 (367)	2.78 (403)	2.91 (422)
70%	5.69 (825)	6.02 (873)	6.69 (970)	7.36 (1,067)	7.69 (1,115)
Density 0.29 kg/dm^3 (18 lb/ft^3)					
10%	5.81 (842)	6.15 (892)	6.83 (990)	7.51 (1,089)	7.85 (1,138)
40%	7.10 (1,030)	7.52 (1,090)	8.35 (1,211)	9.19 (1,333)	9.60 (1,392)
70%	20.98 (3,042)	22.21 (3,220)	24.68 (3,579)	27.15 (3,937)	28.38 (4,115)
Density 0.48 kg/dm^3 (30 lb/ft^3)					
10%	15.30 (2,219)	16.20 (2,349)	18.00 (2,610)	19.80 (2,871)	20.70 (3,002)
40%	20.70 (3,002)	21.92 (3,178)	24.35 (3,531)	26.79 (3,885)	28.00 (4,060)
60%	38.42 (5,571)	40.68 (5,899)	45.20 (6,554)	49.72 (7,209)	51.98 (7,537)

This page intentionally left blank.

8.2 Maintenance Program

This section describes the maintenance program used to ensure continued performance of the TRUPACT–III package.

8.2.1 Structural and Pressure Tests

8.2.1.1 Containment Vessel Pressure Testing

Perform structural pressure testing on the containment vessel (i.e., the CSA) per the requirements of Section 8.1.3.2, *Containment Vessel Pressure Testing*, once every five years. Upon completing the structural pressure test, perform leakage rate testing per the requirements of Section 8.1.4, *Fabrication Leakage Rate Tests*.

8.2.1.2 Interior Cavity Surfaces Inspection

Annual inspection shall be performed of the accessible interior surfaces of the payload cavity for chemically induced corrosion. After removal of the payload loading system, perform a visual inspection for indications of interior surface corrosion. Should evidence of corrosion exist, a liquid penetrant inspection of the interior surfaces shall be performed per ASME Boiler and Pressure Vessel Code, Section V[1], Article 6, and ASME Boiler and Pressure Vessel Code, Section III[2], Division 1, Subsection NB, Article NB–5000. Indications of cracking or distortion shall be evaluated in accordance with the cognizant quality assurance program.

Once the packaging is placed into service, at a maximum interval of five (5) years, an examination shall be performed on the accessible interior surfaces for evidence of chemically induced stress corrosion. This examination shall consist of a liquid penetrant inspection of all accessible welds and adjacent base metal (minimum 13 mm [0.5 in.] on each side of the weld), and shall be performed per ASME Boiler and Pressure Vessel Code, Section V, Article 6, and ASME Boiler and Pressure Vessel Code, Section III, Division 1, Subsection NB, Article NB–5000, as delineated on the drawings in Appendix 1.3.1, *Packaging General Arrangement Drawings*. Indications of cracking or distortion shall be evaluated in accordance with the cognizant quality assurance program prior to implementing corrective actions.

8.2.2 Maintenance/Periodic Leakage Rate Tests

This section provides the generalized procedure for maintenance/periodic leakage rate testing of the containment vessel penetrations during routine maintenance, or at the time of seal replacement or

[1] American Society of Mechanical Engineers (ASME) Boiler and Pressure Vessel Code, Section V, *Nondestructive Examination*, 2004 Edition, 2005 and 2006 Addenda.

[2] American Society of Mechanical Engineers (ASME) Boiler and Pressure Vessel Code, Section III, *Rules for Construction of Nuclear Power Plant Components*, 2004 Edition, 2005 and 2006 Addenda.

seal area repair. Maintenance leakage rate testing shall follow the guidelines of Section 7.4, *Maintenance Leakage Rate Test*, and Section 7.5, *Periodic Leakage Rate Test*, of ANSI N14.5[3].

Maintenance/periodic leakage rate testing shall be performed on the main O–ring seal and vent port insert O–ring seal for the containment structural assembly (CSA) in accordance with Section 8.2.2.2, *Helium Leakage Rate Testing the Main Containment O–ring Seal*, and 8.2.2.3, *Helium Leakage Rate Testing the Vent Port Insert O–ring Seal*. Each leakage rate test shall meet the acceptance criteria delineated in Section 8.2.2.1, *Maintenance/Periodic Leakage Rate Test Acceptance Criteria.*

8.2.2.1 Maintenance/Periodic Leakage Rate Test Acceptance Criteria

Maintenance/periodic leakage rate test acceptance criteria are identical to the criteria delineated in Section 8.1.4.1, *Fabrication Leakage Rate Test Acceptance Criteria.*

8.2.2.2 Helium Leakage Rate Testing the Main Containment O–ring Seal

1. The maintenance/periodic leakage rate test of the main containment O–ring seal (inner) shall be performed following the guidelines of Section A.5.4, *Evacuated Envelope – Gas Detector*, of ANSI N14.5.
2. The CSA shall be assembled with both main O–ring seals installed into the closure lid. If not previously tightened, tighten the closure bolts to 1,480 – 1,720 N–m (1,092 – 1,269 lb_f–ft) torque as shown in Appendix 1.3.1, *Packaging General Arrangement Drawings.*
3. Remove the vent port locking ring and the vent port dust plug, and back–off or remove the vent port retaining ring and vent port insert. Install an adapter to the vent port to allow gas flow to and from the cavity.
4. Connect a vacuum pump to the adapter on the vent port, and evacuate the payload cavity to 90% vacuum or better (i.e., ≤10% ambient atmospheric pressure).
5. Remove the seal test port plug in the closure lid. Install an adapter to the seal test port.
6. Install a helium mass spectrometer leak detector to the adapter on the seal test port. Evacuate through the seal test port until the vacuum is sufficient to operate the helium mass spectrometer leak detector.
7. Provide a helium atmosphere inside the payload cavity by backfilling with helium gas to a pressure slightly greater than atmospheric pressure, i.e., +7, -0 kPa (+1, -0 psig).
8. Perform the helium leakage rate test to the requirements of Section 8.1.4.1, *Fabrication Leakage Rate Test Acceptance Criteria.* If, after repeated attempts, the main containment O–ring seal fails to pass the leakage rate test, isolate the leak path and, prior to repairing the leak path and repeating the leakage rate test, record on a nonconformance report and disposition prior to final acceptance in accordance with the cognizant quality assurance program.
9. If the vent port retaining ring/vent port insert was removed, remove the vent port adapter and re–install the vent port retaining ring/vent port insert; tighten to 370 – 430 N–m (273 – 317 lb_f–ft) torque.

[3] ANSI N14.5–1997 (or later), *American National Standard for Radioactive Materials – Leakage Tests on Packages for Shipment,* American National Standards Institute, Inc. (ANSI).

10. If the vent port retaining ring/vent port insert was not removed, tighten the vent port retaining ring/vent port insert to 370 – 430 N–m (273 – 317 lb_f–ft) torque using the vent port adapter.
11. Install the seal test port plug; tighten to 8 – 12 N–m (5 – 9 lb_f–ft) torque.
12. If the helium leakage rate testing of the vent port insert O–ring seal is to be performed immediately following this test, Steps 13 through 15 may be omitted.
13. If not previously removed, remove the vent port adapter.
14. Install the vent port locking ring; tighten to 370 – 430 N–m (273 – 317 lb_f–ft) torque.
15. Install the vent port dust plug; tighten to 90 – 110 N–m (66 – 81 lb_f–ft) torque.

8.2.2.3 Helium Leakage Rate Testing the Vent Port Insert O–ring Seal

The vent port insert O–ring seal test may be performed either with the closure lid assembled to or with the closure lid removed from the body of the TRUPACT–III packaging, as described in the following sections.

8.2.2.3.1 Testing with the Closure Lid Assembled to the Body

1. The maintenance/periodic leakage rate test of the vent port insert O–ring seal shall be performed following the guidelines of Section A.5.4, *Evacuated Envelope – Gas Detector*, of ANSI N14.5.
2. If this test immediately follows the testing from Section 8.2.2, *Helium Leakage Rate Testing the Main Containment O–ring Seal* (i.e., helium atmosphere already exists in the payload cavity, and the vent port retaining ring/vent port insert is closed and properly tightened), proceed to Step 9.
3. The CSA shall be assembled as shown in Appendix 1.3.1, *Packaging General Arrangement Drawings*.
4. Remove the vent port locking ring and vent port dust plug.
5. Install an adapter to the internal threads of the vent port and retract the vent port retaining ring/vent port insert to allow gas to flow to and from the payload cavity.
6. Connect a vacuum pump to the evacuation envelope and evacuate the envelope to 90% vacuum or better (i.e., ≤10% ambient atmospheric pressure).
7. Provide a helium atmosphere inside the payload cavity by backfilling with helium gas to a pressure slightly greater than atmospheric pressure, i.e., +7, -0 kPa (+1, -0 psig).
8. Utilizing an adaptor, tighten the vent port retaining ring to 370 – 430 N–m (273 – 317 lb_f–ft) torque.
9. If previously removed, install the vent port adapter to the vent port.
10. Install a helium mass spectrometer leak detector to the adapter on the vent port. Evacuate through the vent port until the vacuum is sufficient to operate the helium mass spectrometer leak detector.
11. Perform the helium leakage rate test to the requirements of Section 8.1.4.1, *Fabrication Leakage Rate Test Acceptance Criteria*. If, after repeated attempts, the vent port insert O–ring seal fails to pass the leakage rate test, isolate the leak path and, prior to repairing the leak path and repeating the leakage rate test, record on a nonconformance report and disposition prior to final acceptance in accordance with the cognizant quality assurance program.

12. Remove the vent port adapter.
13. Install the vent port locking ring; tighten to 370 – 430 N–m (273 – 317 lb_f–ft) torque.
14. Install the vent port dust plug; tighten to 90 – 110 N–m (66– 81 lb_f–ft) torque.

8.2.2.3.2 Testing with the Closure Lid Removed from the Body

As an alternative to Section 8.2.2.3.1, *Testing with the Closure Lid Assembled to the Body*, the vent port insert O–ring seal test may be performed with the assembled closure lid separate from the body. Operational steps are the same as established in Section 8.2.2.3.1, except that instead of utilizing the TRUPACT–III payload cavity to establish the required helium atmosphere, a localized envelope is established over the ∅50–mm vent port on the inside surface of the closure lid.

8.2.3 Component and Material Tests

8.2.3.1 Fasteners

All threaded components shall be inspected annually for deformed or stripped threads. Damaged components shall be repaired or replaced prior to further use. The threaded components to be visually inspected include the closure lid bolts, the overpack cover attachment bolts, the vent port insert, retaining ring, and locking ring, the vent port dust plug, the seal test port plug, the body helium fill access plugs, the body helium fill port plug, and all internal threads (i.e., holes and the optional threaded inserts, if applicable).

Regardless of condition, closure lid bolts and overpack cover attachment bolts shall be replaced after no more than 250 service cycles. A service cycle is defined as two tightening operations.

8.2.3.2 Seal Areas and Grooves

8.2.3.2.1 Seal Area Routine Inspection and Repair

Before each use and at the time of seal replacement, the sealing surfaces on the closure lid and body shall be visually inspected for damage that could impair the sealing capabilities of the TRUPACT–III packaging. Perform surface finish inspections for the body flange, and the O–ring grooves and mating sealing surfaces on the closure lid. Damage shall be corrected prior to further use (e.g., using emery cloth restore sealing surfaces) to the surface finish specified in Section 8.2.3.2.2, *Surface Finish of Sealing Areas*.

Upon completion of containment seal area repairs, perform a leakage rate test per the applicable section of Section 8.2.2, *Maintenance/Periodic Leakage Rate Tests*.

8.2.3.2.2 Surface Finish of Sealing Areas

The surface finish for the main O–ring sealing regions shall be a 0.8 micro–mm (32 micro–inches) finish, or better, to maintain package configuration and performance to design criteria. If the surface condition is determined to exceed 0.8 micro–mm (32 micro–inches), repair the surface per the requirements of Section 8.2.3.2.1, *Seal Area Routine Inspection and Repair*.

8.2.4 Thermal Tests

No thermal tests are necessary to ensure continued performance of the TRUPACT–III packaging.

8.2.5 Miscellaneous Tests

8.2.5.1 Valves and Rupture Discs

The TRUPACT–III packaging does not contain any valves or rupture discs on the containment vessel.

8.2.5.2 Gaskets

Containment boundary O–ring seals and the debris shield silicone foam insert shall be replaced within the 12–month period prior to shipment or when damaged (whichever is sooner), per the size and material requirements delineated on the drawings in Appendix 1.3.1, *Packaging General Arrangement Drawings*. Following containment O–ring seal replacement and prior to a loaded shipment, the new O–ring seals shall be leakage rate tested to the requirements of Section 8.2.2, *Maintenance/Periodic Leakage Rate Tests*.

8.2.5.3 Shielding

The TRUPACT–III packaging does not contain any biological shielding.

8.2.5.4 Passive Filters

The function of the passive polyethylene filters that are installed on the closure lid shall be verified within the 12–month period prior to shipment or when damaged (whichever is sooner). Verification of the passive filter function is determined by applying an air supply to one side of the filter to ensure air passes through the filter. Should a passive filter be determined to fail the function test or is damaged, the filter shall be replaced per the size and material requirements delineated on the drawings in Appendix 1.3.1, *Packaging General Arrangement Drawings*.

This page intentionally left blank.